Award Number: DAMD17-00-1-0420

TITLE: Effect of Angiogenic Growth on Tumor Growth, Vascular Function, and the Development of Hypoxic Therapeutic Resistance

PRINCIPAL INVESTIGATOR: Bruce M. Fenton, Ph.D.

CONTRACTING ORGANIZATION: University of Rochester
Rochester, New York 14627

REPORT DATE: May 2003

TYPE OF REPORT: Final

PREPARED FOR: U.S. Army Medical Research and Materiel Command
Fort Detrick, Maryland 21702-5012

REPORT DOCUMENTATION PAGE

Form Approved
OMB No. 074-0188

1. AGENCY USE ONLY (Leave blank)	2. REPORT DATE	3. REPORT TYPE AND DATES COVERED
	May 2003	Final (1 May 2002 - 30 Apr 2003)

4. TITLE AND SUBTITLE
Effect of Angiogenic Growth on Tumor Growth, Vascular Function, and the Development of Hypoxic Therapeutic Resistance

5. FUNDING NUMBERS
DAMD17-00-1-420

6. AUTHOR(S)
Bruce M. Fenton, Ph.D.

7. PERFORMING ORGANIZATION NAME(S) AND ADDRESS(ES)
University of Rochester
Rochester, New York 14627

E-Mail: bruce.fenton@rochester.edu

8. PERFORMING ORGANIZATION REPORT NUMBER

9. SPONSORING / MONITORING AGENCY NAME(S) AND ADDRESS(ES)
U.S. Army Medical Research and Materiel Command
Fort Detrick, Maryland 21702-5012

10. SPONSORING / MONITORING AGENCY REPORT NUMBER

11. SUPPLEMENTARY NOTES

12a. DISTRIBUTION / AVAILABILITY STATEMENT
Approved for Public Release; Distribution Unlimited

12b. DISTRIBUTION CODE

13. ABSTRACT (Maximum 200 Words)

The primary objectives of this grant were to determine the effects of either angiogenic growth factor overexpression or inhibition on mammary tumor pathophysiology. We evaluated four transfected human breast tumors and two murine mammary carcinoma lines by developing new methods for image analysis to quantify tumor vascular structure and function as well as micro-regional hypoxia. A particular emphasis was the comparison of several antiangiogenic strategies, including endostatin, anti-VEGFR-2, and Celebrex, to quantitate the pathophysiological response to each. Overall effects on tumor oxygenation varied temporally as a function of the specific treatment and among the tumor lines and implantation sites. Even within a tumor type, response could vary significantly among animals. Further more detailed studies are clearly warranted to determine what specific factors distinguish responders from nonresponders prior to treatment. These findings are clinically relevant in terms of clarifying the relationships among angiogenesis, tumor vascular function, and metastatic potential, and have improved our understanding of the physiological links between growth factor expression and the development of therapeutically resistant tumor cell subpopulations. Given the observed dependence of tumor oxygenation on angiogenic and antiangiogenic factors, this work clearly demonstrates that the precise scheduling of conventional therapies with antiangiogenic strategies, specifically those targeting VEGF, can be critical.

14. SUBJECT TERMS
angiogenesis, tumor vasculature, tumor oxygenation, hypoxia, tumor pathophysiology, therapeutic resistance

15. NUMBER OF PAGES
185

16. PRICE CODE

17. SECURITY CLASSIFICATION OF REPORT	18. SECURITY CLASSIFICATION OF THIS PAGE	19. SECURITY CLASSIFICATION OF ABSTRACT	20. LIMITATION OF ABSTRACT
Unclassified	Unclassified	Unclassified	Unlimited

Table of Contents

Introduction:

The primary objectives of this grant were to determine the *in vivo* consequences of angiogenic growth factor overexpression by breast cancer cells. Based on the MCF-7 human breast carcinoma cell line, which has previously been used to study the effects of growth factor overexpression on its estrogen-dependent and poorly metastatic phenotype, several transfected cell lines were derived, each overexpressing a different angiogenic factor. Incorporating a combination of techniques, we have investigated changes in tumor vascular configuration and function in four human mammary carcinoma lines: parental MCF-7 tumors (an estrogen dependent, slowly growing tumor which expresses low FGF levels), and four MCF-7 transfectants (overexpressing either FGF_1 (fibroblast growth factor 1), FGF_4, $VEGF_{121}$ (vascular endothelial growth factor – isoform 121), and $VEGF_{165}$). Anatomical and perfused blood vessel distributions were quantified using image analysis of fluorescent and immunohistochemical sections. In addition, tumor micro-regional hypoxic development was quantified using the hypoxia marker, EF5.

This proposal was clinically relevant in terms of clarifying the relationships between angiogenesis, tumor vascular function, and metastatic potential, and furthers our understanding of the physiological links between growth factor expression and the development of therapeutically resistant tumor cell subpopulations. In response to the suggestions of the reviewers, Aim 3 was shifted to emphasize measuring pathophysiological response to several antiangiogenic strategies. This information is of use both in designing new therapies to specifically target tumor blood vessels (including antiangiogenic agents and antibodies to the primary angiogenic growth factors), and in predicting the effects of combining recently proposed antiangiogenic strategies with ongoing conventional treatment modalities. Since the balance between angiogenesis inhibitors and activators may differ in different tumors, this improved understanding of the underlying physiology aids in the design of specific interventions that selectively block angiogenesis in a particular carcinogenesis pathway, raising the prospects for combined modality clinical strategies in which angiogenesis inhibitors play a key role.

Body:

In completing the objectives of this proposal, a key factor was the continued improvement and implementation of image processing methodologies and equipment. To better understand the complex relationships between tumor vascular configuration and the development of micro-regional hypoxia, zonal analysis techniques were developed (see Publication 3 in Appendix) that allowed sequentially stained sections to be revisited at the same spatial coordinates. Briefly, the goal was to spatially quantitate hypoxic marker binding as a function of distance from the nearest blood vessel. Several refinements to previous imaging methods were implemented: 1) hypoxia marker images were quantified in terms of their intensity levels, thus providing an analysis of the gradients in hypoxia with increasing distances from blood vessels, 2) zonal imaging masks were derived, which permit spatial sampling of images at precisely defined distances from blood vessels, as well as the omission of necrotic artifacts, 3) thresholding techniques were applied to omit holes in the tissue sections, and 4) distance mapping was utilized to define vascular spacing. Our previous 3-CCD camera has now been replaced with a cooled Retiga digital camera (under separate funding). This provides not only improved spatial resolution, but also enhanced pixel depth (12-bit gray level or 36-bit

color), allowing hypoxia marker intensities to be quantified over a much greater range. Although this required rewriting the Image Pro and Visual Basic macros that control the image processing, overall efficiency was increased by roughly 100% and much larger image montages can now be acquired, thus allowing a more comprehensive sampling of the histological sections.

Effect of angiogenic growth factor overexpression on tumor pathophysiology:

As outlined in the original Statement of Work, the primary objectives of this proposal were to clarify the interdependencies between tumor angiogenic growth factor overexpression and tumor pathophysiological changes. To determine whether micro-regional vascular perfusion and oxygen delivery keep pace with increased tumor growth, a combination of techniques was used to measure anatomical vessel spacing, angiogenic vessel spacing, perfused vessel spacing, and intravascular oxygen availability. For Aim 1, pathophysiological measurements were performed in MCF-7 human mammary tumors, including three transfectants that overexpressed various angiogenic growth factors (MCF-7/VEGF121, MCF-7/VEGF165, MCF-7/FGF-1, and MCF-7/FGF-4) as well as two murine mammary tumors (MCa-4 and MCa-35), which were not originally proposed, but were later included to provide a less costly method of evaluating some of the anti-angiogenic approaches. Aim 2 was closely related to Aim 1 in terms of tumor models and served to delineate the effects of tumor vascular changes on the development of hypoxia, both as a function of angiogenic growth factor expression.

Findings related to the pathophysiological consequences of angiogenic growth factor overexpression in MCF-7 tumors are summarized in Publications 6 and 7 and Abstracts 2, 13, 14, and 17 (Appendix). These manuscripts resulted from a collaboration that was established, during this grant period, between our laboratory and that of Dr. Shi-Yuan Cheng at the University of Pittsburgh. Our laboratory had already developed the FGF-1 and FGF-4 overexpressing transfectants, and Dr. Cheng's laboratory provided additional transfectants that overexpressed different isoforms of VEGF. In addition, we contributed our advanced image processing techniques to the Pittsburgh group to allow improvement quantitative measures of changes in tumor vascular configuration and hypoxia.

To summarize the first paper: vascular endothelial growth factor (VEGF) is an intensively studied molecule that has significant potential, both in stimulating angiogenesis and as a target for antiangiogenic approaches. We utilized MCF-7 breast cancer cells transfected with either of two of the major VEGF isoforms, $VEGF_{121}$ or $VEGF_{165}$, or fibroblast growth factor-1 (FGF-1) to distinguish the effects of these factors on tumor growth, vascular function, and oxygen delivery. While each transfectant demonstrated substantially increased tumorigenicity and growth rate compared to vector controls, only $VEGF_{121}$ produced a combination of significantly reduced total and perfused vessel spacing, as well as a corresponding reduction in overall tumor hypoxia. Such pathophysiological effects are of potential importance, since antiangiogenic agents designed to block VEGF isoforms could in turn result in the development of therapeutically unfavorable environments. If antiangiogenic agents are also combined with conventional therapies such as irradiation or chemotherapy, microregional deficiencies in oxygenation could play a key role in ultimate therapeutic success.

While VEGF is well accepted as an important modulator of tumor growth and vascular development, specific pathophysiological alterations associated with the different VEGF isoforms are less well understood. The current work reaffirms the notion that different VEGF isoforms lead to distinct differences in tumor vascular structure when compared at the same implantation site. In addition, we found that such vascular changes are, in some cases, directly associated with alterations in tumor oxygenation. In previous studies, results have varied widely in terms of both tumor growth rate and vascular density when different tumor models and implantation sites were considered. Guo, et al. (3) demonstrated that microenvironmental factors may be important, comparing $VEGF_{121}$ and $VEGF_{165}$ transfected glioma cell lines implanted either subcutaneously (*s.c.*) or intracranially (*i.c.*). $VEGF_{165}$ transfectants grew much more rapidly than wild-type at either location, with a corresponding increase in vascular density at both. Interestingly, $VEGF_{121}$ transfectants exhibited enhanced vessel growth only when implanted orthotopically in the brain. Using transfected fibrosarcoma cell lines, Grunstein et al. (2) proposed a model in which the different VEGF isoforms preferentially recruit blood vessels to either the tumor interior or periphery. It was suggested that these vascular patterns could possibly relate to the diffusibility of the $VEGF_{121}$ versus the $VEGF_{165}$. In this model, $VEGF_{120}$ overexpressing tumors tended to more effectively recruit systemic vessels, but failed to develop adequate internal vascularization (2), while $VEGF_{164}$ tumors were capable of inducing both external and internal vascular expansion. In human melanoma transfectants, overall growth rate of the tumors correlated only with amount of secretable VEGF, rather than on which specific VEGF isoform was overexpressed (5). Although $VEGF_{121}$ tumors were more densely vascularized at the tumor periphery (with more central necrosis), $VEGF_{165}$ tumors produced a much more densely vascularized plexus of blood vessels overall.

In the current study, human MCF-7 cells were implanted orthotopically in the mammary fat pad. Growth rates of $VEGF_{121}$ and $VEGF_{165}$ transfectants were significantly higher than vector controls and essentially equal to each other, while FGF-1 tumors grew at a somewhat less rapid rate. Both $VEGF_{121}$ and $VEGF_{165}$ produced densely arcading networks of blood vessels of increased vascular diameter. In contrast to both the fibrosarcomas and melanomas, however, spatial heterogeneities in vascular spacing were generally not observed. On average, neither total nor perfused vascular spacing varied as a function of distance from the tumor surface for any of the MCF-7 transfectants, although roughly half of the $VEGF_{165}$ tumors demonstrated a reduction in vasculature in the tumor center compared to periphery. Also, in contrast to previous reports in other models, MCF-7 $VEGF_{121}$ transfectants were much more evenly vascularized than the $VEGF_{165}$, as measured by the reduction in vascular spacing. Although the reasons for these disparate findings are unclear, spatially dependent vascular heterogeneities could possibly be related to either specific implantation site or differences in tumor volume.

A key advantage in our method of measuring vascular spacing, rather than the more commonly reported "vessels/field" or "positive pixels/mm^2", is that vascular spacing is more closely related to the ability of the blood vessels to uniformly supply the tumor with oxygen and nutrients. Especially in tumors containing an uneven distribution of vessels, determinations of mean vascular density can be highly misleading in terms of tumor oxygen delivery. For example, a tumor with a highly localized cluster of dense vascularization could have an overall vascular density equal to that of a tumor having a

reduced but homogeneous distribution of vessels. Clearly, micro-regional efficiencies in the delivery of either oxygen or chemotherapeutic agents would be quite different between the two. Such differences are apparent when using our "distance map" measurements of vascular spacing, which depends on vessel number, size, and spatial distribution. Although neither perfused vessel spacing nor tumor hypoxia was significantly altered in the $VEGF_{165}$ tumors, $VEGF_{121}$ tumors demonstrated significant changes in both. This decrease in perfused vessel spacing suggests that these vessels are more efficiently distributed in the $VEGF_{121}$ tumors, which is supported by the significant decrease in overall tumor hypoxia observed in these tumors.

Finally, FGF-1 transfectants have also been reported to form large, vascularized tumors and to confer a more malignant phenotype upon MCF-7 cells, without estrogen supplementation (6). In the current studies, FGF-1 overexpression led to a substantial increase in tumor growth rate, with a significant decrease in the perfused vessel spacing. Conceivably, this increase in perfused vasculature could translate to an increased opportunity for these tumor cells to invade into the circulation and metastasize (6).

A major unanswered question raised by this and previous studies is why $VEGF_{121}$ and $VEGF_{165}$ isoforms have such disparate effects on vascular structure and function among different tumor models. Although tumorigenicity and vascular growth were increased by both in all of the previously cited tumor models, specific alterations in vascular morphology were distinctly different. Interestingly, it has been reported that while $VEGF_{121}$ is the predominant form expressed in human breast carcinomas (4) and melanomas (5), the $VEGF_{165}$ variant is predominant in glioblastomas (1). This is intriguing in view of the fact that the vascular modification associated with $VEGF_{121}$ or $VEGF_{165}$ transfectants of the three tumor types do not necessarily follow this same pattern. In breast tumors, the predominant variant, $VEGF_{121}$, was also the more effective in inducing extensive tumor vascularization when overexpressed in that model. In melanomas and gliomas, however, an entirely different relationship holds true, and in each case, the predominant isoform is the less important in terms of promoting vascular development (3, 5). Previous studies have speculated that differences in vascular configuration between $VEGF_{121}$ and $VEGF_{165}$ may be related to variations in heparin binding, isoform size, or diffusivity (3, 5). It has also been hypothesized that variations in isoform expression may confer differential advantages on tumors as they expand in the different sites, each of which may possess different requirements for neovascularization (2). Further detailed studies are needed to determine whether vascular response is primarily dictated by the immediate microenvironment of the tumor, including proximity to nearby preexisting host vessels, or instead related to local balances among additional angiogenic growth factors and inhibitors.

Dr. Cheng's manuscript (first author: Dr. Guo, Publication 6 in Appendix) provides additional insight into the dependence on estrogen of tumor growth and vascular growth in MCF-7 transfectants. To summarize: alteration of the phenotype of breast cancers from estrogen-dependent to estrogen-independent growth often leads to the failure of anti-estrogenic tumor therapies. This manuscript demonstrates that overexpression of VEGF by estrogen-dependent MCF-7 breast cancer cells could abolish estrogen-dependent tumor growth in ovariectomized mice. In the absence of estrogen, MCF-7 VEGF-expressing tumors with increased vessel density showed growth kinetics similar to, or even greater than that of parental MCF-7 tumors with estrogen-

supplementation. Overexpression of VEGF by MCF-7 cells also stimulated cell proliferation in culture. These data suggest that stimulation of MCF-7 tumor angiogenesis and growth by VEGF is mediated by both autocrine and paracrine mechanisms. VEGF is a major angiogenic factor in breast tumor progression. This factor is expressed at high levels in breast cancers compared to normal breast tissue, and suppression of VEGF function inhibits breast tumor formation. Results show that expression of VEGF isoforms,$VEGF_{121}$, or $VEGF_{165}$, by MCF-7 cells at high levels stimulated both E2-independent and E2-dependent breast tumor growth in mice. Moreover, we also obtained several V121 or V165 cell clones that secreted VEGF at lower levels. These low VEGF-expressing cell clones did not show enhancement of tumor growth in E2-treated mice, nor formed tumors in non-E2-treated mice. This observation is in agreement with previous reports. With lower expression of the VEGF isoforms by MCF-7 cells, moderate augmentation on E2-dependent breast tumor growth in ovariectomized mice was seen. In another study, although MCF-7 $VEGF_{165}$-expressing tumors responded vigorously to estrogen stimulation in promoting tumorigenesis, the V165 cells could only form E2-independent tumors in ovariectomized mice when implanted with Matrigel. Thus, threshold levels of VEGF expression in breast cancer cells may be critical for the acquisition of the estrogen-independent phenotype in human breast cancers. This hypothesis is clinically relevant since high levels of VEGF proteins could be detected in primary breast cancer specimens, especially in hypoxic regions.

Immunohistochemical studies:

Over this grant period, several new immunohistochemical staining approaches were successfully optimized and implemented. These included Apotag for apoptosis, Ki-67 staining for proliferation, panendothelial cell antigen for endothelial cells (in tumor lines in which our standard CD31 staining is nonspecific for endothelial cells), VEGF, and thick section perfusion imaging (DiOC7). Preliminary studies were also completed in validating an alternative endogenous hypoxia marker, NDRG1, by comparison with our standard EF5 staining. Other staining techniques were less successful in our frozen sections, including $\alpha v\beta 3$ (for which a specific mouse antibody is still unavailable), $\beta 3$, α-smooth muscle actin (nonspecific in our tumor models), and desmin, the combination of which we were hoping to be able to use to distinguish mature blood vessels (associated with pericytes or smooth muscle cells) from less stable, more angiogenic vessels. We also tried some alternative perfusion markers (lectins), with limited success, in an effort to develop an alternative to our somewhat toxic $DiOC_7$ perfusion, but these agents had fairly weak signal and were too expensive for routine usage.

Antiangiogenic strategies and angiogenic growth factor administration:

The goal of Aim 3 in the original Statement of Work was to quantify functional changes in vascular perfusion and oxygen delivery in these same tumor models following the administration of angiogenic growth factors. In response to the suggestions of the original review committee, an additional major focus of this aim was to quantify changes in tumor pathophysiology following antiangiogenic strategies. In view of the highly intriguing results observed in our preliminary experiments, which measured vascular and oxygenation changes in response to antiangiogenic treatment, our primary focus in Aim 3 shifted in favor of the administration of antiangiogenic rather than angiogenic factors. In

this regard, since we were not familiar with specific doses and scheduling for many of these agents, we performed most of the experiments in more economical murine tumor models, rather than the very slow-growing and more expensive human xenografts.

Since endostatin had received a large amount of favorable publicity several years ago, in terms of striking tumor regressions, we first initiated a collaboration with Dr. Brian Grimwood at the New York State Department of Health (Wadsworth Center), to provide us with the recombinant endostatin. These studies resulted in numerous abstracts (Abstracts 1, 5, 6, 10, 12, 13, 18) and manuscripts (Publications 1, 4, 5). At the same time, my Co-investigator, Dr. Ding investigated the administration of endostatin plasmid and angiostatin on these same tumor models (see Publication 2 and Abstracts 3, 4, 7, 8, 11), as well as FGF-1, FGF-2, FGF-4, and VEGF (Publications 9, 10). In addition to the endostatin and angiostatin, we also studied celecoxib and meloxicam (Publications 1, 8 and Abstracts 2, 9), and most recently, an antibody to VEGFR-2, DC101, which we obtained through a collaboration we initiated with ImClone Systems (see Abstracts 15, 16). To summarize some of the most interesting results from these manuscripts and abstracts:

Endostatin has been shown to potently inhibit both tumor angiogenesis and the growth of experimental tumors, primarily through reduction of endothelial cell migration and proliferation with minimal direct effects on tumor cells (Publication 4). Recent studies have demonstrated that this agent can also enhance the antitumor effects of radiation when administered before or during radiotherapy. The current work was undertaken to investigate the effects of short-term recombinant endostatin administration on tumor microregional perfusion and hypoxic marker uptake in two murine mammary carcinomas, the poorly differentiated and highly vascularized MCa-35 tumor, and the well differentiated and less vascularized MCa-4. Specifically, the question was whether endostatin could produce pathophysiological changes in the tumor microenvironment, most notably alterations in oxygen delivery, that could lead to alterations in tumor radiosensitivity. Although antiangiogenic treatment might be expected to lead to a reduction in tumor blood flow, overall oxygenation was improved in one tumor model and unchanged in the other following short-term endostatin administration. Using recently devised image analysis techniques that allow correlation of multiply stained images of the same tumor frozen sections, changes in tumor hypoxia, apoptosis, and proliferation were quantified as a function of distance from the nearest anatomical or perfused blood vessel. In MCa-35 tumors, three daily doses of endostatin (20 mg/kg) had no effect on total or perfused vessel numbers, tumor hypoxia, or tumor growth. In MCa-4 tumors, total and perfused vessel counts were unchanged following endostatin, but tumor growth was inhibited by 30% and overall tumor hypoxia significantly decreased. Results suggest an initial increased vascular functionality in the endostatin treated tumors, without substantial alterations in tumor oxygen consumption rates. Following cessation of endostatin in the MCa-4 tumors, total and perfused vessel counts as well as vessel functionality decreased significantly with tumor growth, in conjunction with an increase in overall tumor necrosis. In summary, these results demonstrate striking intertumoral disparities in pathophysiological response following short-term endostatin administration. In those tumors in which hypoxia is reduced, acute treatment could prove extremely beneficial when combined with irradiation, providing that optimal treatment schedules

can be defined. Improved predictive assays are clearly needed to characterize and select such tumors.

Antiangiogenic therapy with endostatin in animals requires multiple and prolonged administration of the protein. Gene therapy could provide an alternative approach to continuous local delivery of this antiangiogenic factor *in vivo* (Publication 2, Abstracts 1,4,8). Established MCa-4 murine mammary carcinomas, grown in immunodeficient mice, were treated with intratumoral injection of endostatin plasmid at 7-day intervals. At the time of sacrifice, 14 days after the first injection, endostatin-treated tumor weights were 51% of controls ($P < 0.01$). Tumor growth inhibition was accompanied by a marked reduction in total vascular density. Specifically, computerized image analysis showed a 18–21% increase in the median distances between tumor cells and both the nearest anatomical (CD31-stained) vessel [48.1 6 3.8 versus 38.3 6 1.6 mm ($P < 0.05$)] and the nearest tumor-specific (CD105-stained) vessel [48.5 6 1.5 versus 39.8 6 1.5 mm ($P < 0.01$)]. An increased apoptotic index of tumor cells in endostatin-treated tumors [3.2 6 0.5% versus 1.9 6 0.3% ($P < 0.05$)] was observed in conjunction with a significant decrease in tumor perfused vessels ($DiOC_7$ staining), and an increase in tumor cell hypoxia (EF5 staining). Hypoxia resulting from endostatin therapy most likely caused a compensatory increase of in situ vascular endothelial growth factor (VEGF) and VEGF receptor mRNA expression. Increased immunoreactivity of endostatin staining in endostatin-treated tumors was also associated with an increased thrombospondin-1 staining [1.12 6 0.16 versus 2.44 6 0.35]. Our data suggest that intratumoral delivery of the endostatin gene efficiently suppresses murine mammary carcinoma growth and support the potential utility of the endostatin gene for cancer therapy.

In comparing all of our antiangiogenic strategies, the most effective agent in slowing tumor growth was clearly the anti-VEGFR-2 (DC101). We therefore devoted quite a bit of effort to quantifying accompanying changes in tumor vasculature and oxygen delivery. Although the manuscripts reporting these results are in progress, this work has been presented at two meetings (Abstracts 15 and 16). To summarize: DC101 has been shown to result in substantial tumor growth inhibition and enhanced radiosensitization in numerous tumor models. Since antiangiogenic treatments are likely to be ultimately combined with conventional therapies, it is vital to understand accompanying acute and chronic alterations in tumor pathophysiology. In the current study, two murine mammary carcinomas were grown orthotopically in C3H/HeJ mice: poorly differentiated, highly vascularized, MCa-35 tumors, and well-differentiated, less vascularized MCa-4 tumors. DC101 treatment (45 mg/kg every 3 days) was initiated at tumor volumes of either 50 mm^3 (early) or 500 mm^3 (late). Using computer analysis of multiple-field image montages from frozen tumor sections: 1) total blood vessels were identified using anti-CD31, 2) perfused vessels were found using *i.v.* injection of fluorescent $DiOC_7$, and 3) tumor hypoxia was quantified by uptake of the EF5 hypoxia marker. DC101 produced significant tumor growth inhibition for both tumor types, although somewhat more pronounced for the MCa-4. For the MCa-4 tumors, DC101 produced no alterations in total vessels densities, but significantly fewer perfused vessels ($p = 0.03$) and increased overall tumor hypoxia ($p = 0.03$). Zonal analysis of hypoxia variations as a function of distance from perfused vessels also suggested a decrease in oxygen delivery capacity in the early treated tumors, with no corresponding change in tumor oxygen consumption rate. For the late initiation treatments in MCa-4 tumors, DC101 again produced

significant tumor growth inhibition, with no alterations in total vessel counts. Here, however, perfused vessel counts were not decreased and tumor hypoxia was not increased, suggesting a relative enhancement of radiosensitivity and drug delivery in comparison to early treatment tumors. For the MCa-35 tumors, pathophysiological responses were quite different. Following DC101, overall hypoxia was unchanged, but total and perfused vessel counts were strikingly decreased ($p = 0.001$ and $p = 0.02$, respectively). Although oxygen delivery capacity significantly declined with increasing tumor volume, perivascular hypoxia levels in treated MCa-35 tumors were not significantly different from controls for large or small tumors. In conclusion, treatment-induced, temporal variations in tumor oxygenation clearly have important implications in terms of the timing of subsequent therapies, and predictive assays of tumor response are critically needed. Further studies are in progress to better characterize the underlying rationale for the differential response in these tumors, including spatial measurements of endogenous pro- and anti-angiogenic cytokine levels as well as differences in vessel angiogenic status.

Key Research Accomplishments:

- Several sophisticated improvements to the automated image analysis techniques were developed and implemented: 1) zonal imaging masks were derived, which permit spatial sampling of images at precisely defined distances from blood vessels, as well as the omission of necrotic artifacts, 2) thresholding techniques were applied to automatically remove holes in the tissue sections, and 3) distance mapping methods were introduced to more accurately define vascular spacing. Visual Basic macros were also formulated to automatically acquire and link the data among the imaging, spreadsheet, and plotting software. Zonal image analysis of multiple immunohistochemically stained images from the same frozen tumor sections provides pathophysiological information unobtainable from the individual images.
- Overexpression of FGF-1, FGF-4, $VEGF_{121}$, and $VEGF_{165}$ resulted in enhanced tumor growth rate, increased vascularity and reduced tumor hypoxia. While each transfectant demonstrated substantially increased tumorigenicity and growth rate compared to vector controls, only $VEGF_{121}$ produced a combination of significantly reduced total and perfused vessel spacing, as well as a corresponding reduction in overall tumor hypoxia. Such pathophysiological effects are of potential importance, since antiangiogenic agents designed to block VEGF isoforms could in turn result in the development of therapeutically unfavorable environments and, in turn, select for more aggressive tumor phenotypes.
- Experiments studying the acute effects of endostatin (3 daily doses) on MCa-4 and MCa-35 mammary tumor lines demonstrated that although antiangiogenic treatment had generally been predicted to lead to reductions in tumor blood flow, oxygenation was actually improved in one tumor model and unchanged in the other following short-term endostatin administration. These pathophysiological changes have significant implications in terms of combining endostatin with conventional therapies and suggest that acute endostatin administration could serve to improve radioresponse, based solely on improvements in oxygenation.

- Studies investigating longer term endostatin treatments (10 doses) were completed on 68 MCa-4 tumors. Surprisingly, when orthotopic transplantations were used (in contrast to the *i.m.* transplants used for the acute administrations), no effect on tumor growth was observed following 10 daily doses.
- Early initiation DC101 treatment produced decreased tumor growth, diminished vessel function, and increased hypoxia. Surprisingly, tumor growth suppression continued despite cessation of drug at day 20. The pathophysiological changes observed in small volume tumors were transient. By the time tumors reached volumes of >700 mm^3, perfused vessel spacing and hypoxia levels for treated and control tumors were equal. Late initiation DC101 treatment similarly reduced the tumor growth rate, but had no effect on tumor oxygenation, vascular spacing, or vessel function.
- DC101 treatment was more effective in the MCa-4 murine tumors than in the MCa-35, the latter distinguished by increased VEGF levels, vascularity, and metastatic potential (mutant p53), implying that endogenous expression of angiogenic cytokines could directly influence individual tumor response to receptor-targeted therapies. These pathophysiological results demonstrate a significant decrease in tumor vascular function and oxygenation following DC101 and suggest that appropriate scheduling must be devised when combining this agent with conventional treatments such as chemo- and radiotherapy. Perhaps the most interesting finding from these experiments was that antiangiogenic-induced reductions in tumor oxygenation can be transient in nature. Thus although such treatments could compromise treatment if administered immediately prior to radiotherapy, the exact scheduling is critical.

Reportable Outcomes:

Manuscripts:

1) Fenton, BM, P Okunieff, and I Ding. Characterization of the effects of antiangiogenic agents on tumor pathophysiology, Am J Clin Oncol 24(5):453-457, 2001.

2) I Ding, JZ Sun, BM Fenton, WM Liu, P Kimsely, P Okunieff, and W Min, Intratumoral administration of endostatin plasmid inhibits vascular growth and perfusion in MCa-4 mammary carcinomas, Cancer Res 61:526-531, 2001.

3) Fenton, BM, SF Paoni, BK Beauchamp, and I Ding. Zonal image analysis of tumor vascular perfusion, hypoxia, and necrosis. Br J Cancer 86:1831-1836, 2002.

4) Fenton, BM, SF Paoni, BG Grimwood, and I Ding. Disparate effects of endostatin on tumor vascular perfusion and hypoxia in two murine mammary carcinomas. Int J Radiat Oncol Biol Phys (accepted with revisions), 2003.

5) Fenton, BM, SF Paoni, BK Beauchamp, B Tran, L Liang, B Grimwood, and I Ding. Evaluation of microregional variations in tumor hypoxia following the administration of endostatin. Adv Expt Med Biol 510:19-24, 2003.

6) Guo, P, Q Fang, H-Q Tao, CA Schafer, BM Fenton, I Ding, B Hu, and S-Y Cheng. Overexpression of VEGF by MCF-7 breast cancer cells promotes estrogen-independent tumor growth in vivo. Cancer Res (in press), 2003.

7) Fenton, BM, SF Paoni, WM Liu, L Zhang, S-Y Cheng, and I Ding. Overexpression of VEGF121, but not VEGF165 or FGF-1, improves oxygenation in MCF-7 breast tumors. Br J Cancer (submitted), 2003.

8) W Liu, Y Chen, W Wang, P Keng, J Finkelstein, D Hu, L Liang, M Guo, B Fenton, P Okunieff and I Ding. Combination of radiation and Celebrex™ (celecoxib) reduce mammary and lung tumor growth, Am J Clin Oncol (in press), 2003.

9) Okunieff, P, Fenton, BM, Zhang, L, Kern, FG, Wu, T, Greg, JR, and Ding, I. Fibroblast growth factors (FGFs) increase breast tumor growth rate, metastases, blood flow, and oxygenation without significant change in vascular density, Adv Expt Med Biol (in press), 2003.

10) Ding, I, Liu, WM, Sun, JZ, Paoni, SF, Hernady, E, Fenton, BM, and Okunieff, P. FGF1 and VEGF mediated angiogenesis in KHT tumor-bearing mice, Adv Expt Med Biol (in press), 2003.

Abstracts and Presentations:

1) 2000 Eleventh International Congress in the Chemical Modifiers of Cancer Treatment Series, Banff, Alberta, Canada. Administration of endostatin plasmid inhibits angiogenesis and tumor growth and in nude but not C3H mice. P Okunieff, J Sun, W Liu, Y Jiang, B Fenton, and I Ding

2) 2001 First Radiation Therapy Oncology Group Workshop for Translational Research, Tampa, FL. "Effect of Angiogenesis Factor Expression on Tumor Vascular Distribution and Function", B Fenton.

3) 2001 American Association for Cancer Research Meeting, New Orleans, LA. Endostatin-mediated antitumor and antiangiogenesis: inhibition of murine MCa-35 mammary tumor growth and metastasis are associated with decreased tumor structural and perfused vessels, JZ Sun, WM Liu, CR Yang, W Min, P Keng, B Fenton, P Okunieff, and I Ding.

4) 2001 International Workshop on the Tumor Microenvironment and Its Cancer Therapies, Atlanta, GA. Alteration of cytokine and chemokine mRNA expression in MCa-4 murine mammary carcinomas following intratumoral administration of endostatin plasmid. I Ding, J Sun, L Liang, W Liu, W Min, P Okunieff and B Fenton.

5) 2001 International Society for Oxygen Transport to Tissue Meeting, Philadelphia, PA. Effect of endostatin administration on tumor growth inhibition, vascular perfusion, and hypoxia in murine mammary carcinomas. BM Fenton, S Paoni, B Beauchamp, B Tran, L Liang, BG Grimwood, and I Ding.

6) 2001 University of Rochester 5th Annual Cancer Center Symposium, Rochester, NY. Alterations in tumor growth, perfusion, hypoxia, and oxygen consumption following administration of endostatin. B Fenton, S Paoni, B Beauchamp, L Liang, B Grimwood, B Tran, and I Ding.

7) 2001 University of Rochester 5th Annual Cancer Center Symposium, Rochester, NY. Endostatin and angiostatin induce tumor and endothelial cell apoptosis through the down-regulation of VEGF/Akt signal transduction pathway. WM Liu, P Keng, CR Yang, B Fenton, P Okunieff and I Ding.

8) 2002 American Association for Cancer Research Meeting, San Francisco, CA. Mouse endostatin protein and endostatin plasmid have differential effects on esophageal and mammary carcinomas at various growth stages. I Ding, M Guo, DP Hu, WM Liu, YD Ding, LD Wang, B Grimwood, D Beer, P Okunieff, and BM Fenton.

9) 2002 American Association for Cancer Research Meeting, San Francisco, CA. Celecoxib-mediated antitumor effects in murine mammary carcinomas: association of two signal transduction pathways involved in DNA damage and apoptosis. W Liu, BM Fenton, P Keng, P Okunieff and I Ding.

10) 2002 Radiation Research Meeting, Reno, Nevada. Alterations in tumor growth, perfusion, hypoxia, and oxygen consumption following administration of endostatin. B Fenton, S Paoni, B Beauchamp, L Liang, B Grimwood, B Tran, and I Ding.

11) 2002 Radiation Research Meeting, Reno, Nevada. Endostatin and angiostatin induce tumor and endothelial cell apoptosis through the down-regulation of VEGF/Akt signal transduction pathway, W Liu, P Keng, C-R Yang, B Fenton, B Grimwood, P Okunieff, and I Ding.

12) 2002 Banbury Center Meeting on "Endostatin: Structure, Function, and Application", Cold Spring Harbor Laboratory, Disparate effects of endostatin on tumor vascular perfusion and hypoxia in two murine mammary carcinomas, BM Fenton, SF Paoni, BG Grimwood, and I Ding.

13) 2002 Era of Hope Department of Defense Breast Cancer Research Program Meeting, Orlando, Florida. Effect of antiangiogenic agents on tumor vasculature and oxygenation in mammary carcinomas. BM Fenton and I Ding.

14) 2002 Era of Hope Department of Defense Breast Cancer Research Program Meeting, Orlando, Florida. Overexpression of VEGF enhances estrogen-dependent and estrogen-independent growth of MCF-7 breast tumors. P Guo, Q Fang, I Ding, B Fenton, B Hu, and S-Y Cheng.

15) 2002 University of Rochester 6th Annual Cancer Center Symposium, Rochester, NY. VEGF receptor-2 blocking antibody inhibits mammary tumor growth, vascular perfusion, and oxygenation, BM Fenton, SF Paoni, WM Liu, and I Ding.

16) 2003 American Association for Cancer Research Meeting, Washington, D.C. Effects of vascular endothelial growth factor receptor-2 antibody on vascular function and tumor hypoxia in two disparate murine mammary carcinomas. BM Fenton, SF Paoni, and I Ding.

17) 2003 American Association for Cancer Research Meeting, Washington, D.C. Overexpression of VEGF by MCF-7 breast cancer cells enhances estrogen-dependent and estrogen-independent tumor growth. P Guo, Q Fang, H Tao, A Schafer, B Fenton, I Ding, B Hu, and S Cheng.

18) 2003 Tumor Microenvironment Workshop, Miami, FL. Effect of antiangiogenic strategies on the pathophysiology and progression of spontaneous and transplanted mammary tumors. BM Fenton, SF Paoni, and I Ding.

List of Personnel

Bruce Fenton, PhD – Principal Investigator
Ivan Ding, MD – Co-investigator
Scott Paoni – Laboratory Technician
Brian Beauchamp – Laboratory Technician

Conclusions:

The primary objectives of this grant were to quantitatively measure the effects of both angiogenic growth factor overexpression and angiogenic inhibition on mammary tumor pathophysiology. We evaluated four transfected human breast tumors and two murine mammary carcinoma lines by developing sophisticated new image analysis methods to quantify tumor vascular structure and function in relation to micro-regional hypoxia. In view of upcoming clinical strategies involving the combination of antiangiogenic approaches with conventional therapies, a particular emphasis was a comparison of the pathophysiological effects of several different antiangiogenic strategies. These included endostatin, DC101, and Celebrex. One of our most striking findings was the substantial intertumoral response to the different agents. Effects not only varied markedly among animals of a given tumor model, but could be totally opposite when comparing different models or different implantation sites. Different antiangiogenic agents also has varied effects. In response to short-term administration of endostatin, MCa-4 tumors demonstrated a significant increase in tumor oxygenation and substantial growth delay, while MCa-35 tumors exhibited no response at all. Response to DC101 was quite the opposite. Here, tumor oxygenation and perfusion decreased substantially in conjunction with a striking decrease in tumor growth rate. Clearly, these disparate effects on tumor oxygenation and perfusion have significant implications in terms of combining such agents with conventional therapies. This proposal is clinically important in terms of clarifying the relationships between angiogenesis, tumor vascular function, and metastatic potential, and has improved our understanding of the physiological links between growth factor expression and the development of therapeutically resistant tumor cell subpopulations. Given the observed dependence of tumor oxygenation on angiogenic and antiangiogenic factors, this work clearly demonstrates that the precise scheduling of conventional therapies with antiangiogenic strategies, specifically those targeting VEGF, can be critical. The current results emphasize the importance of developing suitable surrogate markers of tumor response, both to decide which types of agents can be effectively combined with radiation or chemotherapy and to predict which tumors will respond in the first place. Further more detailed studies are clearly warranted to define what specific factors distinguish responders from nonresponders prior to treatment. Over the course of this grant, hundreds of tumors were frozen and analyzed with our existing staining techniques and measurements. As we continue to improve and add to our methodologies, these same archival specimens will be recut and subjected to additional analyses.

References:

1. R.A.Berkman, M.J.Merrill, and W.C.Reinhold, Expression of the vascular permeability factor/vascular endothelial growth factor gene in central nervous system neoplasms, J Clin Invest 91:153 (1993).

2. J.Grunstein, J.J.Masbad, R.Hickey, F.Giordano, and R.S.Johnson, Isoforms of vascular endothelial growth factor act in a coordinate fashion to recruit and expand tumor vasculature, Molecular & Cellular Biology 20:7282 (2000).

3. P.Guo, L.Xu, S.Pan, R.A.Brekken, S.T.Yang, G.B.Whitaker, M.Nagane, P.E.Thorpe, J.S.Rosenbaum, H.H.Su, W.K.Cavenee, and S.Y.Cheng, Vascular endothelial growth factor isoforms display distinct activities in promoting tumor angiogenesis at different anatomic sites, Cancer Res 61:8569 (2001).

4. M.Relf, S.Lejeune, P.E.Scott, S.Fox, K.Smith, R.Leek, A.Moghaddam, R.Whitehouse, R.Bicknell, and A.L.Harris, Expression of the angiogenic factors vascular endothelial cell growth factor, acidic and basic fibroblast growth factor, tumor growth factor beta-1, platelet-derived endothelial cell growth factor, placenta growth factor, and pleiotrophin in human primary breast cancer and its relation to angiogenesis, Cancer Research 57:963 (1997).

5. J.L.Yu, J.W.Rak, G.Klement, and R.S.Kerbel, Vascular endothelial growth factor isoform expression as a determinant of blood vessel patterning in human melanoma xenografts, Cancer Res 62:1838 (2002).

6. L.Zhang, S.Kharbanda, D.Chen, J.Bullocks, D.L.Miller, I.Y.F.Ding, J.Hanfelt, S.W.McLeskey, and F.G.Kern, MCF-7 breast carcinoma cells overexpressing FGF-1 form vascularized, metastatic tumors in ovariectomized or tamoxifen-treated nude mice, Oncogene 15:2093 (1997).

Appendices:

Copies of 11 submitted and published manuscripts, plus 18 abstracts are included.

Am J Clin Oncol (CCT) 24(5): 453–457, 2001.

Characterization of the Effects of Antiangiogenic Agents on Tumor Pathophysiology

Bruce M. Fenton, Ph.D., Brian K. Beauchamp, B.S., Scott F. Paoni, M.S., Paul Okunieff, M.D., and Ivan Ding, M.D.

A variety of strategies have been proposed to control tumor growth and metastasis by inhibiting tumor angiogenesis. To optimally combine such antiangiogenic approaches with conventional therapy, improved methods are needed to characterize the underlying pathophysiologic changes. The objective of the current work was to demonstrate the utility of a combination of recently developed immunohistochemical and image analysis techniques in quantitating changes in tumor vasculature and hypoxia. Murine MCa-35 mammary carcinomas were frozen after administration of two COX-2 inhibitors: meloxicam and celecoxib (Celebrex). Total blood vessels were visualized using anti-CD31 staining, perfused vessels by intravenous injection of $DiOC_7$, and tumor hypoxia by EF5 uptake. Although both agents produced similar reductions in tumor volume compared with untreated tumors, varied effects on tumor vasculature and hypoxia were noted. Meloxicam reduced total vessel numbers significantly, whereas celecoxib had no effect. Both drugs substantially increased perfused vessel densities. Although mean hypoxic marker uptake was unchanged from matched controls, intratumor EF5 heterogeneities were significantly different between drugs. The results suggest that COX-2 inhibitors can have varying effects on tumor pathophysiology. Successful use of these drugs to enhance radiation response will likely require optimization of drug choice, dose schedule, and direct physiologic monitoring.

Key Words: Angiogenesis—Tumor oxygenation—Hypoxia—Celecoxib—Meloxicam.

During the past several years, a variety of strategies have been proposed to control tumor growth and metastatic spread by inhibiting tumor angiogenesis.[1] Despite a growing interest in the translation of these agents to clinical studies, the underlying pathophysiologic changes associated with the different antiangiogenic approaches remain relatively unexplored. Given the proposed clinical combination of angiogenic inhibitors and radiotherapy,[2–4] temporal changes in tumor vascular distribution and oxygenation are of particular relevance.

Inhibitors of the cyclooxygenases, COX-1 and COX-2, have received increasing attention, initially as antiinflammatory drugs and more recently as potential anticancer agents. Overexpression of COX-2 has been demonstrated in human tumors[5,6] and has been shown to mediate cell cycle progression, apoptosis, angiogenesis, and metastasis.[7–9] Selective COX-2 inhibitors have been shown useful not only for the prevention or regression of human and experimental tumors,[10–12] but also for the potentiation of tumor radioresponse.[3]

The primary objective of the current studies was to demonstrate that the pathophysiologic effects of antiangiogenic agents can be quantified using a combination of recently developed immunohistochemical methods combined with computerized image analysis. As an illustration of these techniques, we will present preliminary results regarding changes in tumor volume, hypoxia, and blood vessel growth after administration of two COX-2 inhibitors: meloxicam, which is 13 times more selective for inhibition of COX-2 than COX-1,[13] and celecoxib, which is more than 300 times more selective for COX-2.[14] After five to seven daily doses of either celecoxib or meloxicam, total and perfused blood vessel distributions as well as uptake of the EF5 hypoxic marker were quantified in MCa-35 mammary carcinomas in relation to untreated controls. These studies demonstrate that although these two drugs have similar effects on tumor growth delay, underlying pathophysiologic alterations are strikingly different.

METHODS

Animal Model

Cells from MCa-35 murine mammary carcinomas (3×10^6) were inoculated in the mammary fat pads of 6- to 8-week-old female C3H/HeJ mice (The Jackson Laboratory, Bar Harbor, ME). Tumors volumes were measured by calipers and the formula: volume = $1/2\ a^2b$, where a and b are the minor and major tumor axes, respectively. Guidelines for the humane treatment of animals were followed as approved by the University Committee on Animal Resources.

From the Department of Radiation Oncology, University of Rochester Medical Center, Rochester, New York, U.S.A.

Supported by National Institutes of Health grant CA52586 and DOD grant DAMD17-00-1-0420.

Address correspondence and reprint requests to Dr. Bruce M. Fenton, Box 704, University of Rochester Medical Center, Rochester, NY 14642, U.S.A.

Drug Treatments

COX-2 inhibitors were administered daily for 5 days at a dose of 50 mg/kg/d by oral gavage for celecoxib (Searle, Chicago, IL), or 7 days at a dose of 40 mg/kg/d by intraperitoneal injection for meloxicam (Calbiochem, San Diego, CA).

Injection of Perfusion Markers and EF5 Hypoxic Marker

Localized areas of tumor hypoxia were assessed in frozen tissue sections by immunohistochemical identification of sites of 2-nitroimidazole metabolism as described previously.[15] A pentafluorinated derivative (EF5) of etanidazole was injected intravenously 1 hour before tumor freezing (0.2 ml of 10 mmol/l EF5), a time at which EF5 has been shown to be well distributed throughout even poorly perfused regions of the tumor.[16] Protein conjugates of EF5 have been previously used to immunize mice from which ELK3-51 monoclonal antibodies were developed.[17] These antibodies are extremely specific for the EF5 drug adducts that form when the drug is incorporated by hypoxic cells. Regions of high EF5 metabolism were visualized immunochemically using a fluorochrome (Cy3, Amersham Pharmacia Biotech, Inc., Piscataway, NJ, U.S.A.) conjugated to the ELK3-51 antibody. To visualize blood vessels open to flow, an intravascular injected stain was used ($DiOC_7$) (Molecular Probes, Eugene, OR). This agent was injected in the tail vein 1 minute before tumor freezing at a concentration of 1.0 mg/kg (dissolved in 75% dimethyl sulfoxide in phosphate-buffered saline), and it has been shown to provide optimal visualization of tumor blood vessels by preferentially staining cells immediately adjacent to the vessels.[15,18]

Immunohistochemistry and Image Analysis

Immediately after cryostat sectioning, tumor slices were imaged for $DiOC_7$ perfusion staining using a Nikon microscope, digitized, background-corrected, and image-analyzed using Image-Pro software (Media Cybernetics, Silver Spring, MD) and a 800-MHz Pentium computer, as previously described in detail.[15] Color images from adjacent microscope fields were automatically acquired and digitally combined. Each section was scanned under each of three different staining conditions. First, epi-illumination images of the fluorescent green $DiOC_7$ staining were obtained immediately after the sections were sliced on the cryostat. After the immunohistochemical staining procedures were completed, the tumor section was returned to the microscope stage and rescanned and fluorescent red-orange images were obtained showing the distribution of the EF5/Cy3 hypoxic marker staining. Finally, matching brownish-red stained images of the CD31 endothelial staining were acquired. The CD31 (anatomical blood vessels) and $DiOC_7$ (perfused blood vessels) images were enhanced by first using the Image-Pro "color segmentation" to identify appropriate blood vessels.[15] Specific colors were interactively selected and accumulated to obtain optimal discrimination between vessels and stroma, and a binary image of the selected colors was created. To quantify vessel distributions, a rectangular matrix of sampling points was computer superimposed over the selected tumor montage, and the distances from each sampling point to the nearest total or perfused blood vessel were then determined.[19] Fluorescent image montages of the EF5/Cy3 staining were quantified using the Image-Pro "histogram" tool to count the number of image pixels of each red intensity.

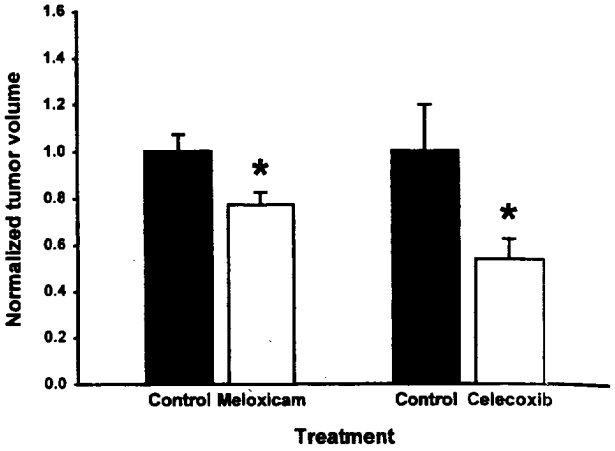

FIG. 1. Effects of either meloxicam (N = 6, 40 mg/kg for 7 days) or celecoxib (N = 10, 50 mg/kg for 5 days) on tumor volume (mean ± SEM). Tumor volumes are normalized to control volumes, which were approximately 400 mm^3 for the celecoxib controls and 800 mm^3 for the meloxicam controls. Tumor volumes were significantly reduced for both meloxicam ($p = 0.036$) and celecoxib ($p = 0.043$).

Statistical Analysis

Tumor means were compared using Student t test and were considered significant for $p < 0.05$.

RESULTS

Separate experiments were performed to quantitate the pathophysiologic effects of either celecoxib or meloxicam on MCa-35 carcinomas, but drug administration was initiated at somewhat larger tumor volumes for the meloxicam (200 mm^3 versus 100 mm^3 for celecoxib). Therefore, results in the following figures are normalized to corresponding untreated controls to reduce the effects of final tumor volume on comparisons between drugs. Figure 1 illustrates changes in normalized tumor volume after 5 or 7 days treatment. Both drugs resulted in significant decreases in tumor growth rate, with a somewhat more pronounced effect for the celecoxib (47% decrease, $p = 0.043$) than for the meloxicam (23% decrease, $p = 0.036$).

Quantitative image analysis results are summarized in Figure 2A for the total vessel staining and Figure 2B for the perfused vessels. Here, tumor blood vessels are characterized in terms of the median distance between tumor cells and the nearest blood vessel, which represents the median distance the oxygen or nutrients would need to diffuse to reach all points in the tumor (note that this quantity is inversely related to vascular density). Distances to the nearest blood vessel (Fig. 2A) were significantly increased for the meloxicam-treated tumors ($p = 0.015$), demonstrating a substantial reduction in total vessel densities in these tumors. In contrast, total blood vessel distances in celecoxib-treated tumors were unchanged. For perfused blood vessels, both drugs pro-

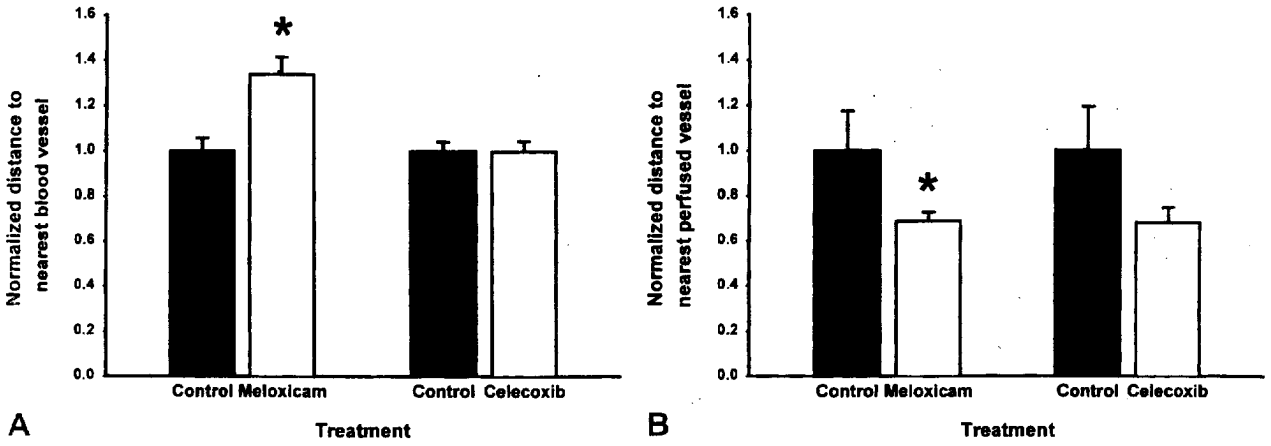

FIG. 2. A. Normalized distance to nearest total blood vessel (anti-CD31 staining) for meloxicam (N = 8, $p = 0.015$) and celecoxib (N = 7, $p = 0.90$) -treated tumors versus their respective controls (mean ± SEM). **B.** Normalized distance to nearest perfused blood vessel ($DiOC_7$ staining) for meloxicam ($p = 0.048$) and celecoxib ($p = 0.32$) -treated tumors versus controls.

duced substantial reductions in the mean distance, although for celecoxib the decrease was not statistically significant ($p = 0.048$ for meloxicam and $p = 0.32$ for celecoxib).

Figure 3 summarizes changes in tumor hypoxia, as determined by uptake of the hypoxic marker, EF5. In view of the substantial increase in numbers of perfused vessels after either celecoxib or meloxicam, tumor hypoxia would perhaps be expected to decrease after either treatment. Nonetheless, mean overall EF5/Cy3 intensities were unchanged after either drug in comparison with untreated controls (Fig. 3A). Intratumor heterogeneities in EF5 binding (as evaluated by the mean of the variance in EF5/Cy3 intensities within tumors) were markedly different between the two COX-2 inhibitors (Fig. 3B). Meloxicam tended to increase the variance, whereas celecoxib had the opposite effect, suggesting a much more uniform distribution of oxygenation in the celecoxib-treated tumors. Because of the marked intertumor heterogeneities, however, neither of these changes in variance was significant.

DISCUSSION

The primary objective of this study was to illustrate the utility of combining several recently developed immunohistochemical and computerized image analysis techniques to provide a quantitative characterization of tumor pathophysiologic changes after antian-

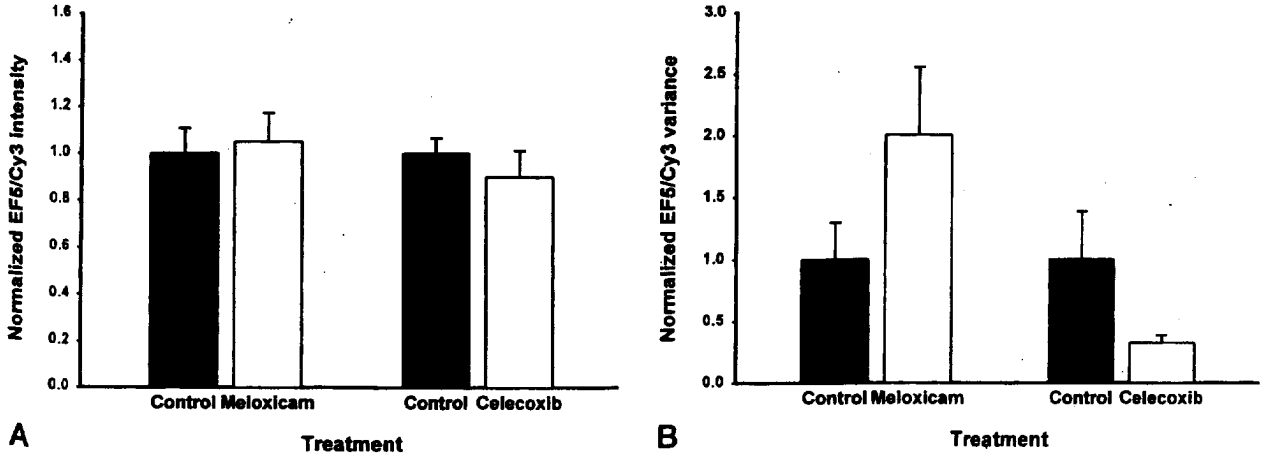

FIG. 3. A. Normalized EF5/Cy3 intensities for meloxicam (N = 8, $p = 0.42$) and celecoxib (N = 6, $p = 0.76$) -treated tumors versus their respective controls (mean ± SEM). **B.** Normalized EF5/Cy3 variance for meloxicam ($p = 0.20$) and celecoxib ($p = 0.23$) -treated tumors versus their respective controls.

giogenic therapy. Although a wide range of sophisticated immunohistochemical methods have been previously published, including markers for tumor cell and endothelial cell apoptosis, proliferation, total vascular density, and necrosis,[20] indices of functional vasculature and tumor oxygenation have rarely been included. These types of functional assays may be of particular relevance in predicting the consequences of combining antiangiogenic therapies with either radiation or chemotherapy.

As seen in the current preliminary results, total vascular spacing as determined by anti-CD31 staining was unaffected in tumors treated with celecoxib. However, vascular perfusion increased markedly in these tumors, with a corresponding reduction in intratumor heterogeneities in the distribution of hypoxic microregions. Even though the overall levels of hypoxic marker binding were unchanged after celecoxib treatment, the reduction in hypoxia heterogeneity, presumably brought about by a more uniform distribution of perfusion, would likely predict for a COX-2 mediated enhancement in radioresponse.

For the meloxicam-treated tumors, several key differences were noted. First, the striking decrease in total vasculature after meloxicam administration suggests a possible increase in the ratio of endothelial cell apoptosis to proliferation and indicates that meloxicam could possibly have more of an effect on newly sprouting, nonperfused, angiogenic blood vessels. The fact that increased numbers of vessels are perfused in the meloxicam-treated tumors hints that some slowdown in tumor cell proliferation may also be occurring, possibly producing an improvement in perfusion through a reduction in tumor cell pressure on the blood vessels. Despite the improvements in perfusion, pronounced heterogeneities in the distribution of hypoxia persist in the meloxicam-treated tumors, which could also be related to the fact that these tumors are larger than the corresponding celecoxib-treated tumors. Again, these could be indicative of substantial differences in absolute flow rates among perfused blood vessels. Clearly, additional studies are required to fully understand the complex pathophysiologic and molecular relationships.

In the clinic, measurements of the pathophysiologic responses to these Cox-2 inhibitors could provide valuable information regarding changes in tumor oxygenation after antiangiogenic therapies. Such determinations could also be useful in identifying which Cox-2 inhibitors are most efficacious for potentiating radioresponse in individual tumors. For instance, when combining such approaches with radiotherapy, the primary goal is to deliver the antiangiogenic agents in such a way that tumor hypoxia is reduced at the time of irradiation. In predicting radioresponse, quantification of EF5/Cy3 intensity distributions appears the most promising. Phase I clinical trials on this marker have recently been initiated[21] and have documented patterns of EF5 binding consistent with diffusion-limited hypoxia in human sarcomas.[22]

Three approaches are possible in the clinic: 1) pretreatment needle biopsies could be used to determine microregional heterogeneities in hypoxia distributions, both to predict response to radiotherapy and to design appropriate drug/dose schedules with concurrent radiation; 2) needle biopsies could be obtained before and after antiangiogenic treatment to quantify changes in tumor hypoxia after various agents; and 3) tumor biopsies could be obtained after surgery to compare hypoxia in treated versus untreated tumors. In this way, different Cox-2 inhibitors could be quantitatively ranked in terms of their abilities to enhance conventional therapies. Through such direct monitoring of both structural and functional indices of tumor pathophysiology, a more rational basis could be provided for optimization of drug choice, dose schedule, and timepoints for combinations of antiangiogenic agents and either radiation or chemotherapy.

REFERENCES

1. Hagedorn M, Bikfalvi A. Target molecules for anti-angiogenic therapy: from basic research to clinical trials [Review]. *Crit Rev Oncol Hematol* 2000;34:89–110.
2. Hanna NN, Seetharam S, Mauceri HJ, et al. Autitumor interaction of short-course endostatin and ionizing radiation. *Cancer J* 2000; 6:287–93.
3. Kishi K, Petersen S, Petersen C, et al. Preferential enhancement of tumor radioresponse by a cyclooxygenase-2 inhibitor. *Cancer Res* 2000;60:1326–31.
4. Gorski DH, Beckett MA, Jaskowiak NT, et al. Blockade of vascular endothelial growth factor stress response increases the antitumor effects of ionizing radiation. *Cancer Res* 1999;59:3374–8.
5. Joki T, Heese O, Nikas DC, et al. Expression of cyclooxygenase 2 (COX-2) in human glioma and in vitro inhibition by a specific COX-2 inhibitor, NS-398. *Cancer Res* 2000;60:4926–31.
6. Chan G, Boyle JO, Yang EK, et al. Cyclooxygenase-2 expression is up-regulated in squamous cell carcinoma of the head and neck. *Cancer Res* 1999;59:991–4.
7. Tsujii M, Kawano S, Tsuji W, et al. Cyclooxygenase regulates angiogenesis induced by colon cancer cells. *Cell* 1998;93:705–16.
8. Murata H, Kawano S, Tsuji S, et al. Cyclooxygenase-2 overexpression enhances lymphatic invasion and metastasis in human gastric carcinoma. *Am J Gastroenterol* 1999;94:451–5.
9. Tsujii M, Kawano S, DuBois RN. Cyclooxygenase-2 expression in human colon cancer cells increases metastatic potential. *Proc Natl Acad Sci USA* 1997;94:3336–40.
10. Liu XH, Kirschenbaum A, Yao S, et al. Inhibition of cyclooxygenase-2 suppresses angiogenesis and the growth of prostate cancer in vivo. *J Urol* 2000;164:820–5.
11. Masferrer JL, Leahy KM, Koki AT, et al. Antiangiogenic and antitumor activities of cyclooxygenase-2 inhibitors. *Cancer Res* 2000;60:1306–11.
12. Gupta RA, DuBois RN. Translational studies on Cox-2 inhibitors in the prevention and treatment of colon cancer. *Ann NY Acad Sci* 2000;910:196–204.
13. Hussey JJ, Tisdale MJ. Effect of the specific cyclooxygenase-2 inhibitor meloxicam on tumour growth and cachexia in a murine model. *Int J Cancer* 2000;87:95–100.
14. Masferrer JL, Isakson PC, Seibert K. Cyclooxygenase-2 inhibitors: a new class of anti-inflammatory agents that spare the gastrointestinal tract. *Gastroenterol Clin North Am* 1996;25:363–72.

15. Fenton BM, Paoni SF, Lee J, et al. Quantification of tumor vascular development and hypoxia by immunohistochemical staining and HbO_2 saturation measurements. *Br J Cancer* 1999;79: 464–71.
16. Fenton BM, Lord EM, Paoni SF. Effects of radiation on tumor intravascular oxygenation, vascular configuration, hypoxic development, and survival. *Radiat Res* 2001;155:360–8.
17. Lord EM, Harwell L, Koch CJ. Detection of hypoxic cells by monoclonal antibody recognizing 2-nitroimidazole adducts. *Cancer Res* 1993;53:5721–6.
18. Trotter MJ, Chaplin DJ, Olive PL. Use of a carbocyanine dye as a marker of functional vasculature in murine tumours. *Br J Cancer* 1989;59:706–9.
19. Fenton BM, Way BW. Vascular morphometry of KHT and RIF-1 murine sarcomas. *Radiother Oncol* 1993;28:57–62.
20. Bruns CJ, Liu W, Davis DW, et al. Vascular endothelial growth factor is an in vivo survival factor for tumor endothelium in a murine model of colorectal carcinoma liver metastases. *Cancer* 2000;89:488–99.
21. Evans SM, Hahn S, Pook DR, et al. Detection of hypoxia in human squamous cell carcinoma by EF5 binding. *Cancer Res* 2000;60: 2018–24.
22. Evans SM, Hahn SM, Magarelli DP, et al. Hypoxia in human intraperitoneal and extremity sarcomas. *Int J Radiat Oncol Biol Phys* 2001;49:587–96.

[CANCER RESEARCH Vol. 61, 526–531, January 15, 2001]

Intratumoral Administration of Endostatin Plasmid Inhibits Vascular Growth and Perfusion in MCa-4 Murine Mammary Carcinomas[1]

Ivan Ding, Jian Zhong Sun, Bruce Fenton, Wei Min Liu, Paul Kimsely, Paul Okunieff, and Wang Min[2]

Departments of Radiation Oncology [I. D., J. Z. S., B. F., W. M. L., P. O.], Pediatrics [P. K.], and Medicine [W. M.], University of Rochester School of Medicine, Rochester, New York 14642

ABSTRACT

Endostatin, a fragment of the COOH-terminal domain of mouse collagen XVIII is a recently demonstrated endogenous inhibitor of tumor angiogenesis and endothelial cell growth. Antiangiogenic therapy with endostatin in animals requires multiple and prolonged administration of the protein. Gene therapy could provide an alternative approach to continuous local delivery of this antiangiogenic factor *in vivo*. Established MCa-4 murine mammary carcinomas, grown in immunodeficient mice, were treated with intratumoral injection of endostatin plasmid at 7-day intervals. At the time of sacrifice, 14 days after the first injection, endostatin-treated tumor weights were 51% of controls ($P < 0.01$). Tumor growth inhibition was accompanied by a marked reduction in total vascular density. Specifically, computerized image analysis showed a 18–21% increase in the median distances between tumor cells and both the nearest anatomical (CD31-stained) vessel [48.1 ± 3.8 *versus* 38.3 ± 1.6 μm ($P < 0.05$)] and the nearest tumor-specific (CD105-stained) vessel [48.5 ± 1.5 *versus* 39.8 ± 1.5 μm ($P < 0.01$)]. An increased apoptotic index of tumor cells in endostatin-treated tumors [3.2 ± 0.5% *versus* 1.9 ± 0.3% ($P < 0.05$)] was observed in conjunction with a significant decrease in tumor perfused vessels ($DiOC_7$ staining), and an increase in tumor cell hypoxia (EF5 staining). Hypoxia resulting from endostatin therapy most likely caused a compensatory increase of *in situ* vascular endothelial growth factor (VEGF) and VEGF receptor mRNA expression. Increased immunoreactivity of endostatin staining in endostatin-treated tumors was also associated with an increased thrombospondin-1 staining [1.12 ± 0.16 *versus* 2.44 ± 0.35]. Our data suggest that intratumoral delivery of the endostatin gene efficiently suppresses murine mammary carcinoma growth and support the potential utility of the endostatin gene for cancer therapy.

INTRODUCTION

Angiogenesis, the formation of new blood vessels, is essential for both critical physiological processes (wound healing) and lethal pathological conditions (tumor growth and atherosclerosis; Refs. 1–3). Numerous studies have shown that tumor growth is dependent on angiogenesis (4–7), thus providing a rationale for antiangiogenic therapy. Endostatin is one of the most potent endogenous angiogenesis inhibitors discovered to date. Interestingly, it inhibits pathologic vascular growth while allowing for normal processes. For example, both tumor growth (8) and atherosclerosis (9, 10) are inhibited in experimental animal models, whereas wound healing is unaffected. M_r 20,000 endostatin is a proteolytic polypeptide derived from its parent protein (collagen XVIII; Refs. 8, 11, 12). *In vitro* studies have shown that endostatin specifically inhibits endothelial proliferation without a direct effect on tumor or other nonneoplastic cell growth (12–15). Whether administrated as recombinant protein (14, 16), plasmid injection (17–19), or gene transfection (20), endostatin inhibits tumor growth, with reduction of virtually all tumor neovascularization and without detectable systemic toxicity in preclinical models.

To be effective, antiangiogenic therapy with endostatin in tumor-bearing mice requires prolonged administration and high doses of recombinant protein (8, 14). In addition, production of the functional polypeptide has proven difficult, perhaps because of its physical properties and because of variations in the purification procedures utilized by different laboratories (15, 21). However, some preliminary data have shown that local or systemic administration of endostatin is an effective means of application in cancer therapy. A few groups have demonstrated that antiangiogenic gene therapy with viral vectors is a potentially useful approach for inhibiting tumor growth in mouse models (22–23). Although viral vectors have high transfection efficiency and are commonly used in experimental systems, safety issues and the toxicity of these viral vectors likely precludes their use as an i.v. agent. In contrast, we and others have shown that systematically delivered endostatin plasmid possesses low toxicity and high effective antitumor action (17–19). In the current study, we investigated whether intratumoral injection of endostatin plasmid once a week for 2 weeks inhibited mammary tumor growth. We also explored the underlying physiological and molecular mechanisms of endostatin-mediated antitumoral effects.

MATERIALS AND METHODS

Endostatin Plasmid. A plasmid containing an expression cassette for mouse endostatin was constructed as described previously (18). The coding sequence of endostatin comprises the COOH-terminal 184 ammo acid residues of collagen XVIII. This sequence was directly amplified by PCR from liver cDNA. Plasmids were grown under kanamycin selection in host strain DH5α and purified by alkaline lysis and chromatographic methods using Endofree kit (Qiagen, Valencia, CA). Purified plasmid had the following specifications: <50 Eu/mg endotoxin; <1% protein: and <5% (wt/wt) chromosomal DNA.

Murine Mammary Tumor Models and Treatment. Isotransplants of the murine mammary carcinoma MCa-4 were used. Frozen MCa-4 tumor cells were inoculated i.m. into the hind limbs of 6–8-week-old female BALB/c (nu/nu) mice (National Cancer Institute, NIH, Frederick, MD). Tumors were selected for endostatin plasmid treatment when they reached volumes of between 150 and 250 mm^3 (as measured by calipers and the formula: Volume = $Diameter^3/6$). Endotoxin-free endostatin plasmid (45 μg) was injected once a week for 2 weeks into the tumor in the right thigh. All of the tumors (right and left) were averaged. Equal volumes of saline and vector were injected as controls in separate mice. Mice were sacrificed 7 days after the second injection. Tumors were removed, examined, and frozen for later immunohistochemistry or RNA isolation. Guidelines for the humane treatment of animals were followed as approved by the University Committee on Animal Resources.

Measurement of Anatomical (CD31), Perfused ($DiOC_7$), and Angiogenic (CD105) Blood Vessels. Immunohistochemistry methods have previously been described in detail (24). To visualize blood vessels open to flow, an i.v. injected stain, $DiOC_7$ (Molecular Probes, Engene, OR), was utilized. Injections were administered i.v. at a concentration of 1.0 mg/kg, 1 min prior to freezing. This dose and schedule has been shown to provide optimal visualization of tumor vasculature by preferentially staining cells immediately adjacent to blood vessels. $DiOC_7$-stained vessels emit green fluorescence when excited by blue light. CD31 antibody staining (PharMingen, San Diego, CA) was used for visualizing total structural vessels. In addition, an anti-CD105

Received 4/3/00; accepted 11/8/00.

The costs of publication of this article were defrayed in part by the payment of page charges. This article must therefore be hereby marked *advertisement* in accordance with 18 U.S.C. Section 1734 solely to indicate this fact.

[1] Supported by NIH Grants CA11051-25A2 (to P. O., J. Z. S., W. M. L., and I. D.), CA52586 (to B. F.), and University of Rochester starting fund (to W. M.).

[2] To whom requests for reprints should be addressed, at Center for Cardiovascular Research, Department of Medicine, Box 679, University of Rochester, Rochester, NY 14642. Phone: (716) 273-1499; Fax: (716) 275-9895; E-mail: Wang_min@urmc.rochester.edu.

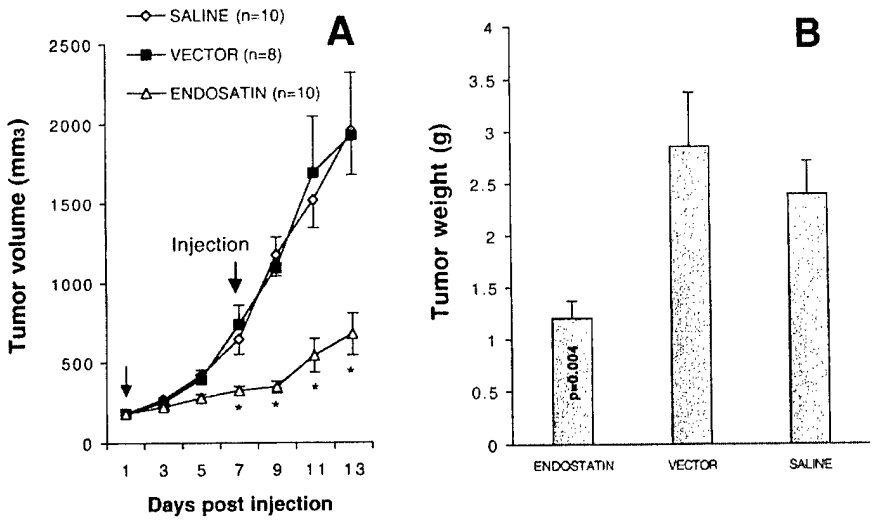

Fig. 1. Injection of endostatin inhibited MCa-4 tumor growth. *A*, saline-, vector-, and endostatin-treated tumors were measured, and volumes were calculated as mean ± SE. Significant differences were found between controls and endostatin-treated tumors 7 days after treatment. *B*, all of the mice were killed 14 days after the first endostatin treatment. Tumor weight (mean ± SE) is shown.

antibody (PharMingen) that was recently reported to specifically identify vascular neogenesis was also utilized. CD105 is strongly expressed in activated endothelial cells of various human tumors, including breast cancer, but is either undetectable or only weakly present in mature blood vessels of normal tissues (25–26).

EF5/Cy3 Hypoxia Marker. Localized areas of tumor hypoxia were assessed in frozen tissue sections by immunohistochemical identification of sites of 2-nitroimidazole metabolism. A pentafluorinated derivative of etanidazole (EF5) was injected i.v. 1 h before tumor freezing. Protein conjugates of EF5 have been previously used to immunize mice from which monoclonal antibodies were developed (27). These antibodies are extremely specific for the EF5 drug adducts that form when the drug is incorporated by hypoxic cells, and one of these, ELK3-51, has been well characterized. Regions of high EF5 metabolism in tumors (hypoxic regions) were visualized and the area of staining quantified immunochemically using a fluorochrome (Cy3) conjugated to the ELK3-51 antibody and computerized imaging techniques.

Imaging and Image Analysis. For each frozen tumor, 4.0-μm sections were cut using a cryostat. The stained sections were imaged using an epi-fluorescence-equipped microscope, digitized (3-CCD camera), background-corrected, and image-analyzed using Image Pro software (Media Cybernetics) and a 450-MHz Pentium computer. Color images from adjacent microscope fields were automatically acquired and digitally combined to form 4 × 4 montages of the tumor cross-section (using a motorized stage and controller). For each section, two peripheral and two interior image montages were obtained. Each section was then scanned under each of three staining conditions. First, epi-illumination images of the fluorescent green $DiOC_7$ staining (perfused vessels) were obtained immediately after the 4.0-μm sections were sliced on the cryostat. After the immunohistochemical staining procedures were completed, the same tumor section used for the $DiOC_7$ imaging was returned to the microscope stage and automatically rescanned using the same coordinates as for the initial 4 × 4 montages. Using transmitted light, matching montages of the CD31 (anatomical vessels) and CD105 (angiogenic vessels) were obtained. Briefly, the image montages were processed to enhance the contrast between background and either CD31 staining or $DiOC_7$ staining. The quantitative vascular information was analyzed using custom FORTRAN programs to perform a "closest individual" analysis. Briefly, the distances from computer-superimposed sampling points to the nearest blood vessel were determined. The cumulative frequency distribution of these distances provides the probability of encountering vessels within any specified distance from the tumor cells. Median distances to the nearest anatomical or perfused blood vessel were used for statistical comparisons.

RNase Protection Assay. Tumor tissue RNA from each treatment group (n = 4–6 mice) was isolated by pulverizing the frozen tissue and dissolving it in TRIzol reagent (MRC, Cincinnati, OH). RNAse protection was performed using established multiprobe template sets (PharMingen) as described previously (27). The apoptosis set includes: antiapoptotic genes: *Bcl-2, bcl-X, bcl-W*, and *bfl-1*; and apoptotic genes: *Bax, Bak*, and *Bad*. Two internal controls, L32 and GAPDH,[3] were used to monitor RNA loading. The quantitation of mRNA expression level tested for each sample was measured using a Cyclone PhosphorImager (HP Company, Meriden, CT). Relative mRNA expression levels were ratios of targeted gene divided by *L32* or *GAPDH* genes.

Western Blot Analysis. Cell lysates were prepared from frozen tumor tissues (n = 2) and separated by SDS-PAGE on 12% (w/v) polyacrylamide gels and electrotransferred onto Millipore polyvinylidene difluoride membranes in 25 mM Tris, 192 mM glycine. Membranes were blocked in Tris-buffered saline (20 mM Tris-HCl, 137 mM NaCl) containing 0.05% Tween 20 and 5% nonfat dry milk for 60 min at room temperature. The blots were then incubated overnight at 4°C in blocking solution with the 1:1000 goat-antimurine endostatin antibody (R&D Systems, Minneapolis, MN). Thereafter, membranes were washed in Tris-buffered saline and incubated with horseradish peroxidase-conjugated antigoat IgG (1:3000) in blocking solution for 1 h. The blots were visualized by chemiluminescence using the Pierce ECL system (Pierce, Rockford, Illinois).

***In Situ* Hybridization.** For *in situ* localization of VEGF and it receptor gene expression in tumor tissue, we followed procedures previously published from our laboratory (28). Briefly, tumor tissue was fixed in 10% formalin or 2% paraformaldehyde, and cross-sections were then cut. Sections of tissue were placed on specially prepared slides (acid-washed and T3-aminopropyl triethoxysilane-coated), then deparaffinized, rehydrated, proteinase K-digested, and hybridized with VEGF and VEGFR riboprobes labeled with [^{33}P]UTP. After washing, sections were prepared for autoradiography using NBTII emulsion. After autoradiography and staining, slides were analyzed by bright- and dark-field microscopy. Backgrounds for these studies were determined by using the sense stand RNA probe. As a positive control for hybridization, some sections were hybridized for a constitutively expressed mRNA, such as GAPDH, analyzed for cell-specific expression of the molecule of interest. The location of overexpression was identified histologically.

RESULTS

The effects of intratumoral injection of endostatin plasmid (45 μg/mouse/two injections) on MCa-4 tumor growth are shown in Fig. 1. There was a substantial tumor growth delay in endostatin-treated tumors compared with saline- or vector-treated controls (Fig. 1*A*). Tumor growth inhibition was only slightly greater in the right (directly treated) compared with the left thigh tumors, and because the differences did not achieve statistical significance, the data were

[3] The abbreviations used are: VEGF, vascular endothelial growth factor; VEGFR, VEGF receptor; GAPDH, glyceraldehyde-3-phosphate dehydrogenase.

Table 1 *MCa-4 tumor-bearing nude mice treated with endostatin plasmid injections*

Injection of endostatin inhibited anatomic and angiogenic vessels and induced tumor apoptosis in MCa-4 tumors. Tumor proliferation and necrosis index were not significantly altered.

	Median distance to tumor vessels		Tumor Cells		
	CD31 (μm)	CD105 (μm)	% of apoptosis	% of mitosis	% of necrosis
Saline	38.29 ± 1.56	39.75 ± 1.45	1.90 ± 0.32	3.60 ± 0.62	14.87 ± 2.90
Vector	41.47 ± 1.13	44.26 ± 1.57	2.02 ± 0.32	4.35 ± 0.41	11.31 ± 0.79
Endostatin	48.10 ± 3.76[a]	48.51 ± 1.48[b]	3.22 ± 0.45[a]	3.56 ± 0.22	8.62 ± 1.84

[a] $P < 0.05$.
[b] $P < 0.01$.

combined. This is consistent with our previous observation that endostatin expressed in local tissues can release into the circulation and elicit systemic inhibition of tumor growth and metastasis (18, 19). Inhibition of tumor growth was statistically significant beginning 7 days after injection of endostatin plasmid ($P < 0.05$). All of the mice were killed 14 days after the first endostatin treatment. There was a significant reduction of tumor weight in endostatin-treated animals compared with controls (Fig. 1*B*). Repeating the first experiment with the same number of mice and treatment schedules again demonstrated significant reduction in MCa-4 tumor growth. As in the original experiment, the treated tumors (right leg) had slightly greater growth inhibition than the opposite leg (left) tumors.

To examine the effect of endostatin on vascular growth, anatomical vessels (CD31 staining) and angiogenic vessels (CD105 staining) in the tumors were measured and quantified "Materials and Methods"). As shown in Table 1, endostatin-treated tumors had a significant reduction in total anatomical vessels and angiogenic vessels. Tumor proliferation and necrosis index were not significantly altered. In contrast, decreased blood vessel density was associated with a significant increase in tumor cell apoptosis. The increase in apoptotic index was 1.7-fold [3.2 ± 0.45 *versus* 1.9 ± 0.3 for saline ($P < 0.05$); 2.0 ± 0.3 for vector-treated). An RNase protection assay also showed that endostatin-treated tumors had a significant (28%) reduction in *bfl-1* mRNA, as well as 21–26% decrease of *bak* and *bad* mRNA gene expression compared with controls ($P < 0.05$) as shown in Fig. 2. No other differential mRNA expression was observed in the other apoptotic gene (*bax*), or antiapoptotic genes (*bcl-2, bcl-2*, and *bcl-X*) between endostatin-treated and control animals.

The effects of endostatin on tumor functional vessels and oxygenation were evaluated using $DiOC_7$ and EF5 staining 14 days after the first endostatin treatment. As shown in Fig. 3, endostatin-treated tumors had a 13% increase in median distance to the nearest perfused vessel compared with saline controls ($P = 0.053$). In the same experiment, we also observed that endostatin-treated tumors showed a significant reduction in CD31- and CD105-stained vessels ($P < 0.01$). Vector-treated tumors also had decreased numbers of perfused vessels compared with saline controls, most likely because of the larger sizes of the tumors (3.4 ± 0.8 g for vector *versus* 2.5 ± 0.5 g for saline) in this treatment group (Fig. 1*B*). Unpublished studies have shown an inverse relationship between perfusion and tumor volumes in numerous tumor models.[4]

The most extensive hypoxia marker uptake, however, was observed in endostatin-treated tumors, despite their smaller tumor size (Fig. 3). The reduction in number of perfused vessels and the increase in tumor hypoxia were associated with an elevation of local tumor VEGF and VEGFR mRNA expression, as detected by *in situ* hybridization (Fig. 4).

Endostatin-treated tumors also showed increased levels of thrombospondin-1 protein by immunohistochemistry (Fig. 5). Both thrombospondin-1 (Fig. 5*B*) and endostatin protein (Fig. 5*A*) were detected in cellular ($a-c$) or stromal ($a'-c'$) compartment.

DISCUSSION

In the present study, we have shown that intratumoral injection of endostatin plasmid once a week for 2 weeks inhibits murine mammary MCa-4 tumor growth in nude mice. The reduction of tumor growth rate is associated with decreased numbers of tumor anatomical vessels, angiogenic vessels, and perfused vessels. Endostatin-treated tumors also have an increased tumor cell apoptotic index and increased tumor cell hypoxia, which are most likely associated with secondary induction of tumor cell VEGF and VEGFR mRNA expression as well as with elevation of local thrombospondin-1 protein expression.

Application of antiangiogenic growth factors for gene therapy has been recently used in several tumor models (17, 18). We initially reported the systemic inhibition of tumor growth and metastasis by i.m. administration of the endostatin gene formulated with synthetic polymer in murine Renca and Lewis lung carcinomas, and tumor volume was 40% of control at 13-day posttreatment (18). More recently, we reported that i.v. injection of a mixture of liposome with endostatin plasmid inhibited tumor growth and metastases (19). A similar study has been reported by Chen *et al.* in human mammary MDA-MB435 xenograft (17). Preclinical gene therapy models, therefore, suggest that this approach to antiangiogenic growth factor therapy will be efficacious. In contrast, achieving tumor regression with recombinant protein has been difficult and requires frequent high-dose injections in animal tumors. Our results and those of others have demonstrated that local or systemic administration of nonviral endostatin plasmid significantly inhibits the growth of several tumor types, including lung, breast, kidney, and sarcoma tumors (17–19). Response, however, is limited to the slowing of tumor growth without complete regression for established tumors. The efficacy may be dependent on tumor type, vector type, and plasmid administration route and dose, as well as the formulation of agents.

Regression of transplanted tumors is a more difficult undertaking than preventing tumor formation when using any cytotoxic or antiangiogenic therapy. Using a transgenic mouse model of a spontaneous pancreatic β-islet cell tumor, Bergers *et al.* (29) recently reported that recombinant endostatin effectively prevented the promotion from

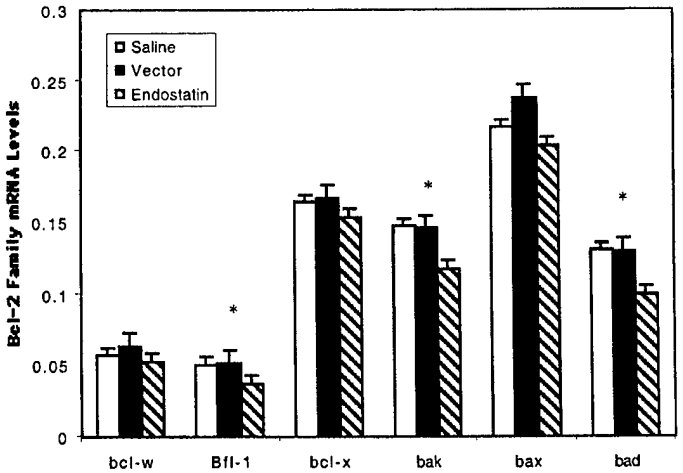

Fig. 2. Injection of endostatin regulated mRNA expression of Bcl-2 family genes in MCa-4 tumor. Saline-, vector-, and endostatin-treated tumors were collected 14 days after treatment, and 30 μg total RNA were used for RNase protection assay. Relative mRNA expression levels were presented as ratio of targeted gene divided by loading control *L32* or *GAPDH* genes (mean ± SD; $n = 5$ mice).

[4] Unpublished observations.

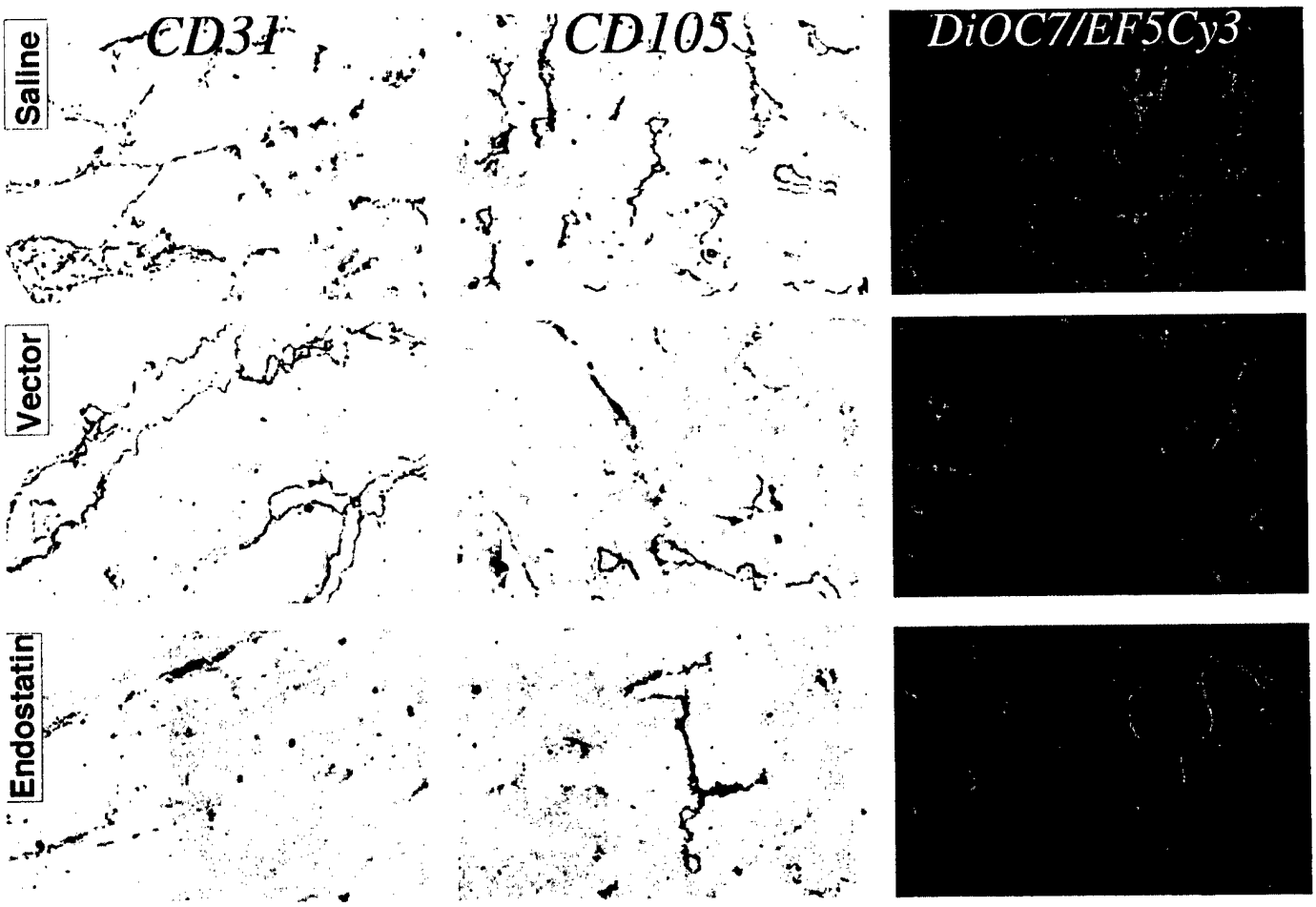

Fig. 3. Injection of endostatin inhibits anatomic, angiogenic, and perfused vessels in MCa-4 tumor. Saline-, vector-, and endostatin-treated tumors were collected 14 days after treatment. Anatomic, angiogenic, and perfused vessels were visualized by CD31, CD105, and $DiOC_7$ staining. Endostatin-treated tumors had a significantly reduced vessel density among all of the three vessel types. Endostatin-treated tumors also showed an increase in EF5 hypoxia marker uptake (*orange staining*).

hyperplastic lesion to small tumor formation but poorly inhibited established tumor growth (progression stage). In our transplantable MCa-4 tumor and others, endostatin succeeded in slowing tumor growth in established tumors as described previously (17–20). The antitumoral action of endostatin should, therefore, be further investigated at different stages of carcinogenesis. Ultimately, we may find that the greatest utility for endostatin is in preventing metastases rather than in inhibiting established tumors (18–19).

Endostatin is believed to specifically inhibit endothelial cell proliferation rather than tumor cell growth (12–15). The underlying molecular mechanisms of antiangiogenesis are presumably related to an increase in endothelial cell apoptosis (13), or an alteration of cell cycle (21). In our animal model, the effects of endostatin-mediated antiangiogenesis are consistent with previous studies. In addition, we quantitatively demonstrated that endostatin-treated tumors showed a clear decrease in perfused vessel density and an increase in tumor cell hypoxia, and that the effects were long lasting, with physiological effects still manifesting 14 days after initial treatment. Direct inhibi-

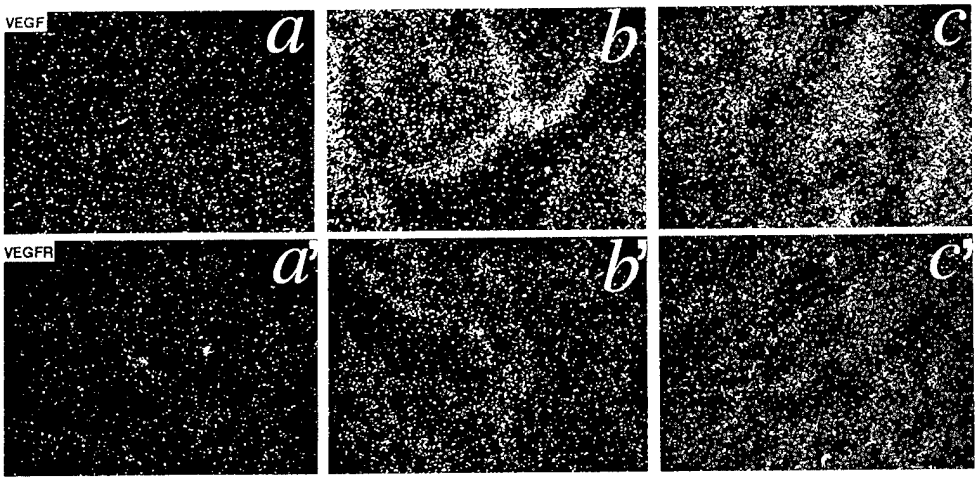

Fig. 4. Overexpression of VEGF and VEGFR mRNA in endostatin-treated tumors by *in situ* hybridization in MCa-4 tumors. Saline-, vector-, and endostatin-treated tumors were collected 14 days after treatment, and ^{33}P-labeled antisense riboprobe for VEGF (a–c) or VEGFR (a'–c') was hybridized. Radiographs are shown in dark field. Endostatin-treated tumors (c and c') had elevated VEGF and VEGFR mRNA expression compared with that of untreated tumors (a and a'). Vector-treated tumor (b and b') also showed increased VEGF and VEGFR expression, which was probably attributable to the fact that vector-treated tumors were larger in size than untreated tumors.

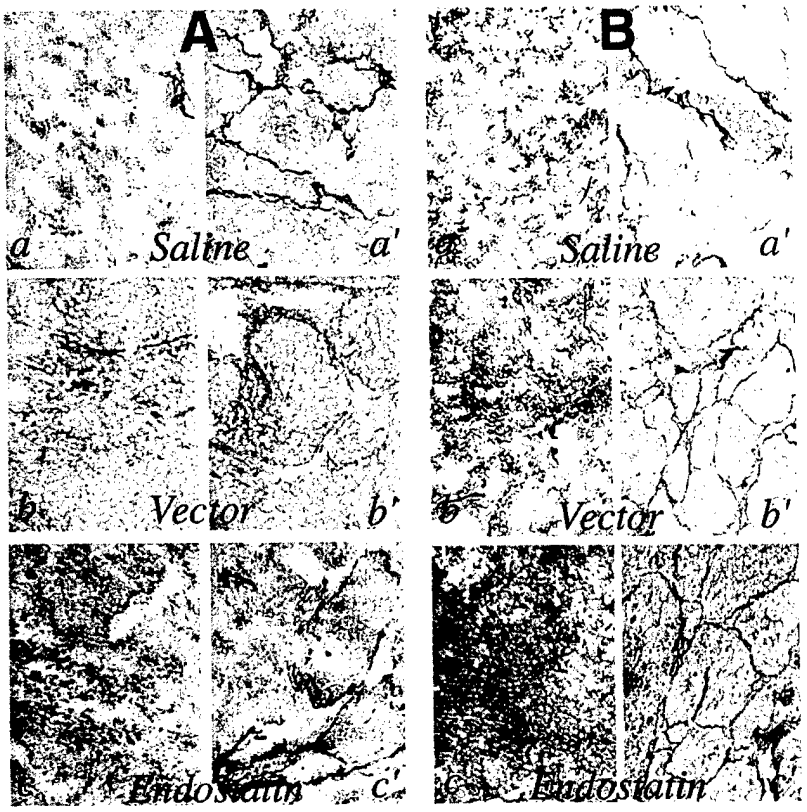

Fig. 5. Expression of thrombospondin-1 protein in endostatin-treated tumors by immunohistochemistry in MCa-4 tumors. Saline-, vector-, and endostatin-treated tumors were collected 14 days after initial treatment and antiendostatin antibody (*A*) or antithrombospondin-1 antibody (*B*) was hybridized with these sections. (*a–c*), cellular staining pattern; (*a'–c'*), stromal staining pattern. Endostatin-treated tumors showed the transgene expression and had elevated thrombospondin-1 protein expression.

tion of tumor structural vessels, angiogenic vessels, and perfused vessels can explain the observed endostatin-mediated antitumoral effects. Although we believe that the tumor cell apoptosis was secondary to ischemia, our observation leaves open the possibility that endostatin has direct apoptotic effects on tumor tissue. Likewise, tumor necrosis and apoptosis may have been attributable to ischemia, reperfusion injury, or some as-yet-unexplained indirect endostatin-induced cytotoxicity.

We favor a direct effect of endostatin on tumor vascularity, resulting indirectly in tumor growth reduction. Consistent with this hypothesis, endostatin-treated MCa-4 tumors had a similar proliferative rate to that of controls as measured by mitotic figures (Table 1), which suggests that the tumor cell cycle was not altered by endostatin. Reduced vascularity, however, can deprive tumors of their nutrient supply, and, thus, proliferation can result in environmentally deprived progeny, leading to apoptosis or necrosis after division. Kirsch *et al.* (30) showed that recombinant angiostatin-treated gliomas caused both neoplastic and endothelial cell apoptosis. They concluded that endothelial cell apoptosis results from vessel thrombosis or regression of pre-existing vessels. In our study, we counted only the tumor cell apoptotic numbers, because very few endothelial cells displayed an apoptotic appearance on the basis of morphology. Thus, we cannot confirm (or refute) the observation of Kirsch *et al.* (30). Regarding molecules important in promoting or inhibiting apoptosis, there were mixed responses. The antiapoptotic gene *bfl-1* decreased, but so did the apoptotic genes *bad* and *bak*. Ischemia and reperfusion injury, therefore, appear more important in generating the necrosis and apoptosis than any hypothetical direct endostatin-mediated apoptosis. It is possible, however, that endothelial cells from different tumor types may respond differently to endostatin (20).

Endostatin may exert biological effects directly or indirectly by altering expression of other growth-related molecules. One possible mechanism is a down-regulation of angiogenic molecules by endostatin. Because multiple cell types, such as tumor cells, endothelial cells, activated macrophages, and tumor fibroblasts, in tumors produce angiogenic and antiangiogenic growth factors, and because many angiogenic growth factors can also be mobilized from the extracellular matrix, endostatin-mediated regulation of angiogenic growth factor gene expression is extremely complex and difficult to assess. Kirsch *et al.* (30) treated three types of malignant gliomas and found a significant reduction of VEGF mRNA by Northern analysis, but an elevation of FGF2 3 weeks after angiostatin treatment. They hypothesized that angiostatin-mediated antiangiogenesis in gliomas may be secondary to down-regulation of certain angiogenic growth factors or to up-regulation of antiangiogenic factors. We found an up-regulation of VEGF and VEGFR mRNA as well as up-regulation of thrombospondin-1 protein expression in endostatin-treated MCa-4 breast tumors. In contrast to Kirsch *et al.* (30), our results demonstrated that VEGF and VEGFR were up-regulated rather than down-regulated. These differences could suggest that: (*a*) the balance of angiogenic and antiangiogenic growth factors as well as their gene regulation may be time-dependent during endostatin treatment. Sampling at different times after endostatin treatment may result in differential gene expression; (*b*) expression of angiogenic or antiangiogenic growth factors may be tumor size- or tumor histologic type-dependent; (*c*) endostatin may exert its effects through different mechanisms in different tumors, animal strains, or species; and (*d*) expression of angiogenic/antiangiogenic factors may be responding to independent stimuli. We believe that tumor hypoxia induced the VEGF and VEGFR mRNA expression, and the up-regulation of thrombospondin-1 may be triggered by endostatin through specific signaling pathways.

In summary, endostatin inhibits tumor growth by reducing structural, angiogenic, and perfused tumor vessels. A lack of adequate blood supply leads to tumor hypoxia and probably accounts for tumor cell apoptosis and the up-regulation of VEGF and VEGFR. Thrombospondin-1 also increased, which suggests that endostatin may regulate this antiangiogenic peptide. However, the molecular mecha-

nisms for endostatin-mediated antiangiogenesis are still unknown at present. Different mechanisms may exist for *in vitro* and *in vivo* models. *In vitro*, several issues need to be addressed: (*a*) is there a receptor or endostatin-related cell surface molecule on endothelial cells? and (*b*) if so, what are the signal transduction pathway and target genes? If not, how does it inhibit angiogenesis and is it via stromal effects? In animal models, we also need to consider: (*a*) does endostatin act on tumor cells through direct or indirect pathways? (*b*) if by indirect pathways, is it by regulation of other angiogenic or antiangiogenic factors in endothelial, inflammatory, or tumor cells? and (*c*) can endostatin induce tumor regression rather than just slow growth, and under what circumstances? These mechanistic questions are now under investigation in our laboratory.

REFERENCES

1. Bout, J. C., Soncin, F., and Vandenbunder, B. Therapeutic prospects of angiogenesis inhibitors in cancerology (in French). Rev. Mal. Respir., *16:* 854–855, 1999.
2. Keshet, E. and Ben-Sasson, S. A. Anticancer drug targets: approaching angiogenesis. J. Clin. Investig., *104:* 1497–1501, 1999.
3. Cao, Y. Therapeutic potentials of angiostatin in the treatment of cancer. Haematologica, *84:* 643–650, 1999.
4. Folkman, J. Angiogenesis in cancer, vascular, rheumatoid and other disease. Nat. Med., *1:* 27–31, 1995.
5. Folkman, J. Angiogenesis inhibitors generated by tumors. Mol. Med. *1:* 120–122, 1995.
6. Hahnfeldt, P., Panigraphy, D., Folkman, J., and Hlatky, L. Tumor development under angiogenic signaling: a dynamical theory of tumor growth, treatment response, and postvascular dormancy. Cancer Res., *59:* 4770–4775, 1999.
7. Le Querrec, A., Duval, D., and Tobelem, G. Tumour angiogenesis, Bailliere's Clin. Haematol., *6:* 711–730, 1993.
8. O'Reilly, M. S., Boehm, T., Shing, Y., Fukai, N., Vasios, G., Lane, W. S., Flynn, E., Birkhead, J. R., Olsen, B. R., and Folkman, J. Endostatin: an endogenous inhibitor of angiogenesis and tumor growth. Cell, *88:* 277–285, 1997.
9. Dejana, E. Research on the endothelium and new therapeutic strategies in tumors and cardiovascular diseases (in Italian). Recenti Prog. Med., *90:* 64–68, 1999.
10. Gottlieb, S. Endostatin may stop the progression of atherosclerosis. Br. Med. J., *318:* 1030B, 1999.
11. Sasaki, T., Larsson, H., Kreuger, J., Salmivirta, M., Claesson-Welsh, L., Lindahl, U., Hohenester, E., and Timpl, R. Structural basis and potential role of heparin/heparan sulfate binding to the angiogenesis inhibitor endostatin. EMBO J., *18:* 6240–6248, 1999.
12. Sasaki, T., Fukai, N., Mann, K., Gohring, W., Olsen, B. R., and Timpl, R. Structure, function and tissue forms of the C-terminal globular domain of collagen XVIII containing the angiogenesis inhibitor endostatin. EMBO J., *17:* 4249–4256, 1998.
13. Dhanabal, M., Ramchandran, R., Waterman, M. J., Lu, H., Knebelmann, B., Segal, M., and Sukhatme, V. P. Endostatin induces endothelial cell apoptosis. J. Biol. Chem., *274:* 11721–11726, 1999.
14. Dhanabal, M., Ramchandran, R., Volk, R., Stillman, I. E., Lombardo, M., Iruela-Arispe, M. L., Simons, M., and Sukhatme, V. P. Endostatin: yeast production, mutants, and antitumor effect in renal cell carcinoma. Cancer Res., *59:* 189–197, 1999.
15. Taddei, L., Chiarugi, P., Brogelli, L., Cirri, P., Magnelli, L., Raugei, G., Ziche, M., Granger, H. J., Chiarugi, V., and Ramponi, G. Inhibitory effect of full-length human endostatin on *in vitro* angiogenesis. Biochem. Biophys. Res. Commun., *263:* 340–345, 1999.
16. Yamaguchi, N., Anand-Apte, B., Lee, M., Sasaki, T., Fukai, N., Shapiro, R., Que, I., Lowik, C., Timpl, R., and Olsen, B. R. Endostatin inhibits VEGF-induced endothelial cell migration and tumor growth independently of zinc binding. EMBO J., *18:* 4414–4423, 1999.
17. Chen, Q. R., Kumar, D., Stass, S. A., and Mixson, A. J. Liposomes complexed to plasmids encoding angiostatin and endostatin inhibit breast cancer in nude mice. Cancer Res., *59:* 3308–3312, 1999.
18. Blezinger, P., Wang, J., Gondo, M., Quezada, A., Mehrens, D., French, M., Singhal, A., Sullivan, S., Rolland, A., Ralston, R., and Min, W. Systemic inhibition of tumor growth and tumor metastases by intramuscular administration of the endostatin gene. Nat. Biotechnol., *17:* 343–348, 1999.
19. Blezinger, P., Yin, G., Xie, L., Wang, J., Matar, M., Bishop, J. S., and Min, W. Intravenous delivery of an endostatin gene complexed in cationic lipid inhibits systemic angiogenesis and tumor growth in murine models. Angiogenesis, *3:* 205–210, 1999.
20. Yoon, S. S., Eto, H., Lin, C. M., Nakamura, H., Pawlik, T. M., Song, S. U., and Tanabe, K. K. Mouse endostatin inhibits the formation of lung and liver metastases. Cancer Res., *59:* 6251–6256, 1999.
21. Dhanabal, M., Volk, R., Ramchandran, R., Simons, M., and Sukhatme, V. P. Cloning, expression, and *in vitro* activity of human endostatin. Biochem. Biophys. Res. Commun., *258:* 345–352, 1999.
22. Tanaka, T., Cao, Y., Folkman, J., and Fine, H. A. Viral vector-targeted antiangiogenic gene therapy utilizing an angiostatin complementary DNA. Cancer Res., *58:* 3362–3369, 1998.
23. Nguyen, J. T., Wu, P., Clouse, M. E., Hlatky, L., and Terwilliger, E. F. Adeno-associated virus-mediated delivery of antiangiogenic factors as an antitumor strategy. Cancer Res., *58:* 5673–5677, 1998.
24. Fenton, B. M., Paoni, S. F., Lee, J., Koch, C. J., and Lord, E. M. Quantification of tumour vasculature and hypoxia by immunohistochemical staining and HbO_2 saturation measurements. Br. J. Cancer., *79:* 464–471, 1999.
25. Altomonte, M., Montagner, R., Fonsatti, E., Colizzi, F., Cattarossi, I., Brasoveanu, L. I., Nicotra, M. R., Cattelan, A., Natali, P. G., and Maio, M. Expression and structural features of endoglin (CD105), a transforming growth factor β1 and β3 binding protein, in human melanoma. Br. J. Cancer., *74:* 1586–1591, 1996.
26. Bodey, B., Bodey, B., Jr., Siegel, S. E., and Kaiser, H. E. Over-expression of endoglin (CD105): a marker of breast carcinoma-induced neo-vascularization. Anticancer Res., *18:* 3621–3628, 1998.
27. Lord, E. M., Harwell, L., and Koch, C. J. Detection of hypoxic cells by monoclonal antibody recognizing 2-nitroimidazole adducts. Cancer Res., *53:* 5721–5726, 1993.
28. McGrath, K. E., Koniski, A. D., Maltby, K. M., McGann, J. K., and Palis, J. Embryonic expression and function of the chemokine SDF-1 and its receptor, CXCR4. Dev. Biol., *213:* 442–456, 1999.
29. Bergers, G., Javaherian, K., Lo, K. M., Folkman, J., and Hanahan, D. Effects of angiogenesis inhibitors on multistage carcinogenesis in mice. Science (Washington DC), *284:* 808–812, 1999.
30. Kirsch, M., Strasser, J., Allende, R., Bello, L., Zhang, J., and Black, P. M. Angiostatin suppresses malignant glioma growth *in vivo*. Cancer Res., *58:* 4654–4659, 1998.

[CANCER RESEARCH Vol. 61, 526–531, January 15, 2001]

Intratumoral Administration of Endostatin Plasmid Inhibits Vascular Growth and Perfusion in MCa-4 Murine Mammary Carcinomas[1]

Ivan Ding, Jian Zhong Sun, Bruce Fenton, Wei Min Liu, Paul Kimsely, Paul Okunieff, and Wang Min[2]

Departments of Radiation Oncology [I. D., J. Z. S., B. F., W. M. L., P. O.], Pediatrics [P. K.], and Medicine [W. M.], University of Rochester School of Medicine, Rochester, New York 14642

ABSTRACT

Endostatin, a fragment of the COOH-terminal domain of mouse collagen XVIII is a recently demonstrated endogenous inhibitor of tumor angiogenesis and endothelial cell growth. Antiangiogenic therapy with endostatin in animals requires multiple and prolonged administration of the protein. Gene therapy could provide an alternative approach to continuous local delivery of this antiangiogenic factor *in vivo*. Established MCa-4 murine mammary carcinomas, grown in immunodeficient mice, were treated with intratumoral injection of endostatin plasmid at 7-day intervals. At the time of sacrifice, 14 days after the first injection, endostatin-treated tumor weights were 51% of controls ($P < 0.01$). Tumor growth inhibition was accompanied by a marked reduction in total vascular density. Specifically, computerized image analysis showed a 18–21% increase in the median distances between tumor cells and both the nearest anatomical (CD31-stained) vessel [48.1 ± 3.8 *versus* 38.3 ± 1.6 μm ($P < 0.05$)] and the nearest tumor-specific (CD105-stained) vessel [48.5 ± 1.5 *versus* 39.8 ± 1.5 μm ($P < 0.01$)]. An increased apoptotic index of tumor cells in endostatin-treated tumors [3.2 ± 0.5% *versus* 1.9 ± 0.3% ($P < 0.05$)] was observed in conjunction with a significant decrease in tumor perfused vessels ($DiOC_7$ staining), and an increase in tumor cell hypoxia (EF5 staining). Hypoxia resulting from endostatin therapy most likely caused a compensatory increase of *in situ* vascular endothelial growth factor (VEGF) and VEGF receptor mRNA expression. Increased immunoreactivity of endostatin staining in endostatin-treated tumors was also associated with an increased thrombospondin-1 staining [1.12 ± 0.16 *versus* 2.44 ± 0.35]. Our data suggest that intratumoral delivery of the endostatin gene efficiently suppresses murine mammary carcinoma growth and support the potential utility of the endostatin gene for cancer therapy.

INTRODUCTION

Angiogenesis, the formation of new blood vessels, is essential for both critical physiological processes (wound healing) and lethal pathological conditions (tumor growth and atherosclerosis; Refs. 1–3). Numerous studies have shown that tumor growth is dependent on angiogenesis (4–7), thus providing a rationale for antiangiogenic therapy. Endostatin is one of the most potent endogenous angiogenesis inhibitors discovered to date. Interestingly, it inhibits pathologic vascular growth while allowing for normal processes. For example, both tumor growth (8) and atherosclerosis (9, 10) are inhibited in experimental animal models, whereas wound healing is unaffected. M_r 20,000 endostatin is a proteolytic polypeptide derived from its parent protein (collagen XVIII; Refs. 8, 11, 12). *In vitro* studies have shown that endostatin specifically inhibits endothelial proliferation without a direct effect on tumor or other nonneoplastic cell growth (12–15). Whether administrated as recombinant protein (14, 16), plasmid injection (17–19), or gene transfection (20), endostatin inhibits tumor growth, with reduction of virtually all tumor neovascularization and without detectable systemic toxicity in preclinical models.

To be effective, antiangiogenic therapy with endostatin in tumor-bearing mice requires prolonged administration and high doses of recombinant protein (8, 14). In addition, production of the functional polypeptide has proven difficult, perhaps because of its physical properties and because of variations in the purification procedures utilized by different laboratories (15, 21). However, some preliminary data have shown that local or systemic administration of endostatin is an effective means of application in cancer therapy. A few groups have demonstrated that antiangiogenic gene therapy with viral vectors is a potentially useful approach for inhibiting tumor growth in mouse models (22–23). Although viral vectors have high transfection efficiency and are commonly used in experimental systems, safety issues and the toxicity of these viral vectors likely precludes their use as an i.v. agent. In contrast, we and others have shown that systematically delivered endostatin plasmid possesses low toxicity and high effective antitumor action (17–19). In the current study, we investigated whether intratumoral injection of endostatin plasmid once a week for 2 weeks inhibited mammary tumor growth. We also explored the underlying physiological and molecular mechanisms of endostatin-mediated antitumoral effects.

MATERIALS AND METHODS

Endostatin Plasmid. A plasmid containing an expression cassette for mouse endostatin was constructed as described previously (18). The coding sequence of endostatin comprises the COOH-terminal 184 ammo acid residues of collagen XVIII. This sequence was directly amplified by PCR from liver cDNA. Plasmids were grown under kanamycin selection in host strain DH5α and purified by alkaline lysis and chromatographic methods using Endofree kit (Qiagen, Valencia, CA). Purified plasmid had the following specifications: <50 Eu/mg endotoxin; <1% protein: and <5% (wt/wt) chromosomal DNA.

Murine Mammary Tumor Models and Treatment. Isotransplants of the murine mammary carcinoma MCa-4 were used. Frozen MCa-4 tumor cells were inoculated i.m. into the hind limbs of 6–8-week-old female BALB/c (nu/nu) mice (National Cancer Institute, NIH, Frederick, MD). Tumors were selected for endostatin plasmid treatment when they reached volumes of between 150 and 250 mm^3 (as measured by calipers and the formula: Volume = Diameter^3/6). Endotoxin-free endostatin plasmid (45 μg) was injected once a week for 2 weeks into the tumor in the right thigh. All of the tumors (right and left) were averaged. Equal volumes of saline and vector were injected as controls in separate mice. Mice were sacrificed 7 days after the second injection. Tumors were removed, examined, and frozen for later immunohistochemistry or RNA isolation. Guidelines for the humane treatment of animals were followed as approved by the University Committee on Animal Resources.

Measurement of Anatomical (CD31), Perfused ($DiOC_7$), and Angiogenic (CD105) Blood Vessels. Immunohistochemistry methods have previously been described in detail (24). To visualize blood vessels open to flow, an i.v. injected stain, $DiOC_7$ (Molecular Probes, Engene, OR), was utilized. Injections were administered i.v. at a concentration of 1.0 mg/kg, 1 min prior to freezing. This dose and schedule has been shown to provide optimal visualization of tumor vasculature by preferentially staining cells immediately adjacent to blood vessels. $DiOC_7$-stained vessels emit green fluorescence when excited by blue light. CD31 antibody staining (PharMingen, San Diego, CA) was used for visualizing total structural vessels. In addition, an anti-CD105

Received 4/3/00; accepted 11/8/00.

The costs of publication of this article were defrayed in part by the payment of page charges. This article must therefore be hereby marked *advertisement* in accordance with 18 U.S.C. Section 1734 solely to indicate this fact.

[1] Supported by NIH Grants CA11051-25A2 (to P. O., J. Z. S., W. M. L., and I. D.), CA52586 (to B. F.), and University of Rochester starting fund (to W. M.).

[2] To whom requests for reprints should be addressed, at Center for Cardiovascular Research, Department of Medicine, Box 679, University of Rochester, Rochester, NY 14642. Phone: (716) 273-1499; Fax: (716) 275-9895; E-mail: Wang_min@urmc.rochester.edu.

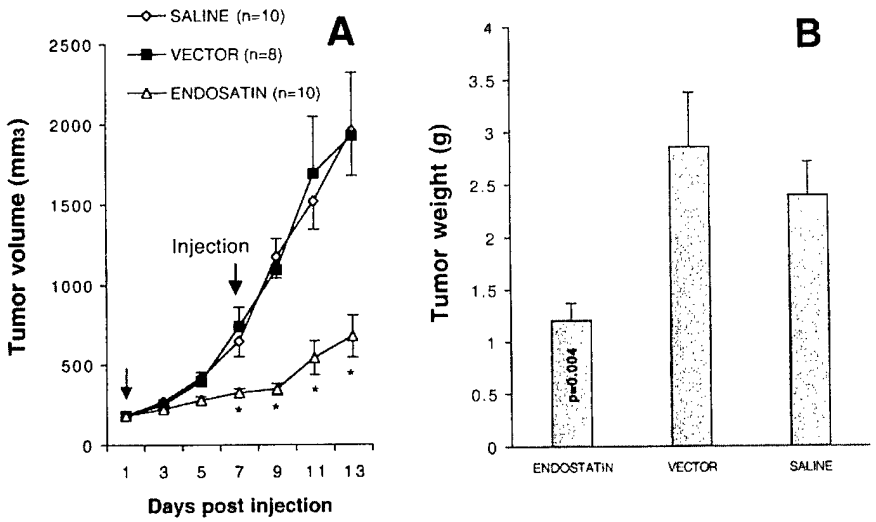

Fig. 1. Injection of endostatin inhibited MCa-4 tumor growth. *A*, saline-, vector-, and endostatin-treated tumors were measured, and volumes were calculated as mean ± SE. Significant differences were found between controls and endostatin-treated tumors 7 days after treatment. *B*, all of the mice were killed 14 days after the first endostatin treatment. Tumor weight (mean ± SE) is shown.

antibody (PharMingen) that was recently reported to specifically identify vascular neogenesis was also utilized. CD105 is strongly expressed in activated endothelial cells of various human tumors, including breast cancer, but is either undetectable or only weakly present in mature blood vessels of normal tissues (25–26).

EF5/Cy3 Hypoxia Marker. Localized areas of tumor hypoxia were assessed in frozen tissue sections by immunohistochemical identification of sites of 2-nitroimidazole metabolism. A pentafluorinated derivative of etanidazole (EF5) was injected i.v. 1 h before tumor freezing. Protein conjugates of EF5 have been previously used to immunize mice from which monoclonal antibodies were developed (27). These antibodies are extremely specific for the EF5 drug adducts that form when the drug is incorporated by hypoxic cells, and one of these, ELK3-51, has been well characterized. Regions of high EF5 metabolism in tumors (hypoxic regions) were visualized and the area of staining quantified immunochemically using a fluorochrome (Cy3) conjugated to the ELK3-51 antibody and computerized imaging techniques.

Imaging and Image Analysis. For each frozen tumor, 4.0-μm sections were cut using a cryostat. The stained sections were imaged using an epi-fluorescence-equipped microscope, digitized (3-CCD camera), background-corrected, and image-analyzed using Image Pro software (Media Cybernetics) and a 450-MHz Pentium computer. Color images from adjacent microscope fields were automatically acquired and digitally combined to form 4 × 4 montages of the tumor cross-section (using a motorized stage and controller). For each section, two peripheral and two interior image montages were obtained. Each section was then scanned under each of three staining conditions. First, epi-illumination images of the fluorescent green $DiOC_7$ staining (perfused vessels) were obtained immediately after the 4.0-μm sections were sliced on the cryostat. After the immunohistochemical staining procedures were completed, the same tumor section used for the $DiOC_7$ imaging was returned to the microscope stage and automatically rescanned using the same coordinates as for the initial 4 × 4 montages. Using transmitted light, matching montages of the CD31 (anatomical vessels) and CD105 (angiogenic vessels) were obtained. Briefly, the image montages were processed to enhance the contrast between background and either CD31 staining or $DiOC_7$ staining. The quantitative vascular information was analyzed using custom FORTRAN programs to perform a "closest individual" analysis. Briefly, the distances from computer-superimposed sampling points to the nearest blood vessel were determined. The cumulative frequency distribution of these distances provides the probability of encountering vessels within any specified distance from the tumor cells. Median distances to the nearest anatomical or perfused blood vessel were used for statistical comparisons.

RNase Protection Assay. Tumor tissue RNA from each treatment group (n = 4–6 mice) was isolated by pulverizing the frozen tissue and dissolving it in TRIzol reagent (MRC, Cincinnati, OH). RNAse protection was performed using established multiprobe template sets (PharMingen) as described previously (27). The apoptosis set includes: antiapoptotic genes: *Bcl-2, bcl-X, bcl-W*, and *bfl-1*; and apoptotic genes: *Bax, Bak*, and *Bad*. Two internal controls, L32 and GAPDH,[3] were used to monitor RNA loading. The quantitation of mRNA expression level tested for each sample was measured using a Cyclone PhosphorImager (HP Company, Meriden, CT). Relative mRNA expression levels were ratios of targeted gene divided by *L32* or *GAPDH* genes.

Western Blot Analysis. Cell lysates were prepared from frozen tumor tissues (n = 2) and separated by SDS-PAGE on 12% (w/v) polyacrylamide gels and electrotransferred onto Millipore polyvinylidene difluoride membranes in 25 mM Tris, 192 mM glycine. Membranes were blocked in Tris-buffered saline (20 mM Tris-HCl, 137 mM NaCl) containing 0.05% Tween 20 and 5% nonfat dry milk for 60 min at room temperature. The blots were then incubated overnight at 4°C in blocking solution with the 1:1000 goat-antimurine endostatin antibody (R&D Systems, Minneapolis, MN). Thereafter, membranes were washed in Tris-buffered saline and incubated with horseradish peroxidase-conjugated antigoat IgG (1:3000) in blocking solution for 1 h. The blots were visualized by chemiluminescence using the Pierce ECL system (Pierce, Rockford, Illinois).

***In Situ* Hybridization.** For *in situ* localization of VEGF and it receptor gene expression in tumor tissue, we followed procedures previously published from our laboratory (28). Briefly, tumor tissue was fixed in 10% formalin or 2% paraformaldehyde, and cross-sections were then cut. Sections of tissue were placed on specially prepared slides (acid-washed and T3-aminopropyl triethoxysilane-coated), then deparaffinized, rehydrated, proteinase K-digested, and hybridized with VEGF and VEGFR riboprobes labeled with [^{33}P]UTP. After washing, sections were prepared for autoradiography using NBTII emulsion. After autoradiography and staining, slides were analyzed by bright- and dark-field microscopy. Backgrounds for these studies were determined by using the sense stand RNA probe. As a positive control for hybridization, some sections were hybridized for a constitutively expressed mRNA, such as GAPDH, analyzed for cell-specific expression of the molecule of interest. The location of overexpression was identified histologically.

RESULTS

The effects of intratumoral injection of endostatin plasmid (45 μg/mouse/two injections) on MCa-4 tumor growth are shown in Fig. 1. There was a substantial tumor growth delay in endostatin-treated tumors compared with saline- or vector-treated controls (Fig. 1*A*). Tumor growth inhibition was only slightly greater in the right (directly treated) compared with the left thigh tumors, and because the differences did not achieve statistical significance, the data were

[3] The abbreviations used are: VEGF, vascular endothelial growth factor; VEGFR, VEGF receptor; GAPDH, glyceraldehyde-3-phosphate dehydrogenase.

Table 1 *MCa-4 tumor-bearing nude mice treated with endostatin plasmid injections*

Injection of endostatin inhibited anatomic and angiogenic vessels and induced tumor apoptosis in MCa-4 tumors. Tumor proliferation and necrosis index were not significantly altered.

	Median distance to tumor vessels		Tumor Cells		
	CD31 (μm)	CD105 (μm)	% of apoptosis	% of mitosis	% of necrosis
Saline	38.29 ± 1.56	39.75 ± 1.45	1.90 ± 0.32	3.60 ± 0.62	14.87 ± 2.90
Vector	41.47 ± 1.13	44.26 ± 1.57	2.02 ± 0.32	4.35 ± 0.41	11.31 ± 0.79
Endostatin	48.10 ± 3.76[a]	48.51 ± 1.48[b]	3.22 ± 0.45[a]	3.56 ± 0.22	8.62 ± 1.84

[a] $P < 0.05$.
[b] $P < 0.01$.

combined. This is consistent with our previous observation that endostatin expressed in local tissues can release into the circulation and elicit systemic inhibition of tumor growth and metastasis (18, 19). Inhibition of tumor growth was statistically significant beginning 7 days after injection of endostatin plasmid ($P < 0.05$). All of the mice were killed 14 days after the first endostatin treatment. There was a significant reduction of tumor weight in endostatin-treated animals compared with controls (Fig. 1*B*). Repeating the first experiment with the same number of mice and treatment schedules again demonstrated significant reduction in MCa-4 tumor growth. As in the original experiment, the treated tumors (right leg) had slightly greater growth inhibition than the opposite leg (left) tumors.

To examine the effect of endostatin on vascular growth, anatomical vessels (CD31 staining) and angiogenic vessels (CD105 staining) in the tumors were measured and quantified "Materials and Methods"). As shown in Table 1, endostatin-treated tumors had a significant reduction in total anatomical vessels and angiogenic vessels. Tumor proliferation and necrosis index were not significantly altered. In contrast, decreased blood vessel density was associated with a significant increase in tumor cell apoptosis. The increase in apoptotic index was 1.7-fold [3.2 ± 0.45 *versus* 1.9 ± 0.3 for saline ($P < 0.05$); 2.0 ± 0.3 for vector-treated). An RNase protection assay also showed that endostatin-treated tumors had a significant (28%) reduction in *bfl-1* mRNA, as well as 21–26% decrease of *bak* and *bad* mRNA gene expression compared with controls ($P < 0.05$) as shown in Fig. 2. No other differential mRNA expression was observed in the other apoptotic gene (*bax*), or antiapoptotic genes (*bcl-2, bcl-2*, and *bcl-X*) between endostatin-treated and control animals.

The effects of endostatin on tumor functional vessels and oxygenation were evaluated using $DiOC_7$ and EF5 staining 14 days after the first endostatin treatment. As shown in Fig. 3, endostatin-treated tumors had a 13% increase in median distance to the nearest perfused vessel compared with saline controls ($P = 0.053$). In the same experiment, we also observed that endostatin-treated tumors showed a significant reduction in CD31- and CD105-stained vessels ($P < 0.01$). Vector-treated tumors also had decreased numbers of perfused vessels compared with saline controls, most likely because of the larger sizes of the tumors (3.4 ± 0.8 g for vector *versus* 2.5 ± 0.5 g for saline) in this treatment group (Fig. 1*B*). Unpublished studies have shown an inverse relationship between perfusion and tumor volumes in numerous tumor models.[4]

The most extensive hypoxia marker uptake, however, was observed in endostatin-treated tumors, despite their smaller tumor size (Fig. 3). The reduction in number of perfused vessels and the increase in tumor hypoxia were associated with an elevation of local tumor VEGF and VEGFR mRNA expression, as detected by *in situ* hybridization (Fig. 4).

Endostatin-treated tumors also showed increased levels of thrombospondin-1 protein by immunohistochemistry (Fig. 5). Both thrombospondin-1 (Fig. 5*B*) and endostatin protein (Fig. 5*A*) were detected in cellular (*a–c*) or stromal (*a′–c′*) compartment.

DISCUSSION

In the present study, we have shown that intratumoral injection of endostatin plasmid once a week for 2 weeks inhibits murine mammary MCa-4 tumor growth in nude mice. The reduction of tumor growth rate is associated with decreased numbers of tumor anatomical vessels, angiogenic vessels, and perfused vessels. Endostatin-treated tumors also have an increased tumor cell apoptotic index and increased tumor cell hypoxia, which are most likely associated with secondary induction of tumor cell VEGF and VEGFR mRNA expression as well as with elevation of local thrombospondin-1 protein expression.

Application of antiangiogenic growth factors for gene therapy has been recently used in several tumor models (17, 18). We initially reported the systemic inhibition of tumor growth and metastasis by i.m. administration of the endostatin gene formulated with synthetic polymer in murine Renca and Lewis lung carcinomas, and tumor volume was 40% of control at 13-day posttreatment (18). More recently, we reported that i.v. injection of a mixture of liposome with endostatin plasmid inhibited tumor growth and metastases (19). A similar study has been reported by Chen *et al.* in human mammary MDA-MB435 xenograft (17). Preclinical gene therapy models, therefore, suggest that this approach to antiangiogenic growth factor therapy will be efficacious. In contrast, achieving tumor regression with recombinant protein has been difficult and requires frequent high-dose injections in animal tumors. Our results and those of others have demonstrated that local or systemic administration of nonviral endostatin plasmid significantly inhibits the growth of several tumor types, including lung, breast, kidney, and sarcoma tumors (17–19). Response, however, is limited to the slowing of tumor growth without complete regression for established tumors. The efficacy may be dependent on tumor type, vector type, and plasmid administration route and dose, as well as the formulation of agents.

Regression of transplanted tumors is a more difficult undertaking than preventing tumor formation when using any cytotoxic or antiangiogenic therapy. Using a transgenic mouse model of a spontaneous pancreatic β-islet cell tumor, Bergers *et al.* (29) recently reported that recombinant endostatin effectively prevented the promotion from

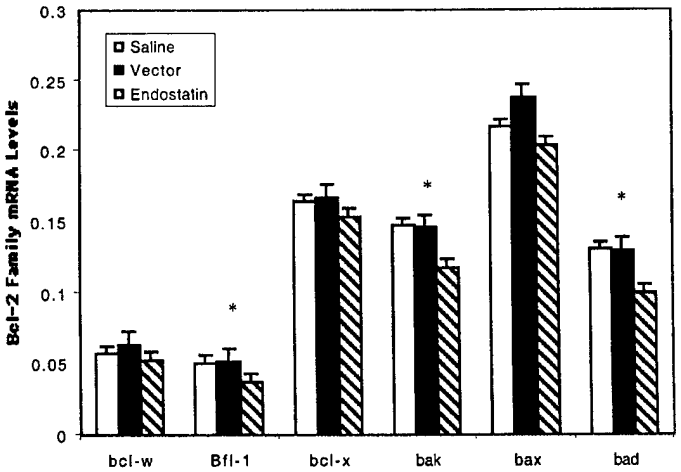

Fig. 2. Injection of endostatin regulated mRNA expression of Bcl-2 family genes in MCa-4 tumor. Saline-, vector-, and endostatin-treated tumors were collected 14 days after treatment, and 30 μg total RNA were used for RNase protection assay. Relative mRNA expression levels were presented as ratio of targeted gene divided by loading control *L32* or *GAPDH* genes (mean ± SD; $n = 5$ mice).

[4] Unpublished observations.

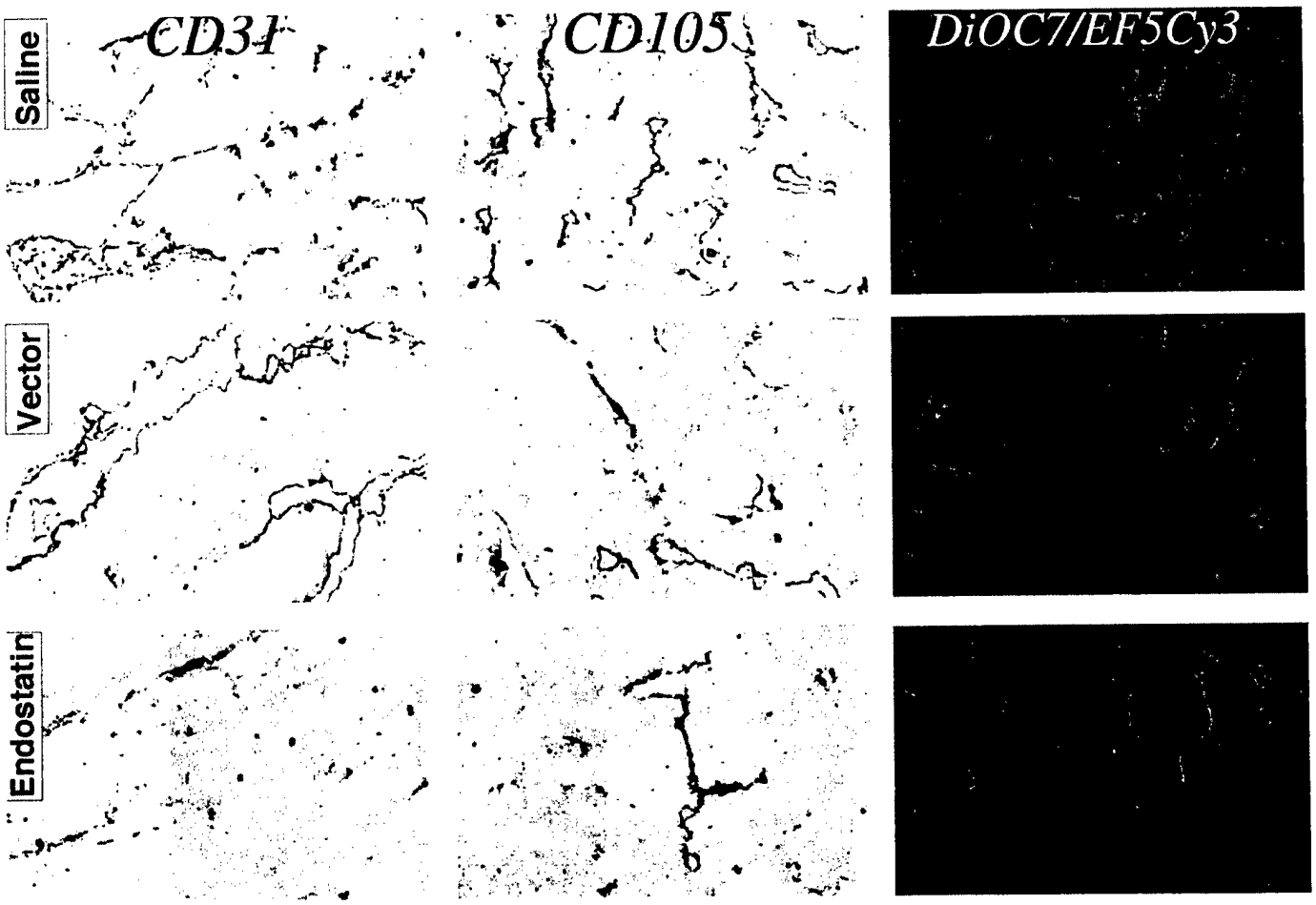

Fig. 3. Injection of endostatin inhibits anatomic, angiogenic, and perfused vessels in MCa-4 tumor. Saline-, vector-, and endostatin-treated tumors were collected 14 days after treatment. Anatomic, angiogenic, and perfused vessels were visualized by CD31, CD105, and $DiOC_7$ staining. Endostatin-treated tumors had a significantly reduced vessel density among all of the three vessel types. Endostatin-treated tumors also showed an increase in EF5 hypoxia marker uptake (*orange staining*).

hyperplastic lesion to small tumor formation but poorly inhibited established tumor growth (progression stage). In our transplantable MCa-4 tumor and others, endostatin succeeded in slowing tumor growth in established tumors as described previously (17–20). The antitumoral action of endostatin should, therefore, be further investigated at different stages of carcinogenesis. Ultimately, we may find that the greatest utility for endostatin is in preventing metastases rather than in inhibiting established tumors (18–19).

Endostatin is believed to specifically inhibit endothelial cell proliferation rather than tumor cell growth (12–15). The underlying molecular mechanisms of antiangiogenesis are presumably related to an increase in endothelial cell apoptosis (13), or an alteration of cell cycle (21). In our animal model, the effects of endostatin-mediated antiangiogenesis are consistent with previous studies. In addition, we quantitatively demonstrated that endostatin-treated tumors showed a clear decrease in perfused vessel density and an increase in tumor cell hypoxia, and that the effects were long lasting, with physiological effects still manifesting 14 days after initial treatment. Direct inhibi-

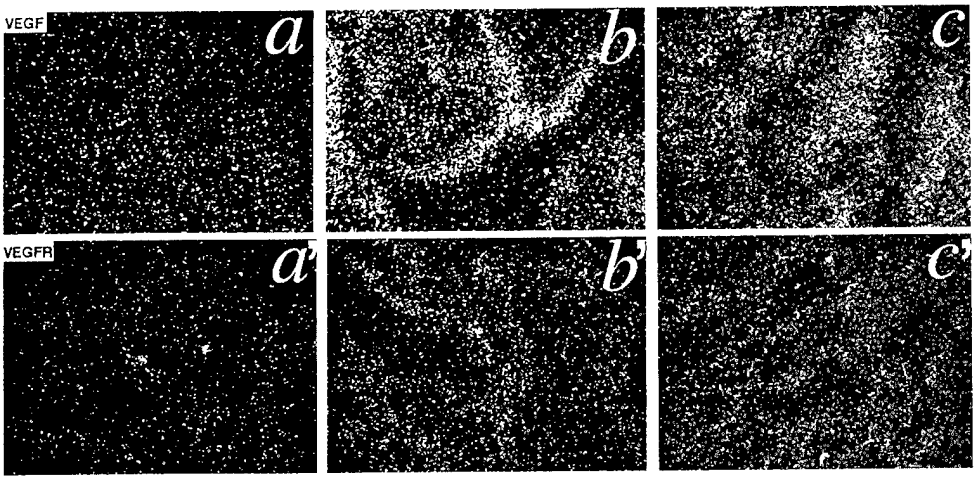

Fig. 4. Overexpression of VEGF and VEGFR mRNA in endostatin-treated tumors by *in situ* hybridization in MCa-4 tumors. Saline-, vector-, and endostatin-treated tumors were collected 14 days after treatment, and ^{33}P-labeled antisense riboprobe for VEGF (*a–c*) or VEGFR (*a'–c'*) was hybridized. Radiographs are shown in dark field. Endostatin-treated tumors (*c* and *c'*) had elevated VEGF and VEGFR mRNA expression compared with that of untreated tumors (*a* and *a'*). Vector-treated tumor (*b* and *b'*) also showed increased VEGF and VEGFR expression, which was probably attributable to the fact that vector-treated tumors were larger in size than untreated tumors.

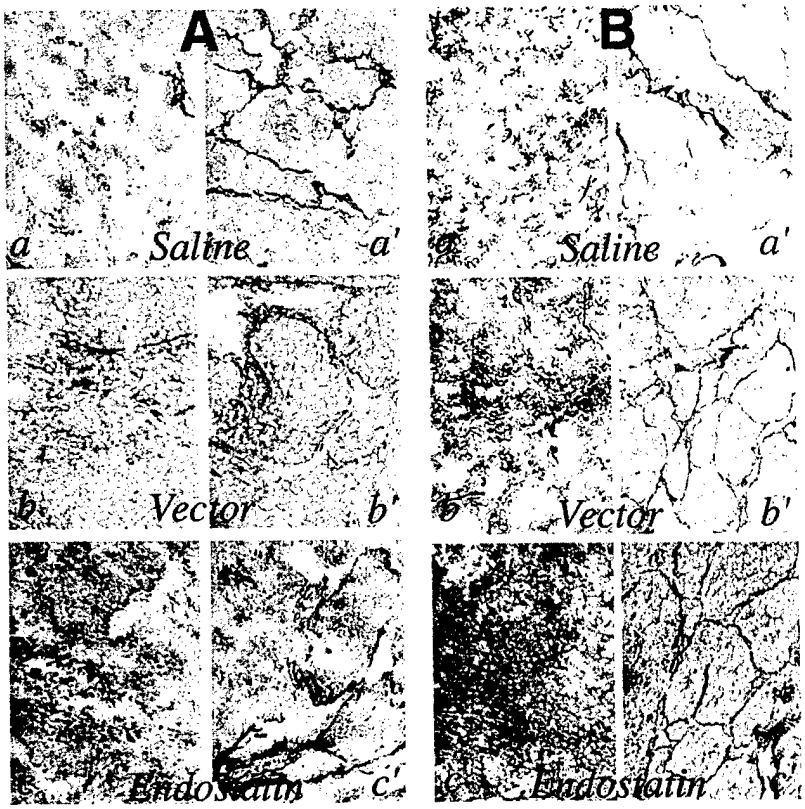

Fig. 5. Expression of thrombospondin-1 protein in endostatin-treated tumors by immunohistochemistry in MCa-4 tumors. Saline-, vector-, and endostatin-treated tumors were collected 14 days after initial treatment and antiendostatin antibody (*A*) or antithrombospondin-1 antibody (*B*) was hybridized with these sections. (*a–c*), cellular staining pattern; (*a'–c'*), stromal staining pattern. Endostatin-treated tumors showed the transgene expression and had elevated thrombospondin-1 protein expression.

tion of tumor structural vessels, angiogenic vessels, and perfused vessels can explain the observed endostatin-mediated antitumoral effects. Although we believe that the tumor cell apoptosis was secondary to ischemia, our observation leaves open the possibility that endostatin has direct apoptotic effects on tumor tissue. Likewise, tumor necrosis and apoptosis may have been attributable to ischemia, reperfusion injury, or some as-yet-unexplained indirect endostatin-induced cytotoxicity.

We favor a direct effect of endostatin on tumor vascularity, resulting indirectly in tumor growth reduction. Consistent with this hypothesis, endostatin-treated MCa-4 tumors had a similar proliferative rate to that of controls as measured by mitotic figures (Table 1), which suggests that the tumor cell cycle was not altered by endostatin. Reduced vascularity, however, can deprive tumors of their nutrient supply, and, thus, proliferation can result in environmentally deprived progeny, leading to apoptosis or necrosis after division. Kirsch *et al.* (30) showed that recombinant angiostatin-treated gliomas caused both neoplastic and endothelial cell apoptosis. They concluded that endothelial cell apoptosis results from vessel thrombosis or regression of pre-existing vessels. In our study, we counted only the tumor cell apoptotic numbers, because very few endothelial cells displayed an apoptotic appearance on the basis of morphology. Thus, we cannot confirm (or refute) the observation of Kirsch *et al.* (30). Regarding molecules important in promoting or inhibiting apoptosis, there were mixed responses. The antiapoptotic gene *bfl-1* decreased, but so did the apoptotic genes *bad* and *bak*. Ischemia and reperfusion injury, therefore, appear more important in generating the necrosis and apoptosis than any hypothetical direct endostatin-mediated apoptosis. It is possible, however, that endothelial cells from different tumor types may respond differently to endostatin (20).

Endostatin may exert biological effects directly or indirectly by altering expression of other growth-related molecules. One possible mechanism is a down-regulation of angiogenic molecules by endostatin. Because multiple cell types, such as tumor cells, endothelial cells, activated macrophages, and tumor fibroblasts, in tumors produce angiogenic and antiangiogenic growth factors, and because many angiogenic growth factors can also be mobilized from the extracellular matrix, endostatin-mediated regulation of angiogenic growth factor gene expression is extremely complex and difficult to assess. Kirsch *et al.* (30) treated three types of malignant gliomas and found a significant reduction of VEGF mRNA by Northern analysis, but an elevation of FGF2 3 weeks after angiostatin treatment. They hypothesized that angiostatin-mediated antiangiogenesis in gliomas may be secondary to down-regulation of certain angiogenic growth factors or to up-regulation of antiangiogenic factors. We found an up-regulation of VEGF and VEGFR mRNA as well as up-regulation of thrombospondin-1 protein expression in endostatin-treated MCa-4 breast tumors. In contrast to Kirsch *et al.* (30), our results demonstrated that VEGF and VEGFR were up-regulated rather than down-regulated. These differences could suggest that: (*a*) the balance of angiogenic and antiangiogenic growth factors as well as their gene regulation may be time-dependent during endostatin treatment. Sampling at different times after endostatin treatment may result in differential gene expression; (*b*) expression of angiogenic or antiangiogenic growth factors may be tumor size- or tumor histologic type-dependent; (*c*) endostatin may exert its effects through different mechanisms in different tumors, animal strains, or species; and (*d*) expression of angiogenic/antiangiogenic factors may be responding to independent stimuli. We believe that tumor hypoxia induced the VEGF and VEGFR mRNA expression, and the up-regulation of thrombospondin-1 may be triggered by endostatin through specific signaling pathways.

In summary, endostatin inhibits tumor growth by reducing structural, angiogenic, and perfused tumor vessels. A lack of adequate blood supply leads to tumor hypoxia and probably accounts for tumor cell apoptosis and the up-regulation of VEGF and VEGFR. Thrombospondin-1 also increased, which suggests that endostatin may regulate this antiangiogenic peptide. However, the molecular mecha-

nisms for endostatin-mediated antiangiogenesis are still unknown at present. Different mechanisms may exist for *in vitro* and *in vivo* models. *In vitro*, several issues need to be addressed: (*a*) is there a receptor or endostatin-related cell surface molecule on endothelial cells? and (*b*) if so, what are the signal transduction pathway and target genes? If not, how does it inhibit angiogenesis and is it via stromal effects? In animal models, we also need to consider: (*a*) does endostatin act on tumor cells through direct or indirect pathways? (*b*) if by indirect pathways, is it by regulation of other angiogenic or antiangiogenic factors in endothelial, inflammatory, or tumor cells? and (*c*) can endostatin induce tumor regression rather than just slow growth, and under what circumstances? These mechanistic questions are now under investigation in our laboratory.

REFERENCES

1. Bout, J. C., Soncin, F., and Vandenbunder, B. Therapeutic prospects of angiogenesis inhibitors in cancerology (in French). Rev. Mal. Respir., *16:* 854–855, 1999.
2. Keshet, E. and Ben-Sasson, S. A. Anticancer drug targets: approaching angiogenesis. J. Clin. Investig., *104:* 1497–1501, 1999.
3. Cao, Y. Therapeutic potentials of angiostatin in the treatment of cancer. Haematologica, *84:* 643–650, 1999.
4. Folkman, J. Angiogenesis in cancer, vascular, rheumatoid and other disease. Nat. Med., *1:* 27–31, 1995.
5. Folkman, J. Angiogenesis inhibitors generated by tumors. Mol. Med. *1:* 120–122, 1995.
6. Hahnfeldt, P., Panigraphy, D., Folkman, J., and Hlatky, L. Tumor development under angiogenic signaling: a dynamical theory of tumor growth, treatment response, and postvascular dormancy. Cancer Res., *59:* 4770–4775, 1999.
7. Le Querrec, A., Duval, D., and Tobelem, G. Tumour angiogenesis, Bailliere's Clin. Haematol., *6:* 711–730, 1993.
8. O'Reilly, M. S., Boehm, T., Shing, Y., Fukai, N., Vasios, G., Lane, W. S., Flynn, E., Birkhead, J. R., Olsen, B. R., and Folkman, J. Endostatin: an endogenous inhibitor of angiogenesis and tumor growth. Cell, *88:* 277–285, 1997.
9. Dejana, E. Research on the endothelium and new therapeutic strategies in tumors and cardiovascular diseases (in Italian). Recenti Prog. Med., *90:* 64–68, 1999.
10. Gottlieb, S. Endostatin may stop the progression of atherosclerosis. Br. Med. J., *318:* 1030B, 1999.
11. Sasaki, T., Larsson, H., Kreuger, J., Salmivirta, M., Claesson-Welsh, L., Lindahl, U., Hohenester, E., and Timpl, R. Structural basis and potential role of heparin/heparan sulfate binding to the angiogenesis inhibitor endostatin. EMBO J., *18:* 6240–6248, 1999.
12. Sasaki, T., Fukai, N., Mann, K., Gohring, W., Olsen, B. R., and Timpl, R. Structure, function and tissue forms of the C-terminal globular domain of collagen XVIII containing the angiogenesis inhibitor endostatin. EMBO J., *17:* 4249–4256, 1998.
13. Dhanabal, M., Ramchandran, R., Waterman, M. J., Lu, H., Knebelmann, B., Segal, M., and Sukhatme, V. P. Endostatin induces endothelial cell apoptosis. J. Biol. Chem., *274:* 11721–11726, 1999.
14. Dhanabal, M., Ramchandran, R., Volk, R., Stillman, I. E., Lombardo, M., Iruela-Arispe, M. L., Simons, M., and Sukhatme, V. P. Endostatin: yeast production, mutants, and antitumor effect in renal cell carcinoma. Cancer Res., *59:* 189–197, 1999.
15. Taddei, L., Chiarugi, P., Brogelli, L., Cirri, P., Magnelli, L., Raugei, G., Ziche, M., Granger, H. J., Chiarugi, V., and Ramponi, G. Inhibitory effect of full-length human endostatin on *in vitro* angiogenesis. Biochem. Biophys. Res. Commun., *263:* 340–345, 1999.
16. Yamaguchi, N., Anand-Apte, B., Lee, M., Sasaki, T., Fukai, N., Shapiro, R., Que, I., Lowik, C., Timpl, R., and Olsen, B. R. Endostatin inhibits VEGF-induced endothelial cell migration and tumor growth independently of zinc binding. EMBO J., *18:* 4414–4423, 1999.
17. Chen, Q. R., Kumar, D., Stass, S. A., and Mixson, A. J. Liposomes complexed to plasmids encoding angiostatin and endostatin inhibit breast cancer in nude mice. Cancer Res., *59:* 3308–3312, 1999.
18. Blezinger, P., Wang, J., Gondo, M., Quezada, A., Mehrens, D., French, M., Singhal, A., Sullivan, S., Rolland, A., Ralston, R., and Min, W. Systemic inhibition of tumor growth and tumor metastases by intramuscular administration of the endostatin gene. Nat. Biotechnol., *17:* 343–348, 1999.
19. Blezinger, P., Yin, G., Xie, L., Wang, J., Matar, M., Bishop, J. S., and Min, W. Intravenous delivery of an endostatin gene complexed in cationic lipid inhibits systemic angiogenesis and tumor growth in murine models. Angiogenesis, *3:* 205–210, 1999.
20. Yoon, S. S., Eto, H., Lin, C. M., Nakamura, H., Pawlik, T. M., Song, S. U., and Tanabe, K. K. Mouse endostatin inhibits the formation of lung and liver metastases. Cancer Res., *59:* 6251–6256, 1999.
21. Dhanabal, M., Volk, R., Ramchandran, R., Simons, M., and Sukhatme, V. P. Cloning, expression, and *in vitro* activity of human endostatin. Biochem. Biophys. Res. Commun., *258:* 345–352, 1999.
22. Tanaka, T., Cao, Y., Folkman, J., and Fine, H. A. Viral vector-targeted antiangiogenic gene therapy utilizing an angiostatin complementary DNA. Cancer Res., *58:* 3362–3369, 1998.
23. Nguyen, J. T., Wu, P., Clouse, M. E., Hlatky, L., and Terwilliger, E. F. Adeno-associated virus-mediated delivery of antiangiogenic factors as an antitumor strategy. Cancer Res., *58:* 5673–5677, 1998.
24. Fenton, B. M., Paoni, S. F., Lee, J., Koch, C. J., and Lord, E. M. Quantification of tumour vasculature and hypoxia by immunohistochemical staining and HbO_2 saturation measurements. Br. J. Cancer., *79:* 464–471, 1999.
25. Altomonte, M., Montagner, R., Fonsatti, E., Colizzi, F., Cattarossi, I., Brasoveanu, L. I., Nicotra, M. R., Cattelan, A., Natali, P. G., and Maio, M. Expression and structural features of endoglin (CD105), a transforming growth factor β1 and β3 binding protein, in human melanoma. Br. J. Cancer., *74:* 1586–1591, 1996.
26. Bodey, B., Bodey, B., Jr., Siegel, S. E., and Kaiser, H. E. Over-expression of endoglin (CD105): a marker of breast carcinoma-induced neo-vascularization. Anticancer Res., *18:* 3621–3628, 1998.
27. Lord, E. M., Harwell, L., and Koch, C. J. Detection of hypoxic cells by monoclonal antibody recognizing 2-nitroimidazole adducts. Cancer Res., *53:* 5721–5726, 1993.
28. McGrath, K. E., Koniski, A. D., Maltby, K. M., McGann, J. K., and Palis, J. Embryonic expression and function of the chemokine SDF-1 and its receptor, CXCR4. Dev. Biol., *213:* 442–456, 1999.
29. Bergers, G., Javaherian, K., Lo, K. M., Folkman, J., and Hanahan, D. Effects of angiogenesis inhibitors on multistage carcinogenesis in mice. Science (Washington DC), *284:* 808–812, 1999.
30. Kirsch, M., Strasser, J., Allende, R., Bello, L., Zhang, J., and Black, P. M. Angiostatin suppresses malignant glioma growth *in vivo*. Cancer Res., *58:* 4654–4659, 1998.

British Journal of Cancer (2002) 86, 1831 – 1836

www.bjcancer.com

Zonal image analysis of tumour vascular perfusion, hypoxia, and necrosis

BM Fenton*[,1], SF Paoni[1], BK Beauchamp[1] and I Ding[1]

[1]*Department of Radiation Oncology, University of Rochester Medical Center, Rochester, New York, NY 14642, USA*

A number of laboratories are utilising both hypoxia and perfusion markers to spatially quantify tumour oxygenation and vascular distributions, and scientists are increasingly turning to automated image analysis methods to quantify such interrelationships. In these studies, the presence of regions of necrosis in the immunohistochemical sections remains a potentially significant source of error. In the present work, frozen MCa-4 mammary tumour sections were used to obtain a series of corresponding image montages. Total vessels were identified using CD31 staining, perfused vessels by $DiOC_7$ staining, hypoxia by EF5/Cy3 uptake, and necrosis by haematoxylin and eosin staining. Our goal was to utilise image analysis techniques to spatially quantitate hypoxic marker binding as a function of distance from the nearest blood vessel. Several refinements to previous imaging methods are described: (1) hypoxia marker images are quantified in terms of their intensity levels, thus providing an analysis of the gradients in hypoxia with increasing distances from blood vessels, (2) zonal imaging masks are derived, which permit spatial sampling of images at precisely defined distances from blood vessels, as well as the omission of necrotic artifacts, (3) thresholding techniques are applied to omit holes in the tissue sections, and (4) distance mapping is utilised to define vascular spacing.
British Journal of Cancer (2002) **86,** 1831 – 1836. doi:10.1038/sj.bjc.6600343 www.bjcancer.com

Keywords: hypoxia markers; image processing; immunohistochemistry; tumour oxygenation

The relationship between tumour hypoxia and therapeutic response has been well documented in the literature for quite some time, and direct measures of tumour oxygenation have been shown to correlate with both long-term survival (Hockel *et al*, 1996) and the occurrence of distant metastases (Brizel *et al*, 1996). Two of the more prominent techniques for measuring tumour hypoxia are: (1) the Eppendorf electrode for determination of tumour pO_2 levels, and (2) nitroimidazole hypoxia markers, e.g., EF5, NITP, and pimonidazole, which covalently bind to hypoxic tumour cells and allow immunohistochemical or flow cytometric determination of hypoxia distributions (Koch *et al*, 1995; Hodgkiss and Wardman, 1992; Raleigh *et al*, 1987). The presence of tumour necrosis can have substantial effects on each of these types of measurements. With the Eppendorf technique, necrotic regions result in a reduction in measured pO_2 levels that is not reflective of a corresponding reduction in clonogenic survival of the tumour cells (Fenton *et al*, 1995). This leads to overestimates of the fraction of radiobiologically resistant tumour cells. In the case of hypoxia markers, regions of necrosis can also lead to inaccurate predictions in overall tumour hypoxia. Since these drugs are not metabolized in necrotic areas, such regions appear well oxygenated and lead instead to an underestimate of overall tumour hypoxia.

Several recent studies have described methods for quantifying hypoxia marker distribution as a function of distance from either perfused or anatomical blood vessels. The first (Rijken *et al*, 2000) is an elegant, multiparameter analysis of vascularity, perfusion, and hypoxia that characterises uptake of two hypoxia markers, NITP and pimonidazole, in relation to perfused vasculature. The second (Vukovic *et al*, 2001) focuses primarily on the spatial distribution of EF5 in relation to total vasculature. A potential limitation in each of these studies is the characterisation of hypoxia marker labelled cells as either positive or negative, thus ignoring any information regarding relative intensity of the marker. Since hypoxia clearly increases continuously with increasing distance from blood vessels, such a conversion of hypoxia marker intensity levels to binary images results in the loss of potentially important information regarding intermediate regions of hypoxia.

The current work presents several refinements of earlier methods: (1) Hypoxia marker images are quantified in terms of their intensity levels, thus providing an analysis of the rate at which hypoxia increases with increasing distances from blood vessels. This measurement is directly related to oxygen consumption by the tumour tissue and provides an estimate of intravascular oxygen levels. (2) Improved image analysis techniques are described for defining zonal imaging masks, thereby permitting spatial sampling of immunohistochemical images at precisely defined distances from blood vessels. (3) Thresholding techniques are described for removing artifactual holes in the tissue sections. (4) Distance mapping is used to define vascular spacing. Although previous studies (Vukovic *et al*, 2001; Rijken *et al*, 2000) have used adjacent sections for the removal of gross necrosis, the current study utilized haematoxylin and eosin staining of the same frozen sections used for hypoxia marker and vascular imaging.

MATERIALS AND METHODS

Tumour model

Cells from MCa-4 murine mammary carcinomas were inoculated into the mammary fat pads of C3H/HeJ mice. Guidelines for the

*Correspondence: B Fenton; Box 704, University of Rochester Medical Center, Rochester, NY 14642, USA; E-mail: bruce.fenton@rochester.edu
Received 10 December 2001; revised 4 April 2002; accepted 4 April 2002

humane treatment of animals were followed as approved by the University Committee on Animal Resources and meet the standards required by the UKCCCR guidelines (Workman *et al*, 1998).

$DiOC_7$ perfusion marker and EF5 hypoxic marker

To visualise blood vessels open to flow, an intravascular injected stain, $DiOC_7$, was injected 1 min prior to tumour freezing (Trotter *et al*, 1989). This agent has been shown to provide optimal visualisation of tumour blood vessels by preferentially staining cells immediately adjacent to the vessels (Fenton *et al*, 1999). Localised areas of tumour hypoxia were assessed in 9 μm frozen tissue sections by immunohistochemical identification of sites of 2-nitroimidazole metabolism as described previously (Fenton *et al*, 1999). A pentafluorinated derivative (EF5) of etanidazole was injected i.v. 1 h before tumour freezing, at which time the EF5 has been shown to be well distributed throughout even poorly perfused regions of the tumour (Fenton *et al*, 2001a). Regions of high EF5 metabolism were visualised immunohistochemically using a fluorochrome (Cy3, Amersham) conjugated to the ELK3-51 monoclonal antibody. This antibody is extremely specific for the EF5 drug adducts that form when the drug is incorporated by hypoxic cells (Lord *et al*, 1993). Both the EF5 (made by the NCI) and the ELK3-51 were obtained from the University of Pennsylvania Imaging Service Center (C Koch, Director).

Immunohistochemistry and image acquisition

Tumour sections were imaged using a Nikon microscope (20× objective), digitised (FlashPoint frame grabber and Sony DXC9000 3CCD camera), background-corrected, and image-analysed using Image-Pro software (version 4.5, Media Cybernetics, Silver Spring, MD, USA) with a 800 MHz Pentium computer, as previously described (Fenton *et al*, 1999). Colour images from the same 16 adjacent microscope fields were automatically acquired and digitally combined under four different staining conditions, using a Prior computer interfaced stage and Prior controller to revisit the same stage co-ordinates. First, epi-illumination images of the fluorescent green $DiOC_7$(3) staining were obtained immediately after the sections were sliced on the cryostat. Following immunohistochemical staining, the tumour section was returned to the same stage co-ordinates, and fluorescent red–orange images were acquired of the distribution of the EF5/Cy3. Next, using transmitted light, matching brownish–red montages of the CD31 endothelial staining were acquired. Finally, sections were stained for haematoxylin and eosin and again imaged at the same coordinates.

Image processing techniques

To quantitate microregional EF5/Cy3 intensities variations as a function of distance from perfused blood vessels, methods somewhat similar to those of Rijken *et al* (2000) were utilised. As summarised in Figure 1, CD31 (total blood vessels) and $DiOC_7$ (perfused blood vessels) stained images were enhanced by first using colour segmentation to identify blood vessels (Fenton *et al*, 1999). For CD31 staining, specific intensity thresholds (using the HSI colour model) were interactively selected and accumulated to obtain optimal discrimination of vessels and stroma, and a binary image of the selected colours was created (Figure 1A). For $DiOC_7$ staining, the Image-Pro 'automatic bright' thresholding was used (Figure 1B). For counting either perfused or total vessels, objects of area less than 10 μm^2 (roughly 3.5 μm^2 in diameter, to eliminate nonvascular artifacts) were removed, and an area of interest was outlined to omit sectioning artifacts and normal tissue. This binary image was next inverted and a 'distance filter' applied, which replaces the intensity of each pixel with an intensity proportional to the distance of that pixel from the nearest vessel (Figure 1C). Thus, pixels immediately adjacent to the vessels were assigned intensity 1 in the new image, and the intensities of more distant pixels increase by one grey level for each one pixel increase in distance from the vessel edge. This distance filtered image was then successively thresholded and binarized to select regions of the image within specific distances from vessels. For example, thresholding between 1–20 grey levels selects a zone 1–20 pixels away from a vessel, 21–40 selects a zone from 21–40 pixels away from a vessel, and so on. Figure 1D illustrates the binary image resulting from thresholding between grey levels of 21–40, which selects a region within approximately 21–40 microns of the nearest vessel, since each pixel is approximately one micron square.

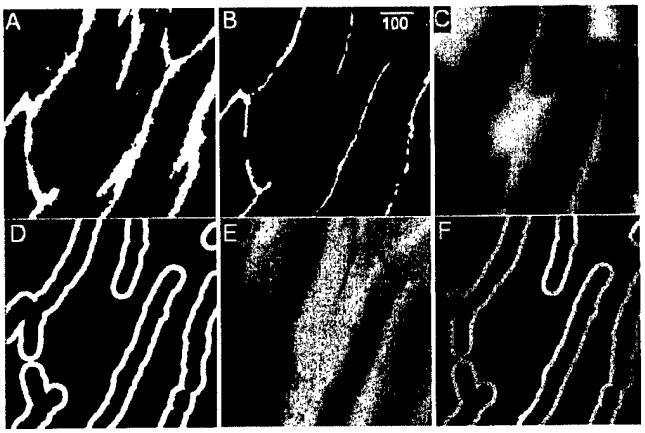

Figure 1 Zonal image analysis procedures: (**A**) binary image of total blood vessels (CD31 stained vessels are shown in white), (**B**) binary image of perfused vessels ($DiOC_7$ vessels shown in white, scale=100 μm), (**C**) distance map of perfused blood vessels, (**D**) zonal mask of pixels 21–40 μm from perfused vessels, (**E**) EF5/Cy3 staining (lighter shades correspond to increased tumour hypoxia), (**F**) logical 'AND' of the zonal mask and EF5/Cy3 images, which selectively samples the distribution of EF5/Cy3 intensities within this specific zone.

For the EF5/Cy3 images (Figure 1E), holes in the immunohistochemical sections were automatically removed by interactively thresholding on the image to convert the pixel intensities of holes in the tissue section to zero. Finally, the binary 'mask' (Figure 1D) was combined with the corresponding EF5/Cy3 image (Figure 1E), using the logical 'AND' to obtain an image in which only those regions of the EF5/Cy3 image within the 21–40 μm zone are included (Figure 1F). This allows the determination of the EF5/Cy3 intensity distribution within a precisely defined distance from the blood vessels. Using the same sequence of steps, EF5/Cy3 intensities within each successive concentric zone were also obtained and median intensity levels were plotted as a function of distance from the nearest perfused or total vessel.

Regions of gross necrosis were selected visually from the haematoxylin and eosin images and outlined using the multiple area of interest (AOI) tool. Regions inside or outside of the AOI were converted to a binary mask (set to black or white, respectively), and percent gross necrosis was determined by the Image-Pro intensity 'range statistics' function. Finally, necrosis correction was applied to the zonal analysis by performing a logical 'AND' on the binary necrosis image and the corresponding zonal EF5/Cy3 image (Figure 1F). This converts necrotic intensities to zero while leaving other intensities unaltered, and the zero intensity regions are excluded from the analysis.

RESULTS

Figure 2 presents EF5/Cy3 intensities as a function of distance from the nearest total blood vessel, each point representing the median EF5/Cy3 intensity within a specific 20 μm wide zone (as detailed

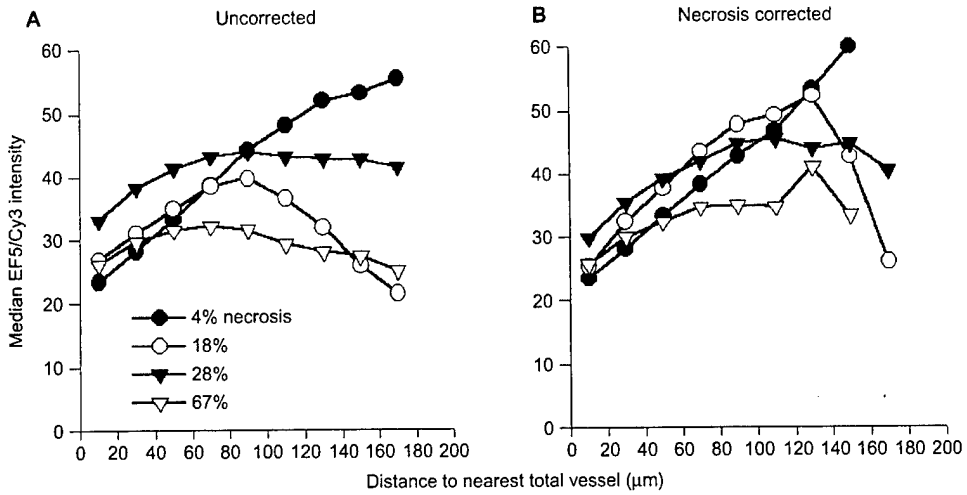

Figure 2 Effect of necrosis on median EF5/Cy3 intensities as a function of distance from nearest total blood vessel (CD31 staining). Each curve is based on the combination of four image montages from a single untreated tumour, and percentages of gross necrosis and tumour volumes are as follows: filled circles=4%, 520 mm^3; open circles=18%, 900 mm^3; filled triangles=28%, 1150 mm^3; open triangles=67%, 1770 mm^3. Intensities are presented as the median intensity within each 20 μm wide zone.

in Materials and Methods). The four curves in each panel correspond to MCa-4 tumours of increasing tumour volume, with correspondingly increasing percentages of gross necrosis. The slopes of these curves are directly related to the oxygen consumption of the surrounding tumour cells. Thus, steeper slopes, which are indicative of a rapid increase in hypoxia with increasing distance from the perfused vessels, correspond to increased consumption rates. Median EF5/Cy3 intensities of the innermost zone (1–20 μm from the vessels) are most reflective of the adjacent intravascular oxygen levels.

In Figure 2A, the filled circles correspond to a tumour of 4% gross necrosis, and median EF5/Cy3 intensities increase progressively with increasing distance from the nearest total blood vessel (reflecting the expected increase in tumour hypoxia with increasing distance from a vessel). With increasing percentages of necrosis, the curves of Figure 2A become less predictable, and in some cases tend to become less rather than more hypoxic at the longest distances from the vessels. In Figure 2B, gross necrotic regions have been removed as detailed in the Materials and Methods, and the analyses of Figure 2A have been repeated. Although the curves are altered somewhat by this correction, the unexpected decrease in hypoxia at the highest distances was still observed for some tumours (in particular the open circles). This decrease is possibly due to the influence of regions of necrosis that were too small to be included in the gross necrosis correction, which would be more likely to be found near nonfunctional vessels than near perfused blood vessels. In addition, the fraction of the total tumour area included in a given zone decreases at increasing distances from the vessels, due to the overlap of adjacent zones from nearby vessels (especially for the total vessels, which are more densely distributed). At distances greater than 140 μm, zones around total vessels can encompass less than 1% of the total tumour area, leading to an increase in sampling variability in these zones.

Figures 3A and B depict analyses similar to those of Figure 2, but plotted as a function of distance from perfused vessels rather than total blood vessels. Compared with Figure 2A, the median intensities for the 0–20 zone (nearest the blood vessels) in Figure 3A are decreased. This shift is due to the inclusion of nonfunctional vessels in the total vessel plots of Figure 2A. Tumour cells around these vessels will more likely be hypoxic, and the shift between the total and perfused intensity plots is therefore a reflection of vessel functionality in a given tumour. Thus the larger intensity shift for the tumour represented by the solid triangles is suggestive of a higher proportion of nonfunctional vessels in this particular tumour, compared with the remaining three tumours. For the uncorrected analyses (Figure 3A), all tumours showed a distinct peak in EF5/Cy3 intensities at distances between 100–150 μm, followed by a distinct decline. After necrosis correction (Figure 3B), the shape of each of these curves was dramatically altered such that EF5/Cy3 intensities generally tended to plateau at distances of about 120–130 μm from the nearest vessel.

Figure 4 presents the effects of tumour growth, antiangiogenic treatment, and irradiation, to illustrate the influence of different pathophysiological alterations on zonal variations in hypoxia. Untreated controls are plotted as filled symbols (filled circles=840 mm^3 tumour volume and filled triangles=1280 mm^3). For three of the four curves in Figure 4 (those in which tumour volumes are closely matched), a peak in EF5/Cy3 intensities is observed at the 140–160 μm zone. However, for the larger volume tumours (filled triangles), this peak is shifted to the left. During tumour growth, tumour cells tend to either outgrow or compress their own vasculature, leading to an overall increase in hypoxia (as evidenced by the upward shift in EF5/Cy3 intensities compared to the smaller volume controls) and necrosis. In support of such an increase in necrosis, the larger volume curve takes a downward turn at shorter distances from perfused blood vessels than does the smaller volume curve (since necrotic areas do not metabolize EF5, such regions will remain black and decrease median EF5/Cy3 intensities).

The effect of three daily doses of the anti-angiogenic agent, endostatin (20 mg/kg/day), is shown by the open circles. Here, a slight but insignificant improvement in both intravascular and tumour oxygenation is apparent. EF5/Cy3 intensities are similar for the zone immediately surrounding the blood vessels (1–20 μm distances), and these intensities increase with increasing distance from a vessel at approximately the same rate as for controls. The effect of a single dose of 30 Gy irradiation on this curve is quite different (as shown by the open triangles). Compared to volume-matched controls (filled circles), irradiated tumours had slightly lower intravascular oxygen levels (as evidenced by the intensities at the shortest distance zone), and the slope of the curve is substantially less steep. This decrease in slope in the irradiated tumours could be indicative of a decrease in oxygen consumption in the radiation-sterilized tumour cells or an increased proportion of quiescent cells.

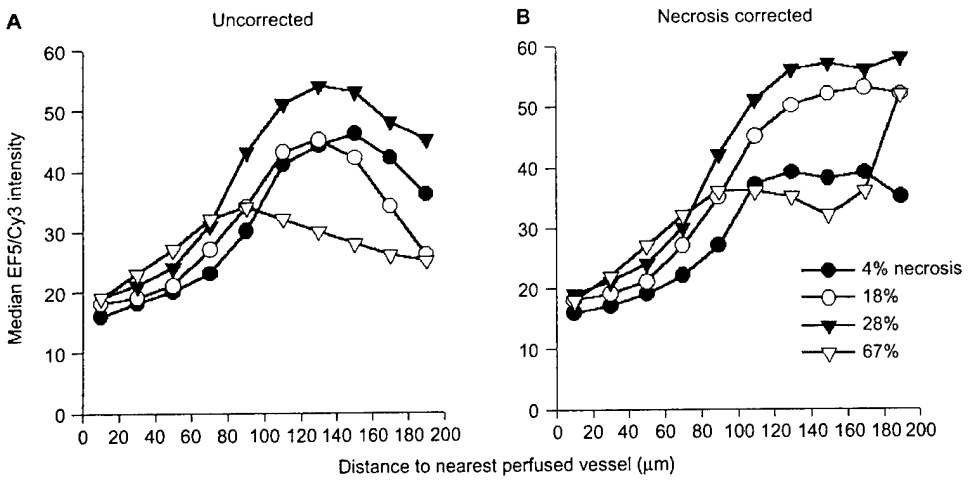

Figure 3 Effect of necrosis on median EF5/Cy3 intensities as a function of distance from nearest perfused blood vessel ($DiOC_7$ staining). Each curve is based on images from the same untreated tumours of Figure 2. See Figure 2 for legend.

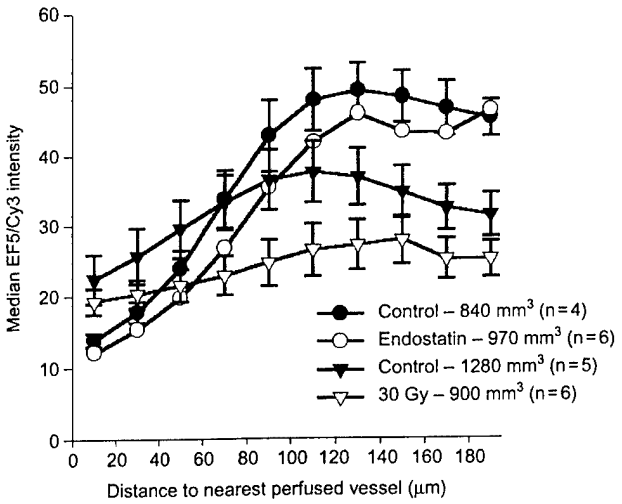

Figure 4 Effect of tumour volume and treatment on median EF5/Cy3 intensities as a function of nearest perfused ($DiOC_7$ staining) blood vessel (mean ± s.e.m., based on 4–6 tumours per group). filled circles=840 mm^3 controls, open circles=970 mm^3 endostatin treated tumours, filled triangles=1280 mm^3 controls, open triangles=900 mm^3 30 Gy irradiated tumours (none corrected for necrosis). For clarity, the s.e.m. are omitted for the 30 Gy and 1280 mm^3 control tumours.

DISCUSSION

Both Eppendorf micro-electrode measurements and hypoxia marker uptake have been extensively used for gauging inter- and intratumoral variations in oxygenation. A disadvantage of the Eppendorf is that pO_2 levels can only be obtained at discrete locations along the needle track (roughly every 400 μm), although multiple tracks can also be measured. In contrast, immunohistochemical staining of hypoxia markers permits microregional variations in hypoxia to be spatially mapped in two dimensions across an entire tumour section. By comparing the hypoxia marker images with corresponding images of vessel staining, proliferation markers, or angiogenic/anti-angiogenic cytokines, relationships among a variety of pathophysiological factors can also be correlated (Fenton *et al*, 2001b; Wijffels *et al*, 2001; Rijken *et al*, 2000; Zeman *et al*, 1993).

Although image analysis techniques are an indispensable aid in quantifying these types of images, automated counting procedures are not necessarily straight-forward. Perhaps the most difficult step in the analysis is the separation of countable objects from background using either image thresholding or colour segmentation. Previous studies have evaluated the effect of different threshold choices on hypoxic fraction, as determined by percentage hypoxia marker positive pixels (Rijken *et al*, 2000). These authors found that changing the threshold intensity by only two levels in either direction (in an image with 256 grey levels) resulted in a change of from 14–21% in the calculated hypoxic fraction for NITP staining. A change of four levels in the threshold intensity resulted in up to a 57% increase in the calculated hypoxic fraction. As these authors recommend, the selection of a constant threshold is essential when attempting to classify hypoxic tumours cells as simply positive or negative. An advantage of the current methods is that the hypoxia marker intensity levels of each pixel are also quantified. This means that the selection of an arbitrary threshold of hypoxia is not required. Constant threshold settings can be used for defining vascular structures, providing the fluorescent intensities or colours of the objects are sufficiently different from background (Vukovic *et al*, 2001; Rijken *et al*, 2000). However, images of immunostained sections can vary substantially under fluorescent and especially transmission microscopy, even within a given experiment. In such cases, manual thresholding or colour segmentation is often necessary for each image.

When analysing the intensities of fluorescently conjugated hypoxia markers, an essential first step is the calibration of the illumination source, as has been previously described in detail (Jenkins *et al*, 2000). To next quantify the distribution of hypoxia marker uptake, the most common approach has been to measure the percentage of the tumour section that is positively stained (Raleigh *et al*, 2001). Although this analysis is relatively straight-forward and corresponds to the notion of tumour hypoxic fraction, a substantial amount of information is not taken into account. Another approach has been to measure mean hypoxia marker intensities (Evans *et al*, 2001; Fenton, 2001; Fenton *et al*, 2001b), which again provides only an overall appraisal of changes in tumour hypoxia. Here, results can be especially misleading in the presence of large regions of necrosis, which do not metabolize EF5. Since hypoxia marker uptake has been clearly shown to depend proportionately on tissue pO_2 levels (Jenkins *et al*, 2000; Koch *et al*, 1995), both intensity changes of the markers and their relationships to surrounding blood vessels are vital to fully describe microregional pathophysiological gradients.

Another potential problem in the automated analysis of vascular images lies in the determination of vascular density. The field shown in Figure 1B clearly includes five perfused blood vessels (based on the total vessel staining shown in Figure 1A). However, an automated count of this image would result in a much higher number of objects, corresponding to each of the discrete segments of each vessel. Although various image filtering operations can be utilized to close the gaps between these segments, such operations can also dramatically alter parameters such as vessel diameters and areas. Single vessels can also meander in and out of a thin frozen section and therefore be counted multiple times. Both of these difficulties are minimized by an alternative method for analysing vascular spacing, based on the perfused vessel distance map shown in Figure 1C. Following distance map filtering, individual pixel intensities are converted to levels directly proportional to the distances between tumour cells and the nearest blood vessel. If this distance map is next combined with a predefined image of white grid points (e.g., 50 μm spacing) on a black background using the image multiplication operator, the distance map intensities can be spatially sampled, which are directly proportional to the distribution of distances to the nearest vessel. This provides a histogram of the distribution of distances that oxygen and nutrients must diffuse to reach all points in the tumour, and an increase in this median distance thus corresponds to a decrease in vascularity. Although somewhat less intuitive than vascular density measures, the median of these distances provides a much more reliable method for quantifying changes in vascular spacing than does vascular density when using automated image analysis techniques.

It is possible that out-of-plane vessels may be an additional contributory factor to the decrease in hypoxia observed at higher distances from blood vessels. Since all images are based on two-dimensional slices through the tumours, vessels outside of the image plane are ignored. Thus EF5/Cy3 intensities could be locally reduced despite the absence of visible perfused vessels. Although this could potentially alter the relationship between EF5/Cy3 intensity and distance to the nearest vessel, such occurrences are expected, for the most part, to follow the distribution of visible vessels. Regions with high vascular densities will thus be more likely to have accompanying out of plane branches than regions of low vascular density. Although such out of plane branches would result in a decrease in absolute EF5/Cy3 intensities in associated regions, the effects should be similar for different treatment groups and are not expected to mask relative differences among groups.

The currently described zonal analysis of EF5/Cy3 intensities provides a comprehensive description of changes in tumour hypoxia as a function of distance to the nearest blood vessel. Compared with previous methods that utilize either dilation filters (Rijken *et al*, 2000) or square masks (Vukovic *et al*, 2001), these improved techniques permit the limits of each zone to be precisely defined based on a combination of distance mapping and thresholding operations. Although the presence of necrotic regions can have substantial effects on relative EF5/Cy3 intensities at increasing distances from vessels, these artifacts can be minimized if the analysis is limited to regions less than approximately 100–120 μm from blood vessels. This means that a laborious manual definition of necrotic regions from the H&E images is unnecessary if the zonal analysis is limited to this distance range. From this type of microregional analysis, relative changes in tumour cell oxygen consumption rates and intravascular oxygenation (which relates to vascular functionality) can both be estimated. Finally, by comparing changes in the distributions of hypoxic marker intensities around total *vs* perfused vessels, a relative index of the proportion of functional blood vessels in a given tumour can also be derived.

ACKNOWLEDGEMENTS

Financial support was provided by NIH Grant CA52586 and DOD Grant DAMD17-00-1-0420.

REFERENCES

Brizel DM, Scully SP, Harrelson JM, Layfield LJ, Bean JM, Prosnitz LR, Dewhirst MW (1996) Tumor oxygenation predicts for the likelihood of distant metastases in human soft tissue sarcoma. *Cancer Res* **56:** 941–943

Evans SM, Hahn SM, Magarelli DP, Zhang PJ, Jenkins WT, Fraker DL, Hsi RA, Mckenna WG, Koch CJ (2001) Hypoxia in human intraperitoneal and extremity sarcomas. *Int J Radiat Oncol Biol Phys* **49:** 587–596

Fenton BM (2001) Influence of hydralazine administration on oxygenation in spontaneous and transplanted tumor models. *Int J Radiat Oncol Biol Phys* **49:** 799–808

Fenton BM, Kiani MF, Siemann DW (1995) Should direct measurements of tumor oxygenation relate to the radiobiological hypoxic fraction of a tumor? *Int J Radiat Oncol Biol Phys* **33:** 365–373

Fenton BM, Lord EM, Paoni SF (2001a) Effects of radiation on tumor intravascular oxygenation, vascular configuration, hypoxic development, and survival. *Radiat Res* **155:** 360–368

Fenton BM, Lord EM, Paoni SF (2001b) Intravascular HBO_2 saturations, perfusion and hypoxia in spontaneous and transplanted tumor models. *Int J Cancer* **93:** 693–698

Fenton BM, Paoni SF, Lee J, Koch CJ, Lord EM (1999) Quantification of tumor vascular development and hypoxia by immunohistochemical staining and HbO_2 saturation measurements. *Br J Cancer* **79:** 464–471

Hockel M, Schlenger K, Aral B, Mitze M, Schaffer U, Vaupel P (1996) Association between tumor hypoxia and malignant progression in advanced cancer of the uterine cervix. *Cancer Res* **56:** 4509–4515

Hodgkiss RJ, Wardman P (1992) The measurement of hypoxia in tumours. *BJR Suppl* **24:** 105–110

Jenkins WT, Evans SM, Koch CJ (2000) Hypoxia and necrosis in rat 9L glioma and Morris 7777 hepatoma tumors: Comparative measurements using EF5 binding and the Eppendorf needle electrode. *Int J Radiat Oncol Biol Phys* **46:** 1005–1017

Koch CJ, Evans SM, Lord EM (1995) Oxygen dependence of cellular uptake of EF5 [2-(2-nitro-1H-imidazol-1-yl)-N-(2,2,3,3,3-pentafluoropropyl)acetamide] – analysis of drug adducts by fluorescent antibodies *vs* bound radioactivity. *Br J Cancer* **72:** 869–874

Lord EM, Harwell L, Koch CJ (1993) Detection of hypoxic cells by monoclonal antibody recognizing 2-nitroimidazole adducts. *Cancer Res* **53:** 5721–5726

Raleigh JA, Chou SC, Bono EL, Thrall DE, Varia MA (2001) Semiquantitative immunohistochemical analysis for hypoxia in human tumors. *Int J Radiat Oncol Biol Phys* **49:** 569–574

Raleigh JA, Miller GG, Franko AJ, Koch CJ, Fuciarelli AF, Kelly DA (1987) Fluorescent immunohistochemical detection of hypoxic cells in spheroids and tumors. *Br J Cancer* **56:** 395–400

Rijken PFJW, Bernsen HJJA, Peters JPW, Hodgkiss RJ, Raleigh JA, van der Kogel AJ (2000) Spatial relationship between hypoxia and the (perfused) vascular network in a human glioma xenograft: A quantitative multi-parameter analysis. *Int J Radiat Oncol Biol Phys* **48:** 571–582

Trotter MJ, Chaplin DJ, Olive PL (1989) Use of a carbocyanine dye as a marker of functional vasculature in murine tumours. *Br J Cancer* **59:** 706–709

Vukovic V, Haugland HK, Nicklee T, Morrison AJ, Hedley DW (2001) Hypoxia-inducible Factor-1alpha is an intrinsic marker for hypoxia in cervical cancer xenografts. *Cancer Res* **61:** 7394–7398

Wijffels KI, Kaanders JH, Marres HA, Bussink J, Peters HP, Rijken MSP, van den Hoogen FJ, de Wilde PC, van der Kogel AJ (2001) Patterns of proliferation related to vasculature in human head-and-neck carcinomas before and after transplantation in nude mice. *Int J Radiat Oncol Biol Phys* **51:** 1346–1353

Workman P, Twentyman P, Balkwill F, Balmain A, Chaplin D, Double J, Embleton J, Newell D, Raymond R, Stables J, Stephens T, Wallace J (1998) United Kingdom co-ordinating committee on cancer research (UKCCCR) Guidelines for the welfare of animals in experimental neoplasia (Second edition). *Br J Cancer* **77:** 1 – 10

Zeman EM, Calkins DP, Cline JM, Thrall DE, Raleigh JA (1993) The relationship between proliferative and oxygenation status in spontaneous canine tumors. *Int J Radiat Oncol Biol Phys* **27:** 891 – 898

DISPARATE EFFECTS OF ENDOSTATIN ON TUMOR VASCULAR PERFUSION AND HYPOXIA IN TWO MURINE MAMMARY CARCINOMAS

Bruce M. Fenton, Ph.D.[1], Scott F. Paoni, M.S.,

Brian G. Grimwood, Ph.D., and Ivan Ding, M.D.

Department of Radiation Oncology (B.M.F., S.F.P., I.D.),

University of Rochester Medical Center, Rochester, NY 14642, and

Wadsworth Center, NY State Department of Health (B.G.G.), Albany, NY 12201

The authors would like acknowledge the technical assistance of Mr. Brian Beauchamp, Dr. Li Liang, and Dr. Weimin Liu. Financial support was provided by NIH Grant CA52586 and DOD Grant DAMD17-00-1-0420.

Running Title: Endostatin effects on tumor perfusion and hypoxia

[1]To whom correspondence should be sent at:

Address: Box 704, University of Rochester Medical Center, Rochester, NY 14642

Telephone: 585-275-7911

Fax: 585-273-1042

Email: bruce.fenton@rochester.edu

ABSTRACT:
Purpose: Recent results in the literature have demonstrated that the antiangiogenic agent, endostatin, can enhance antitumor effects when administered prior to or during radiotherapy. In order to better understand the underlying pathophysiological basis for this radiosensitization, the current study investigated whether short-term endostatin administration may be linked alterations in tumor vascular perfusion and oxygen delivery.
Methods and Materials: Three daily doses of recombinant endostatin (20 mg/kg) were administered to two murine mammary carcinomas, the highly vascularized MCa-35 and the less vascularized and more differentiated MCa-4. Image analysis techniques were used to quantify: 1) total and perfused vascular spacing, and 2) changes in tumor hypoxia as a function of distance from the nearest blood vessel.
Results: In MCa-35 tumors, endostatin had no effect on vessel spacing, tumor hypoxia, or tumor growth. In MCa-4 tumors, total and perfused vessel spacings were also unchanged, but tumor growth was inhibited and tumor hypoxia significantly decreased. Tumors that responded to endostatin treatment demonstrated an increased vascular functionality without corresponding alterations in tumor oxygen consumption rate.
Conclusions: Striking intertumoral disparities in pathophysiological properties were observed between responders and nonresponders following short-term endostatin administration. Such disparate effects could have substantial implications in determining ultimate therapeutic effectiveness when antiangiogenic agents are combined with conventional therapies.

Key Words: antiangiogenesis, blood flow, hypoxia marker, image analysis, tumor oxygenation

INTRODUCTION

The dependence of tumor growth on the concomitant development of new blood vessels (angiogenesis) has been documented in numerous reports beginning over 30 years ago (1-3). Both experimental and clinical studies have utilized a number of therapeutic approaches with a wide variety of antiangiogenic drugs (4;5). Endostatin, a fragment of collagen XVIII, has been shown to potently inhibit both tumor angiogenesis and the growth of experimental tumors, primarily through inhibition of endothelial cell migration and proliferation, as well as induction of endothelial cell apoptosis, with minimal direct effects on tumor cells (6-8). Several studies have also demonstrated that short courses of naturally occurring antiangiogenic factors, such as endostatin and angiostatin, can enhance the antitumor effects of radiation when administered before or during radiotherapy (9;10). *In vitro* studies by these same authors have demonstrated that endostatin enhances the cytotoxic effects of irradiation on endothelial cells but not on tumor cells.

In addition to directly targeting the endothelial compartment, endostatin could also conceivably alter tumor radiosensitivity through pathophysiological changes in the tumor microenvironment, most notably alterations in blood flow and oxygen delivery. In general, antiangiogenic approaches would probably be expected to decrease tumor oxygen levels through reductions in tumor vasculature, as has been recently reported in response to anti-VEGFR-2 treatment (11). However, the situation is complicated by the

relationship between the relative proliferation rates of endothelial cells versus tumor cells, making predictions difficult. The current work was undertaken to investigate the effects of endostatin on tumor microregional perfusion and hypoxia, to clarify such underlying pathophysiological changes. Since the primary purpose was to quantitate the immediate pathophysiological response, a relatively short-term course of only three days of endostatin treatments was administered. During this brief period, untreated tumors tripled in volume, suggesting a significant concomitant growth in neovasculature. By applying a combination of immunohistochemical staining and zonal image analysis on multiple images taken from the same frozen sections, microregional changes in hypoxia were detailed in relation to vascular function.

METHODS AND MATERIALS

Tumor models. Tumor cells (3×10^6, suspended in saline) from MCa-4 or MCa-35 murine mammary carcinomas were inoculated *i.m.* into the upper legs of 6-8 week-old female C3H/HeJ mice (The Jackson Laboratory, Bar Harbor, ME). Tumor volumes were measured by calipers and the formula: volume = π diameter^3/6. Guidelines for the humane treatment of animals were followed as approved by the University Committee on Animal Resources.

Expression, purification, and administration of mouse endostatin (rmNYendo). Mouse cDNA, provided by T. Boehm (Children's Hospital, Harvard Medical School, Boston, MA) in the pET 11d was amplified by PCR. After sequence verification, the gene was cloned into the pMAL-p2 vector (New England Biolabs, Beverly, MA), which created a fusion protein consisting of maltose binding protein, a Factor Xa susceptible sequence, and endostatin, following established procedures (12). After induction and extraction from the periplasm by polymyxin B, the soluble fusion protein was purified by chromatography on Q-sepharose, digested with Factor Xa, and rechromatographed on Q-sepharose. The rmNYendo preparations were then examined for homogeneity and molecular weight by SDS-PAGE and mass spectroscopy, and stored at 4 degrees C. When tumors had grown to between 200-400 mm^3, recombinant murine endostatin was administered *i.p.* at 20 mg/kg for three consecutive days. Tumors were frozen at 3, 6, or 7 days following initiation of treatment.

$DiOC_7$ perfusion marker and EF5 hypoxic marker. To visualize blood vessels open to flow, an intravascular stain, $DiOC_7$, (Molecular Probes, Eugene, OR) was injected that preferentially stains cells immediately adjacent to the vessels (13). Localized areas of tumor hypoxia were assessed in 9.0 μm frozen tissue sections by immunohistochemical identification of sites of 2-nitroimidazole metabolism (14). A pentafluorinated derivative (EF5) of etanidazole was injected *i.v.* one hour before tumor freezing, at which time the EF5 has been shown to be well distributed throughout the tumor (15). Regions of high EF5 metabolism were visualized immunohistochemically using a fluorochrome (Cy3, Amersham, Piscataway, NJ) conjugated to the ELK3-51 antibody, which is extremely specific for the EF5 adducts that form when the drug is incorporated by hypoxic cells (16). Both the EF5 (made by the NCI) and the ELK3-51 were obtained from the University of Pennsylvania Imaging Service Center (C. Koch, Director).

Immunohistochemistry and image acquisition. Tumor sections were imaged using a 20× objective, digitized (Sony DXC9000 3CCD camera), background-corrected, and

image-analyzed using Image-Pro software (Media Cybernetics, Silver Spring, MD) (14). Color image montages from 16 adjacent microscope fields in each of four tumor regions (a total area of 15.5 mm^2) were automatically acquired and digitally combined under four different staining conditions. First, images of the $DiOC_7$ were obtained immediately after the sections were sliced on the cryostat. Following staining, the section was returned to the same stage coordinates, and both EF5/Cy3 and anti-CD31 (Pharmingen, San Diego, CA) images were acquired. Finally, sections were stained and imaged for hematoxylin and eosin (H&E). Anti-CD105 staining (Pharmingen), which is reportedly more specifically reactive with endothelial cells of blood vessels in tissues undergoing angiogenesis (17), was also utilized on selected tumors.

Image analysis – Zonal hypoxia analysis. To quantitate microregional EF5/Cy3 intensity variations (hypoxia) as a function of distance from perfused blood vessels, zonal analysis methods were utilized, as previously described in detail (18). Briefly, $DiOC_7$(3) images were first automatically color segmented to identify perfused blood vessels, and a binary image of the selected colors was created. This image was inverted and a "distance filter" applied, which replaces the intensity of each pixel with an intensity proportional to the distance of that pixel from the nearest perfused vessel. Thus, pixels immediately adjacent to the vessels were assigned intensity 1, and intensities of more distant pixels were increased by one gray level for each one pixel increase in distance from the vessel. This distance filtered image was successively thresholded and binarized to select regions of the image within specific distances around perfused vessels. For example, thresholding between 1-20 gray levels selects a zone from 1-20 pixels away from a vessel. This binary mask was then multiplied by the corresponding EF5/Cy3 image to obtain an image in which only those regions of the EF5/Cy3 image within each zone were included, and mean EF5/Cy3 zonal intensities were determined.

Image analysis – Vascular spacing and percent necrosis. Following distance map filtering of the vascular images, individual pixel intensities were converted to levels directly proportional to the distances between tumor cells and the nearest blood vessel. This distance map was combined with a predefined image of white grid points on a black background using the image multiplication operator to obtain a spatial sampling of the distance map intensities, which are directly proportional to the distribution of distances to the nearest vessel (18). Finally, regions of gross necrosis were visually selected on the H&E images and outlined with the Image Pro multiple area of interest (AOI) tool. Percentage necrosis was found by converting AOIs to objects, creating a mask, and using pseudo-color to determine the % area.

Image analysis – Detection of apoptosis and proliferation. Apoptotic assays were performed on 5 micron frozen sections following the directions from the Intergen Apoptag Fluorescein In Situ Apoptosis Detection Kit (Purchase, NY). Proliferation assays were also performed on adjacent frozen sections using a rat anti-mouse Ki-67 monoclonal antibody (clone TEC-3 from Dako Corporation, Capinteria, Ca) and a mouse anti-rat HRP-conjugated secondary antibody (Jackson Immunoresearch Laboratories, West Grove, PA) with AEC detection (Vector, Burlingame, CA). Both stains were quantified using zonal analysis methods similar to those described above. Instead of determining image intensity, however, zonal distributions of % area positive staining were determined using color segmentation methods to select positively stained cells.

Statistical Analysis. Tumor means were compared using the Student's t-test or the

Mann-Whitney Rank Sum test and were considered significant for $p < 0.05$. Slopes and intercepts of the zonal analyses were compared using multiple linear regressions on log transformed EF5 intensities.

RESULTS

Tumor growth delay. To determine the overall effects of short-term administration of endostatin on tumor growth, tumor diameters were measured daily beginning at the start of treatment. Figure 1 summarizes the results for both MCa-4 and MCa-35 tumors. At day 3 (1 day following the last endostatin dose), treated MCa-4 tumors were somewhat smaller than untreated controls, and by day 7, differences were more substantial ($p = 0.05$). For the MCa-35 tumors, no alterations in tumor growth were observed following endostatin administration.

Percentage necrosis. Percentage gross necrosis was determined in treated and control MCa-4 tumors at days 3 and 7 (Table I). Although a trend towards reduced necrosis was evident in the day 3 endostatin treated tumors (6.5 % necrosis versus 18.3 % for controls), this was not significant ($p = 0.07$). Within the treated tumors, however, necrosis increased significantly to 31.4 % at day 7 ($p = 0.002$), similar to the 25.2 % necrosis observed in the day 7 control tumors. Since untreated tumors were much larger at this time (1600 mm^3 versus 1200 mm^3 for endostatin treated tumors), % necrosis would also have been expected to be higher in these tumors.

Vascular and hypoxia marker staining. Figure 2 presents representative immunohistochemical staining for MCa-4 versus MCa-35 tumors and illustrates the disparate vascular and hypoxia marker staining observed. Figure 1A shows the anti-CD31 staining of blood vessels in the MCa-4 tumors, a well-differentiated murine mammary tumor. Figure 1B details regions of EF5 uptake (tumor hypoxia) in the same section. A high degree of colocalization exists, with increased hypoxia marker intensities almost invariably found at locations distant from the nearest blood vessel. For the MCa-35 tumors (Figures 2C and 2D), a more aggressive, poorly differentiated mammary tumor, vascular densities were much higher and demonstrated little of the glandular structure of the MCa-4 tumors. Vessel diameters were also substantially reduced in the MCa-35 tumors, quite unlike the large sinusoidal vessels of the MCa-4 tumors. In line with the increased vascular densities, hypoxia marker intensities were significantly reduced throughout the MCa-35 tumors.

Total and perfused vessel spacing. Quantitative results from the image analysis of the total and perfused blood vessels in the two tumor types are presented in Figure 3. Here, tumor blood vessels are characterized in terms of the median distance between tumor cells and the nearest total (CD31 staining) or perfused ($DiOC_7$ staining) blood vessel, which represents the median distance that oxygen or nutrients require to diffuse to all regions of the tumor (14). For the untreated MCa-4 tumors (Figure 3A), neither total nor perfused vessel spacings changed significantly between days 3 and 7. Median distances to the nearest perfused vessel were substantially higher in comparison to total vessel distances, however, reflecting the high proportion of nonperfused vessels in these tumors. For the endostatin treated MCa-4 tumors, distances to the nearest total or perfused vessel were also not significantly different from controls at either day 3 or 7, although a trend towards increased distances was observed for the day 7 endostatin tumors ($p = 0.06$). Within the endostatin treated group, total and perfused distances increased significantly between days 3 and 7 ($p < 0.001$ and $p < 0.009$, respectively),

indicating a decrease in vessel numbers in the period immediately following cessation of endostatin. Total vessel spacing was also determined using anti-CD105 staining, which has been proposed as a preferential marker of endothelial cells in angiogenic tissues (17). However, distances to anti-CD105 and anti-CD31 stained vessels were equivalent for both endostatin treated and control tumors (data not shown).

For the MCa-35 tumors (Figure 3B), no differences in either perfused or total vessel spacing were observed between treated and control tumors. However, perfused vessel distances increased significantly ($p < 0.04$) between days 3 and 6 for both treated and control tumors, most likely reflective of the decrease in perfusion with increasing tumor volume reported that has been previously reported in other tumor models (19). Compared with MCa-4 tumors, both total and perfused distances were significantly lower.

Overall hypoxia marker uptake. In the MCa-4 tumors (Figure 4A), overall hypoxia (median EF5/Cy3 intensity) was reduced immediately following endostatin treatment, compared to control tumors ($p = 0.05$), but returned to control levels by day 7. In contrast, no differences between controls and treated tumors were found in the MCa-35 tumors (Figure 4B). As expected, however, hypoxia increased with increasing tumor volume for both treated and controls.

Zonal analysis of hypoxia. Figure 5 presents EF5/Cy3 intensities as a function of distance from the nearest perfused blood vessel, each point corresponding to the median EF5/Cy3 intensity within a specific 20 micron wide zone. These results do not provide information regarding overall changes in hypoxia, but instead detail alterations in oxygen delivery and tumor oxygen consumption in relation to individual blood vessels. EF5/Cy3 intensities within the first 20 micron zone are most closely related to adjacent intravascular oxygen levels. Slopes of the curves, which depend on the rate of increase in hypoxia with increasing distance from the perfused vessels, are in part reflective of oxygen consumption rates in the surrounding tumor cells.

Comparing day 3 MCa-4 tumors (Figures 5A & B), endostatin produced a slight but insignificant decrease in tumor hypoxia within each zone. Since the slopes of the endostatin and control curves are not significantly different ($p = 0.94$) , oxygen consumption rates were most likely not substantially altered by treatment. By day 7, the slope of the endostatin curve had become significantly more steep in relation to the untreated curve ($p = 0.039$). Thus, despite the fact that total and perfused vascular spacings were equivalent in treated and untreated tumors at this time, oxygen was consumed somewhat more quickly adjacent to the endostatin tumor vessels. For both treated and control tumors, the curves were shifted significantly upward ($p = 0.007$ and $p = 0.002$) at day 7, indicating a decrease in oxygen delivery with increasing tumor volume.

In contrast to MCa-4 tumors, hypoxia marker intensities did not significantly increase with distance from perfused vessels in untreated MCa-35 tumors (Figure 5C). This is likely due to the much higher density of perfused vessels in the MCa-35 tumors (Figure 4). Since the immunostained images of Fig 2C are based on a two-dimensional slice, out-of-plane vessels can also contribute. Due to the overlapping effects of such adjacent blood vessels, such a highly vascularized tumor is less likely to contain significant regions of hypoxia. This is evidenced by the fact that hypoxia marker intensities throughout the day 3 MCa-35 tumors (Figure 5C) are very similar to the intensities immediately adjacent to the vessels in the MCa-4 tumors (Figure 5A).

Although the number of perfused vessels in untreated MCa-35 tumors had decreased substantially by day 6 (Figure 3B), hypoxia marker intensities were essentially unchanged in relation to distance from the nearest perfused vessel (Figure 5D). This suggests that many of the perfused vessels at day 3 were either essentially nonfunctional or superfluous, i.e., more functional vessels were initially present than were required to oxygenate the tumor. For the treated MCa-35 tumors, the slope of the curve increased significantly ($p = 0.02$) between days 3 and 6, indicating either an increase in consumption in these tumors or a decrease in the overlapping oxygen delivery among adjacent out-of-plane vessels as the number of perfused vessels declined. In comparison to the MCa-4 tumors, however, hypoxia remained much lower in all MCa-35 treatment groups.

Figure 6 presents the relationships between total and perfused vessel zonal analyses for each of the four MCa-4 tumor groups. These comparisons highlight changes in vessel function with treatment and tumor growth. Therefore, if most of the blood vessels in a given tumor are of similar functionality, the total and perfused curves will tend to overlap (Figure 6B). Similarly, as a rising proportion of the vessels become nonfunctional, the curves will tend to separate, such that increased levels of hypoxia will be found around the total vessels in relation to the perfused vessels (Figure 6A). Comparing Figures 6A and 6B, a large proportion of the vessels in the untreated tumors are initially nonfunctional at day 3, but improve by day 7. For the endostatin treated tumors (Figures 6C & 6D), the opposite effect is observed. At day 3 most vessels are functional, but by day 7 overall oxygen delivery decreases in the total vessels. For the MCa-35 tumors, total and perfused zonal analysis curves were essentially overlapping for all four treatment groups (data not shown).

Proliferation and apoptosis. Tumor cell proliferation and apoptosis zonal analyses were also performed in relation to perfused vessels for the MCa-4 tumors. As expected, % area Ki-67 staining decreased and % area apoptosis increased with increasing distance from perfused blood vessels. However, differences among treatment groups were not significant (data not shown).

DISCUSSION

Since the antiangiogenic effects of endostatin were first described nearly five years ago (6), numerous *in vivo* studies have detailed the effectiveness of recombinant endostatin on both tumor growth suppression (20) and regression (21-23). Dose dependent effects have been described in the Lewis lung carcinoma (6), and a dose of 20 mg/kg/day has been shown to produce significant tumor inhibition in a variety of tumor models (6;21-23). Numerous *in vitro* studies have clearly demonstrated that endostatin acts through the inhibition of endothelial cell proliferation, migration, and invasion (6;24). More recent studies have also suggested that endostatin effects may be mediated through a down-regulation of VEGF expression within the tumor (25;26). The present work was undertaken primarily to elucidate the effects of short-term endostatin administration on tumor pathophysiological properties, most notably vascular perfusion and oxygen delivery. Given that antiangiogenic agents will likely be combined with radiation therapy, it is critical to understand accompanying alterations in tumor oxygenation as well as to define optimal timepoints for delivery of radiation. Since different tumor types have been shown to exhibit quite disparate responses to the same antiangiogenic therapy (27), a secondary objective was to contrast endostatin effects in

two dissimilar murine mammary carcinomas, highly vascularized MCa-35 mammary carcinomas versus less vascularized MCa-4 tumors.

For both MCa-4 and MCa-35 tumors, numbers of perfused vessels tended to decrease with increasing tumor volume, most likely due to compression of the existing vessels as the tumor cells proliferated in an increasingly constrained space. Although endostatin had no effect on MCa-35 tumor growth, growth of MCa-4 tumors was markedly inhibited by day 3, as we have previously reported following injection of endostatin plasmid (22). We initially hypothesized that this inhibition was due to a slowdown in vascular development, which would presumably lead to an overall decrease in oxygenation as the tumor cells outgrew the existing vasculature. Surprisingly, neither total nor perfused vessel counts were significantly reduced in the MCa-4 tumors, somewhat in contrast to previous studies that have reported a decrease in total blood vessels after more extended administration of either recombinant endostatin (28) or the endostatin gene (28;29).

Although one might predict a reduction in tumor vascular density following endostatin, Folkman et al. (30) have pointed out that antiangiogenic treatments may also result in unchanged or even increased vascular counts. Thus while a decrease in vessel density strongly suggests that an antiangiogenic agent is working, the absence of such a decrease is inconclusive and indicates only that the endothelial and tumor cell proliferation rates are in balance. When an angiogenic treatment is administered short-term, the situation is even more complicated. Here, an initial decrease in endothelial cell proliferation could progressively lead to: 1) hypoxia, 2) a subsequent upregulation of angiogenic growth factors, and 3) a net gain in blood vessels. Clearly, results are highly dependent on the specific timepoint chosen and could differ at later times if the balance between the various factors changes. Temporal fluctuations in vascular volume have been reported following antiangiogenic treatments in window chamber tumors (31). In the current study, neither total nor perfused vessel spacings were significantly altered despite a significant reduction in tumor volume in the MCa-4 tumors. This suggests that either a parallel decrease in tumor cell proliferation or an increase in tumor cell apoptosis (28) may also be occurring. Although endostatin produced a slight overall increase in apoptosis and a slight decrease in proliferation in the current work, neither was significantly different from controls, in contrast to previous reports of a significant decrease in tumor cell proliferation following endostatin (26). In the previous study, however, a much longer course of endostatin treatment was administered. In the present work, necrosis was somewhat higher in the day 7 endostatin treated tumors than in the larger day 7 controls.

A second unanticipated finding in the MCa-4 tumors was a decrease in overall tumor hypoxia following short-course endostatin treatment, rather than the expected increase in hypoxia as the tumor presumably outgrows its vasculature. This could be due to either an increase in oxygen delivery (higher blood flow rate) or a decrease in tumor oxygen consumption rate, both of which would permit the available oxygen to diffuse further from the blood vessels. Based on the zonal analyses of Figure 5, oxygen levels in the endostatin treated tumors were not significantly different from controls, either immediately adjacent to perfused blood vessels or at increasing distances from the vessels. Since relative increases in hypoxia with increasing distance from the perfused vessels were similar between the two groups, oxygen consumption rate was most likely

not significantly altered. Functionality in the endostatin treated tumors was increased, however, as shown in Figure 6. This combination of an increased vessel functionality, a trend towards more perfused vessels, and a constant rate of oxygen consumption could explain the observed decrease in overall hypoxia of the endostatin treated MCa-4 tumors.

Despite a reduction in tumor volume, vascular density was not reduced in the MCa-4 tumors at day 3; instead, vascular functionality was improved and tumor hypoxia reduced. Since previous work has shown that tumors contain a significant fraction of immature blood vessels, and it has been hypothesized that either withdrawal of vascular endothelial growth factor (32) or administration of antiangiogenic agents (33) could prune inefficient vascular sprouts (34), endostatin administration could conceivably lead to the establishment of more efficient flow paths. In fact, previous work has demonstrated an increase in tumor oxygenation following antiangiogenic therapy, despite a reduction in vascular density, suggesting that it is the quality of vascular organization rather than the quantity of vessels that is important (35). Such a vascular stabilization could substantially improve vascular function in the short term, without significantly changing overall vascular densities.

In the current study, short term endostatin treatment eventually led to a marked decrease in vascular density as the tumors continued to grow without a parallel expansion of the vasculature. Ultimately, tumor growth rate was reduced due to the deficiencies in oxygen and nutrient supply. By day 7, hypoxia had increased in the endostatin treated tumors, and vascular spacing was comparable to controls despite the much smaller size of the treated tumors. At this time, vascular function in the treated tumors was also substantially reduced. Thus, while vessels in untreated tumors became somewhat more functional as the tumor grew, the opposite was true in the endostatin treated tumors, where vascular functionality decreased with increasing tumor volume. Previous reports of a decrease in blood vessel maturation following endostatin (36) could also account for these findings.

Several investigators have reported improvements in radioresponse when combining antiangiogenic agents with radiotherapy (9;10). Potent antitumor synergism was seen when angiostatin, another endogenous inhibitor of angiogenesis, was combined with radiation, but only if this agent was administered prior to or concurrent with irradiation (10). In general, however, such studies have not supported the idea that tumor oxygenation is the primary factor. When combining endostatin and irradiation, Hanna et al. (9) suggested that the endothelial compartment was the more likely target, rather than an enhancement of tumor cell radiosensitivity. As shown by the current zonal analysis of total blood vessels, short-term endostatin treatment resulted in vessels that were temporarily much more effective in delivering oxygen than the untreated controls. Four days after cessation of treatment, however, vascular function had deteriorated and was worse than in control tumors of larger volume. Although neither the total nor perfused vessel counts were significantly altered, overall hypoxia was much lower in the endostatin treated MCa-4 tumors. This suggests that short-term administration of endostatin could provide a beneficial enhancement of tumor radiosensitivity if given immediately prior to radiotherapy.

In contrast to the MCa-4 tumors, endostatin had no effect on either tumor growth rate or pathophysiology in the MCa-35 tumors. However, both total and perfused vascular densities were substantially higher in the MCa-35 tumors compared to the MCa-

4. In line with this increased vascularity, overall tumor hypoxia was significantly lower in the MCa-35 tumors and was essentially invariant with either tumor growth or treatment. In addition, hypoxia did not increase with increasing distance from the blood vessels in the MCa-35 tumors. This relatively homogeneous distribution of oxygen was most likely due to the combination of a more uniform distribution of blood vessels with a higher proportion of perfused vessels. Whether or not endostatin is less effective in such highly vascularized tumors remains to be conclusively proven.

In summary, the current studies demonstrate that murine mammary tumors of contrasting pathophysiology and differentiation status can differ substantially in their response to short-course endostatin treatment. While MCa-4 tumors responded robustly to endostatin in terms of growth rate and pathophysiological function, more vascularized MCa-35 tumors showed essentially no response. These disparate effects could have substantial implications in determining the ultimate effectiveness of combinations of antiangiogenic agents with conventional therapies. Further work is needed to elucidate which specific factors led to these disparate outcomes, and whether alterations in the overall balance of angiogenic versus antiangiogenic factors or levels of specific angiogenic cytokines may be the more critical factors. To fully realize the potential of antiangiogenic approaches, predictive assays are clearly needed to distinguish among responders and nonresponders. Both pathophysiological and molecular alterations must be characterized in additional tumor models, following acute and extended schedules of endostatin administration. For this purpose, zonal analysis of proliferation, apoptosis, and hypoxia markers permits the acquisition of a wealth of comprehensive pathophysiological information.

REFERENCES

(1) Folkman J. Tumor angiogenesis: Therapeutic implications. N Engl J Med 1971; 21:1182-1186.

(2) Fidler IJ. Angiogenesis and cancer metastasis [Review]. Cancer Journal 2000; 6(Suppl 2):S134-S141.

(3) Folkman J. The role of angiogenesis in tumor growth. [Review]. Seminars in Cancer Biology 1992; 3:65-71.

(4) Gasparini G. The rationale and future potential of angiogenesis inhibitors in neoplasia [Review]. Drugs 1999; 58(1):17-38.

(5) Carmeliet P, Jain RK. Angiogenesis in cancer and other diseases [Review]. Nature 2000; 407(6801):249-257.

(6) O'Reilly MS, Boehm T, Shing Y, Fukai N, Vasios G, Lane WS et al. Endostatin: An endogenous inhibitor of angiogenesis and tumor growth. Cell 1997; 88:277-285.

(7) Dhanabal M, Ramchandran R, Waterman MJ, Lu H, Knebelmann B, Segal M et al. Endostatin induces endothelial cell apoptosis. J Biol Chem 1999; 274(17):11721-11726.

(8) Kisker O, Becker CM, Prox D, Fannon M, D'Amato R, Flynn E et al. Continuous administration of endostatin by intraperitoneally implanted osmotic pump improves the efficacy and potency of therapy in a mouse xenograft tumor model. Cancer Res 2001; 61(20):7669-7674.

(9) Hanna NN, Seetharam S, Mauceri HJ, Beckett MA, Jaskowiak NT, Salloum RM et al. Antitumor interaction of short-course endostatin and ionizing radiation. Cancer Journal 2000; 6(5):287-293.

(10) Gorski DH, Mauceri HJ, Salloum RM, Gately S, Hellman S, Beckett MA et al. Potentiation of the antitumor effect of ionizing radiation by brief concomitant, exposures to angiostatin. Cancer Res 1998; 58(24):5686-5689.

(11) Bruns CJ, Shrader M, Harbison MT, Portera C, Solorzano CC, Jauch KW et al. Effect of the vascular endothelial growth factor receptor-2 antibody DC101 plus gemcitabine on growth, metastasis and angiogenesis of human pancreatic cancer growing orthotopically in nude mice. Int J Cancer 2002; 102(2):101-108.

(12) Guan C, Li P, Riggs PD. Vectors that facilitate the expression and purification of foreign peptides in Escherichia coli by fusion to maltose binding protein. Gene 1988; 67:21-30.

(13) Trotter MJ, Chaplin DJ, Olive PL. Use of a carbocyanine dye as a marker of functional vasculature in murine tumours. Br J Cancer 1989; 59:706-709.

(14) Fenton BM, Paoni SF, Lee J, Koch CJ, Lord EM. Quantification of tumor vascular development and hypoxia by immunohistochemical staining and HbO_2 saturation measurements. Br J Cancer 1999; 79(3/4):464-471.

(15) Fenton BM, Lord EM, Paoni SF. Effects of radiation on tumor intravascular oxygenation, vascular configuration, hypoxic development, and survival. Radiat Res 2001; 155(2):360-368.

(16) Lord EM, Harwell L, Koch CJ. Detection of hypoxic cells by monoclonal antibody recognizing 2-nitroimidazole adducts. Cancer Res 1993; 53:5721-5726.

(17) Kumar S, Ghellal A, Li C, Byrne G, Haboubi N, Wang JM et al. Breast carcinoma: vascular density determined using CD105 antibody correlates with tumor prognosis. Cancer Res 1999; 59:856-861.

(18) Fenton BM, Paoni SF, Beauchamp BK, Ding I. Zonal image analysis of tumour vascular perfusion, hypoxia, and necrosis. Br J Cancer 2002; 86(11):1831-1836.

(19) Fenton BM, Lord EM, Paoni SF. Intravascular HBO_2 saturations, perfusion and hypoxia in spontaneous and transplanted tumor models. Int J Cancer 2001; 93(5):693-698.

(20) Yokoyama Y, Green JE, Sukhatme VP, Ramakrishnan S. Effect of endostatin on spontaneous tumorigenesis of mammary adenocarcinomas in a transgenic mouse model. Cancer Res 2000; 60(16):4362-4365.

(21) Hahnfeldt P, Panigrahy D, Folkman J, Hlatky L. Tumor development under angiogenic signaling: A dynamical theory of tumor growth, treatment response, and postvascular dormancy. Cancer Res 1999; 59(19):4770-4775.

(22) Ding I, Sun JZ, Fenton B, Liu WM, Kimsely P, Okunieff P et al. Intratumoral administration of endostatin plasmid inhibits vascular growth and perfusion in MCa-4 murine mammary carcinomas. Cancer Res 2001; 61:526-531.

(23) Boehm T, Folkman J, Browder T, O'Reilly MS. Antiangiogenic therapy of experimental cancer does not induce acquired drug resistance. Nature 1997; 390:404-407.

(24) Jouanneau E, Alberti L, Nejjari M, Treilleux I, Vilgrain I, Duc A et al. Lack of antitumor activity of recombinant endostatin in a human neuroblastoma xenograft model. Journal of Neuro-Oncology 2001; 51(1):11-18.

(25) Huang XJ, Wong MKK, Zhao Q, Zhu ZY, Wang KZQ, Huang N et al. Soluble recombinant endostatin purified from Escherichia coli: Antiangiogenic activity and antitumor effect. Cancer Res 2001; 61(2):478-481.

(26) Boehle AS, Kurdow R, Schulze M, Kliche U, Sipos B, Soondrum K et al. Human endostatin inhibits growth of human non-small-cell lung cancer in a murine xenotransplant model. Int J Cancer 2001; 94(3):420-428.

(27) Kozin SV, Boucher Y, Hicklin DJ, Bohlen P, Jain RK, Suit HD. Vascular endothelial growth factor receptor-2-blocking antibody potentiates radiation-induced long-term control of human tumor xenografts. Cancer Res 2001; 61(1):39-44.

(28) Yokoyama Y, Dhanabal M, Griffioen AW, Sukhatme VP, Ramakrishnan S. Synergy between angiostatin and endostatin: Inhibition of ovarian cancer growth. Cancer Res 2000; 60(8):2190-2196.

(29) Kim YM, Hwang S, Pyun BJ, Kim TY, Lee ST, Gho YS et al. Endostatin blocks VEGF-mediated signaling via direct interaction with KDR/Flk-1. J Biol Chem 2002.

(30) Folkman J, Browder T, Palmblad J. Angiogenesis research: guidelines for translation to clinical application. Thromb Haemost 2001; 86(1):23-33.

(31) Hansen-Algenstaedt N, Stoll BR, Padera TP, Dolmans DEJG, Hicklin DJ, Fukumura D et al. Tumor oxygenation in hormone-dependent tumors during vascular endothelial growth factor receptor-2 blockade, hormone ablation, and chemotherapy. Cancer Res 2000; 60(16):4556-4560.

(32) Benjamin LE, Golijanin D, Itin A, Pode D, Keshet E. Selective ablation of immature blood vessels in established human tumors follows vascular endothelial growth factor withdrawal [see comments]. Journal of Clinical Investigation 1999; 103(2):159-165.

(33) Lee JC, Kim DC, Gee MS, Saunders HM, Sehgal CM, Feldman MD et al. Interleukin-12 Inhibits Angiogenesis and Growth of Transplanted but not in Situ Mouse Mammary Tumor Virus-induced Mammary Carcinomas. Cancer Res 2002; 62(3):747-755.

(34) Jain RK. Normalizing tumor vasculature with anti-angiogenic therapy: A new paradigm for combination therapy. Nat Med 2001; 7(9):987-989.

(35) Lee CG, Heijn M, di Tomaso E, Griffon-Etienne G, Ancukiewicz M, Koike C et al. Anti-vascular endothelial growth factor treatment augments tumor radiation

response under normoxic or hypoxic conditions. Cancer Res 2000; 60(19):5565-5570.

(36) Bloch W, Huggel K, Sasaki T, Grose R, Bugnon P, Addicks K et al. The angiogenesis inhibitor endostatin impairs blood vessel maturation during wound healing. FASEB Journal 2000; 14(15):2373-2376.

FIGURE LEGENDS:

Figure 1 – Tumor volume as a function of days from start of treatment (mean ± SE). Endostatin treatments of 20 mg/kg are denoted by the vertical arrows. *A*, MCa-4 curves based on 15 tumors each, of which half were frozen at day 3. *B*, MCa-35 curves based on 11 tumors each, with half frozen at day 3.

Figure 2 – Immunohistochemical staining of *A*, MCa-4 tumor anti-CD31. *B*, MCa-4 tumor EF5/Cy3, *C*, MCa-35 tumor anti-CD31, *D*, MCa-35 tumor EF5/Cy3. More intensely stained regions of *B* and *D* correspond to increased tumor hypoxia. Each image is a 4×4 composite image taken at 200× (area = 15.5 mm^2). Bar = 200 μm.

Figure 3 – Effect of endostatin treatment on median distance (mean ± SE) to the nearest total (open bars) or perfused (cross-hatched bars) blood vessel for MCa-4 (*A*) and MCa-35 (*B*) tumors. Increased median distances correspond to decreased vascular densities. Thus, an increased disparity between the total and perfused bars for a given treatment indicates an increased proportion of nonperfused vessels in that treatment. Data from 22 MCa-4 tumors and 30 MCa-35 tumors.

Figure 4 – Effect of endostatin on tumor hypoxia: Overall mean EF5/Cy3 intensity in (*A*) MCa-4 tumors and (*B*) MCa-35 tumors (mean ± SE). Data from 22 MCa-4 tumors and 30 MCa-35 tumors.

Figure 5 – Effect of endostatin on zonal changes in EF5/Cy3 intensity with increasing distance to the nearest perfused vessel. (*A*) untreated MCa-4 tumors, (*B*) endostatin treated MCa-4 tumors, (*C*) untreated MCa-35 tumors, (*D*) endostatin treated MCa-35 tumors. Data are based on 22 MCa-4 tumors and 30 MCa-35 tumors.

Figure 6 – Effect of endostatin on zonal changes in EF5/Cy3 intensity with increasing distance to the nearest total versus perfused vessel. (*A*) untreated MCa-4 tumors, day 3, (*B*) untreated MCa-4 tumors, day 7, (*C*) endostatin treated MCa-4 tumors, day 3, (*D*) endostatin treated MCa-4 tumors, day 7. Data are based on 22 MCa-4 tumors.

Table I – Effect of Endostatin on % Necrosis (mean ± s.e.)

		Day 4	Day 7
Untreated	Necrosis	18.3 ± 5.0	25.5 ± 12.
	Tumor Volume (mm^3)	950 ± 130	1600 ± 250
Endostatin	Necrosis (%)	6.5 ± 3.0	31.4 ± 1.4
	Tumor Volume (mm^3)	970 ± 150	1200 ± 100

Figure 1

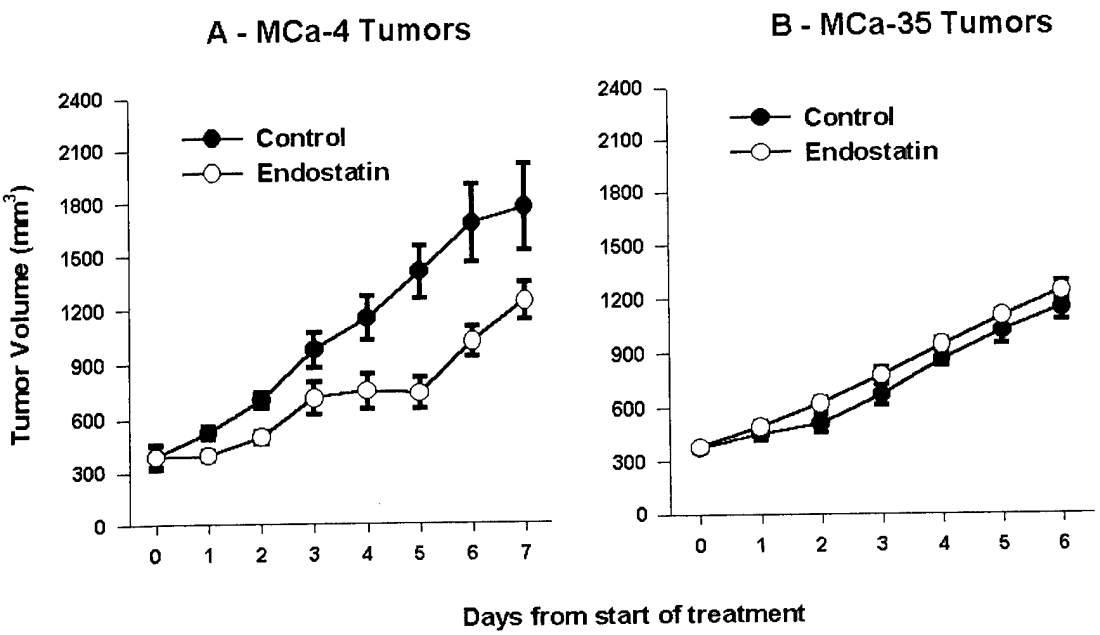
A - MCa-4 Tumors
B - MCa-35 Tumors
Control
Endostatin
Tumor Volume (mm3)
2400
2100
1800
1500
1200
900
600
300
0
0 1 2 3 4 5 6 7
0 1 2 3 4 5 6
Days from start of treatment

Figure 2

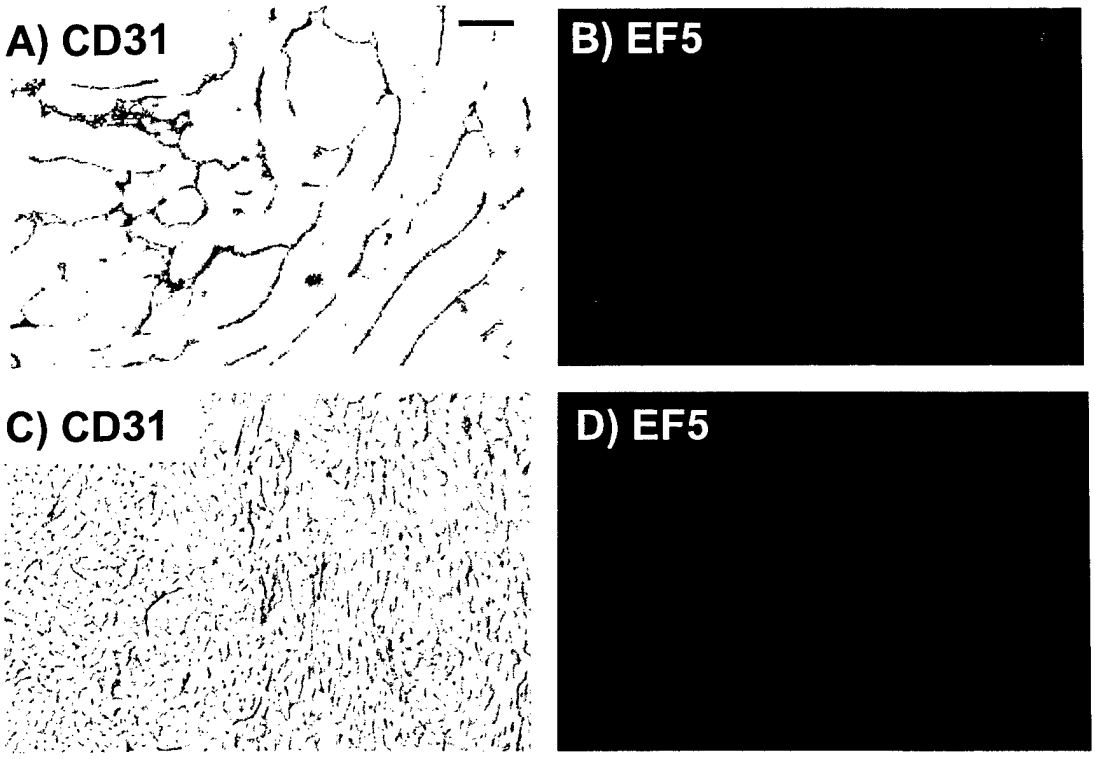

Figure 3

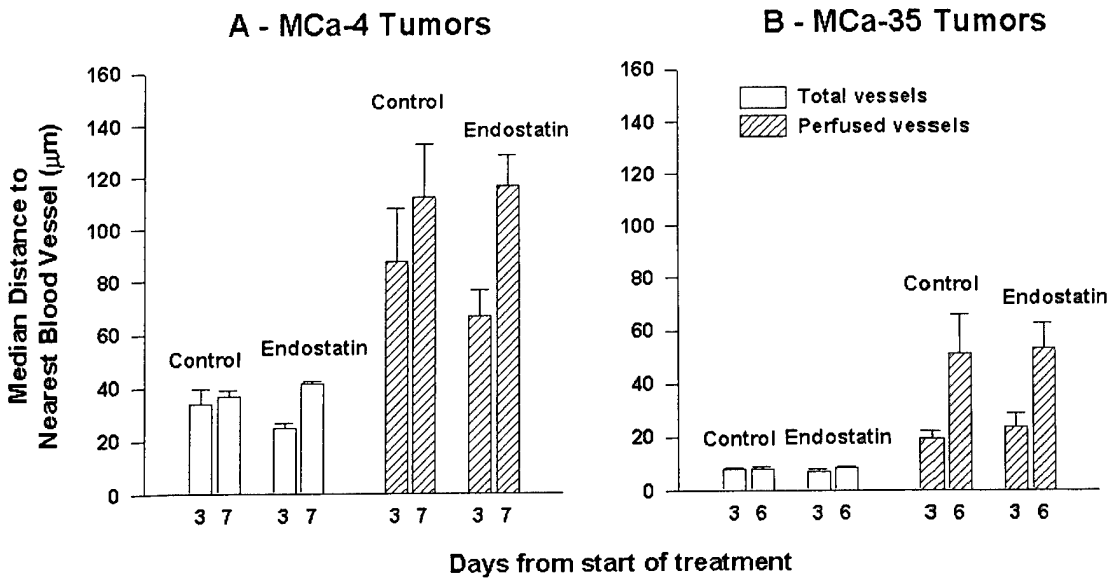
A - MCa-4 Tumors
B - MCa-35 Tumors
Median Distance to Nearest Blood Vessel (μm)
160
140
120
100
80
60
40
20
0
Control
Endostatin
Total vessels
Perfused vessels
3 7 3 7 3 7 3 7
3 6 3 6 3 6 3 6
Days from start of treatment

Figure 4

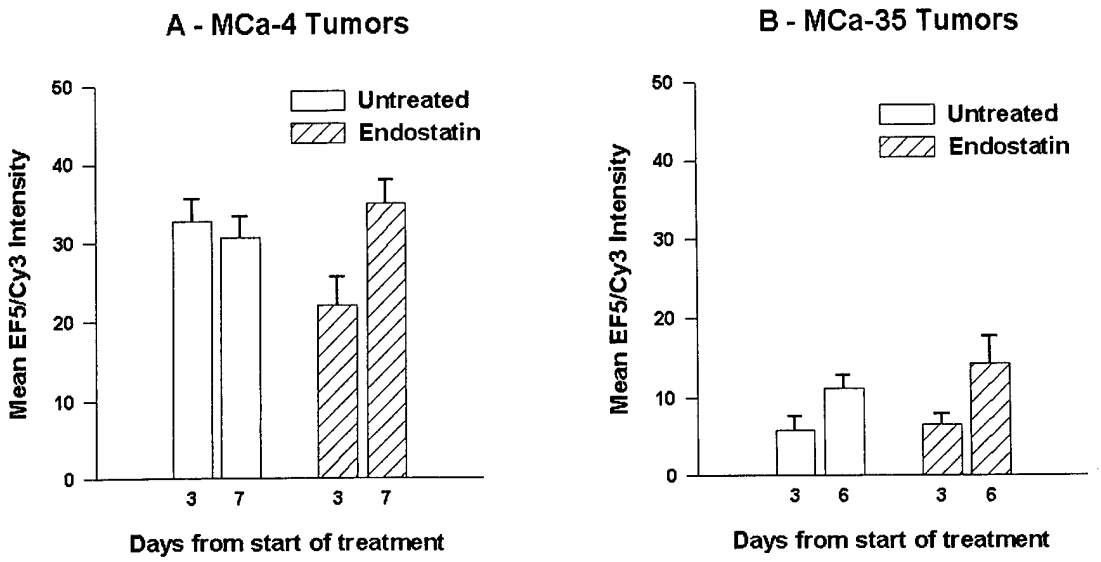
A - MCa-4 Tumors
Mean EF5/Cy3 Intensity
50
40
30
20
10
0
Untreated
Endostatin
3
7
3
7
Days from start of treatment
B - MCa-35 Tumors
Mean EF5/Cy3 Intensity
50
40
30
20
10
0
Untreated
Endostatin
3
6
3
6
Days from start of treatment

Figure 5

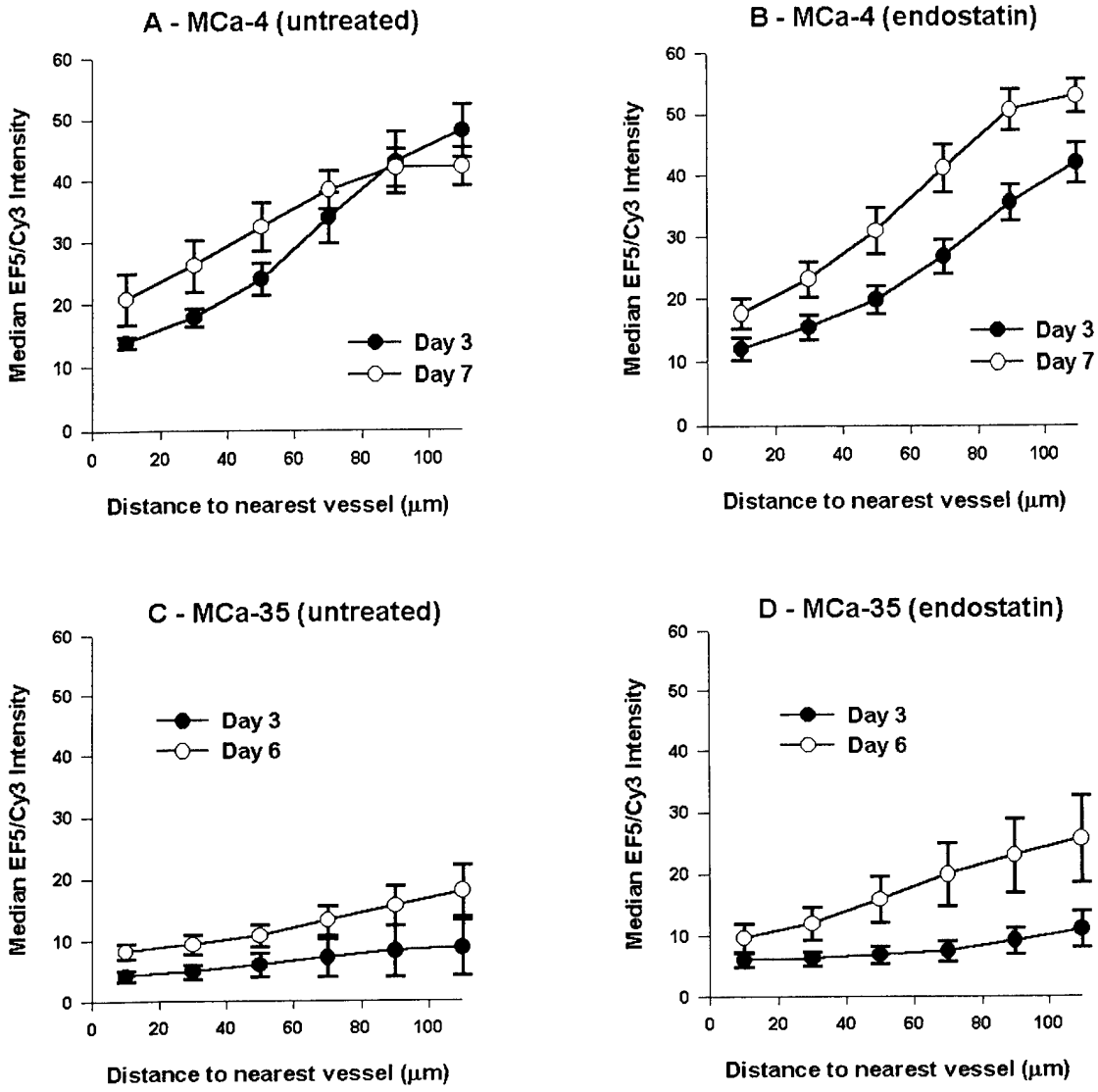
A - MCa-4 (untreated)
B - MCa-4 (endostatin)
C - MCa-35 (untreated)
D - MCa-35 (endostatin)
Median EF5/Cy3 Intensity
Distance to nearest vessel (μm)
Day 3
Day 7
Day 6
0
10
20
30
40
50
60
0
20
40
60
80
100

Figure 6

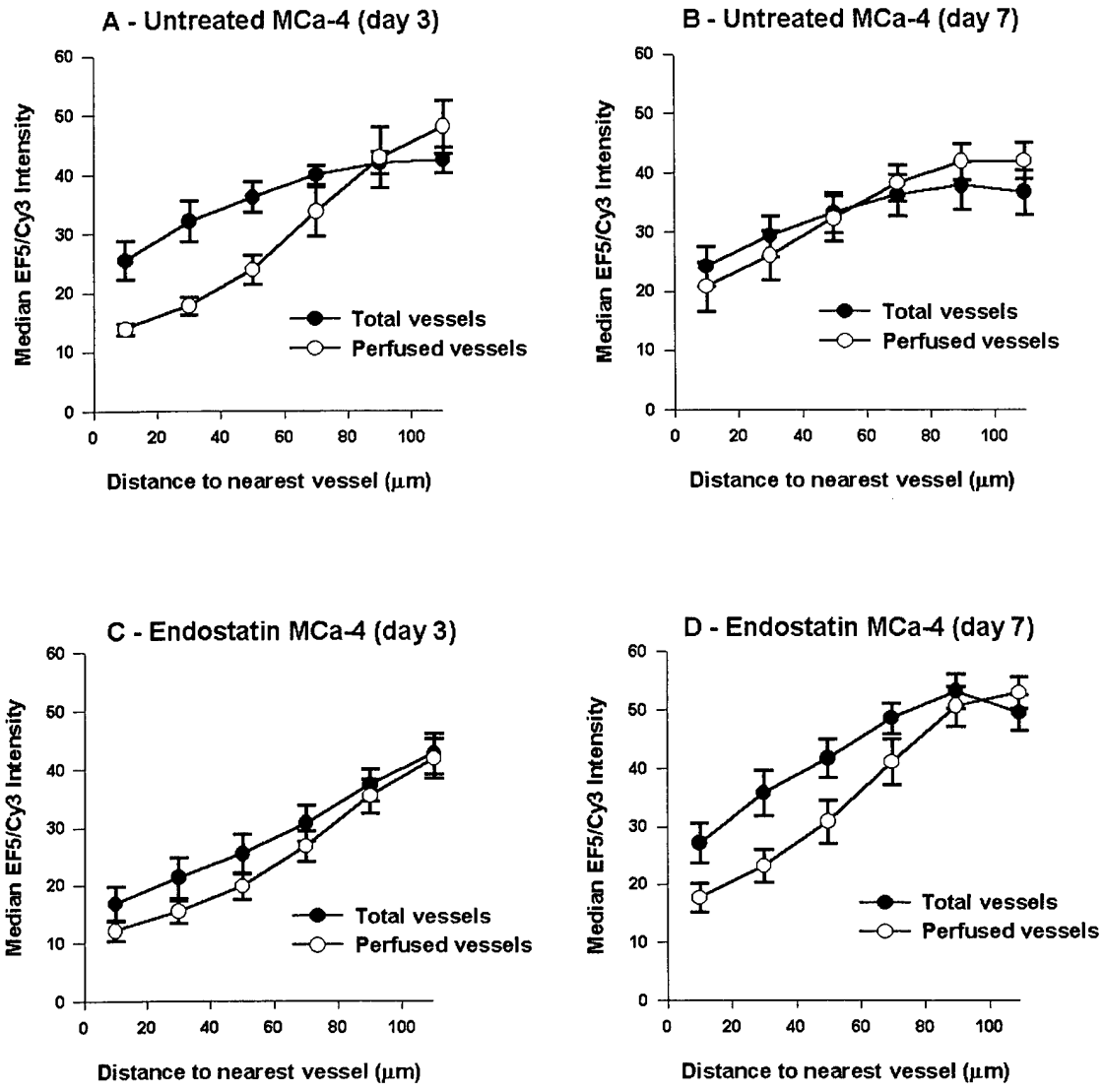
A - Untreated MCa-4 (day 3)
B - Untreated MCa-4 (day 7)
C - Endostatin MCa-4 (day 3)
D - Endostatin MCa-4 (day 7)
Median EF5/Cy3 Intensity
Distance to nearest vessel (μm)
Total vessels
Perfused vessels
0
10
20
30
40
50
60
0
20
40
60
80
100

EVALUATION OF MICROREGIONAL VARIATIONS IN TUMOR HYPOXIA FOLLOWING THE ADMINISTRATION OF ENDOSTATIN

Bruce M. Fenton, Scott F. Paoni, Brian K. Beauchamp, Baohuong Tran, Li Liang, Brian Grimwood, and Ivan Ding*

1. INTRODUCTION

Endostatin, a fragment of collagen XVIII, has been shown to potently inhibit both angiogenesis and the growth of experimental tumors, primarily through inhibition of endothelial cell migration and proliferation with minimal direct effects on tumor cells. Recent studies have also demonstrated that endostatin can enhance the antitumor effects of ionizing radiation, when administered before and during radiotherapy[1]. In order to optimize such combination therapies, an understanding of the accompanying changes in tumor pathophysiology, *i.e.*, oxygenation and blood flow, is clearly of prime importance. The primary aim of the current work was to implement an improved method for determination of the effects of endostatin on the microregional relationship between tumor perfusion and hypoxic marker uptake. By combining information from multiple images taken from the same frozen sections, additional pathophysiological information could be deduced that was unobtainable from the individual images.

2. METHODS

2.1. Animal Model

Cells from MCa-4 murine mammary carcinomas (3×10^6) were inoculated into the mammary fat pads of 6-8 week-old female C3H/HeJ mice (The Jackson Laboratory, Bar

*Bruce M. Fenton, Scott F. Paoni, Brian K. Beauchamp, Baohuong Tran, Li Liang, and Ivan Ding, Department of Radiation Oncology, University of Rochester School of Medicine, Rochester, NY 14642; Brian Grimwood, NY State Department of Health, Albany, NY 12201

Harbor, ME). Tumor volumes were measured by calipers and the formula: volume = ½ a^2b, where a and b are the minor and major tumor axes, respectively. Guidelines for the humane treatment of animals were followed as approved by the University Committee on Animal Resources.

2.2. Drug treatments

When tumors had grown to between 200-400 mm^3, recombinant murine endostatin (rmNYendo) was administered *i.p.* at 20 mg/kg for three consecutive days. Tumors were frozen at either day 4 or day 7, and 9.0 μm frozen sections were cut for later immunohistochemistry and image analysis.

2.3. $DiOC_7$ perfusion marker and EF5 hypoxic marker

To visualize blood vessels open to flow, an intravascular injected stain, $DiOC_7$, was used as described previously[2]. This agent has been shown to provide optimal visualization of tumor blood vessels by preferentially staining cells immediately adjacent to the vessels[3]. Localized areas of tumor hypoxia were assessed in frozen tissue sections by immunohistochemical identification of sites of 2-nitroimidazole metabolism as described previously[3]. A pentafluorinated derivative (EF5) of etanidazole was injected *i.v.* one hour before tumor freezing, at which time the EF5 has been shown to be well distributed throughout even poorly perfused regions of the tumor[4]. Regions of high EF5 metabolism were visualized immunohistochemically using a fluorochrome (Cy3, Amersham) conjugated to the ELK3-51 antibody. This antibody is extremely specific for the EF5 drug adducts that form when the drug is incorporated by hypoxic cells[5].

2.4. Immunohistochemistry and image analysis

Immediately following cryostat sectioning, tumor slices were imaged for $DiOC_7(3)$ perfusion staining using a Nikon microscope, digitized, background-corrected, and image-analyzed using Image-Pro software (Media Cybernetics, Silver Spring, MD) with a 800 MHz Pentium computer, as previously described in detail[3]. Color images from 16 adjacent microscope fields were automatically acquired and digitally combined. Each section was scanned under two different staining conditions. First, epi-illumination images of the fluorescent green $DiOC_7(3)$ staining were obtained immediately after the sections were sliced on the cryostat. Following the immunohistochemical staining procedures, the tumor section was returned to the same coordinates on the microscope stage, and fluorescent red-orange images were acquired showing the distribution of the EF5/Cy3 hypoxic marker staining. To account for variation in the intensity of the 100 W mercury lamp, calibrations images were obtained each day, using a hemocytometer filled with a reference concentration of Cy3 dye, as described in detail by Evans et al.[6]. Pixel intensities were then corrected for each image based on the ratio of the mean red intensities of the corresponding calibration images.

To obtain estimates of overall tumor hypoxia, fluorescent image montages of the EF5/Cy3 staining were quantified using the Image-Pro "histogram" tool to determine the mean intensity of the individual image pixels. To further quantitate microregional EF5/Cy3 intensities variations as a function of distance from perfused blood vessels,

methods somewhat similar to those of Rijken et al.[7] were utilized. As summarized in Figure 1, $DiOC_7(3)$ images were first enhanced using the Image-Pro "color segmentation" tool to identify perfused blood vessels[3]. Specific colors were interactively selected and accumulated to obtain optimal discrimination between vessels and stroma, and a binary image of the selected colors was created (Figure 1A). This image was next inverted and a "distance filter" applied, which replaced the intensity of each pixel with an intensity proportional to the distance of that pixel from the nearest perfused vessel (Figure 1B). Thus, pixels immediately adjacent to the vessels were assigned intensity 1 in the new image, and the intensities of more distant pixels were increased by one gray level for each one pixel increase in distance from the vessel. This distance filtered image was then successively "thresholded" and binarized to select regions of the image within specific distances around perfused vessels. For example, thresholding between 1-20 gray levels selected a zone from 1-20 pixels away from a vessel, 21-40 selected a zone from 21-40 pixels away from a vessel, and so on. Figure 1C illustrates the binary image resulting from thresholding between gray levels of 1-20 (which selects regions within approximately 1-20 microns from the nearest vessel, since each pixel is roughly one micron across). This binary "mask" was then multiplied by the corresponding EF5/Cy3 image (Figure 1D) to obtain an image in which only those regions of the EF5/Cy3 image within the inner zone were included (Figure 1E). Finally, mean EF5/Cy3 intensities within this zone were determined using the Image-Pro "histogram" tool. EF5/Cy3 intensities of successive concentric zones at further distances from the perfused vessels were quantitated similarly and plotted as a function of distance from nearest perfused vessels.

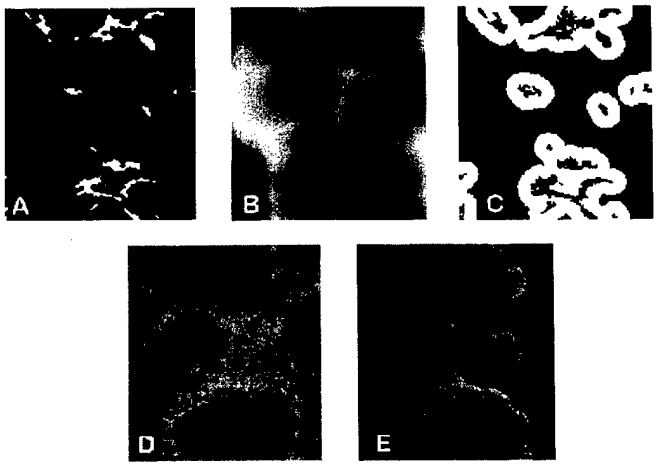

Figure 1 Image analysis procedures: A) binary image of perfused vessels, B) distance filtered image, C) mask from thresholded distance map (includes gray levels from 1-20), D) EF5/Cy3 intensities (lighter intensities correspond to increased hypoxia), E) product of images C and D (selects only those EF5/Cy3 intensities within approximately 20 microns from the perfused vessels.

3. RESULTS

At day four (one day after three daily doses of endostatin), treated tumors were significantly smaller than untreated controls (710±90 mm^3 versus 970±100 mm^3), and by day seven, differences were even more substantial (1670±220 mm^3 versus 1010±80

mm^3). As shown in Figure 2, overall hypoxia (mean EF5/Cy3 intensity) was also significantly reduced in the MCa-4 tumors following three days of endostatin treatment ($p = 0.05$), but returned to control levels by day 7.

Figure 3 presents EF5/Cy3 intensities as a function of distance from the nearest perfused blood vessel, each point corresponding to the mean EF5/Cy3 intensity within a specific 20 micron wide zone (as detailed in Methods). EF5/Cy3 intensities within the first 20 micron zone are most closely related to adjacent intravascular oxygen levels, and the slopes of the curves are reflective of oxygen consumption rates in the surrounding tumor cells. Steeper slopes, which are indicative of a rapid increase in hypoxia with increasing distance from the perfused vessels, therefore correspond to increased consumption rates.

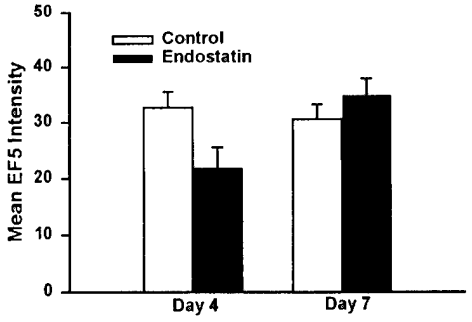

Figure 2 Overall EF5/Cy3 intensity (±SEM). Each bar is the mean of 6 tumors, each of which includes 4 image montages of 16 combined fields (for a total of 64 fields/tumor).

Despite the reduction in overall EF5 intensities at day 4 following endostatin (Figure 2), EF5 intensities within the zone closest to the nearest perfused vessel were not significantly reduced in relation to untreated tumors (Figure 3A), indicating that intravascular oxygen delivery was not substantially changed by treatment. In addition, the minimal difference in the slopes of these two curves suggests, at most, a slight decrease in oxygen consumption rate in the endostatin tumors. At day seven (Figure 3B), EF5 intensities of the zone closest to the blood vessels remain equal for endostatin and untreated tumors, suggesting little difference in intravascular oxygen delivery following treatment. At this time, however, the slope of the endostatin curve is increased in relation to controls, resulting in a significant increase in EF5 intensities for the zones furthest from the blood vessels. This is indicative of an increase in consumption in the endostatin tumors.

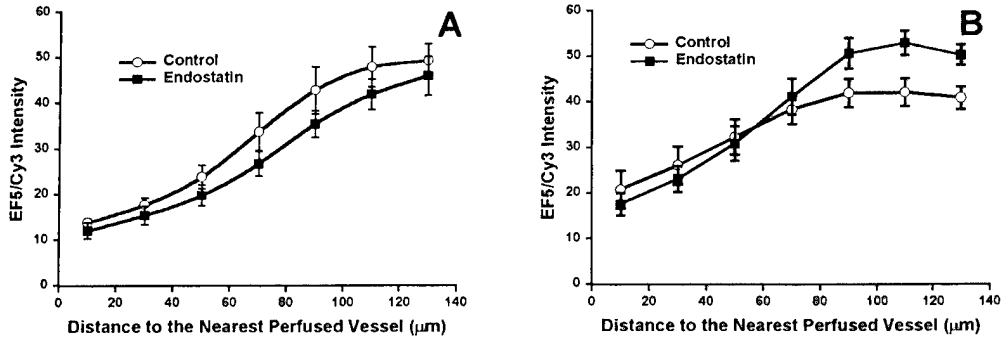

Figure 3 Mean EF5/Cy3 intensity within concentric zones surrounding perfused blood vessels. Each zone is approximately 20 microns in width. A) Day 4 (1 day following completion of treatment), B) Day 7 (4 days following treatment).

4. DISCUSSION

Although commonly used[8,9], changes in overall EF5/Cy3 intensities provide a somewhat oversimplified appraisal of the effects of endostatin on tumor hypoxia and can be misleading if large regions of necrosis are present (which do not metabolize EF5). The zonal analysis of EF5/Cy3 intensities as a function of distance to the nearest perfused vessels permits the acquisition of much more comprehensive information and can be limited to regions immediately surrounding perfused blood vessels, where necrosis would be less likely. From this microregional analysis, differences in tumor cell oxygen consumption rates and relative changes in intravascular oxygenation (which are related to vascular functionality) can both be estimated.

Since all images are based on two-dimensional slices through the tumors, vessels outside of the image plane are ignored. Thus EF5/Cy3 intensities could be locally reduced despite the absence of visible perfused vessels. Although this could potentially alter the relationship between EF5/Cy3 intensity and distance to the nearest vessel, such occurrences are expected to follow the distribution of visible vessels to some extent. Regions with high vascular densities will more likely have accompanying out of plane branches, which will be less likely for regions at large distances from any visible vessels. Although such out of plane branches would result in a decrease in absolute EF5/Cy3 intensities in these regions, the effects should be similar for different treatment groups and are not expected to mask relative differences among groups.

Previous reports of increased endothelial cell apoptosis[1] and decreased angiogenesis[10] following endostatin treatment suggest that this agent could result in a compromised vascular supply and a subsequent increase in tumor hypoxia. Somewhat surprisingly, overall tumor hypoxia was instead reduced following acute administration of endostatin. Since neither oxygen delivery nor consumption appear substantially changed, these results suggest that the relative proportion of functioning vessels may be increased in the endostatin treated tumors. This agrees with the recent proposal that antiangiogenic therapies could serve to improve vascular efficiency through the selective pruning of immature or less functional capillaries[11]. If confirmed in additional experiments, these results could provide an additional rationale for the reported improvement in response observed when combining endostatin with radiotherapy[1]. Further more comprehensive studies are needed to interpret these somewhat puzzling findings. Future experiments will investigate not only whether these increased oxygen levels are transient in nature, but also whether response to fractionated radiotherapy can be enhanced by extended endostatin administration.

5. ACKNOWLEDGMENTS

Financial support was provided by NIH Grant CA52586 and DOD Grant DAMD17-00-1-0420.

6. REFERENCES

1. N.N. Hanna, S. Seetharam, H.J. Mauceri, M.A. Beckett, N.T. Jaskowiak, R.M. Salloum, D. Hari, M. Dhanabal, R. Ramchandran, R. Kalluri, V.P. Sukhatme, D.W. Kufe, and R.R. Weichselbaum,

Antitumor interaction of short-course endostatin and ionizing radiation, *Cancer Journal* **6**:287-293 (2000).

2. M.J. Trotter, D.J. Chaplin, and P.L. Olive, Use of a carbocyanine dye as a marker of functional vasculature in murine tumours, *Br.J.Cancer* **59**:706-709 (1989).
3. B.M. Fenton, S.F. Paoni, J. Lee, C.J. Koch, and E.M. Lord, Quantification of tumor vascular development and hypoxia by immunohistochemical staining and HbO_2 saturation measurements, *Br.J.Cancer* **79**:464-471 (1999).
4. B.M. Fenton, E.M. Lord, and S.F. Paoni, Effects of radiation on tumor intravascular oxygenation, vascular configuration, hypoxic development, and survival, *Radiat.Res.* **155**:360-368 (2001).
5. E.M. Lord, L. Harwell, and C.J. Koch, Detection of hypoxic cells by monoclonal antibody recognizing 2-nitroimidazole adducts, *Cancer Res.* **53**:5721-5726 (1993).
6. S.M. Evans, C.J. Koch, K.M. Laughlin, W.T. Jenkins, T. Vanwinkle, and D.F. Wilson, Tamoxifen induces hypoxia in MCF-7 xenografts, *Cancer Res.* **57**:5155-5161 (1997).
7. P.F.J.W. Rijken, H.J.J.A. Bernsen, J.P.W. Peters, R.J. Hodgkiss, J.A. Raleigh, and A.J. van der Kogel, Spatial relationship between hypoxia and the (perfused) vascular network in a human glioma xenograft: A quantitative multi-parameter analysis, *Int.J.Radiat.Oncol.Biol.Phys.* **48**:571-582 (2000).
8. B.M. Fenton, Influence of hydralazine administration on oxygenation in spontaneous and transplanted tumor models, *Int.J.Radiat.Oncol.Biol.Phys.* **49**:799-808 (2001).
9. S.M. Evans, S.M. Hahn, D.P. Magarelli, P.J. Zhang, W.T. Jenkins, D.L. Fraker, Hsi, RA, W.G. Mckenna, and C.J. Koch, Hypoxia in human intraperitoneal and extremity sarcomas, *Int.J.Radiat.Oncol.Biol.Phys.* **49**:587-596 (2001).
10. M.S. O'Reilly, T. Boehm, Y. Shing, N. Fukai, G. Vasios, W.S. Lane, E. Flynn, J.R. Birkhead, B.R. Olsen, and J. Folkman, Endostatin: An endogenous inhibitor of angiogenesis and tumor growth, *Cell* **88**:277-285 (1997).
11. R.K. Jain, Normalizing tumor vasculature with anti-angiogenic therapy: A new paradigm for combination therapy, *Nat Med* **7**:987-989 (2001).

Overexpression of VEGF by MCF-7 Breast Cancer Cells Promotes Estrogen-independent Tumor Growth *in vivo*[1]

Ping Guo, Quan Fang, Huo-Quan Tao, Christopher A. Schafer, Bruce M. Fenton, Ivan Ding, Bo Hu[2] and Shi-Yuan Cheng[2]

University of Pittsburgh Cancer Institute & Department of Pathology [P. G., Q. F., H.-Q. T., C. A. S., S.-Y. C.] or Medicine [B. H.], Research Pavilion at Hillman Cancer Center, Room 2.19, 5117 Centre Avenue; Pittsburgh, PA 15213-1863

University of Rochester Cancer Center & Department of Radiation Oncology, 601 Elmwood Avenue, Box 704, Rochester, NY 14642 [I. D., B. M. F.]

Running Title:

VEGF promotes estrogen-independent growth of MCF-7 breast cancer

Key Words: Vascular endothelial growth factor, tumor angiogenesis, breast cancer, and estrogen-independent tumor growth.

[1]Supported by grants from Department of Defense, DAMD17-01-1-0375 and DAMD-17-02-1-0584, a developmental fund of University of Pittsburgh Cancer Institute (S.-Y. C); and NIH Grant CA52586 and Department of Defense, DAMD17-00-1-0420 (B. M. F.)

[2]To whom requests for reprint should be addressed, at University of Pittsburgh Cancer Institute & Department of Pathology (S.-Y. C) or Medicine (B.H.), Research Pavilion at Hillman Cancer Center, Suite 2.26, 5117 Centre Avenue; Pittsburgh, PA 15213-1863. Phone: (412) 623-3261; Fax: (412) 623-4840; E-mail: chengs@msx.upmc.edu or hub@msx.upmc.edu

[3]The abbreviations used are: VEGF, vascular endothelial growth factor; VEGF-R, VEGF receptor; NRP-1: neuropilin-1; FGF, fibroblast growth factor; EC, endothelial cell; CM, conditioned media; IHC, Immunohistochemistry; V121 or V165 or LacZ: MCF-7 cells that overexpress $VEGF_{121}$, or $VEGF_{165}$ or LacZ; RT-PCR, reverse transcriptase-polymerase chain reactions; E_2, 17 β-estradiol; VN, vitronectin; FN: fibronectin.

Abstract

Alteration of the phenotype of breast cancers from estrogen-dependent to estrogen-independent growth often leads to the failure of anti-estrogenic tumor therapies. We report that overexpression of VEGF by estrogen-dependent MCF-7 breast cancer cells could abolish estrogen-dependent tumor growth in ovariectomized mice. In the absence of estrogen, MCF-7 VEGF-expressing tumors with increased vessel density showed growth kinetics similar to, or even greater than, that of parental MCF-7 tumors with estrogen-supplementation. Overexpression of VEGF by MCF-7 cells also stimulated cell proliferation in culture. Our data suggest that stimulation of MCF-7 tumor angiogenesis and growth by VEGF is mediated by both autocrine and paracrine mechanisms.

Introduction

Progressive growth of human breast cancers is dependent on estrogen or other estrogenic hormones (1). A considerable number of estrogen-dependent breast tumors often evolve to demonstrate more aggressive and estrogen-independent growth patterns, which are responsible for frequent failures of anti-estrogenic breast cancer therapies (2). Although the molecular events of breast tumorigenesis have been illustrated in great detail, the mechanisms that enable breast cancer cells to acquire the estrogen-independent growth phenotype remains largely unknown. Studies show that estrogen promotes breast cancer progression by interacting with its nuclear receptors, thus regulating a set of genes important for breast cancer growth. Accumulating evidence suggests that acquisition of estrogen-independent breast tumor growth is accompanied by constitutively increased expression of a similar set of the genes that are upregulated by estrogen during estrogen-dependent breast tumor progression (3).

Vascular endothelial growth factor (VEGF)[3], a major angiogenic factor involved in breast cancer progression, is one of the genes that is stimulated by estrogen (4, 5). Functional estrogen-responsive elements in the gene of VEGF have been identified through which estrogen directly regulates VEGF transcription in breast cancer cells (6-8). VEGF produced by breast carcinoma cells stimulates angiogenesis through a paracrine mechanism in tumor endothelial cells (9) and promotes cell growth by an autocrine pathway in tumor cells (10-12). In humans,

VEGF exists as six alternatively spliced isoforms, of which $VEGF_{121}$ and $VEGF_{165}$ are the predominant isoforms (9). VEGF exerts its cellular functions by interacting with VEGF receptors, VEGFR-1, VEGFR-2, as well as a $VEGF_{165}$ receptor, neuropilin-1 (NRP-1). In addition to endothelial cells, VEGF receptors are also found in breast cancer cells (10, 13). Recent studies have shown that both estrogen and VEGF regulate a similar subset of genes in promoting breast cancer progression (5). Therefore, we hypothesize that overexpression of VEGF by estrogen-dependent breast cancer cells could produce an effect on breast cancer progression (acquisition of estrogen-independent growth) similar to the growth stimulation induced by estrogen.

In this report, we show that overexpression of VEGF isoforms, $VEGF_{121}$ or $VEGF_{165}$, by estrogen-dependent MCF-7 breast cells stimulated breast tumor formation in an estrogen-independent fashion in ovariectomized mice, in the absence of 17 β-estradiol (E_2)-treatment. In addition, VEGF strongly stimulated neovascularization in MCF-7 tumors formed either in E_2-treated or non-E_2–treated mice, as well as enhanced estrogen-dependent tumor growth in E_2-treated mice. Our findings suggest that upregulation of VEGF in estrogen-dependent breast cancers contributes to the acquisition of estrogen-independent cancer growth by stimulating tumor angiogenesis and progression through both autocrine and paracrine mechanisms.

Materials and Methods

Cell lines and Reagents. MCF-7 cells were obtained from American Tissue Culture Collection (ATCC, Rockville, MD). MCF-7 cells were cultured using Dulbecco's Modified Eagle's medium (DMEM, Invitrogen/Life Technologies, Grand Island, NY) supplemented with 10% fetal bovine serum (FBS, Hyclone, Salt Lake City, UT), 10μg/ml of insulin (Sigma, St. Louis, MO), and 1% penicillin-streptomycin. All other chemicals and reagents were from Sigma (St. Louis, MO), Fisher Scientific (Hanover Park, IL), or Invitrogen (Rockville, MD).

Generation of MCF-7 cell lines that stably express VEGF or LacZ proteins. Transfected MCF-7 cell clones that stably express VEGF or LacZ were generated by transfecting MCF-7 cells with cDNA inserts of $VEGF_{121,}$ $VEGF_{165,}$ or LacZ in pCEP4 vector. The clones that expressed exogenous $VEGF_{121,}$ $VEGF_{165,}$ or LacZ were expanded and characterized by methods described previously (14).

RNA isolation and RT-PCR analyses. Total RNA was isolated and RT-PCR analyses were performed as described previously (14). Primers for VEGFR-1 were 5'GCACCTTGGTTGTGGCTGAC3' (forward primer) and 5'GGTTTCGCAGGAGGTATGGTG3' (reverse primer). Primers for VEGFR-2 were 5'TATGTCTATGTTCAAGATTAC3' (forward primer) and

5'AAGTTTCTTATGCTGATGCTT3' (reverse primer). The lengths of PCR products were 441 bp for VEGFR-1 and 473 bp for VEGFR-2, respectively.

Tumorigenicity and tissue management. Human MCF-7 breast tumors were established in the mammary fat pads of ovariectomized female nude mice as described previously (15). Briefly, 1 X 10^7 of various types of MCF-7 cells were inoculated into the mammary fat pads of 7 to 8-week old, ovariectomized female nude mice that were or were not implanted with 17-β estradiol (E_2) 60-day slow release pellets (Innovative Research of America, Sarasota, FL). The volumes of the tumors were measured using a caliper every fifth day. At the indicated times, the mice were sacrificed and the tumors were removed and processed (14).

Immunohistochemical (IHC) analyses of the MCF-7 cell derived tumors. IHC analyses were performed on 5 μm cryostat tissue sections of various types of MCF-7 tumors as described previously (14). The following reagents were used for this study: rat anti-mouse CD31 antibody, its isotype control $IgG_{2a,K}$, (BD-PharMingen, San Diego, CA), goat anti-human vitronectin antibody (C-20), goat anti-human fibronectin antibody (C-20, Santa Cruz Biotechnology, Inc., Santa Cruz, CA), mouse monoclonal anti-VEGFR-1 antibody (P3H8A9), rabbit polyclonal anti-VEGFR-2 antibody (T014), and rabbit polyclonal anti-NRP-1 antibody, NP1ECD1A (14). The secondary and tertiary antibodies were from Vector Laboratories (Burlingame, CA) or Jackson

ImmunoResaerch laboratories(West Grove, PA). A DAB elite kit was from Dako Co.(Carpintera, CA). Aqua block was from East Coast Biologics, Inc. (North Berwick, Maine).

Quantitative analyses of blood vessel were performed on serial-cut tumor sections that were stained with the anti-CD31 antibody without counter staining. Five to seven serial-cut tumor sections from each mouse were analyzed. Images (10 to 15 random fields per section) were acquired using a SPOT digital camera (100 X magnification) on an Olympus BX51 microscope using Image Pro Plus software (Version 4.1, Media Cybernetics, L.P., Silver Spring, MD). Blood vessel densities were calculated as the fractional vessel density of the positively stained areas to the total tissue area of the field (14). The mean values of the calculated densities from the serial sections of the separate tumors (4 to 8 individual mice) in each group were used for the quantitative analysis.

Cell proliferation assay. Evaluation of MCF-7 cell proliferation was performed using the Biotrak cell proliferation ELISA system (Amersham Pharmacia Biotech, Piscataway, NJ). Various types of MCF-7 cells were seeded in 96-well plates at 60% confluence and maintained at 37°C in phenol-red free DMEM containing 10% charcoal-treated fetal bovine serum. Twenty-four hours later, the medium was changed to serum-free /phenol-red free DMEM for 48 hrs. 5'-bromo-2'-deoxyuridine (BrdUrd) was then added into the wells for an additional 2 hrs. The cells were fixed and incubated with a peroxidase-conjugated anti-BrdUrd antibody according to

the manufacturer's instructions. The developed color was measured at 450 nm in a microtiter plate spectrophotometer. To assess the effects of extracellular matrix components on enhancing the VEGF stimulated BrdUrd incorporation, 96-well plates were pre-coated with vitronectin (400 ng/ml), or fibronectin (5.0 μg/ml), or Matrigel (1.0 μg/ml, Becton Dickinson Biosciences, Bedford, MA), respectively. The plates were kept at 4°C overnight. The coating solution was then aspirated, and the coated plates were allowed to dry. In blocking experiments, a neutralizing anti-VEGF antibody (10 μg/ml, R&D Systems, Minneapolis, MN) was included in the assays.

Results

Stable expression of $VEGF_{121}$, $VEGF_{165}$, or LacZ proteins in MCF-7 cells. MCF-7 cells were stably transfected with pCEP4 vectors that have a cDNA insert of $VEGF_{121}$, $VEGF_{165}$, or LacZ. Hygromycin-resistant clones were characterized either by Western blotting using an anti-VEGF antibody, or by fluorescence-sorting with a fluorescence-activated cell sorter (FACS) followed by LacZ cell staining (14). Seventeen MCF-7 cell clones that express $VEGF_{121}$ (referred to as V121), 19 MCF-7 cell clones that express $VEGF_{165}$ (referred to as V165), and 6 MCF-7 cell clones that express LacZ (referred to as LacZ) were identified. Each clone of V121 or V165 cells expressed exogenous VEGF proteins at high levels (only 4 representative clones of each type are shown in Fig. 1A), whereas no VEGF was detected in either MCF-7 or LacZ cells by VEGF Western blotting. Similarly, the amounts of VEGF secreted by V121 or V165 clones into conditioned media (CM) were ranged from 288 to 421 ng/ml/10^6 cells after 48-hrs of cell culture (Fig. 1B). In contrast, parental MCF-7 or LacZ cells only secreted 3.0 to 6.0 ng/ml/10^6 cells into the CM. Among the VEGF expressing cell clones, clones 10 and 53 of V121 cells, and clones 35 and 37 of V165 cells were chosen for subsequent studies.

Expression of $VEGF_{121}$ or $VEGF_{165}$ by MCF-7 Cells Enhanced E_2-dependent Breast Tumor Growth. To determine whether expression of $VEGF_{121}$ or $VEGF_{165}$ by MCF-7 cells would enhance MCF-7 breast tumor growth in vivo, MCF-7, LacZ, V121-10, V121-53, V165-35, or

V165-37 cells were implanted orthotopically in ovariectomized nude mice with E_2-supplementation (Fig. 2A and 2B). At 45 days after implantation, 53% or 40% of E_2-treated mice that received MCF-7 or LacZ cells developed tumors, with volumes of 307 ± 42.4 mm^3 (n=6, MCF-7 tumors) or 242 ± 50.6 mm^3 (n=6, LacZ tumors), respectively (Table 1). There were no significant differences in tumor volume or tumor formation between these two groups ($p=0.98$). In contrast, with E_2 treatment, expression of $VEGF_{121}$ or $VEGF_{165}$ not only increased the frequency of MCF-7 tumor formation to 90% (V121 tumors) or 86% (V165 tumors), but also dramatically enhanced tumor growth (1263 ± 214.3 mm^3 for V121 tumors, n=8, $p<0.001$, or 1638 ± 189.5 mm^3 for V165 tumors, n=8, $p<0.001$). In the presence of E_2, $VEGF_{165}$ seemed to have a stronger effect on promoting MCF-7 tumor growth than $VEGF_{121}$ did (Fig. 2 and Table 1, $p<0.05$). Thus, with E_2 treatment, expression of either $VEGF_{121}$ or $VEGF_{165}$ by MCF-7 cells facilitated MCF-7 cancer tumorigenesis.

Expression of $VEGF_{121}$ or $VEGF_{165}$ in MCF-7 Cells Rendered E_2–independent Breast Tumor Growth.

In parallel experiments, MCF-7, LacZ, V121-10, V121-53, V165-35, and V165-37 cells were inoculated separately into the mammary fat pads of ovariectomized mice without E_2-supplementation (Fig. 2A, 2B, and Table 1). Without E_2-treatment, neither MCF-7 nor LacZ cells formed tumors in ovariectomized mice (n=6 in each group). In sharp contrast, 81% of the mice that received V121-10 or V121-53 cells developed tumors at 45-days after inoculation, with

a volume of 830.6 ± 261 mm^3 (n=8, $p<0.002$). Also, 90% of the mice that received V165-35 or V165-37 cells formed tumors, with a volume of 391.4 ± 113.6 mm^3 (n=10, $p<0.0001$). The tumorigenicity experiments (either with or without E_2 treatment) were independently performed a total of 6 times at two different institutions (the laboratory of S.-Y. Cheng at the University of Pittsburgh, Pittsburgh, PA and the laboratories of I. Ding/B. M. Fenton at the University of Rochester, Rochester, NY), with similar results. Therefore, expression of $VEGF_{121}$ or $VEGF_{165}$ by MCF-7 breast cancer cells rendered E_2-independent MCF-7 tumor formation in ovariectomized animals.

$VEGF_{121}$ or $VEGF_{165}$ Enhanced Neovascularization in MCF-7 Breast Tumors in either E_2-treated or Non-E_2-treated Mice. VEGF is a potent stimulator of breast tumor angiogenesis (9). Therefore, we examined whether enhanced tumorigenicity by expression of $VEGF_{121}$ or $VEGF_{165}$ in MCF-7 cells elicited angiogenesis in the various types of MCF-7 tumors. The fractional area of blood vessels for E_2-dependent tumors derived from MCF-7 cells was similar to that of LacZ tumors. (Fig. 3A, a, b, and 3B, p=0.99). In comparison to the MCF-7 tumors in mice with E_2-treatment, the vascular fractional areas in V121 or V165 tumors with E_2-treatment increased by 3.29–fold or 3.45-fold compared to controls (Fig. 3A and 3B, $p<0.001$). To a similar extent, the vascular fractional area of V121 or V165 tumors in mice without E_2-treatment increased by 3.25-fold and 3.77-fold, respectively (Fig. 3A and 3B, $p<0.001$). Thus, overexpression of $VEGF_{121}$ or

$VEGF_{165}$ by the MCF-7 tumors stimulated neovascularization in both E_2-treated and non-E_2-treated mice.

VEGF Receptors Were Expressed in MCF-7 Breast Tumor Cells as well as in Endothelial Cells. VEGF exerts its biological functions through interaction with its functional receptors, VEGFR-1 (Flt-1), VEGFR-2 (Flk-1/KDR) as well as a $VEGF_{165}$ receptor, neuropilin-1 (NRP-1) (9). As shown in Figs. 2, 3, and Table 1, expression of $VEGF_{121}$ or $VEGF_{165}$ enhanced MCF-7 tumor growth and angiogenesis. However, the effect of VEGF-stimulated angiogenesis alone was unlikely to be potent enough to enable E_2-dependent MCF-7 tumor cells to establish E_2-independent tumors in non-E_2-treated mice. We hypothesize that the VEGF produced by V121 or V165 tumor cells might have autocrine effects on MCF-7 tumor cells themselves. These autocrine effects might be similar to the effect of VEGF on cell proliferation of E_2-dependent T47D breast tumor cells (10) or of E_2-independent MDA-MB-231 breast tumor cells (11, 12). Therefore, we examined the expression of VEGFRs in MCF-7 cells and various MCF-7 tumors. In cultured cells, the expressions of VEGFR-1, VEGFR-2, and NRP-1 (data not shown) were detected in MCF-7 cells by RT-PCR analyses, although the expression levels of VEGFR-2 was low (Fig. 4A). There were no significant differences in expression levels of VEGFR-1, VEGFR-2, or NRP-1 among MCF-7, LacZ, V121, and V165 cells (data not shown). In the various types of MCF-7 tumors established in either E_2-treated or non-E_2-treated mice, expression of VEGFR-1 and -2 were detected in most of the tumor vessels (Fig. 4B, arrowheads, data for VEGR-2 is not

shown). The expression of VEGFR-1 and –2 on the vessels correlated with the CD31 staining of the vessels in the various tumors (Figs. 3A and 4B). In corroboration of the expression of mRNAs of VEGFR-1 or NRP-1 in MCF-7 tumor cells (Fig. 4A, data not shown), immunoactivities of an anti-VEGFR-1 antibody (Fig. 4B, arrows), or an anti-NRP-1 antibody (data not shown), but not an anti-VEGFR-2 antibody (data not shown), were found in MCF-7 tumor cells in the various types of MCF-7 tumors. Since $VEGF_{121}$ does not bind to NRP-1, it is plausible that with or without E_2-treatment, $VEGF_{121}$ or $VEGF_{165}$ could promote MCF-7 tumor growth by an autocrine mechanism through interaction with VEGFR-1.

$VEGF_{121}$ or $VEGF_{165}$ Promoted MCF-7 Cell Proliferation potentiated by ECM components. To demonstrate whether VEGF stimulated MCF-7 cell growth through an autocrine pathway, we evaluated the proliferation of various types of MCF-7 cells by assessing the incorporation of BrdUrd into the DNA of these cells. As shown in Fig. 5A, after 48-hrs of serum and E_2 deprivation, quiescent MCF-7 or LacZ cells had comparable levels of DNA synthesis. The percent increase in BrdUrd incorporation was defined as 100% for parental MCF-7 cells. In comparison to those of MCF-7 or LacZ cells, the rates of BrdUrd incorporation of the V121 or V165 cells increased significantly to 143% and 157%, respectively. This stimulation was most likely due to the stimulation by VEGF on V121 or V165 cells, since VEGF-enhanced cell proliferation was inhibited when a neutralizing anti-VEGF antibody (10 μg/ml) was included in the assays (Fig. 5A).

We have previously shown that VN, an ECM ligand that binds to integrins $\alpha_v\beta_3$ or $\alpha_v\beta_5$, potentiates $VEGF_{121}$ or $VEGF_{165}$-stimulated glioma angiogenesis in vivo and EC migration in vitro (14). To assess whether the ECM ligands, VN, or FN, or ECM components (Matrigel) could potentiate VEGF-stimulated MCF-7 tumor cell proliferation under the condition of serum and E_2 deprivation, we performed mitogenic analyses in the presence of VN (Fig. 5B), or FN or Matrigel (data not shown). No enhancements in cell proliferation of the MCF-7 or LacZ cells were seen when the cells were grown in VN (Fig. 5B), or FN or Matrigel (data not shown) coated plates, compared to uncoated controls. In contrast, treatment with VN (Fig. 5B), or FN, or Matrigel (data not shown) on V121 or V165 cells greatly potentiated the mitogenic activities of these cells (increasing from 143% to 175% for V121 cells and from 157% to 200% for V165 cells compared to control cells).

Finally, we determined whether VN or FN was expressed in the various types of MCF-7 tumors. High levels of expression of VN (Fig. 5C) or FN (data not shown) were detected in all types of MCF-7 tumors, in both E_2-treated and non-E_2-treated mice. Taken together, these data suggest that in the absence of E_2, VEGF stimulates mitogenesis of MCF-7 tumor cells by an autocrine mechanism, and ECM components potentiate VEGF-stimulated MCF-7 tumor cell proliferation.

Discussion

During the past three decades, several model systems have been established for studying the process whereby initially estrogen-dependent breast cancer cells acquire estrogen resistance or estrogen-independent growth. Overexpression of fibroblast growth factors-1 (FGF-1) (15) or FGF–4 (16), or c-Jun, (17) by MCF-7 cells enabled E_2-independent MCF-7 tumor growth and stimulated tumor invasion and metastases in ovariectomized mice. However, in vivo, estrogen treatments of mice had no effects on tumor growth (FGF-1 or c-Jun expressing MCF-7 cells) (15, 17) and suppressed tumor formation (FGF-4 expressing MCF-7 cells) (16). On the other hand, E_2-independent, but E_2-responsive MCF-7 sub-lines were also isolated by selecting adriamycin-resistant cell clones (18) or from established MCF-7 tumors in ovariectomized mice (3). Although these two MCF-7 cell sublines formed E_2-independent breast tumors in mice, little was known about the mechanisms that conferred E_2-independence in these two model systems. In the present study, we examined the consequences of overexpression of VEGF by MCF-7 tumors in ovariectomized nude mice with or without E_2-treatment. Expression of $VEGF_{121}$ or $VEGF_{165}$ byMCF-7 cells rendered E_2-independent tumor formation. The growth rates of V121 or V165 tumors were similar to those of tumors derived from estrogen-independent MCF-7 sub-lines (3) or of the parental, estrogen-dependent MCF-7 tumors in E_2-treated mice (Fig. 2 and Table 1). In addition, V121 and V165 tumors remained responsive to estrogen-stimulation *in vivo*, which was also consistent with the response of breast tumors derived from the estrogen-independent MCF-7

sublines (3). Thus, the estrogen-independent but estrogen-responsive phenotype may exemplify a natural progression of development of estrogen-independent growth in breast cancers.

VEGF is a major angiogenic factor in breast tumor progression. This factor is expressed at high levels in breast cancers compared to normal breast tissue, and suppression of VEGF function inhibits breast tumor formation (19). Our results show that expression of VEGF isoforms, $VEGF_{121}$ or $VEGF_{165}$, by MCF-7 cells at high levels stimulated both E_2-independent and E_2-dependent breast tumor growth in mice. Moreover, we also obtained several V121 or V165 cell clones that secreted VEGF at lower levels. These low VEGF-expressing cell clones did not show enhancement of tumor growth in E_2-treated mice, nor formed tumors in non-E_2-treated mice (data not shown). This observation is in agreement with two separate studies reported previously (20, 21). With lower expression of the VEGF isoforms by MCF-7 cells, moderate augmentation on E_2-dependent breast tumor growth in ovariectomized mice was seen (20). In another study, although MCF-7 $VEGF_{165}$-expressing tumors responded vigorously to estrogen stimulation in promoting tumorigenesis, the V165 cells could only form E_2-independent tumors in ovariectomized mice when implanted with Matrigel (21). Thus, threshold levels of VEGF expression in breast cancer cells may be critical for the acquisition of the estrogen-independent phenotype in human breast cancers. This hypothesis is clinically relevant since high levels of VEGF proteins could be detected in primary breast cancer specimens, especially in hypoxic regions (19).

It has been established that estrogen stimulates the expression of VEGF in breast cancers. In vivo, E_2-treatment augments VEGF expression in E_2-induced rat mammary cancer (22). In vitro, E_2 directly regulates VEGF transcription by acting upon the estrogen responsive elements in the VEGF gene in breast cancer cells (6-8). On the other hand, E_2 and VEGF appear to regulate several common genes that are critical for breast cancer progression. Both E_2 and VEGF upregulate the expression of cyclin D1, NFκ-B, and Bcl-2 in breast tumors (E_2) and endothelial cells (VEGF) (23-28). Furthermore, earlier studies have shown that factors induced by E_2 in E_2-dependent MCF-7 cells could partially replace E_2 to promote breast tumor growth (29). Our data corroborate these observations and further demonstrate that during the progression of E_2-dependent breast cancers, up-regulation or constitutive expression of growth factors, such as VEGF, could result in the acquisition of an E_2-independent phenotype. However, since VEGF only regulates a subset of tumor promoting genes, similar to E_2, upregulation of VEGF alone without E_2-treatment is not strong enough to completely replace the stimulatory effects of E_2 together with VEGF on tumorigenicity of MCF-7 breast tumors.

In addition to stimulating breast tumor angiogenesis by a paracrine mechanism, VEGF also promotes breast cancer cell growth, survival, and invasion by an autocrine pathway. Studies have shown that a $VEGF_{165}$ receptor, neuropilin-1 (NRP-1), mediates both VEGF-stimulated survival and invasion for E_2-independent breast cancer cells (10-12). In E_2-dependent T47D breast cancer cells, VEGFR-1 and VEGFR–2 are responsible for VEGF-stimulated mitogenic

and migratory responses (10). In our studies, MCF-7 cells express VEGFR-1 and NRP-1 at high levels, both in vitro and in vivo, whereas the expression of VEGFR-2 was only detected in tumor endothelial cells, but not in the carcinoma cells of the MCF-7 tumors. Since both $VEGF_{121}$ and $VEGF_{165}$ stimulated E_2-dependent and E_2-independent MCF-7 breast tumor growth, and $VEGF_{121}$ does not bind to NRP-1 (30), we propose that augmentation of E_2-dependent MCF-7 tumor growth and acquisition of E_2-independence are likely to be mediated by VEGFR-1, at least in V121 tumors.

In summary, we have shown that overexpression of VEGF by human MCF-7 breast cancers not only enhances E_2-dependent tumor growth, but also enables E_2-independent tumor formation *in vivo*. The stimulation by VEGF of MCF-7 tumor growth is through both a paracrine effect on tumor angiogenesis and an autocrine effect on tumor cell proliferation. Our data suggest that if VEGF is expressed at high levels in breast cancer cells, it could partially replace E_2 stimulation of breast cancer growth. Our results of VEGF-stimulated E_2-dependent or E_2-independent breast cancer growth provide an excellent system to investigate the mechanisms of acquisition of estrogen-independent growth by estrogen-dependent breast cancers. Our findings also indicate the need for targeting the VEGF/VEGFR pathway and other signaling pathways as well as estrogen-ablation in the treatment of human breast cancers.

Figure legends

Figure 1. Overexpression of $VEGF_{121}$ or $VEGF_{165}$ by MCF-7 breast cancer cells. A. Western blot analyses. 30 μg of total protein from the lysates of the various MCF-7 cells or clones was analyzed by immunoblotting. $VEGF_{121}$ or $VEGF_{165}$ ran at 18 KDa or 22 KDa with non-glycosylated (lower band) and glycosylated forms (upper band). **B.** VEGF ELISA analysis. The CM was collected from various types of MCF-7 cells after 48-hrs of cell culture and analyzed with VEGF ELISA kit. Each bar represents the mean ± SEM of three triplicates. Both experiments were performed at least two additional times with similar results.

Figure 2. Overexpression of $VEGF_{121}$ or $VEGF_{165}$ by MCF-7 breast cancers promoted tumorigenicity in both E_2-treated and Non-E_2-treated mice. 1×10^7 of the MCF-7, LacZ, V121, or V165 cells were inoculated into the mammary fat pads of mice implanted with or without 60 day-releasing 17-β estradiol pellets. **A.** Photographs of individual mice inoculated with various types of MCF-7 cells. Breast tumors formed by MCF-7 (a), Lac Z (b), V121 (c and e), or V165 (d and f) cells. Panels a to d: tumors established in E_2-treated mice. Panels e and f: tumors formed in non-E_2-treated mice. Arrows indicate the established MCF-7 tumors. Since no tumors were formed in the non-E_2-treated mice inoculated with MCF-7 or Lac Z cells, photographs were not taken of those mice. **B.** The growth kinetics of the various MCF-7 tumors. Tumor volumes were measured at the indicated times after implantation. Data is shown

as the mean ± SEM (14). Two separate clones from each type of LacZ, V121, or V165 cells were individually inoculated. The experiments included six to ten mice in each group and were preformed 3 separate times each at two different institutions with similar results.

Figure. 3. $VEGF_{121}$ or $VEGF_{165}$ stimulated angiogenesis in MCF-7 breast cancers in both E_2-treated and Non-E_2-treated mice. A. IHC stains of tumor vessels with an anti-CD31 monoclonal antibody. Breast tumors formed by MCF-7 (a), Lac Z (b), V121 (c and e), or V165 (d and f) cells. Panels a to d: tumors established in E_2-treated mice. Panels e and f: tumors developed in non-E_2-treated mice. Since no tumors were formed in the mice that received MCF-7 or LacZ cells without E_2-supplementation, no analysis was done. Arrows indicate blood vessels. Four to eight individual tumor samples of each class from each in vivo experiment were analyzed and the experiments were repeated at least two additional times with similar results. Original magnification: 200X. **B.** Quantitative analysis of the increased fractional vascular area in VEGF-expressed MCF-7 tumors. Representative IHC stains from the various MCF-7 tumors are shown in **A**. Data are means +/- SD. Numbers above each bar indicate the numbers of mice analyzed in each group. Numbers in the parentheses under the X-axis are the differences (in folds) of the VEGF expressing tumors in comparison with parental MCF-7 tumors.

Figure 4. VEGFR-1 is expressed in MCF-7 breast cancer cells in vitro and in vivo. A. RT-PCR analysis on the expression of VEGFRs in human dermal endothelial cells (EC), MCF-7

cells and human U87 glioma cells with (+) or without (-) reverse transcriptase. The length of the PCR product of VEGF-1 or VEGFR-2 was 441 bp or 473 bp, respectively. The arrow indicates a weak VEGFR-2 cDNA fragment detected in MCF-7 cells. N: negative control. The experiments were done three times with identical results. **B.** Expression of VEGFR-1 in various MCF-7 tumors. Panels a to h: IHC analysis of various types of established MCF-7 tumors using a mouse monoclonal anti-VEGFR-1 antibody. Breast tumors formed by MCF-7 (a), Lac Z (b), V121 (c and e), V165 (d and f) cells. Panels a to d: tumors established in E_2-treated mice. Panels e and f: tumors formed in non-E_2-treated mice. Arrowheads indicate blood vessels that were positively stained by the anti-VEGFR-1 antibody. Arrows show tumor cells that expressed VEGFR-1. Six to eight individual tumor samples of each group from each in vivo experiment were analyzed each time and the experiments were repeated at least two additional times with similar staining patterns. Original magnification: 400X.

Figure 5. Vitronectin potentiates MCF-7 cell proliferation stimulated by VEGF. **A** and **B,** cell proliferation assay of various MCF-7 cells using a BrdUrd cell proliferation ELISA system. In some samples, a neutralizing anti-VEGF antibody was included. **A.** Mitogenic activities of the various MCF-7 cells in uncoated 96-well plates. **B.** Mitogenic activities of the various MCF-7 cells in 96-well plates coated with 400 ng/ml of vitronectin. The increased proliferation was calculated as the percentage of that of parental MCF-7 cells. Symbol * denotes statistically significant ($p<0.002$). The assays were performed three times using different cell clones of

various cell passages with similar results. **C.** Expression of vitronectin in various types of established MCF-7 breast tumors. Breast tumors formed by MCF-7 (a), Lac Z (b), V121 (c and e), V165 (d and f) cells. Panels a to d: tumors established in E_2-treated mice. Panels e and f: tumors formed in non-E_2-treated mice. Arrows indicate tumor cells that were positively stained by the anti-VN antibody. Six to eight tumor samples of each group of each in vivo experiment were analyzed and the experiments were repeated at least two additional times with similar results. Original magnification: 400X.

Acknowledgments

This work was initiated in the laboratory of Dr. Webster K. Cavenee at Ludwig Institute for Cancer Research & University of California, San Diego. The authors would like to acknowledge the continuous support of Dr. W. K. Cavenee. We thank Michael Jarzynka and Frank Cackowski for editing this manuscript.

References

1. Dickson, R. B., Johnson, M. D., el-Ashry, D., Shi, Y. E., Bano, M., Zugmaier, G., Ziff, B., Lippman, M. E., and Chrysogelos, S. Breast cancer: influence of endocrine hormones, growth factors and genetic alterations, Adv Exp Med Biol. *330:* 119-41, 1993.

2. Clarke, R., Thompson, E. W., Leonessa, F., Lippman, J., McGarvey, M., Frandsen, T. L., and Brunner, N. Hormone resistance, invasiveness, and metastatic potential in breast cancer, Breast Cancer Res Treat. *24:* 227-39, 1993.

3. Brunner, N., Boulay, V., Fojo, A., Freter, C. E., Lippman, M. E., and Clarke, R. Acquisition of hormone-independent growth in MCF-7 cells is accompanied by increased expression of estrogen-regulated genes but without detectable DNA amplifications, Cancer Res. *53:* 283-90., 1993.

4. Hyder, S. M. and Stancel, G. M. Regulation of angiogenic growth factors in the female reproductive tract by estrogens and progestins, Mol Endocrinol. *13:* 806-11., 1999.

5. Losordo, D. W. and Isner, J. M. Estrogen and angiogenesis: A review, Arterioscler Thromb Vasc Biol. *21:* 6-12., 2001.

6. Hyder, S. M., Nawaz, Z., Chiappetta, C., and Stancel, G. M. Identification of functional estrogen response elements in the gene coding for the potent angiogenic factor vascular endothelial growth factor, Cancer Res. *60:* 3183-90., 2000.

7. Mueller, M. D., Vigne, J. L., Minchenko, A., Lebovic, D. I., Leitman, D. C., and Taylor, R. N. Regulation of vascular endothelial growth factor (VEGF) gene transcription by estrogen receptors alpha and beta, Proc Natl Acad Sci U S A. *97:* 10972-7., 2000.

8. Buteau-Lozano, H., Ancelin, M., Lardeux, B., Milanini, J., and Perrot-Applanat, M. Transcriptional regulation of vascular endothelial growth factor by estradiol and tamoxifen in breast cancer cells: a complex interplay between estrogen receptors alpha and beta, Cancer Res. *62:* 4977-84., 2002.

9. Ferrara, N. Vascular endothelial growth factor: molecular and biological aspects, Curr Top Microbiol Immunol. *237:* 1-30, 1999.

10. Miralem, T., Steinberg, R., Price, D., and Avraham, H. VEGF(165) requires extracellular matrix components to induce mitogenic effects and migratory response in breast cancer cells, Oncogene. *20:* 5511-24., 2001.

11. Bachelder, R. E., Crago, A., Chung, J., Wendt, M. A., Shaw, L. M., Robinson, G., and Mercurio, A. M. Vascular endothelial growth factor is an autocrine survival factor for neuropilin-expressing breast carcinoma cells, Cancer Res. *61:* 5736-40., 2001.

12. Bachelder, R. E., Wendt, M. A., and Mercurio, A. M. Vascular endothelial growth factor promotes breast carcinoma invasion in an autocrine manner by regulating the chemokine receptor CXCR4, Cancer Res. *62:* 7203-6., 2002.

13. Soker, S., Takashima, S., Miao, H. Q., Neufeld, G., and Klagsbrun, M. Neuropilin-1 is expressed by endothelial and tumor cells as an isoform- specific receptor for vascular endothelial growth factor, Cell. *92:* 735-45., 1998.

14. Guo, D. Q., Wu, L. W., Dunbar, J. D., Ozes, O. N., Mayo, L. D., Kessler, K. M., Gustin, J. A., Baerwald, M. R., Jaffe, E. A., Warren, R. S., and Donner, D. B. Tumor necrosis factor employs a protein-tyrosine phosphatase to inhibit activation of KDR and vascular endothelial cell growth factor-induced endothelial cell proliferation, J Biol Chem. *275:* 11216-21., 2000.

15. Zhang, L., Kharbanda, S., Chen, D., Bullocks, J., Miller, D. L., Ding, I. Y., Hanfelt, J., McLeskey, S. W., and Kern, F. G. MCF-7 breast carcinoma cells overexpressing FGF-1 form vascularized, metastatic tumors in ovariectomized or tamoxifen-treated nude mice, Oncogene. *15:* 2093-108., 1997.

16. McLeskey, S. W., Kurebayashi, J., Honig, S. F., Zwiebel, J., Lippman, M. E., Dickson, R. B., and Kern, F. G. Fibroblast growth factor 4 transfection of MCF-7 cells produces cell lines that are tumorigenic and metastatic in ovariectomized or tamoxifen-treated athymic nude mice, Cancer Res. *53:* 2168-77., 1993.

17. Ruohola, J. K., Viitanen, T. P., Valve, E. M., Seppanen, J. A., Loponen, N. T., Keskitalo, J. J., Lakkakorpi, P. T., and Harkonen, P. L. Enhanced invasion and tumor growth of fibroblast growth factor 8b- overexpressing MCF-7 human breast cancer cells, Cancer Res. *61:* 4229-37., 2001.

18. Vickers, P. J., Dickson, R. B., Shoemaker, R., and Cowan, K. H. A multidrug-resistant MCF-7 human breast cancer cell line which exhibits cross-resistance to antiestrogens and hormone-independent tumor growth in vivo, Mol Endocrinol. *2:* 886-92., 1988.

19. Sledge, G. W., Jr. Vascular endothelial growth factor in breast cancer: biologic and therapeutic aspects, Semin Oncol. *29:* 104-10., 2002.

20. Zhang, H. T., Scott, P. A., Morbidelli, L., Peak, S., Moore, J., Turley, H., Harris, A. L., Ziche, M., and Bicknell, R. The 121 amino acid isoform of vascular endothelial growth factor is more strongly tumorigenic than other splice variants in vivo, Br J Cancer. *83:* 63-8, 2000.

21. McLeskey, S. W., Tobias, C. A., Vezza, P. R., Filie, A. C., Kern, F. G., and Hanfelt, J. Tumor growth of FGF or VEGF transfected MCF-7 breast carcinoma cells correlates with density of specific microvessels independent of the transfected angiogenic factor, Am J Pathol. *153:* 1993-2006., 1998.

22. Xie, B., Tam, N. N., Tsao, S. W., and Wong, Y. C. Co-expression of vascular endothelial growth factor (VEGF) and its receptors (flk-1 and flt-1) in hormone-induced mammary cancer in the Noble rat, Br J Cancer. *81:* 1335-43., 1999.

23. Pedram, A., Razandi, M., and Levin, E. R. Extracellular signal-regulated protein kinase/Jun kinase cross-talk underlies vascular endothelial cell growth factor-induced endothelial cell proliferation, J Biol Chem. *273:* 26722-8., 1998.

24. Kim, I., Moon, S. O., Kim, S. H., Kim, H. J., Koh, Y. S., and Koh, G. Y. Vascular endothelial growth factor expression of intercellular adhesion molecule 1 (ICAM-1), vascular cell adhesion molecule 1 (VCAM-1), and E- selectin through nuclear factor-kappa B activation in endothelial cells, J Biol Chem. *276:* 7614-20., 2001.

25. Gerber, H. P., Dixit, V., and Ferrara, N. Vascular endothelial growth factor induces expression of the antiapoptotic proteins Bcl-2 and A1 in vascular endothelial cells, J Biol Chem. *273:* 13313-6., 1998.

26. Prall, O. W., Sarcevic, B., Musgrove, E. A., Watts, C. K., and Sutherland, R. L. Estrogen-induced activation of Cdk4 and Cdk2 during G1-S phase progression is accompanied by increased cyclin D1 expression and decreased cyclin-dependent kinase inhibitor association with cyclin E- Cdk2, J Biol Chem. *272:* 10882-94., 1997.

27. Nakshatri, H., Bhat-Nakshatri, P., Martin, D. A., Goulet, R. J., Jr., and Sledge, G. W., Jr. Constitutive activation of NF-kappaB during progression of breast cancer to hormone-independent growth, Mol Cell Biol. *17:* 3629-39., 1997.

28. Dong, L., Wang, W., Wang, F., Stoner, M., Reed, J. C., Harigai, M., Samudio, I., Kladde, M. P., Vyhlidal, C., and Safe, S. Mechanisms of transcriptional activation of bcl-2 gene expression by 17beta-estradiol in breast cancer cells, J Biol Chem. *274:* 32099-107., 1999.

29. Dickson, R. B., McManaway, M. E., and Lippman, M. E. Estrogen-induced factors of breast cancer cells partially replace estrogen to promote tumor growth, Science. *232:* 1540-3., 1986.

30. Soker, S., Miao, H. Q., Nomi, M., Takashima, S., and Klagsbrun, M. VEGF165 mediates formation of complexes containing VEGFR-2 and neuropilin-1 that enhance VEGF165-receptor binding, J Cell Biochem. *85:* 357-68, 2002.

Figure 1A

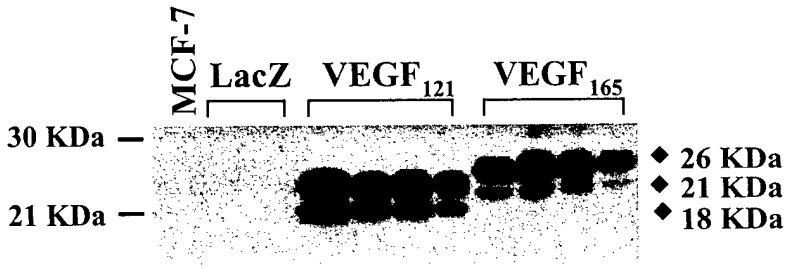

Figure 1B

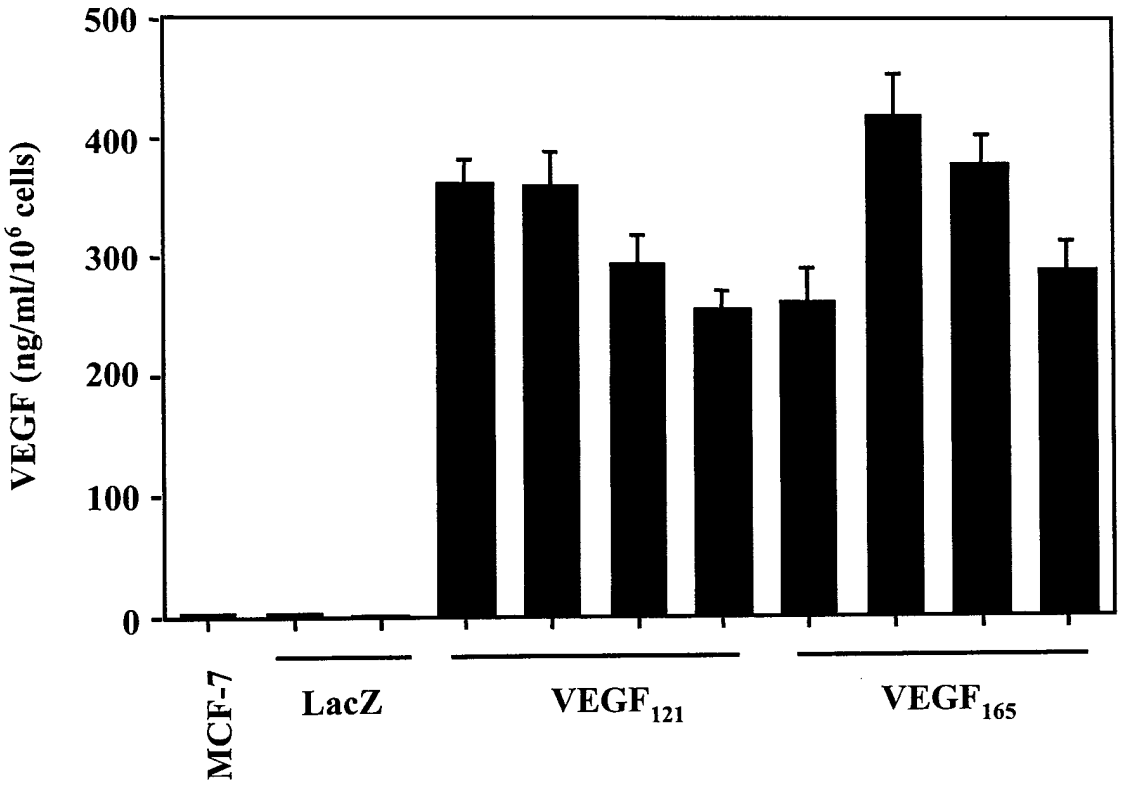
500
400
300
200
100
0
VEGF (ng/ml/10^6 cells)
MCF-7
LacZ
VEGF121
VEGF165

Figure 2A.

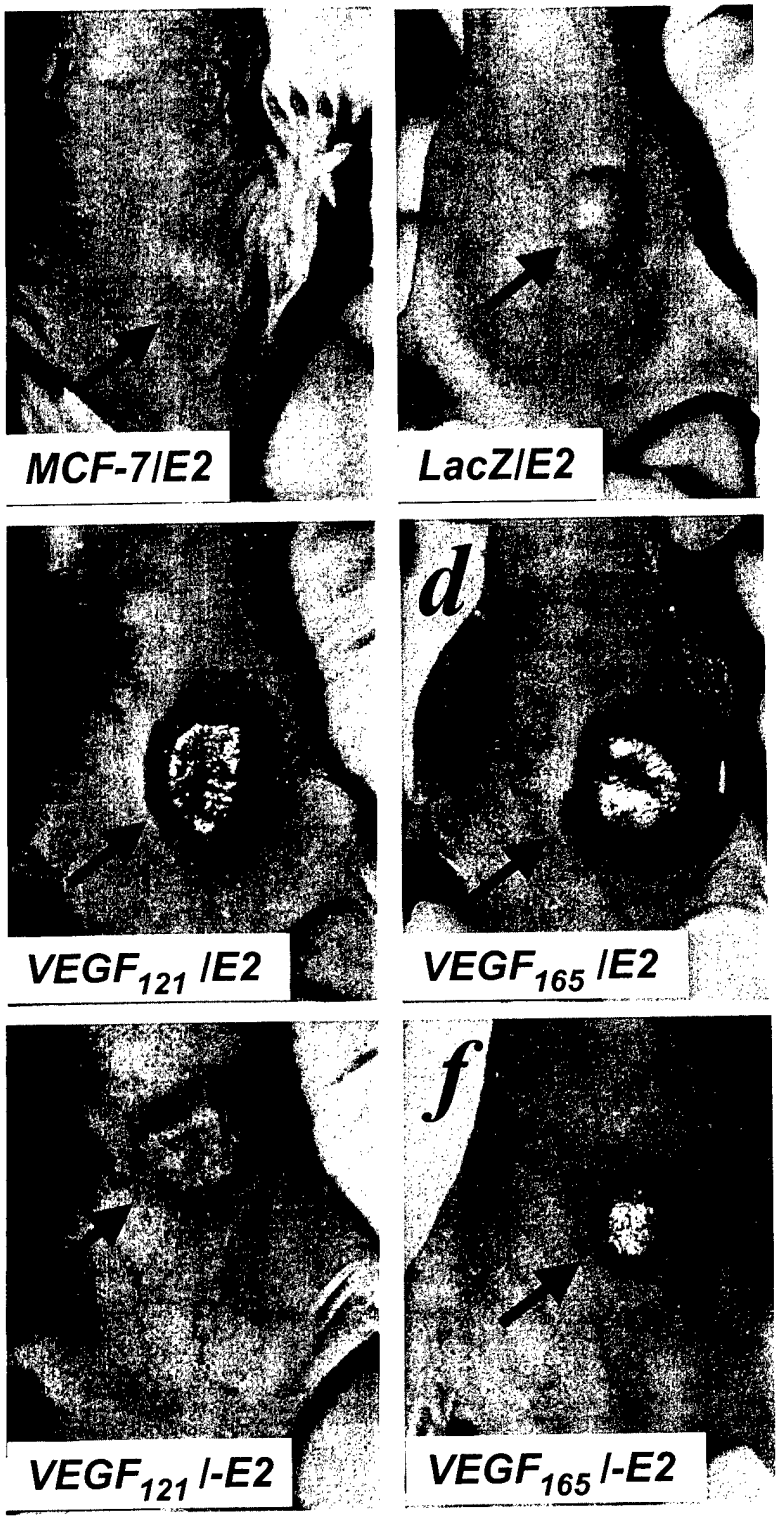
MCF-7/E2
LacZ/E2
VEGF121 /E2
d
VEGF165 /E2
VEGF121 /-E2
f
VEGF165 /-E2

Figure 2B

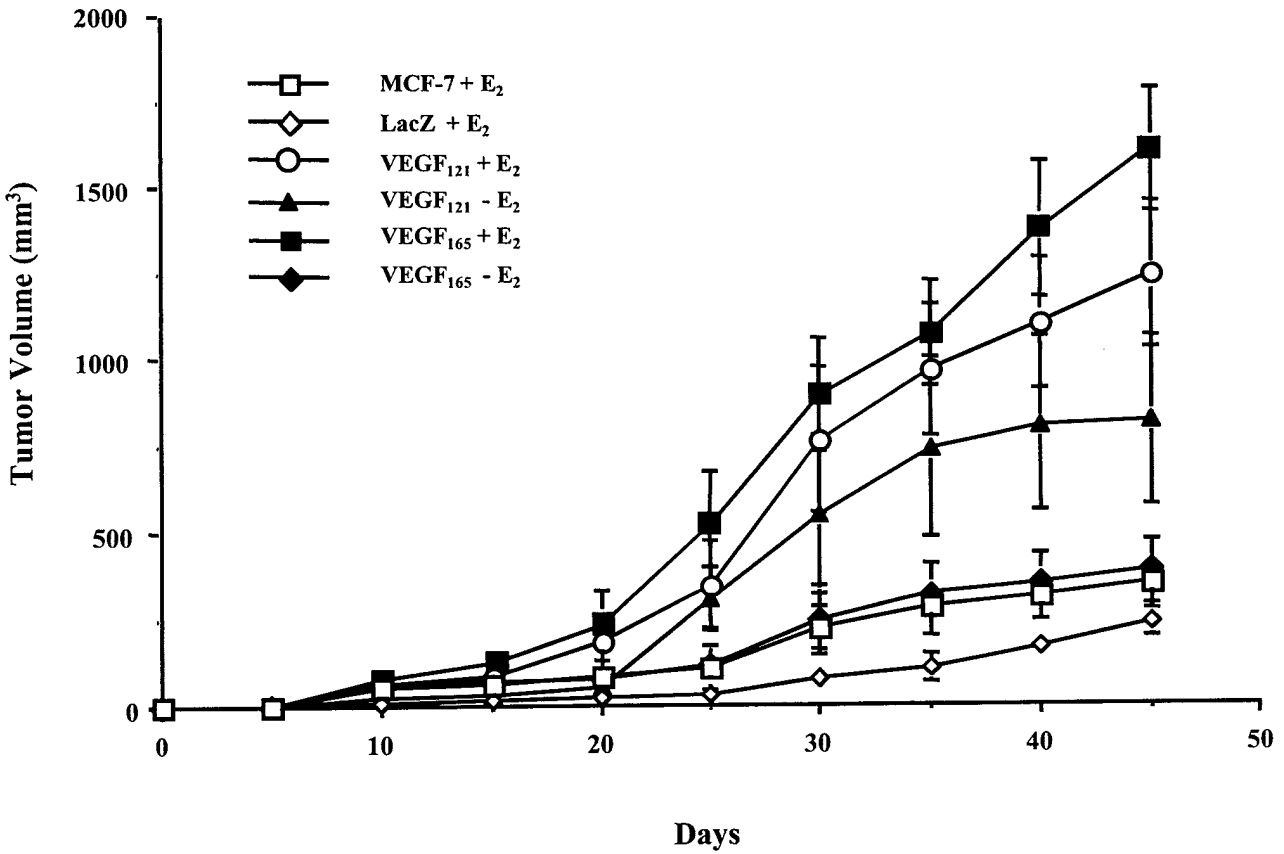
2000
1500
1000
500
0
Tumor Volume (mm3)
0
10
20
30
40
50
Days
MCF-7 + E2
LacZ + E2
VEGF121 + E2
VEGF121 - E2
VEGF165 + E2
VEGF165 - E2

Figure 3A.

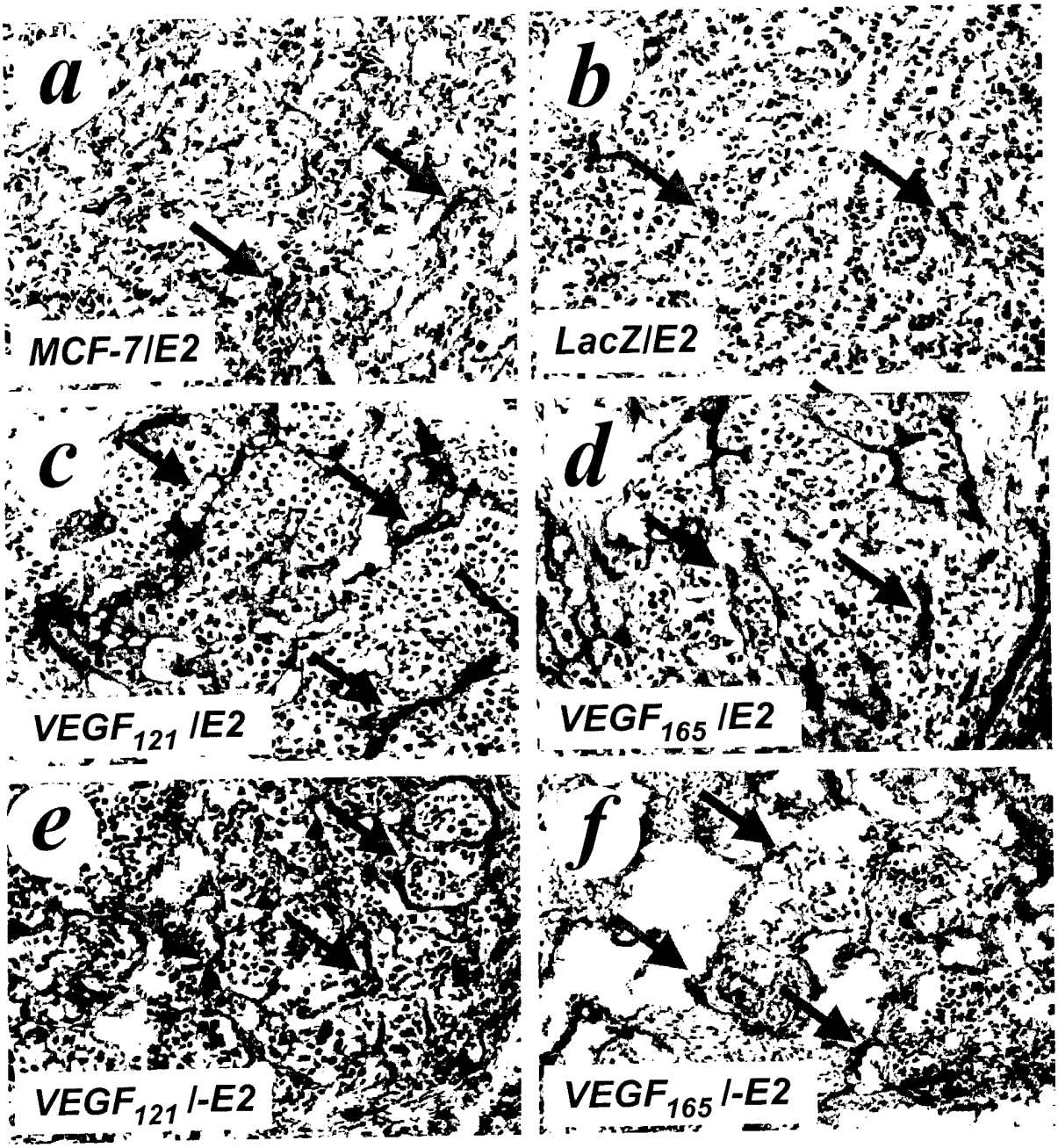
a
MCF-7/E2
b
LacZ/E2
c
VEGF121 /E2
d
VEGF165 /E2
e
VEGF121 /-E2
f
VEGF165 /-E2

Figure 3B

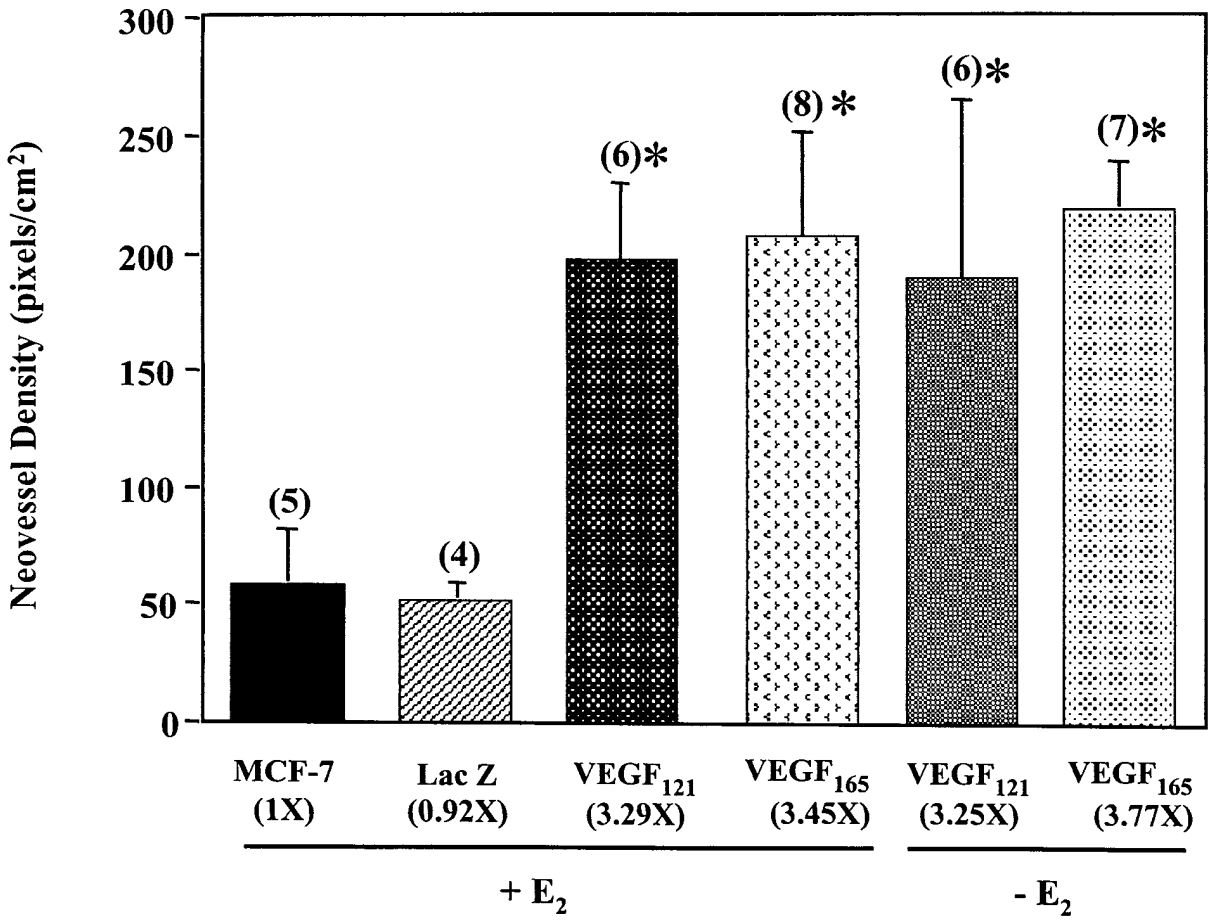
Neovessel Density (pixels/cm²)
300
250
200
150
100
50
0
(5)
(4)
(6)*
(8)*
(6)*
(7)*
MCF-7 (1X)
Lac Z (0.92X)
VEGF121 (3.29X)
VEGF165 (3.45X)
VEGF121 (3.25X)
VEGF165 (3.77X)
+ E2
- E2

Figure 4A

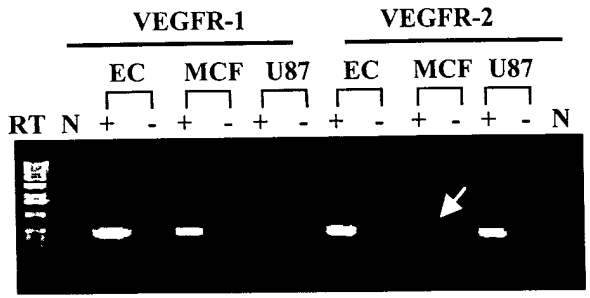

Figure 4B

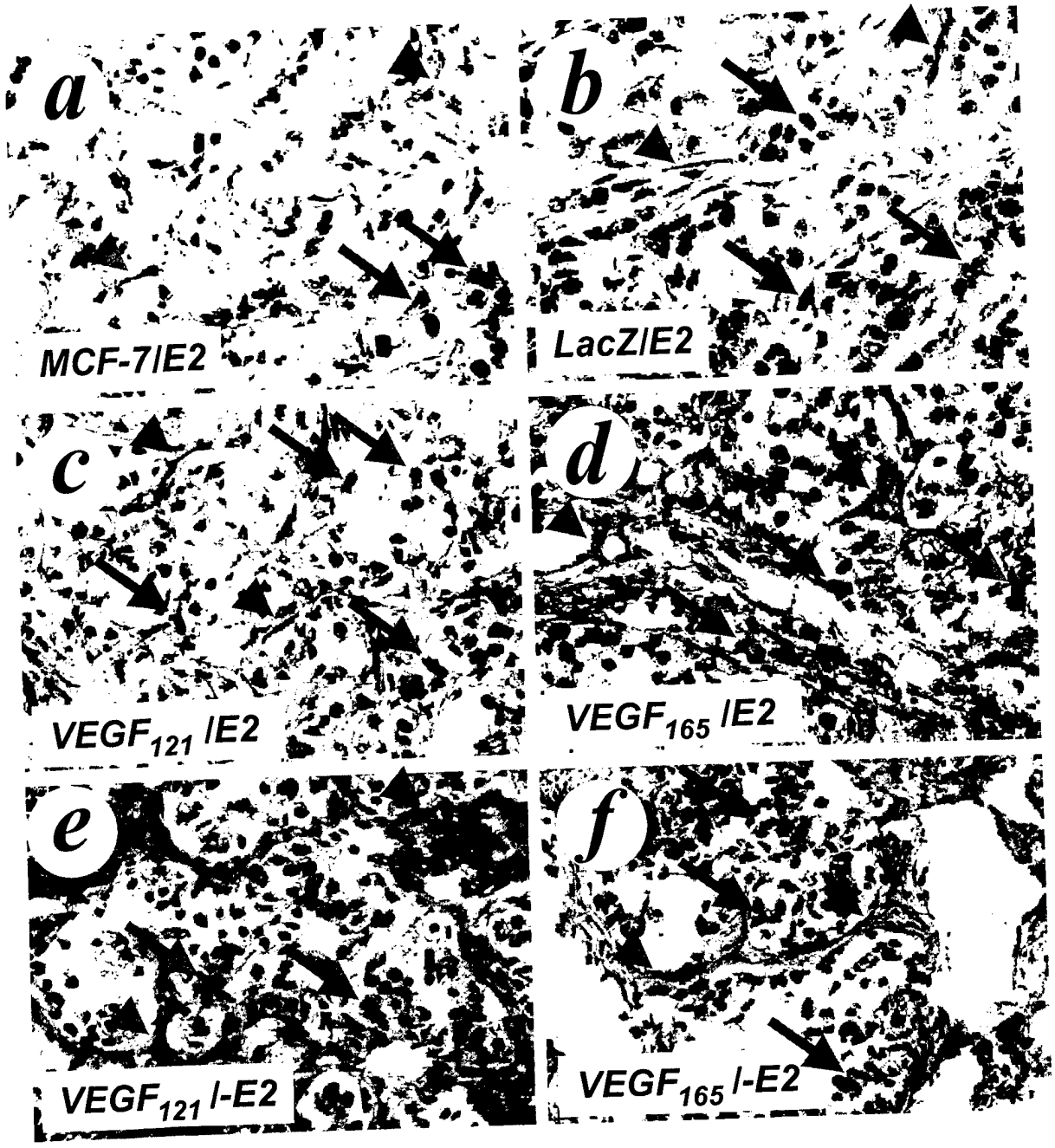
a
MCF-7/E2
b
LacZ/E2
c
VEGF121 /E2
d
VEGF165 /E2
e
VEGF121 /-E2
f
VEGF165 /-E2

Figure 5A

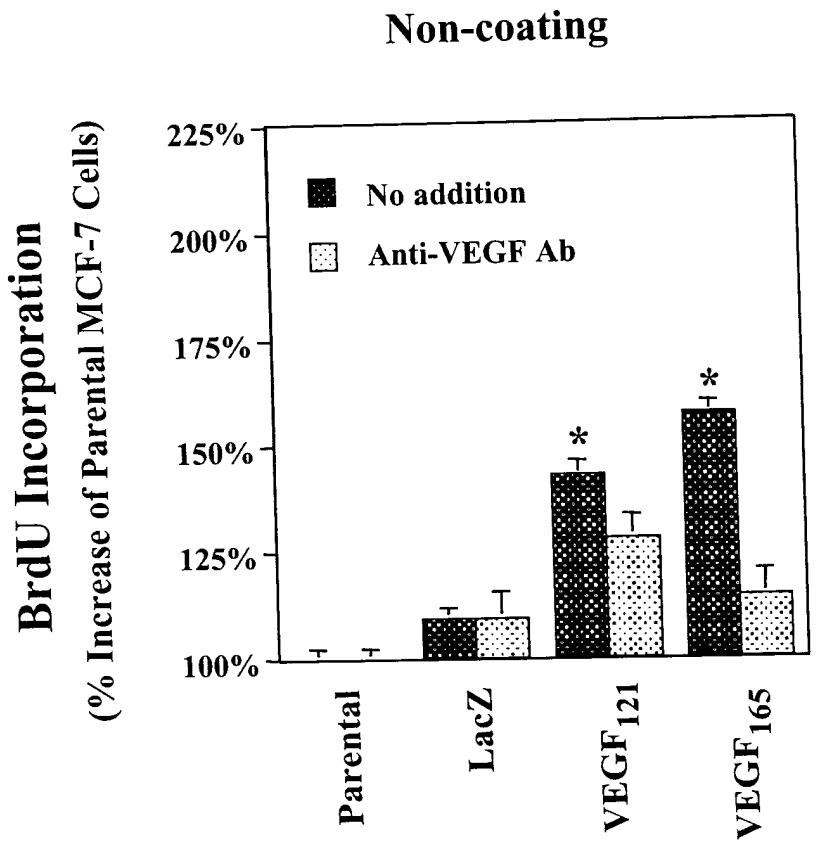
Non-coating
BrdU Incorporation
(% Increase of Parental MCF-7 Cells)
225%
200%
175%
150%
125%
100%
No addition
Anti-VEGF Ab
*
*
Parental
LacZ
VEGF121
VEGF165

Figure 5B

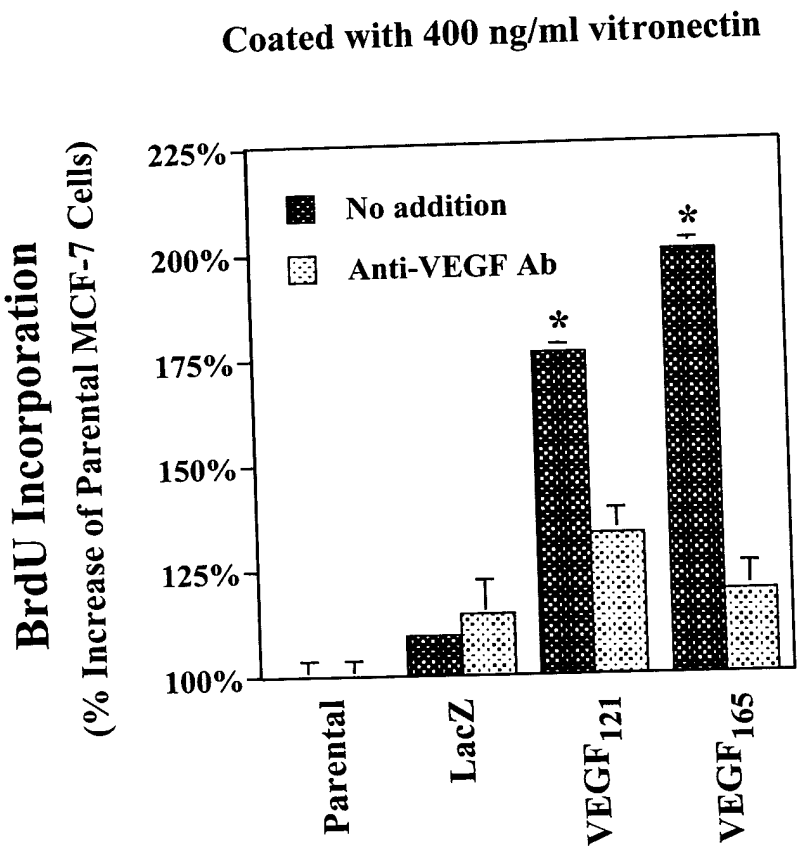
Coated with 400 ng/ml vitronectin
BrdU Incorporation
(% Increase of Parental MCF-7 Cells)
225%
200%
175%
150%
125%
100%
No addition
Anti-VEGF Ab
*
*
Parental
LacZ
VEGF121
VEGF165

Figure 5C

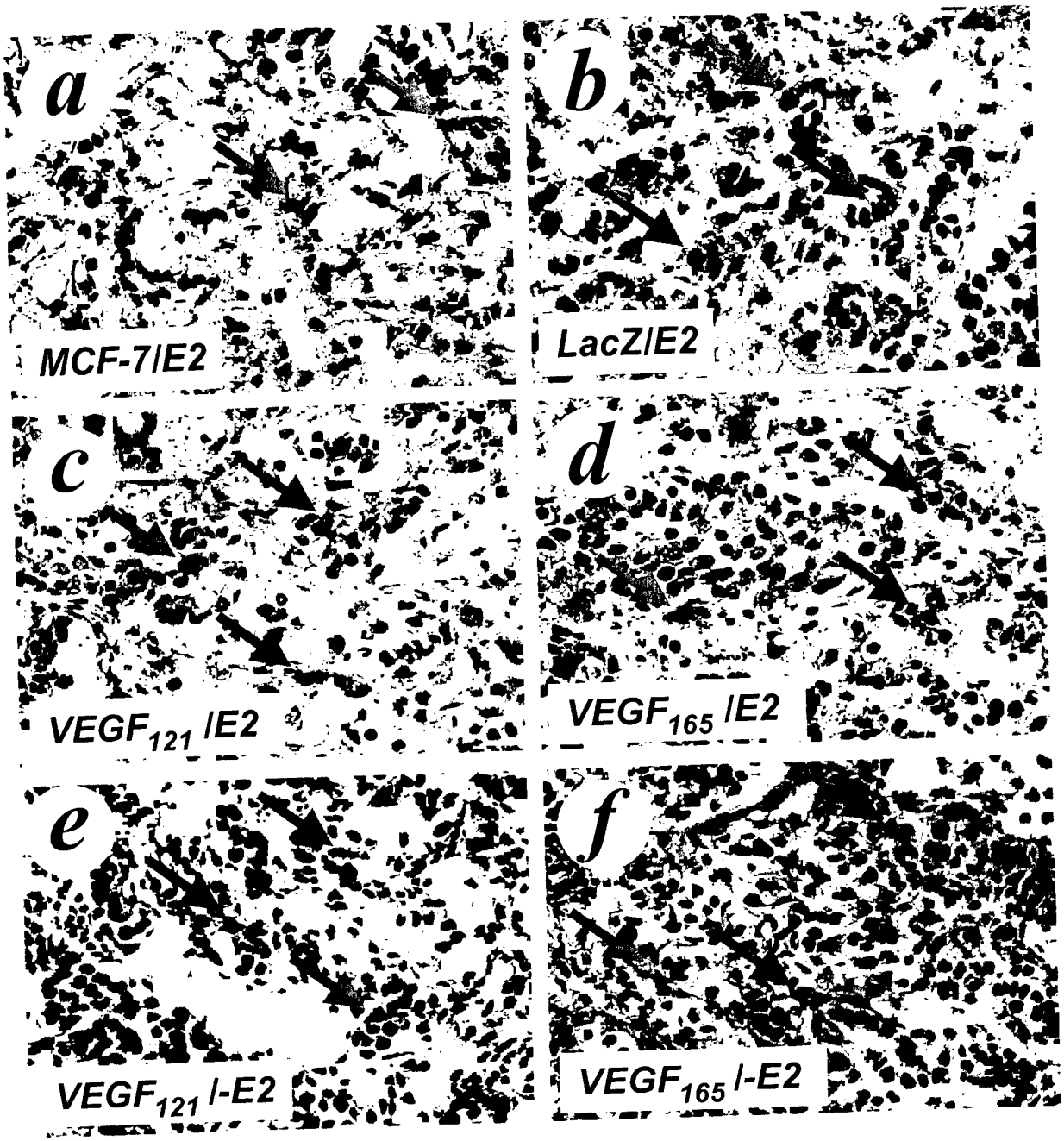
a
MCF-7/E2
b
LacZ/E2
c
VEGF121 /E2
d
VEGF165 /E2
e
VEGF121 /-E2
f
VEGF165 /-E2

Table 1 Tumor growth of MCF-7 VEGF isoform transfectants in nude mice with or without estrogen supplements

Cell Lines	E_2 (-)	E_2 (+)
MCF-7 Parental	0.0 (0%)	307 ± 42.4 (53%)
LacZ	0.0 (0%)[a]	242 ± 50.6 (40%)[b]
$VEGF_{121}$	830 ± 261.8 (81%)[c]	1263 ± 214.3 (90%)[d]
$VEGF_{165}$	391 ± 23.6 (90%)[c]	1638 ± 189.5 (86%)[d]

numbers in parentheses: frequency of the formation of various MCF-7tumors in mice.
a: p=1.00, as compared with tumors derived from MCF-7 cells in non-E_2-treated mice;
b: p=0.98, as compare with tumors derived from MCF-7 cells in E_2-treated mice;
c: p<0.001, as compare with tumors derived from MCF-7 cells in non-E_2-treated mice;
d: p<0.001, as compare with tumors derived from MCF-7 cells in E_2-treated mice;

Overexpression of $VEGF_{121}$, but not $VEGF_{165}$ or FGF-1, Improves Oxygenation in MCF-7 Breast Tumors

Bruce M Fenton[1], Scott F Paoni, Weimin Liu, Shi-Yuan Cheng, Bo Hu, and Ivan Ding

Department of Radiation Oncology, University of Rochester Medical Center, Rochester, NY 14642 (BMF, SFP, WL, ID) and University of Pittsburgh Cancer Institute & Department of Pathology (BH, SYC), Pittsburgh, PA 15213

Pages: 18

Figures: 2

Tables: 1

Running Head: $VEGF_{121}$ improves tumor oxygenation

[1]To whom correspondence should be addressed at Box 704, University of Rochester Medical Center, Rochester, NY 14642; Telephone: 585-275-7911; Fax: 585-273-1042; Email: bruce.fenton@rochester.edu.

Supported by NIH Grant CA52586 (BMF), grants from the Department of Defense: DAMD17-00-1-0420 (BMF), DAMD17-01-1-0375(SYC), and DAMD-17-02-1-0584 (SYC), and the University of Pittsburgh Cancer Institute (SYC).

Abstract

Vascular endothelial growth factor (VEGF) is an intensively studied molecule that has significant potential, both in stimulating angiogenesis and as a target for antiangiogenic approaches. We utilized MCF-7 breast cancer cells transfected with either of two of the major VEGF isoforms, $VEGF_{121}$ or $VEGF_{165}$, or fibroblast growth factor-1 (FGF-1) to distinguish the effects of these factors on tumor growth, vascular function, and oxygen delivery. While each transfectant demonstrated substantially increased tumorigenicity and growth rate compared to vector controls, only $VEGF_{121}$ produced a combination of significantly reduced total and perfused vessel spacing, as well as a corresponding reduction in overall tumor hypoxia. Such pathophysiological effects are of potential importance, since antiangiogenic agents designed to block VEGF isoforms could in turn result in the development of therapeutically unfavorable environments. If antiangiogenic agents are also combined with conventional therapies such as irradiation or chemotherapy, microregional deficiencies in oxygenation could play a key role in ultimate therapeutic success.

Keywords

antiangiogenic, hypoxia, image analysis, perfusion, tumor vasculature

Introduction

Vascular endothelial growth factor (VEGF), perhaps the most critical regulator of angiogenesis in both tumors and normal tissue, is regulated by numerous factors, most notably tissue oxygen level [Shweiki et al., 1992]. VEGF exists as six alternatively spliced isoforms, predominantly $VEGF_{121}$ and $VEGF_{165}$ [Ferrara, 1999], and a number of previous workers have studied vascular changes in tumor lines transfected to overexpress specific isoforms. An almost universal finding among all of the different isoforms has been that overexpression enhances tumorigenesis and tumor progression [Bicknell R, 1997]. In MCF-7 human breast carcinomas specifically, which normally produce low levels of VEGF, $VEGF_{121}$ transfectants formed faster growing, more vascularized tumors in comparison to wild-type [Zhang et al., 1995]. *In vitro* and *in vivo*, $VEGF_{121}$ transfected MCF-7 tumor cells were shown to be much more tumorigenic and angiogenic than $VEGF_{165}$, perhaps due to the enhanced ability of the $VEGF_{121}$ isoform to freely diffuse from the cells producing it [Zhang et al., 2000]. Our previous studies have also shown that overexpression of $VEGF_{121}$ or $VEGF_{165}$ by estrogen-dependent MCF-7 breast cells stimulates breast tumor formation and neovascularization in an estrogen-independent fashion in ovariectomized mice, in the absence of 17 β-estradiol treatment [Guo et al., 2003]. These findings suggested that upregulation of VEGF in estrogen-dependent breast cancer contributes to the acquisition of estrogen-independent cancer growth by stimulating tumor angiogenesis and progression through both autocrine and paracrine mechanisms.

Findings in other tumor cell lines have been somewhat mixed. Using transformed murine fibrosarcoma cells (that initially lack VEGF) to specifically express each of the isoforms, it was found that only $VEGF_{164}$ (the murine version of $VEGF_{165}$) could fully rescue tumor growth [Grunstein et al., 2000]. In this study, vascular densities were unchanged in either the $VEGF_{120}$ or $VEGF_{165}$ transfectants compared to vector controls. In the WM1341B melanoma cell line, however, $VEGF_{165}$ produced much more richly vascularized tumors in transfectants, despite the fact that $VEGF_{121}$ was the predominant isoform in parental cell lines [Yu et al., 2002]. In gliomas, different VEGF isoforms demonstrated different biological activities than each other at the same site, as well as different activities for the same isoform when implanted at different sites [Guo et al., 2001].

Although the effects of $VEGF_{121}$ and $VEGF_{165}$ have been studied in a range of tumor models, techniques have not been available for quantifying corresponding alterations in tumor blood flow and oxygenation until fairly recently. Since several promising antiangiogenic strategies rely on blocking either VEGF or its receptors [Bruns et al., 2002;Gerber et al., 2000], such accompanying pathophysiological changes are clearly of interest. Reductions or enhancements in tumor oxygenation could be especially important when combining antiangiogenic agents with conventional therapies, such as radiotherapy and chemotherapy, each of which directly depends on microregional tumor blood flow and oxygenation. The current work utilized MCF-7 breast cancer cells transfected with either $VEGF_{121}$ or $VEGF_{165}$. In addition, since FGF-1 has been similarly associated with highly vascularized tumors [Zhang et al., 1997], FGF-1 overexpressing transfectants were included for comparison. Using a combination of immunohistochemistry and image analysis techniques, four pathophysiological indices were determined: 1) total vessel spacing, 2) perfused vessel spacing, 3) % vascular area,

and 4) overall tumor hypoxia. Results demonstrate that among these angiogenic growth factors, only $VEGF_{121}$ overexpression produced significant alterations in overall tumor oxygenation.

Materials and Methods

Cell lines and Reagents: MCF-7 cells were obtained from American Tissue Culture Collection (ATCC, Rockville, MD), and MCF-7 cells that stably express VEGF or FGF-1 were generated by transfecting MCF-7 cells with $VEGF_{121}$, $VEGF_{165}$, or FGF-1 cDNA. The clones that highly expressed exogenous $VEGF_{121}$, $VEGF_{165}$, or FGF-1 were expanded and characterized by methods described previously [Zhang et al., 1997;Guo et al., 2001]. Human MCF-7 breast tumors were grown in the mammary fat pads of ovariectomized female nude mice as described previously [Zhang et al., 1997;Guo et al., 2001]. Briefly, 1×10^7 cells were inoculated into the mammary fat pads of 7 to 8-week old, ovariectomized female nude mice that were implanted with 17-β estradiol 60-day slow release pellets (Innovative Research of America, Sarasota, FL). The volumes of the tumors were measured using calipers and the formula $\frac{1}{2}\, ab^2$ (where a and b are the major and minor tumor dimensions).

$DiOC_7$ perfusion marker and EF5 hypoxic marker: To visualize blood vessels open to flow, an intravascular stain, $DiOC_7$, was injected 1 min prior to freezing to preferentially stain cells adjacent to the vessels [Fenton et al., 1999]. Localized areas of tumor hypoxia were assessed in frozen tissue sections by immunohistochemical identification of sites of 2-nitroimidazole metabolism (EF5 binding) [Fenton et al., 1999]. EF5 (from NCI) was injected *i.v.* one hour before tumor freezing, at which time the EF5 is well distributed throughout even poorly perfused regions of the tumor [Fenton et al., 2001]. Regions of high EF5 metabolism were visualized immunohistochemically using a Cy3 fluorochrome conjugated to the ELK3-51 antibody, which is extremely specific for the EF5 drug adducts that form when the drug is incorporated by hypoxic cells [Lord et al., 1993].

Immunohistochemistry and image analysis: Tumor sections were imaged using a 20× objective, digitized (Sony DXC9000 3CCD camera), background-corrected, and image-analyzed using Image-Pro software (Media Cybernetics, Silver Spring, MD) [Fenton et al., 1999]. Color image montages from 16 adjacent microscope fields in each of four tumor regions (encompassing roughly 15 mm^2) were automatically acquired and digitally combined under three different staining conditions. First, images of the $DiOC_7$ were obtained immediately after the frozen sections were sliced on the cryostat. Following staining, the section was returned to the same stage coordinates, and imaged for both hypoxia (EF5) and total vasculature (anti-panendothelial cell antigen, Pharmingen, San Diego, CA). The total vasculature and perfused vasculature images were enhanced using color segmentation to identify appropriate blood vessels [Fenton et al., 1999]. Using "distance map" filtering of the segmented images, individual pixel intensities were converted to levels directly proportional to the distances between tumor cells and the nearest blood vessel [Fenton et al., 2002]. Percentage vascular area (defined as total or perfused vessel area /total tissue area) was also determined using Image Pro software. Finally, fluorescent image montages of the EF5/Cy3 staining were quantified by determining the mean pixel intensity of each image (range: 0-255). CCD camera

settings were set to a constant shutter speed of 1/60, with constant gain, contrast, and brightness settings.

Statistical Analysis: Tumor means were compared using the Student's t-test and differences were considered significant for $p < 0.05$.

Results

Overexpression of $VEGF_{121}$, $VEGF_{165}$, or FGF-1 by MCF-7 cells enhanced estrogen-dependent tumor growth: To determine whether expression of $VEGF_{121}$, $VEGF_{165}$, or FGF-1 by MCF-7 cells enhances MCF-7 breast tumor growth in vivo, MCF-7 vector controls, $VEGF_{121}$, $VEGF_{165}$, or FGF-1 cells were implanted orthotopically. At 45 days post-implantation, 40% of mice that received MCF-7/vector cells developed tumors, and volumes averaged 242 ± 50.6 mm^3. In contrast, expression of $VEGF_{121}$, $VEGF_{165}$, or FGF-1 not only increased the frequency of MCF-7 tumor formation, but also dramatically enhanced tumor growth. As summarized in Table I, tumor volumes were significantly increased for each of the three transfectants in relation to vector controls ($p < 0.001$).

$VEGF_{121}$, $VEGF_{165}$, and FGF-1 have varying effects on tumor vascularity and perfusion: Since tumor vascularity and hypoxia have been shown to vary with tumor volume [Fenton et al., 1988], a separate set of volume-matched tumors were used for the pathophysiological measurements. Mean volumes ± standard errors were as follows: vectors (410±90 mm^3), $VEGF_{121}$ (440±30), $VEGF_{165}$ (570±80), and FGF-1 (440±90). Compared to vector controls, total vessel spacing was significantly decreased in both the $VEGF_{121}$ ($p < 0.001$) and $VEGF_{165}$ ($p = 0.001$) tumors, but unchanged in the FGF-1 tumors (see Figures 1A-D and 2A). Note that this decrease in vascular spacing corresponds to the increased vascularity shown in Figure 1. Perfused vessel spacing (Figure 2B), on the other hand, was significantly decreased for both the $VEGF_{121}$ ($p < 0.001$) and FGF-1 ($p < 0.013$) tumors, but not for the $VEGF_{165}$ ($p = 0.15$) (see Figures 1E-H for representative images of the green perfusion stain superimposed on the orange hypoxia stain). To determine whether vascularity or perfusion varied with depth into the tumor, additional low power image montages (10× objective) were also acquired to contrast vascular spacing in the center (defined by a circular region of diameter 3000 μm) versus the periphery of the tumor cross-section. On average, neither total nor perfused vessel spacing varied significantly with depth into the tumor for any of the four tumor models (data not shown). However, two distinctly different vascular patterns were observed among $VEGF_{165}$ tumors. In roughly half of these tumors, a central region of hypoxia developed that was surrounded by a densely vascularized peripheral rim of vessels (Figure 1I), but in the others, vessels were fairly evenly distributed (Figure 1J).

Vessel diameters and interconnectivity (20 × objective) were also markedly different among the transfectants, as shown in Figures 1A-D. In comparison to vector controls, percentage areas of both total (open bars in Figure 2C) and perfused (filled bars in Figure 2C) vessels were significantly increased for each of the three transfectants, again most strikingly for the $VEGF_{121}$ tumors.

$VEGF_{121}$ overexpression reduces overall tumor hypoxia: Overall tumor hypoxia was characterized by measuring the mean intensity of the Cy3 conjugated antibody to the EF5 hypoxia marker. As summarized in Figure 2D (and shown by the orange staining in Figures 1E-H), overall tumor hypoxia was unchanged in the $VEGF_{165}$ and FGF-1 tumors,

but significantly reduced in the $VEGF_{121}$ tumors ($p = 0.026$) compared to vector controls. This decrease in hypoxia for the $VEGF_{121}$ tumors is in agreement with the striking decrease in perfused vessel spacing observed for these tumors (Figure 2B), which corresponds to a decrease in the distance oxygen must diffuse to reach the tumor cells most distant from the vessels. In the case of the FGF-1 tumors, however, overall tumor hypoxia was unchanged despite a significant (although less pronounced than in the $VEGF_{121}$ tumors) decrease in perfused vessel spacing.

Discussion

While VEGF is well accepted as an important modulator of tumor growth and vascular development, specific pathophysiological alterations associated with the different VEGF isoforms are less well understood. The current work reaffirms the notion that different VEGF isoforms lead to distinct differences in tumor vascular structure when compared at the same implantation site. In addition, we found that such vascular changes are, in some cases, directly associated with alterations in tumor oxygenation.

In previous studies, results have varied widely in terms of both tumor growth rate and vascular density when different tumor models and implantation sites were considered. Guo, et al. [Guo et al., 2001] demonstrated that microenvironmental factors may be important, comparing $VEGF_{121}$ and $VEGF_{165}$ transfected glioma cell lines implanted either subcutaneously (*s.c.*) or intracranially (*i.c.*). $VEGF_{165}$ transfectants grew much more rapidly than wild-type at either location, with a corresponding increase in vascular density at both. Interestingly, $VEGF_{121}$ transfectants exhibited enhanced vessel growth only when implanted orthotopically in the brain.

Using transfected fibrosarcoma cell lines, Grunstein et al. [Grunstein et al., 2000] proposed a model in which the different VEGF isoforms preferentially recruit blood vessels to either the tumor interior or periphery. It was suggested that these vascular patterns could possibly relate to the diffusibility of the $VEGF_{121}$ versus the $VEGF_{165}$. In this model, $VEGF_{120}$ overexpressing tumors tended to more effectively recruit systemic vessels, but failed to develop adequate internal vascularization [Grunstein et al., 2000], while $VEGF_{164}$ tumors were capable of inducing both external and internal vascular expansion. In human melanoma transfectants, overall growth rate of the tumors correlated only with amount of secretable VEGF, rather than on which specific VEGF isoform was overexpressed [Yu et al., 2002]. Although $VEGF_{121}$ tumors were more densely vascularized at the tumor periphery (with more central necrosis), $VEGF_{165}$ tumors produced a much more densely vascularized plexus of blood vessels overall.

In the current study, human MCF-7 cells were implanted orthotopically in the mammary fat pad. Growth rates of $VEGF_{121}$ and $VEGF_{165}$ transfectants were significantly higher than vector controls and essentially equal to each other, while FGF-1 tumors grew at a somewhat less rapid rate. Both $VEGF_{121}$ and $VEGF_{165}$ produced densely arcading networks of blood vessels of increased vascular diameter. In contrast to both the fibrosarcomas and melanomas, however, spatial heterogeneities in vascular spacing were generally not observed. On average, neither total nor perfused vascular spacing varied as a function of distance from the tumor surface for any of the MCF-7 transfectants, although roughly half of the $VEGF_{165}$ tumors demonstrated a reduction in vasculature in the tumor center compared to periphery. Also, in contrast to previous reports in other models, MCF-7 $VEGF_{121}$ transfectants were much more evenly vascularized than the

$VEGF_{165}$, as measured by the reduction in vascular spacing. Although the reasons for these disparate findings are unclear, spatially dependent vascular heterogeneities could possibly be related to either specific implantation site or differences in tumor volume.

A key advantage in our method of measuring vascular spacing, rather than the more commonly reported "vessels/field" or "positive pixels/mm^2", is that vascular spacing is more closely related to the ability of the blood vessels to uniformly supply the tumor with oxygen and nutrients. Especially in tumors containing an uneven distribution of vessels, determinations of mean vascular density can be highly misleading in terms of tumor oxygen delivery. For example, a tumor with a highly localized cluster of dense vascularization could have an overall vascular density equal to that of a tumor having a reduced but homogeneous distribution of vessels. Clearly, micro-regional efficiencies in the delivery of either oxygen or chemotherapeutic agents would be quite different between the two. Such differences are apparent when using our "distance map" measurements of vascular spacing, which depends on vessel number, size, and spatial distribution. Although neither perfused vessel spacing nor tumor hypoxia was significantly altered in the $VEGF_{165}$ tumors, $VEGF_{121}$ tumors demonstrated significant changes in both. This decrease in perfused vessel spacing suggests that these vessels are more efficiently distributed in the $VEGF_{121}$ tumors, which is supported by the significant decrease in overall tumor hypoxia observed in these tumors.

Finally, FGF-1 transfectants have also been reported to form large, vascularized tumors and to confer a more malignant phenotype upon MCF-7 cells, without estrogen supplementation [Zhang et al., 1997]. In the current studies, FGF-1 overexpression led to a substantial increase in tumor growth rate, with a significant decrease in the perfused vessel spacing. Conceivably, this increase in perfused vasculature could translate to an increased opportunity for these tumor cells to invade into the circulation and metastasize [Zhang et al., 1997].

A major unanswered question raised by this and previous studies is why $VEGF_{121}$ and $VEGF_{165}$ isoforms have such disparate effects on vascular structure and function among different tumor models. Although tumorigenicity and vascular growth were increased by both in all of the previously cited tumor models, specific alterations in vascular morphology were distinctly different. Interestingly, it has been reported that while $VEGF_{121}$ is the predominant form expressed in human breast carcinomas [Relf et al., 1997] and melanomas [Yu et al., 2002], the $VEGF_{165}$ variant is predominant in glioblastomas [Berkman et al., 1993]. This is intriguing in view of the fact that the vascular modification associated with $VEGF_{121}$ or $VEGF_{165}$ transfectants of the three tumor types do not necessarily follow this same pattern. In breast tumors, the predominant variant, $VEGF_{121}$, was also the more effective in inducing extensive tumor vascularization when overexpressed in that model. In melanomas and gliomas, however, an entirely different relationship holds true, and in each case, the predominant isoform is the less important in terms of promoting vascular development [Yu et al., 2002;Guo et al., 2001].

Previous studies have speculated that differences in vascular configuration between $VEGF_{121}$ and $VEGF_{165}$ may be related to variations in heparin binding, isoform size, or diffusivity [Yu et al., 2002;Guo et al., 2001]. It has also been hypothesized that variations in isoform expression may confer differential advantages on tumors as they expand in the different sites, each of which may possess different requirements for

neovascularization [Grunstein et al., 2000]. Further detailed studies are needed to determine whether vascular response is primarily dictated by the immediate microenvironment of the tumor, including proximity to nearby preexisting host vessels, or instead related to local balances among additional angiogenic growth factors and inhibitors.

Acknowledgements

The authors would like to thank Dr. Lurong Zhang of the Lombardi Cancer Center, Georgetown University Medical Center, for providing the FGF-1 transfected MCF-7 tumor cell line.

Figure Legends

Figure 1 – Representative immunohistochemical staining of anti-panendothelial cell antigen in panels A-D, with corresponding images of the$DiOC_7$ perfusion marker (green) superimposed over the EF5 hypoxia marker (orange), in panels E-J. Intensely stained orange regions of A, C, and D correspond to increased tumor hypoxia. MCF-7 vector is shown in A and E, $VEGF_{121}$ in B and F, $VEGF_{165}$ in C and G, and FGF-1 in D and H. Each of panels A-H are portions of the original 4×4 composite images taken with a 20× objective, and the bar in panel E equals 100 μm. Panels I and J are entire 4×4 composites taken with a 10× objective (bar in panel I equals 500 μm), illustrating the two general patterns of vascular configuration and hypoxia observed in $VEGF_{165}$ tumors. Peripheral vasculature with centralized hypoxia is shown in panel I and a more randomly distributed pattern of vasculature and hypoxia is shown in panel J.

Figure 2 – Effects of VEGF isoforms and FGF-1 on vascular spacing, % vascular area, and overall hypoxia. Data are presented as median distances (mean ± SE) to the nearest total (A) or perfused (B) blood vessel, and increased median distances correspond to decreased vascular densities. An increased disparity between the total and perfused bars for a given tumor type indicates an increased proportion of nonfunctional vessels in that tumor. Data are averaged over four 4 × 4 image montages (64 fields) from each of 10 MCF-7 vectors (mean volume ± SEM = 410±90 mm^3), 6 $VEGF_{121}$ tumors (440±30)), 5 $VEGF_{165}$ tumors (570±80), and 9 FGF-1 tumors (440±90). (C) Percentage vascular area for total (open bars) and perfused (filled bars) vessels. Asterisks denote statistically significant differences from vector controls. (D) tumor hypoxia, as measured by overall EF5/Cy3 intensity (mean ± SE), again averaged over four 4 × 4 image montages.

References

Berkman RA, Merrill MJ, Reinhold WC (1993) Expression of the vascular permeability factor/vascular endothelial growth factor gene in central nervous system neoplasms. *J Clin Invest* 91: 153-159

Bicknell R (1997) Mechanistic insights into tumour angiogenesis. In *Tumour Angiogenesis*, Bicknell R, Lewis CE, Ferrara N (eds) pp 19-28. Oxford University Press: Oxford

Bruns CJ, Shrader M, Harbison MT, Portera C, Solorzano CC, Jauch KW, Hicklin DJ, Radinsky R, Ellis LM (2002) Effect of the vascular endothelial growth factor receptor-2 antibody DC101 plus gemcitabine on growth, metastasis and angiogenesis of human pancreatic cancer growing orthotopically in nude mice. *Int J Cancer* 102: 101-108

Fenton BM, Lord EM, Paoni SF (2001) Effects of radiation on tumor intravascular oxygenation, vascular configuration, hypoxic development, and survival. *Radiat Res* 155: 360-368

Fenton BM, Paoni SF, Beauchamp BK, Ding I (2002) Zonal image analysis of tumour vascular perfusion, hypoxia, and necrosis. *Br J Cancer* 86: 1831-1836

Fenton BM, Paoni SF, Lee J, Koch CJ, Lord EM (1999) Quantification of tumor vascular development and hypoxia by immunohistochemical staining and HbO_2 saturation measurements. *Br J Cancer* 79: 464-471

Fenton BM, Rofstad EK, Degner FL, Sutherland RM (1988) Cryospectrophotometric determination of tumor intravascular oxyhemoglobin saturations: Dependence on vascular geometry and tumor growth. *J Natl Cancer Inst* 80: 1612-1619

Ferrara N (1999) Vascular endothelial growth factor: molecular and biological aspects. *Curr Top Microbiol Immunol* 237: 1-30

Gerber HP, Kowalski J, Sherman D, Eberhard DA, Ferrara N (2000) Complete inhibition of rhabdomyosarcoma xenograft growth and neovascularization requires blockade of both tumor and host vascular endothelial growth factor. *Cancer Res* 60: 6253-6258

Grunstein J, Masbad JJ, Hickey R, Giordano F, Johnson RS (2000) Isoforms of vascular endothelial growth factor act in a coordinate fashion to recruit and expand tumor vasculature. *Molecular & Cellular Biology* 20: 7282-7291

Guo, P., Fang, Q., Tao, H.-Q., Schafer, A., Fenton, B. M., Ding, I., Hu, B., and Cheng, S.-Y. Overexpression of VEGF by MCF-7 breast cancer cells promotes estrogen-independent tumor growth in vivo. Cancer Research . 2003.
Ref Type: In Press

Guo P, Xu L, Pan S, Brekken RA, Yang ST, Whitaker GB, Nagane M, Thorpe PE, Rosenbaum JS, Su HH, Cavenee WK, Cheng SY (2001) Vascular endothelial growth factor isoforms display distinct activities in promoting tumor angiogenesis at different anatomic sites. *Cancer Res* 61: 8569-8577

Lord EM, Harwell L, Koch CJ (1993) Detection of hypoxic cells by monoclonal antibody recognizing 2-nitroimidazole adducts. *Cancer Res* 53: 5721-5726

Relf M, Lejeune S, Scott PE, Fox S, Smith K, Leek R, Moghaddam A, Whitehouse R, Bicknell R, Harris AL (1997) Expression of the angiogenic factors vascular endothelial cell growth factor, acidic and basic fibroblast growth factor, tumor growth factor beta-1, platelet-derived endothelial cell growth factor, placenta growth factor, and pleiotrophin in human primary breast cancer and its relation to angiogenesis. *Cancer Res* 57: 963-969

Shweiki D, Itin A, Soffer D, Keshet E (1992) Vascular endothelial growth factor induced by hypoxia may mediate hypoxia-initiated angiogenesis. *Nature* 359: 843-845

Yu JL, Rak JW, Klement G, Kerbel RS (2002) Vascular endothelial growth factor isoform expression as a determinant of blood vessel patterning in human melanoma xenografts. *Cancer Res* 62: 1838-1846

Zhang HT, Craft P, Scott PAE, Ziche M, Weich HA, Harris AL, Bicknell R (1995) Enhancement of tumor growth and vascular density by transfection of vascular endothelial cell growth factor into MCF-7 human breast carcinoma cells. *J Natl Cancer Inst* 87: 213-219

Zhang H-T, Scott PAE, Morbidelli L, Peak S, Moore J, Turley.H., Harris AL, Ziche M, Bicknell R (2000) The 121 amino acid isoform of vascular endothelial growth factor is more strongly tumorigenic than other splice variants in vivo. *Br J Cancer* 83: 63-68

Zhang L, Kharbanda S, Chen D, Bullocks J, Miller DL, Ding IYF, Hanfelt J, McLeskey SW, Kern FG (1997) MCF-7 breast carcinoma cells overexpressing FGF-1 form vascularized, metastatic tumors in ovariectomized or tamoxifen-treated nude mice. *Oncogene* 15: 2093-2108

Figure 1

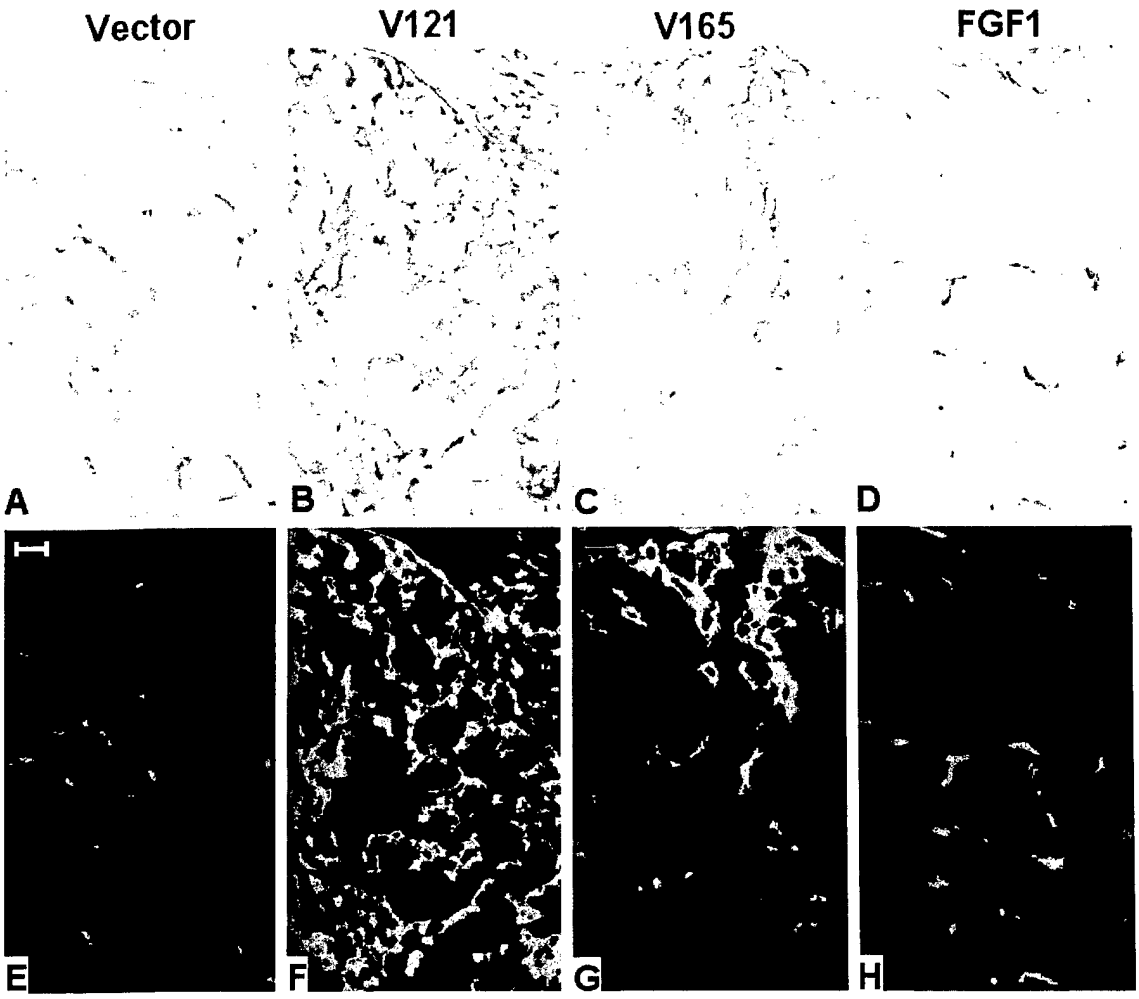

Figure 1 (continued)

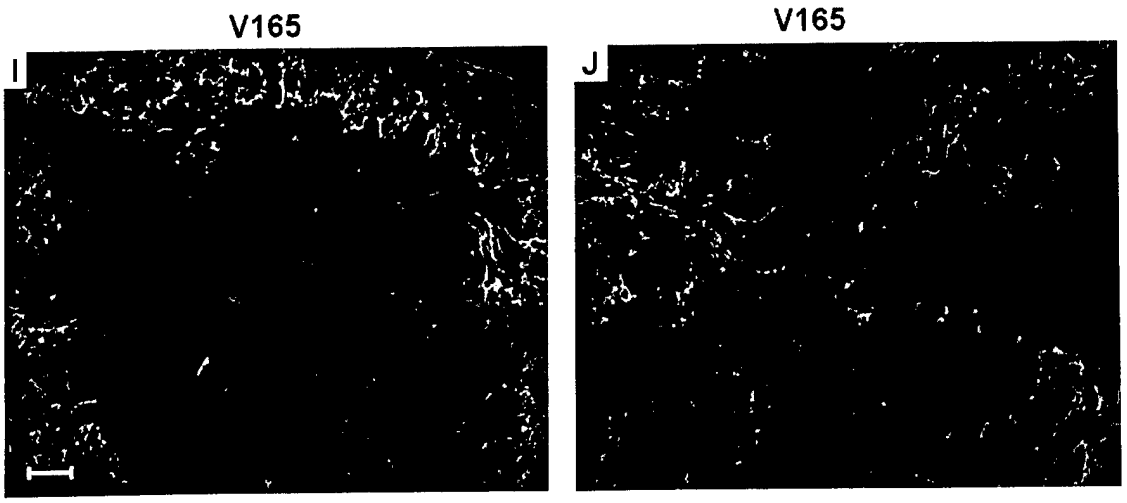

Figure 2

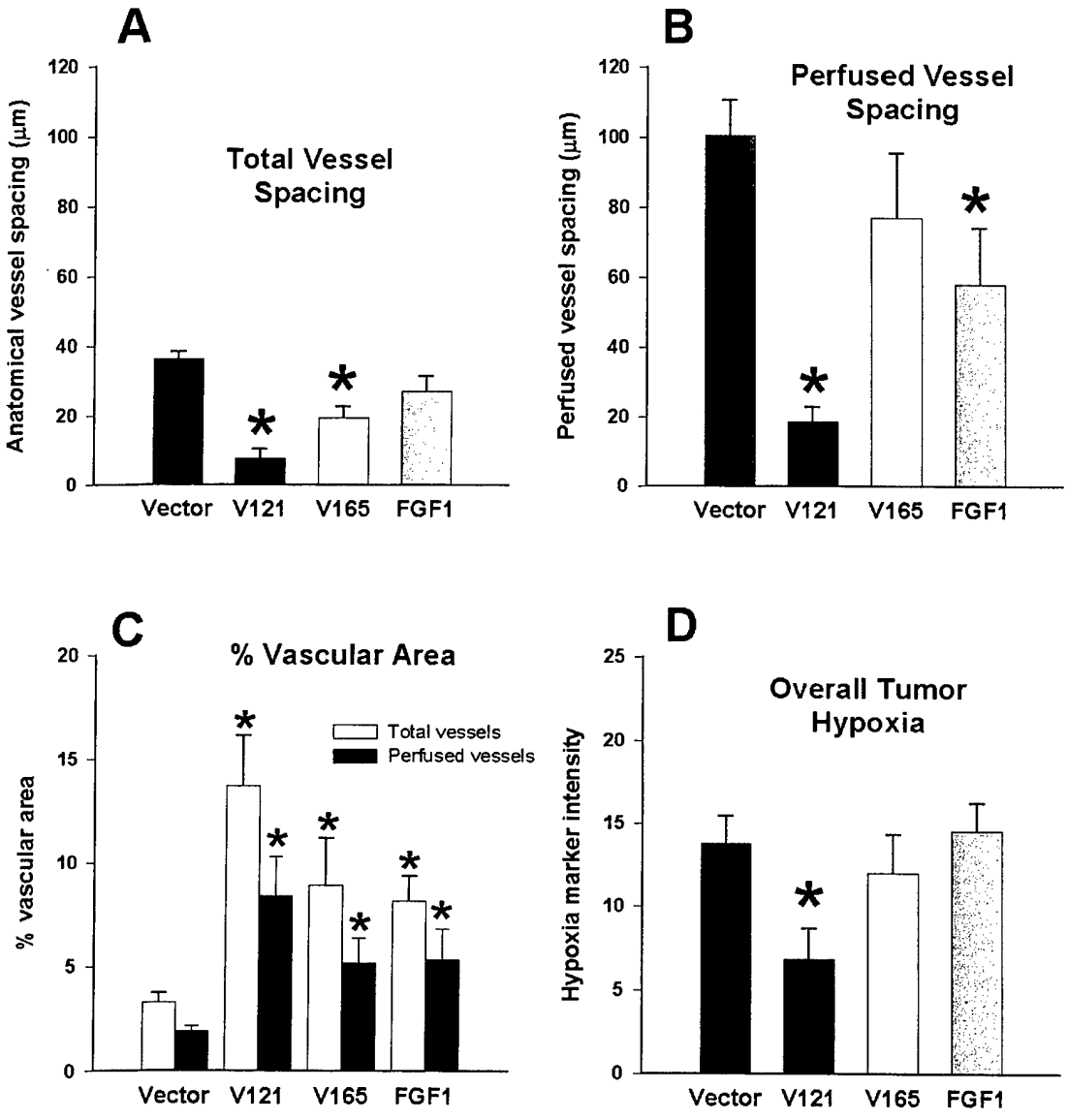
A
Total Vessel Spacing
Anatomical vessel spacing (μm)
120
100
80
60
40
20
0
Vector
V121
V165
FGF1
B
Perfused Vessel Spacing
Perfused vessel spacing (μm)
C
% Vascular Area
Total vessels
Perfused vessels
% vascular area
20
15
10
5
D
Overall Tumor Hypoxia
Hypoxia marker intensity
25

Table I – Tumor Formation Percentage and Tumor Volume at 45 days Post-implantation

	Tumor Formation Frequency (%)	Tumor Volume (mm^3) Mean ± SEM
Vector	40	240 ± 50
$VEGF_{121}$	90	1260 ± 210
$VEGF_{165}$	86	1640 ± 190
FGF-1	74	760 ± 120

Combination of Radiation and Celebrex™ (celecoxib) Reduce Mammary and Lung Tumor Growth

Weimin Liu, Yuhchyau Chen, Wei Wang, Peter Keng, Jacob Finkelstein, Dongping Hu, Li Liang, [redacted], Bruce Fenton, Paul Okunieff and Ivan Ding[1]
Department of Radiation Oncology
University of Rochester, Rochester, NY 14642

Running Title: Radiation and celecoxib reduce tumor growth

Acknowledgment: This work supported in part by NCI/PO1-CA110551-25A2 and a University of Rochester Cancer Center Discovery Grant.

[1]To whom requests for reprints should be addressed, Ivan Ding at University of Rochester School of Medicine, Department of Radiation Oncology, Box 647, 601 Elmwood Avenue, Rochester, NY 14642.
Phone: (716) 275-1985; Fax: (716) 273-3104
E-mail: ivan@radonc.medinfo.rochester.edu

Abstract

The selective cyclooxygenase (COX)-2 inhibitor, celecoxib, alone and in combination with radiation was investigated in vitro and in vivo. Murine mammary tumor line (MCa-35) and human lung carcinoma line (A549) have high and low basal levels of COX-2 protein respectively. Treatment of both tumor cells with celecoxib alone resulted in a dose- and time-dependent reduction of cell number (clonogenic cell death) and tumor cell growth rate in vitro, however, inhibition of tumor cell growth by celecoxib was not correlated with the reduction of COX-2 protein in tumor cells. Although both tumor cell types had similar DNA damage after celecoxib treatment, significant induction of tumor cell apoptosis was only observed in MCa-35. Celecoxib-mediated radiation sensitization also occurred in MCa-35 cells determined by clonogenic assay, in part due to a G2/M arrest at 8-24 hrs after treatment. The tumor growth inhibitory effects of celecoxib were also studied in vivo. It was found that celecoxib inhibited both tumor growth after intragastric administration of celecoxib (5 daily doses of 50 mg/kg). Combined with a single 30 Gy dose of radiation, celecoxib resulted in additive effects on A549 tumors. Celecoxib-treated A549 tumors had marginal reduction of total and perfused blood vessels compared with untreated controls. Reduction of tumor angiogenic cytokine and growth factor mRNA was associated with decreased perfused vessels. Finally, reduction of VEGF protein after celecoxib was also observed in both tumor lines by Western blot. Our results indicate that the selective inhibition of COX-2 combined with radiation has potential application

in radiotherapy, and celecoxib-mediated antitumor effects may act through different mechanisms including direct inhibition of tumor cell proliferation, alteration of tumor cell cycle, and antiangiogenesis.

Introduction

Cyclooxgynase (COX) is a critical enzyme involved in mammalian physiology and several disease conditions (1-3). COX mediated prostglandin (PGs) production has recently been implicated in cancer development and tumor angiogenesis (2, 4-6). Two isoforms cyclooxgynase (COX-1 and COX-2) are coexpressed in both normal and tumor tissues. COX-1 is constitutively expressed in most tissues producing PGs required for normal physiological function, while COX-2 is expressed at relatively low levels but is induced by a variety of agents, including cytokines, growth factors, radiation and stress-related stimuli (7, 8). There is also considerable evidence that suggests a causal relationship between COX-2 overexpression and tumor formation in human and animal tumor models. Therefore, selective overexpression of COX-2 in tumors versus normal tissues makes this enzyme a potential target for cancer therapy. COX inhibitors also participate in radiation-mediated antitumor effects (9). Milas et al. (10) and Furuta et al. (11) have shown that indomethacin enhances the antitumor efficacy of ionizing radiation against PG-producing, transplanted murine sarcomas. Others recently also reported that other COX inhibitors enhanced the radiosensitivity of human prostate carcinoma cells (12, 13). Due to the overexpression of COX-2 in many human malignancies, the recently developed selective COX-2 inhibitors have been extensively investigated in antineoplastic therapy both alone and in combination with radiation (2, 14). In support of this concept, we recently also reported that

celecoxib caused a dramatic enhancement of the in vivo radiation response of esophageal carcinoma cells, and found that celecoxib protected normal soft tissue against damage by radiation (15).

The molecular basis of antitumor effects mediated by COX-2 inhibitors has not been well defined. Antitumor effects of COX-2 inhibitors have been documented, which includes: 1) direct reduction of tumor cell proliferation, 2) the inhibition of angiogenesis and reduction of angiogenic growth factor and cytokine production, 3) the regulation of cytokine and growth factor production by reducing PG production and indirectly affecting tumor cell growth, and 4) increased intrinsic radiosensitivity of tumor cells by alteration of the cell cycle. Celecoxib mediated antitumor effects could be COX-2-dependent or COX-2-independen (16, 17). To investigate the effects of celecoxib on the radiosensitivity of other types of human tumors, we used two carcinoma cell lines with different endogenous COX-2 expression levels in this study. We now report on the in vitro and in vivo effects of the celecoxib alone and in combination with radiation on breast MCa-35 and lung A549 tumor cells.

Material and Methods

Cell Culture

The murine mammary tumor cell line MCa-35 was obtained from Dr. Milas (MD Anderson, Houston TX), and human lung carcinoma cell line A549 cells was obtained from ATCC (Rockville, MD). Tumor cells were grown in DMEM (Life Technologies, Grand Island, NY) supplemented with sodium pyruvate (1 mM), and 10% fetal bovine serum. Cells were grown as monolayers maintained in a humidified 5% CO_2/95% air atmosphere at 37°C.

Cell Growth and Clonogenic Survival Assay

Cultured tumor cells were exposed to different concentrations (1-50 μM) of celecoxib (Pfizer Inc, NY, NY) for various times. Cell numbers were counted by manual cell counts of live cells as assessed with Trypan blue exclusion, and a cell growth curve was generated. For drug clonogenic survival assay, tumor cells were exposed to different concentrations of celecoxib. Colonies were counted at 14 days after drug treatment. For radiation clonogenic assay, celecoxib pre-treated tumor cells (4, 8, 12 and 24 hrs before radiation) were irradiated with varied doses of radiation using a 137Cs source (3.2 Gy/min). Trypsinized cells were then transferred into 60-mm dishes for determination of colony-forming ability. After 14 days of incubation, the dishes were stained with 0.5% crystal violet in methanol, and colonies with >50 cells were counted. Radiation survival curves were then generated. Survival curves were generated by combining data from three independent experiments and fitting the average survival levels by least squares regression using the linear quadratic model.

Cell Cycle and Apoptosis Assays

All of the cultures were subconfluent at the time of collection. Cultured tumor cells were fixed with ice-cold 70% ethanol, stained with propidium iodide, and analyzed using flowcytometer (FCM) as described previously. The BrdU/TUNEL assay (APO-BRDU^{tm}, Phoenix Flow Systems, Inc. San Diego, CA) was performed according to the manufacturer's instructions. Briefly, fixed cells were washed in PBS, suspended in 50μl of TdT buffer with 0.75 μl of TdT enzyme and 8.0 μl of FITC-dUTP and incubated for 60 min. Cell then were rinsed in buffer twice and resuspended in 1ml of propidium iodide/RNase A solution. After incubating the cells in the dark for 30 min at room temperature, the specimens were analyzed using FCM. The percentage of apoptotic cells was recorded.

Tumor Cell DNA Damage Determined by Comet Assay

All of the cultures were subconfluent at the time of collection. Tumor cells were treated with 50 and 100 μM celecoxib for different time periods and collected for determination of DNA damage using Single Cell Gel Electrophoresis (CometAssay™, Trevigne, Inc, Gaithersburg, MD), which was performed according to the manufacturer's instructions. Briefly, celecoxib-treated cells were loaded and immobilized in a bed of low melting point agarose. Following a gentle cell lysis, tumor cells were treated with alkali to unwind and denature the DNA and hydolyze sites of

damage. After electrophoresis and staining of cells with a fluorescent DNA intercalating dye, cells were then visualized under a fluorescence microscope. DNA "comet" tail shape and migration pattern was used to define positive cells with DNA damage.

Western Blotting

Tumor cells were collected as whole cell lysates using lysis buffer (50 mM HEPES, 0.4 M NaCl, 1 mM EDTA, 1 mM DTT, 0.5 mM phenylmethylsulfonyl fluoride, 2 μg/ml aprotinin, 2 μg/ml leupeptin, 5 μg/ml benzamidine, and 1% NP40) and centrifuged at 12,000 rpm for 10 min at 4°C. The protein concentration of the supernatant in each sample was determined using the Bio-Rad Kit (Bio-Rad Laboratories, Hercules, CA) according to the manufacturer's instructions. A total of 50 μg of protein was used for SDS-PAGE. After electrophoresis, the proteins were blotted onto PVDF membrane (NEN, Arlington Heights, IL) and blocked using TBS-T (Tris-buffered saline and 5% nonfat milk in 0.1% Tween 20). The membrane was probed with VEGF and COX-2 polyclonal antibodies (Santa Cruz, SanDiego, CA) in the blocking solution overnight at 4°C. The membrane was washed in TBS-T and incubated for 40 min with antirabbit IgG horseradish peroxidase-conjugated secondary antibody at a 1:2000 dilution in the blocking mixture. The membrane was washed with TBS-T and probed with ECL Plus (Amersham Corp., Piscataway, NJ).

In Vivo Tumor Growth Delay Assay

MCa-35 and A549 tumors were generated by injecting 1 x 10^6 or 10 x 10^6 cell s.c. into the right thighs of C3H/He or nu/nu NCR mice, respectively. When tumors grew to 5 mm in diameter, the mice were given intragastrical celecoxib or vehicle in 0.2 ml for five consecutive days. Control animals received the same volume of vehicle only. After five doses of celecoxib treatment, mice were exposed to a 30 Gy single dose of radiation. To obtain tumor growth curves, tumor-bearing leg diameters were measured daily. Tumor growth delay was expressed as the time in days for tumors in the treated groups to grow from 7 to 12 mm in diameter minus the time in days for tumors in the control group to reach the same size. The groups consisted of 6 (for A549) to 10 (for MCa-35) mice each.

Determination of Vasculature, Oxygenation and Quantitative imaging analysis

Immunohistochemistry methods have previously been described in detail (18). To visualize blood vessels open to flow, a fluorescent dye, $DiOC_7$ (Molecular Probes, Eugene, OR), was administered i.v. at a concentration of 1.0 mg/kg, one minute prior to freezing. CD31 staining was used for determination of total structural vasculature detected using anti-CD31 antibody (PharMingen, SanDiego,CA). Localized areas of tumor hypoxia were assessed in frozen tissue sections by immunohistochemical identification of sites of 2-nitroimidazole metabolism. A pentafluorinated derivative of etanidazole (EF5) was injected i.v. one hour before tumor

freezing. An antibody extremely specific for the EF5 drug adducts that form when the drug is incorporated by hypoxic cells was used to visualize regions of hypoxia (19). For each frozen tumor, a series of 4.0 μm sections were digitized, background-corrected, and image-analyzed. The quantitative vascular information was analyzed using custom Fortran programs to perform a "closest individual" analysis. Briefly, the distances from computer-superimposed sampling points to the nearest blood vessel were determined, and median distances were recorded.

Immunohistochemical Staining Methods

Paraffin sections (4-5 μm thick) are deparaffinized and rehydrated through graded ethanol. The slides were then washed in H_2O and with Tris buffered saline (TBS) containing 0.02% Triton X-100. After 30 min incubation at room temperature with TBS containing 3% normal serum or casein for blocking, the slides were incubated with anti-macrophage antibody, anti-ED1 (Serotec, Raleigh, NC) for 2 hrs. After wash, the slides were incubated with a streptavidin-conjugated secondary antibody followed by reaction with substrate and chromagen (DAB). AEC chromagen can be substituted for DAB. Slides are then counterstained with either methyl green or hematoxylin and cover-slipped. Automated: The A.R.K. (Animal Research Kit from Dako, Carpinteria, CA) technique was followed according to the manufacturer's instructions.

Statistical Methods

Statistical analysis was performed between control and celecoxib-treated groups. Comparisons of means were carried out by Student's t test. Differences with a value of $P < 0.05$ were considered statistically significant.

Results

The effects of celecoxib on growth of MCa-35 and A549 tumor cells was studied by means of both growth curve (Fig1a and 1b) and clonogenic assays (Fig1c and 1d). Celecoxib caused a dose-dependent inhibition of growth rate of tumor cells. 50μM celecoxib effectively inhibited cell growth in both tumor lines. Similarly, celecoxib also increased cell clonogenic death in MCa-35 (Fig1c) and A549 (Fig1d) tumors. 30μM celecoxib reduced clone formation in these tumor cells by 50%. However, celecoxib did not reduce the levels of endogenous COX-2 protein (Fig 1e). In order to determine if reduction of cell proliferation and clonogenic survival by celecoxib is the result of tumor cell apoptosis, TUNEL staining was used to quantitatively determine frequency of apoptotic cells. As shown in Figure 2c, MCa-35 tumor cells had a 4 fold induction of apoptotic cells 8 hr after 50μM celecoxib treatment, but there was no obvious apoptosis in celecoxib-treated A549 cells. Similarly, 10 Gy radiation also significantly induced MCa-35 cell apoptosis compared with A549. Although celecoxib only induced apoptosis in MCa-35 tumor, both tumor cell lines had similar DNA damage determined by Comet assay after celecoxib treatment (Fig 2a and 2b).

Although celecoxib increased radiation sensitization in several animal tumor models, there are no previous reports of breast and lung tumor cell sensitization. As shown in Figure 3, 15-50μM celecoxib radiosensitized cell killing in MCa-35 (Fig 3b and 3c), but not in A549 (Fig 3a). By cell cycle analysis, celecoxib caused an obvious increase of G2/M fraction 8-24 hrs after celecoxib treatment, but it was not observed in A549 cells (Fig 4d). In order to see celecoxib improve tumor radiation sensitization, tumor growth delay study was performed. As shown in Table 1, celecoxib alone caused a reduction of tumor growth in both tumor types, and tumor inhibition was particularly significant in A549 xenografts. However, celecoxib plus radiation delayed tumor growth more profoundly than either agent alone. Although celecoxib treatment did not alter endogenous COX-2 protein levels, it caused a decrease in vascular endothelial growth factor (VEGF) protein expression detected by Western (Fig 4a). Celecoxib-mediated antiangiogenesis in A549 tumors was also determined using the distance between tumor cell to the nearest total or perfused vessels assay. Celecoxib caused a reduction of vascular mass, and reduction of tumor angiogenesis correlated with decreased angiogenic-related cytokine or angiogenic growth factor mRNA expression (Fig 4b, 4c and Fig 5). The implication is that reduction of angiogenic-related molecules in vitro or in vivo by celecoxib may alter tumor cell apoptotic response.

Discussion

In this study, we have shown that the selective COX-2 inhibitor, celecoxib, significantly decreased growth rate and clonogenic survival in both breast and lung tumor cells. The two cell lines had similar DNA damage after celecoxib, but only MCa-35 cells had increased apoptotic cell death. However, inhibition of tumor cell growth and enhancement of tumor cell apoptosis were independent of the endogenous COX-2 protein levels. We also demonstrated that celecoxib had in vitro radiosensitization effects that are at least in part due to the G2/M arrest and apoptosis in MCa-35 cells, but not in A549 tumor line. Furthermore, we observed that celecoxib alone inhibited both tumor growth in vivo, and reduced tumor vascular mass. Likewise, decreased tumor growth in vivo is associated with reduction of angiogenic cytokine and angiogenic growth factor mRNA expression. Inhibition of tumor growth and metastasis by celecoxib has been reported in several tumor types with either COX-2-dependent or COX-2-independent mechanisms (20). Based on our data it appears that cell lines with high COX-2 protein may be more prone to apoptotic than mitotic cell death after celecoxib treatment.

COXs are the key enzymes that mediate the production of PGs from arachidonic acid. Two isoforms of COX have been identified and expressed in both normal and tumor tissues. COX-1 is expressed constitutively, whereas COX-2 can be induced by a number of agents including cytokines, growth factors, and tumor promoters. Overexpression of COX-2 is associated with

tumor formation and progression in both experimental animal tumor models and cancer patients (21). A number of other studies have suggested that: 1) there is an association of overexpression of COX-2 with progression of human malignancy, 2) enhancement of tumor angiogenesis is correlated with COX-2 levels, 3) COX-2 reduces tumor cell apoptosis and increase of tumor cell proliferation, and 4) COX-2 can regulate angiogenic related cytokine or chemokine production. Our study demonstrates that antitumor effects by celecoxib are a complex process including direct tumor cell growth inhibition through DNA damage and subsequent apoptosis, indirect down regulation of angiogenic growth factor gene expression, G2/M delay, and direct antiangiogenic action resulting in reduction of total and perfused vessels in experimental tumor models. Antitumor effects of celecoxib are therefore multifactoral and occur via direct and indirect mechanisms.

Combination of celecoxib and radiation could provide a synergistic way for tumor treatment (13, 14, 22). To our knowledge, this is the first demonstration of celecoxib affecting the intrinsic radiosensitivity of breast tumor cells. Our studies illustrate at least two processes by which COX-2 inhibition can enhance the in vivo response of tumors to radiation, antiangiogenesis and G2/M arrest. Furuta et al. also showed that indomethacin caused accumulation of cells in the G2/M phase of the cell cycle, which is generally considered to be the most sensitive to ionizing radiation. Their data is consistent with our MCa-35 tumors after celecoxib treatment in the

present study. Radiation sensitization after treatment with COX-2 inhibitors has been reported in lung (13), prostate (12), colon and glioma (22) cancer cell lines, antiangiogenic effects of celecoxib have been proposed and may account for the cooperative effects of celecoxib and radiation. Indeed, Elder et al. (23) recently reported a decrease in VEGF and FGFs from cultured human colon carcinoma cell lines in response to COX-2 selective inhibitor. Reduction of angiogenic growth factor may facilitate the induction of apoptosis. Our data shows similar shift of angiogneic factors to lower levels after radiation.

In summary, our findings demonstrate that the selective COX-2 inhibitor celecoxib is cytotoxic and is a DNA damaging agent to both lung and breast carcinoma cells in vitro. Clonogenic survival is at least additive if not radiosensitizing, and may in part be dependent on apoptosis. In vivo studies confirm in vitro results and also support an antiangiogenic component to tumor growth inhibitory effects of celecoxib. The implications for combined radiation and celecoxib in the clinic are significant.

Legends

Fig. 1 Inhibition of cell proliferation with celecoxib is dose-dependant (dose range10-50 μM), but is not dependent on the endogenous COX-2 protein expression in MCa-35 and A549 tumor cell lines. In vitro tumor cell growth curves (a and b). Clonogenic formation 14 days after cell plating (c and d). COX-2 protein detected by Western blot in MCa-35 and A549 tumor cells (e). Data are mean ± 1 SE from 2-3 independent experiments. *, $P < 0.05$ versus no celecoxib control.

Fig. 2 Celecoxib induces DNA damage and apoptosis in both MCa-35 and A549 cells. DNA damaged tumor cells were detected by Comet assay in MCa-35 cells (a), and kinetic induction of Comet cells after celecoxib treatment (b), induction of apoptosis in MCa-35 and A549 tumor cells by celecoxib or by radiation as determined by TUNEL staining and flow cytometry (c). Values are means ± 1 SE.

Fig. 3 Celecoxib effects on clonogenic cell survival and on cell cycle distribution. Clonogenic cell survival curves from cells exposed to various doses of celecoxib and radiation (a+b). Exposure time to celecoxib was altered in c. Change in G2/M fraction of the cell cycle after exposure to celecoxib alone is shown in d. Values are mean ± 1 SE.

Fig. 4 Effect of celecoxib on growth factor expression of tumor cells in vitro and in vivo. Western blot demonstrating VEGF protein expression in MCa-35 and A549 tumor cells after different doses of celecoxib treatment (a). Celecoxib decreased mRNA expression of fibroblast growth factors (b) and other cytokines (TGF-ßs) (c) detected by RNase protection assay. RNA extracts from individual tumors were run on the numbered lanes (b+c).

Fig. 5. Correlation of perfused vessel spacing (μm) with mRNA levels of several angiogenic-related cytokines and growth factors in individual A549 tumors. Open triangles are saline-treated and solid triangles are celecoxib-treated A549 tumors. Lines represent linear regression analysis. After celecoxib treatment, the reduction of angiogenic factors eliminated the usual inverse correlation between angiogenic growth factor expression and vessel spacing.

References

1. Lipsky PE, Brooks P, Crofford LJ, et al. Unresolved issues in the role of cyclooxygenase-2 in normal physiologic processes and disease. *Arch Intern Med* 2000;160:913-20.

2. Milas L. Cyclooxygenase-2 (COX-2) enzyme inhibitors as potential enhancers of tumor radioresponse. *Semin Radiat Oncol* 2001;11:290-9.

3. Howe LR, Subbaramaiah K, Brown AM, et al. Cyclooxygenase-2: a target for the prevention and treatment of breast cancer. *Endocr Relat Cancer* 2001;8:97-114.

4. Kishi K, Milas L, Hunter N, et al. [Recent studies on anti-angiogenesis in cancer therapy] [In Process Citation]. *Nippon Rinsho* 2000;58:1747-62.

5. Ding I, Liang L, Hu DP, et al. Effects of Celebrex on mammary tumor angiogenesis, oxygenation, apoptosis and cytokine gene expression. *Radiation Res 48th Annual Meeting,* 2001.

6. Tsujii M, Kawano S, Tsuji S, et al. Cyclooxygenase regulates angiogenesis induced by colon cancer cells. *Cell* 1998;93:705-16.

7. Dubois RN, Abramson SB, Crofford L, et al. Cyclooxygenase in biology and disease. *Faseb J* 1998;12:1063-73.

8. Williams CS, Tsujii M, Reese J, et al. Host cyclooxygenase-2 modulates carcinoma growth. *J Clin Invest* 2000;105:1589-94.

9. Gupta RA, DuBois RN. Translational studies on Cox-2 inhibitors in the prevention and treatment of colon cancer. *Ann N Y Acad Sci* 2000;910:196-204; discussion 204-6.

10. Milas L, Hirata H, Hunter N, et al. Effect of radiation-induced injury of tumor bed stroma on metastatic spread of murine sarcomas and carcinomas. *Cancer Res* 1988;48:2116-20.

11. Furuta Y, Hunter N, Barkley T, Jr., et al. Increase in radioresponse of murine tumors by treatment with indomethacin. *Cancer Res* 1988;48:3008-13.

12. Palayoor ST, Bump EA, Calderwood SK, et al. Combined antitumor effect of radiation and ibuprofen in human prostate carcinoma cells. *Clin Cancer Res* 1998;4:763-71.

13. Pyo H, Choy H, Amorino GP, et al. A selective cyclooxygenase-2 inhibitor, ns-398, enhances the effect of radiation in vitro and in vivo preferentially on the cells that express cyclooxygenase-2. *Clin Cancer Res* 2001;7:2998-3005.

14. Kishi K, Petersen S, Petersen C, et al. Preferential enhancement of tumor radioresponse by a cyclooxygenase-2 inhibitor. *Cancer Res* 2000;60:1326-31.

15. Ding I, Linang L, Hu DP, et al. Effects of Celebrex on normal tissue fibrosis and mammary tumor control afetr single-dose irradiation. *Radiation Res 48th Annual Meeting*, 2001.

16. Zimmermann KC, Sarbia M, Weber AA, et al. Cyclooxygenase-2 expression in human esophageal carcinoma. *Cancer Res* 1999;59:198-204.

17. Souza RF, Shewmake K, Beer DG, et al. Selective inhibition of cyclooxygenase-2 suppresses growth and induces apoptosis in human esophageal adenocarcinoma cells. *Cancer Res* 2000;60:5767-72.

18. Fenton BM, Paoni SF, Lee J, et al. Quantification of tumour vasculature and hypoxia by immunohistochemical staining and HbO2 saturation measurements. *Br J Cancer* 1999;79:464-71.

19. Lord EM, Harwell L, Koch CJ. Detection of hypoxic cells by monoclonal antibody recognizing 2- nitroimidazole adducts. *Cancer Res* 1993;53:5721-6.

20. Williams CS, Watson AJ, Sheng H, et al. Celecoxib prevents tumor growth in vivo without toxicity to normal gut: lack of correlation between in vitro and in vivo models. *Cancer Res* 2000;60:6045-51.

21. Zhou XM, Wong BC, Fan XM, et al. Non-steroidal anti-inflammatory drugs induce apoptosis in gastric cancer cells through up-regulation of bax and bak. *Carcinogenesis* 2001;22:1393-7.

22. Petersen C, Petersen S, Milas L, et al. Enhancement of intrinsic tumor cell radiosensitivity induced by a selective cyclooxygenase-2 inhibitor. *Clin Cancer Res* 2000;6:2513-20.

23. Elder DJ, Halton DE, Hague A, et al. Induction of apoptotic cell death in human colorectal carcinoma cell lines by a cyclooxygenase-2 (COX-2)-selective nonsteroidal

anti-inflammatory drug: independence from COX-2 protein expression. *Clin Cancer Res* 1997;3:1679-83.

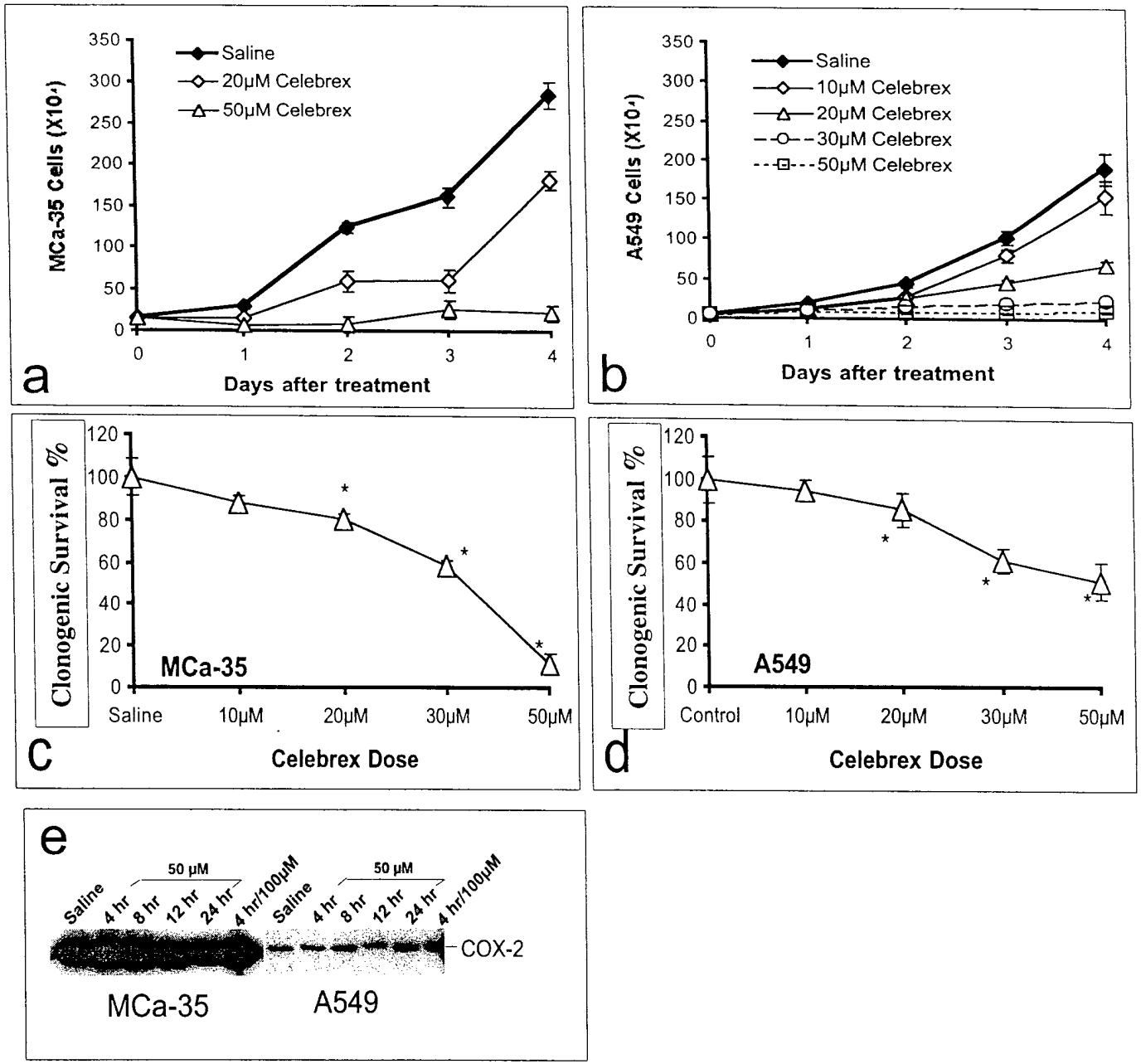
a
MCa-35 Cells (X10⁴)
Saline
20μM Celebrex
50μM Celebrex
Days after treatment
b
A549 Cells (X10⁴)
Saline
10μM Celebrex
20μM Celebrex
30μM Celebrex
50μM Celebrex
Days after treatment
c
Clonogenic Survival %
MCa-35
Saline
10μM
20μM
30μM
50μM
Celebrex Dose
d
Clonogenic Survival %
A549
Control
10μM
20μM
30μM
50μM
Celebrex Dose
e
50 μM
50 μM
Saline
4 hr
8 hr
12 hr
24 hr
4 hr/100μM
COX-2
MCa-35
A549

a

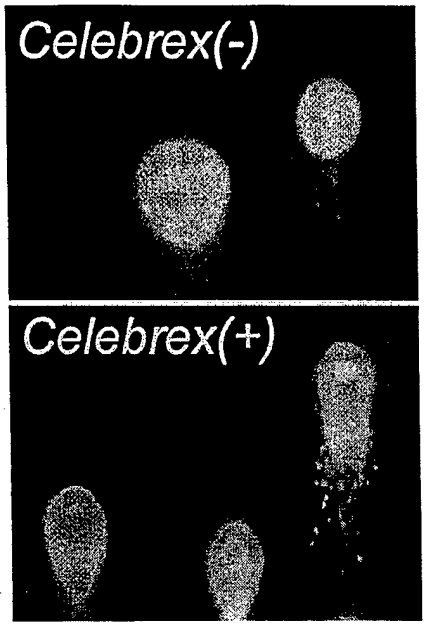
Celebrex(-)
Celebrex(+)

b

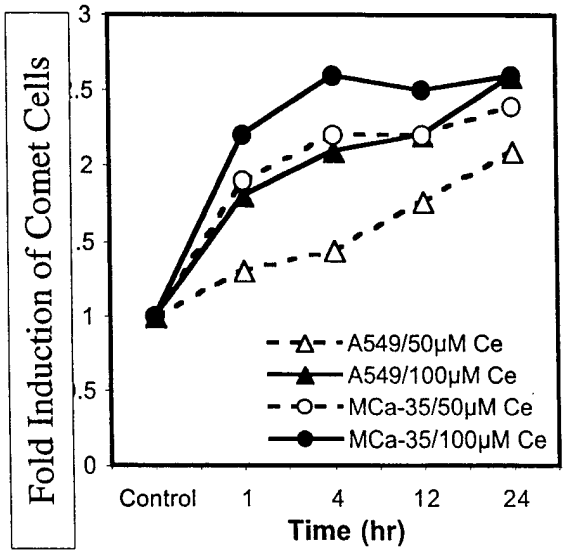
Fold Induction of Comet Cells
3
2
1
0
Control
1
4
12
24
Time (hr)
A549/50μM Ce
A549/100μM Ce
MCa-35/50μM Ce
MCa-35/100μM Ce

c

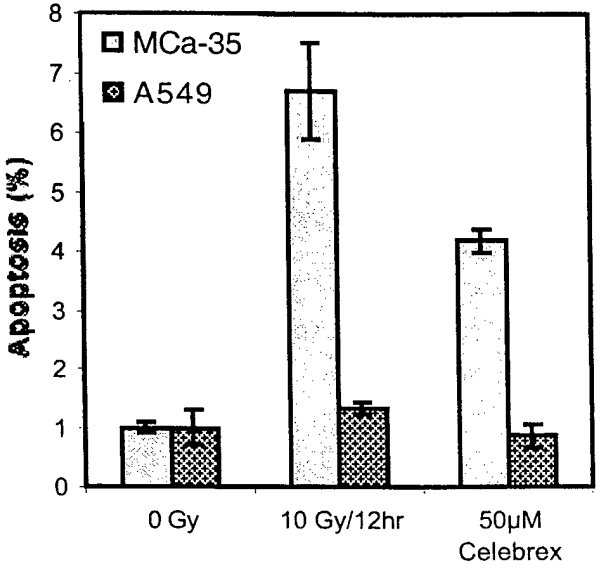
Apoptosis (%)
8
7
6
5
4
3
2
1
0
MCa-35
A549
0 Gy
10 Gy/12hr
50μM Celebrex

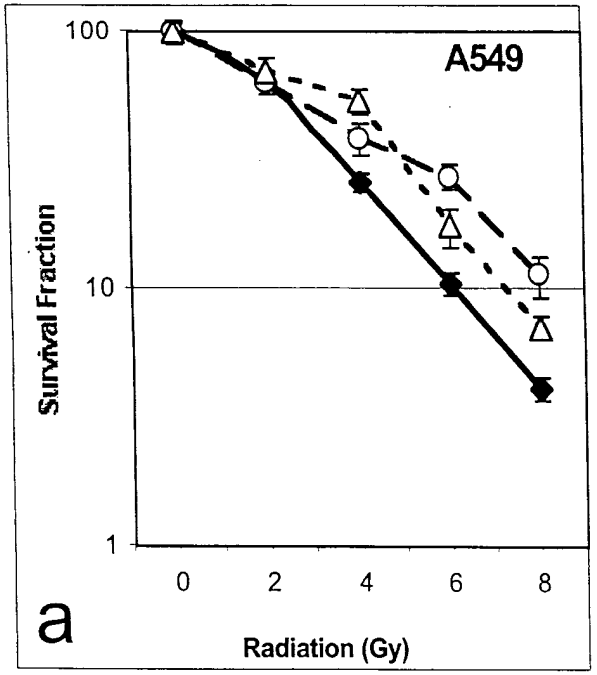
A549
Survival Fraction
100
10
1
0
2
4
6
8
Radiation (Gy)
a

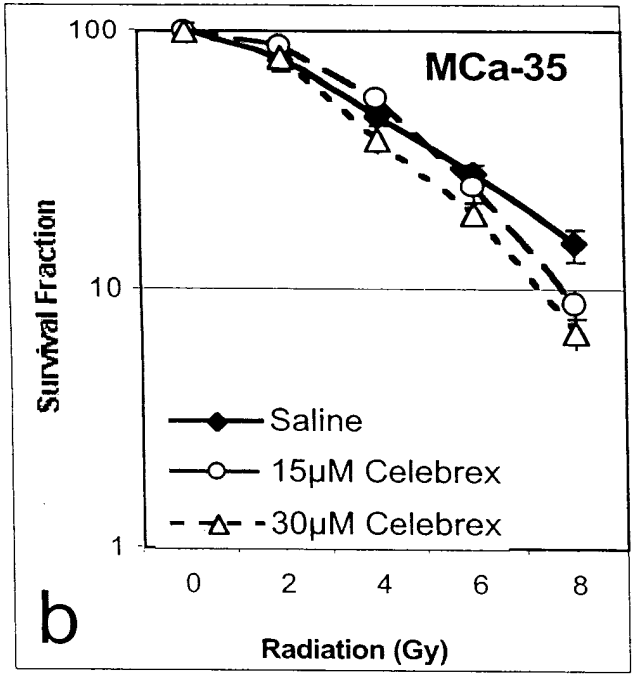
MCa-35
Survival Fraction
100
10
1
Saline
15μM Celebrex
30μM Celebrex
0
2
4
6
8
Radiation (Gy)
b

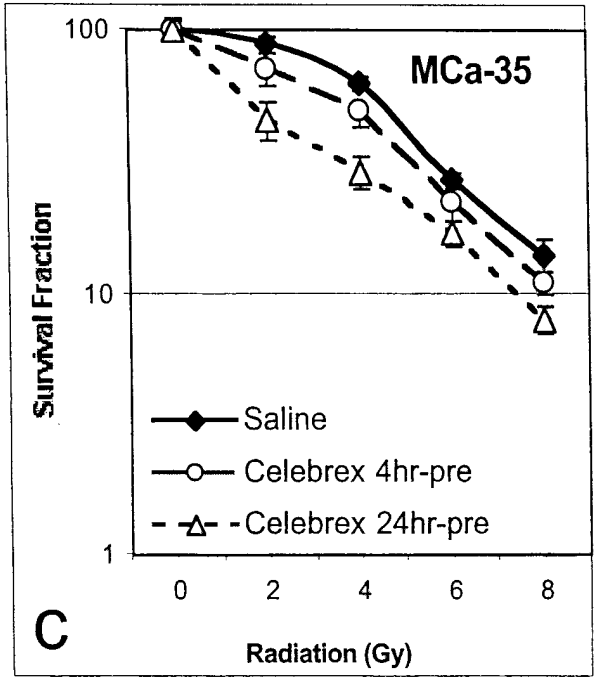
MCa-35
Survival Fraction
100
10
1
Saline
Celebrex 4hr-pre
Celebrex 24hr-pre
0
2
4
6
8
Radiation (Gy)
c

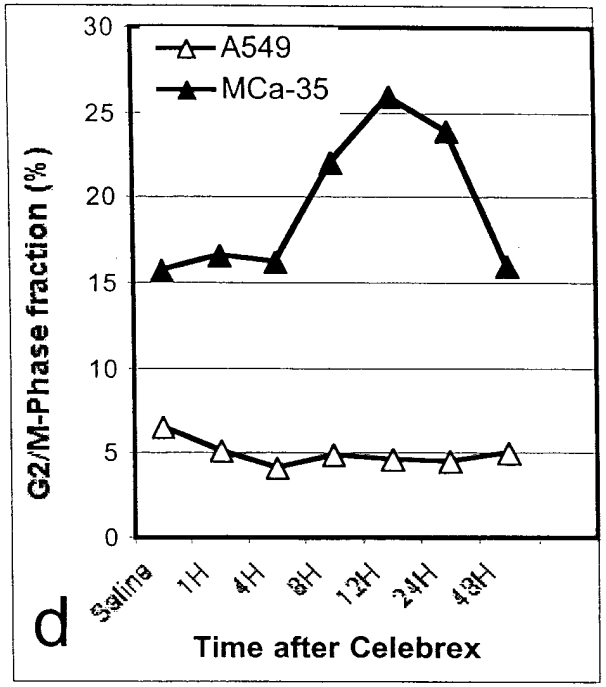
A549
MCa-35
G2/M-Phase fraction (%)
30
25
20
15
10
5
0
Saline
1H
4H
8H
12H
24H
48H
Time after Celebrex
d

Celebrex + Radiation Inhibits Tumor Growth *in-vivo*

(relative tumor volume)

Treatment	MCa-35	A549
Saline	100%	100%
50mg/kg Celebrex	87%	24%
30 Gy single XRT	100%	100%
XRT+ Celebrex	91%	18%

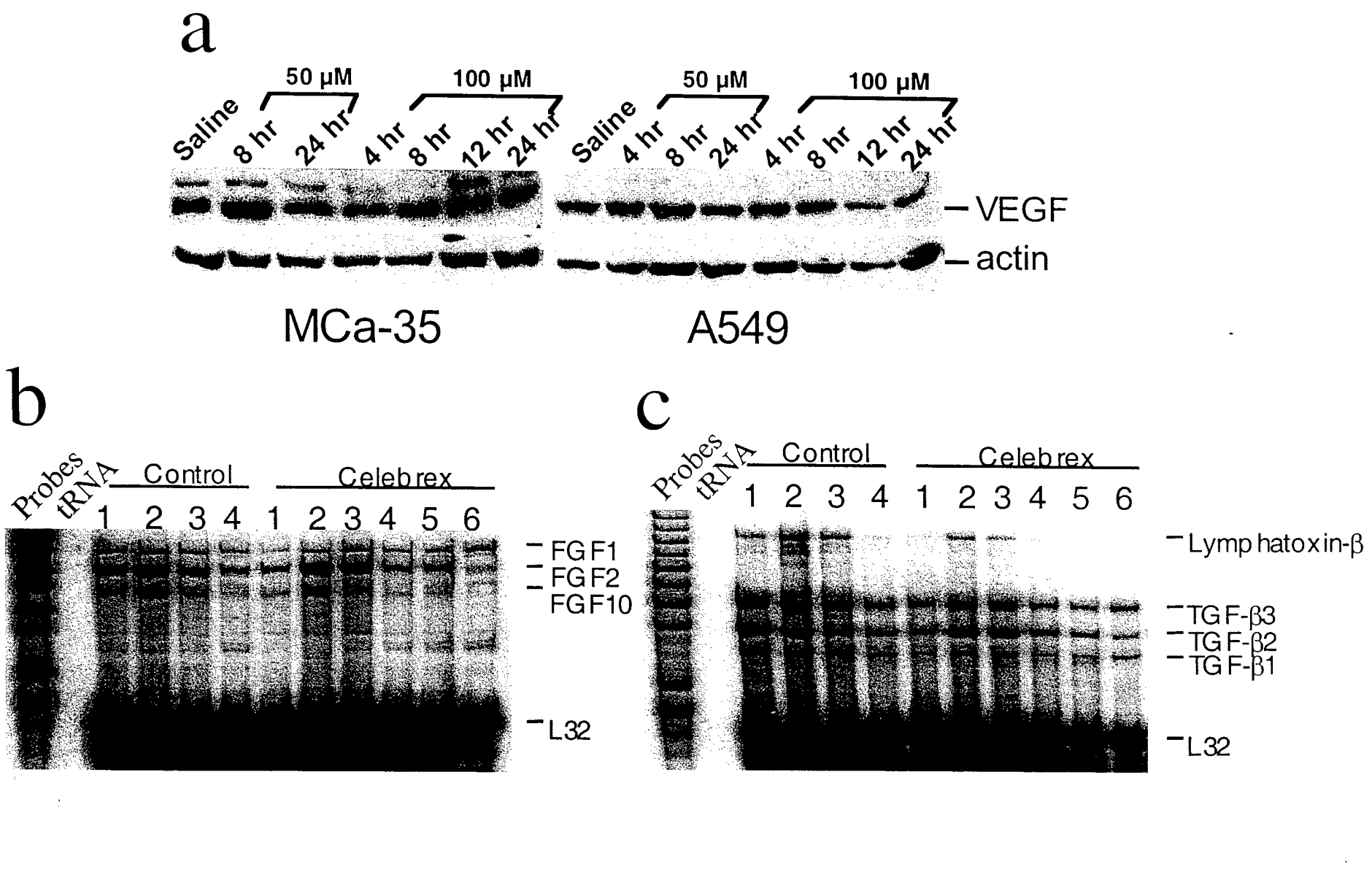
a
50 μM
100 μM
50 μM
100 μM
Saline
8 hr
24 hr
4 hr
8 hr
12 hr
24 hr
Saline
4 hr
8 hr
24 hr
4 hr
8 hr
12 hr
24 hr
VEGF
actin
MCa-35
A549
b
Probes
tRNA
Control
Celebrex
1 2 3 4 1 2 3 4 5 6
FGF1
FGF2
FGF10
L32
c
Probes
tRNA
Control
Celebrex
1 2 3 4 1 2 3 4 5 6
Lymphatoxin-β
TGF-β3
TGF-β2
TGF-β1
L32

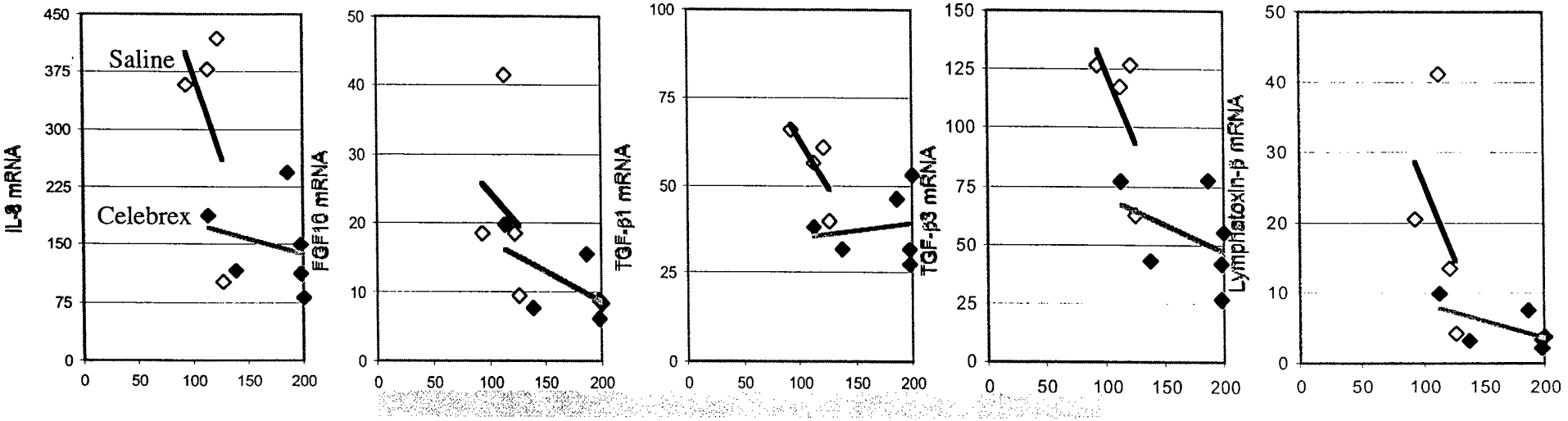
Saline
Celebrex
IL-8 mRNA
FGF10 mRNA
TGF-β1 mRNA
TGF-β3 mRNA
Lymphotoxin-β mRNA
Perfused Vessels Spacing (μM)

FIBROBLAST GROWTH FACTORS (FGFS) INCREASE BREAST TUMOR GROWTH RATE, METASTASES, BLOOD FLOW, AND OXYGENATION WITHOUT SIGNIFICANT CHANGE IN VASCULAR DENSITY

Paul Okunieff[1], Bruce M. Fenton[1], Lurong Zhang[2], Francis G. Kern[3], Timothy Wu[4], J. Robert Greg[4] & Ivan Ding[1]

[1]Department of Radiation Oncology, University of Rochester, Rochester, NY; [2]Department of Cellular and Molecular Biology, Georgetown University, Washington, DC; [3]Southern Research Institute, Birmingham, A; [4]Radiation Oncology Branch, National Cancer Institute, Bethesda, MD

Abstract: Breast tumors expressing no detectable FGFs (MCF-7) were compared with tumors transfected with FGF4 or FGF1 (FGF4/MCF-7 or FGF1/MCF-7), and with MDA-MB-435, which produce endogenous FGF2. Tumor blood flow was measured by ^{133}Xe diffusion, oxygen distribution was measured by Eppendorf pO_2 histography, and vascular density was measured by CD31 staining. Tumors that overexpress angiogenic factors grew at a rate far exceeding that of MCF-7. The FGF producing tumors also had much higher metastatic rates to lung. Tumor blood flow was significantly higher in the two FGF-transfected xenografts compared with the parent MCF7. Median tumor pO_2 was also higher, and tumor oxygenation was preserved even for large tumors. The vascular density as determined by CD31 staining, however, was not markedly increased in tumors overexpressing angiogenic factors. We found that angiogenic factors preserve and augment neovascular function, thus facilitating tumor growth and progression.

Key words: angiogenesis, hypoxia, fibroblast growth factor, blood flow, breast cancer

1. INTRODUCTION

The aggressive malignant phenotype of breast tumors has been attributed to the tumors' ability to generate neovasculature (1, 2). Angiogenic growth factors are the primary signaling peptides that lead to angiogenesis of both normal and neoplastic tissues (2). Among angiogenic factors, fibroblast growth factors (FGFs) are extremely effective at stimulating angiogenesis, facilitating metastases, and promoting tumor growth in both animal and clinical tumor studies (3-7). Neither the mechanism of these angiogenic-related growth factor mediated properties, nor the effect of angiogenic factors on tumor physiology are completely understood. Important questions remain regarding the relative growth effects of these angiogenic factors on the tumor cells themselves compared with their regulation of functioning vasculature. We therefore measured and compared the rate of tumor growth, lung metastasis, and physiological parameters including total blood vessels, blood flow, and oxygenation, in a series of human breast tumor xenografts grown in nude mice. Tumors expressing little or no detectable FGFs (MCF-7) were compared with tumors transfected with FGF4 or FGF1 (FGF4/MCF-7 or FGF1/MCF-7), and with MDA-MB-435, which naturally over-expresses FGF2. Tumor blood flow was measured by ^{133}Xe diffusion, oxygen distribution was measured by Eppendorf pO_2 histography, and vascular density was measured by CD31 staining. We also measured tumor growth rate, tumor take rate, and lung metastasis in these models.

2. METHODS

2.1 Tumor formation in nude mice

MCF-7, MDA-MB-435, FGF1/MCF-7 and FGF4/MCF-7 cells were grown in cell culture dishes in DMEM with 5% fetal bovine serum, and gently scraped into the same medium without serum under sterile conditions. Viable cells were counted using Trypan blue exclusion and a hemocytometer. Cells were harvested by first washing the plates with PBS containing 10 mM EDTA, after which cells were allowed to detach from the dish. Cells were then centrifuged and resuspended into an appropriate volume of medium to give $5x10^6$ viable cells/0.2 ml for injection. Five week old nude mice (Athymic NCR nu/nu, National Cancer Institute, Frederick, MD) were injected with $5x10^6$ cells/site into the mammary fat pad. Tumors of different sizes were chosen at appropriate times after inoculation to determine tumor size-dependent changes in physiological parameters. Tumor

volume, tumor take rate, and lung metastasis were measured and recorded after sacrificing mice. Guidelines for the humane treatment of animals were followed as approved by the University Committee on Animal Resources.

2.2 Tumor blood flow (^{133}Xe clearance)

^{133}Xe ($T_{1/2}$ 5.3 day; γ 81 KV) dissolved in 0.9% NaCl solution was injected directly into the tumors in order to study tumor blood flow. The total volume injected was 10 µl, which contains 60 to 150 mCi and resulted in maximum counting rates of 100,000 to 300,000/min. The mouse was placed in a plastic jug approximately the same size as the diameter of the lead collimator (the collimator shields extraneous radiation from the body of the animal). The collimator has a 1.5 cm diameter bore and is 10 cm in length. The bore exposes the 1.5 inch NaI crystal detector. The tumor was set in front of the collimator bore at an appropriate distance and geometry. The output of the detector was processed with a multichannel analyzer, with counts summed at 3 to 10 sec intervals. The radioactivity from each animal was recorded for at least eight min (range 8 to 60 min, median 18 min), which represents at least one, but usually several, half-times. These lines were plotted semi-logarithmically and fitted by linear regression for computation of the half-times ($T_{1/2}$) of radioisotope clearance (clearance is a single exponential function). The half-times were converted to rates of blood flow as determined by the following formula: blood flow (ml/100 g/min) = 100 l (ln 2/ $T_{1/2}$), where the partition coefficient, l, was determined for samples of the tumors under investigation. The reproducibility of the method is excellent based on repeated studies of single tumors and repeated analysis of data sets. All data analysis was done by a single observer.

2.3 Tumor pO_2 measurements

Tumor pO_2 was determined using a polarographic oxygen electrode system (Eppendorf, Germany, Model 6650). The measurement of tumor pO_2 levels using the Eppendorf pO_2 histograph is a well established procedure for quantifying both human and animal tumor oxygen distributions (8, 9). Estimates of tumor pO_2 were obtained in anesthetized animals using a fine needle Eppendorf electrode probe (needle diameter 270 µm). To measure pO_2, the needle is inserted up to a depth of about 1 mm into the tumor and then moved automatically through the tissue in 0.7 mm increments, followed each time by a 0.3 mm backward step prior to measurement. From three to seven repeated insertions are performed in each tumor, with 7-15 measurements per track, depending on tumor volume. The relative frequency of the pO_2 measurements is automatically calculated and displayed as a

histogram, and tumors are characterized on the basis of median pO_2. The forward motion is chosen such that the net motion will not overlap on a preceding needle location. The reverse motion reduces pressure on the lanced tumor.

2.4 Immunohistochemical staining for CD31

CD31 immunohistochemical staining was carried out on 5 μm thick paraffin embedded tissue sections. Rabbit polyclonal antibody against CD31 were used. Slides were deparaffinized and rehydrated followed by blocking of endogenous peroxidase activity with 0.3% hydrogen peroxide in methanol for 30 min. Incubation with a 1: 1000 dilution of the primary antibody was performed at 4°C overnight, followed by incubation with 1:200 dilution of a biotinylated horse anti-rabbit IgG for 60 min at room temperature and 1:100 dilution of peroxidase-coupled avidin according to the manufacturer's protocol (ABC kit, Vector, Burlingame, CA). The specimens were then stained with 50 μg/ml 3,3'-diaminobenzidine (Sigma Chemical Co., St Louis, MO) in 0.05 m Tris buffered saline containing 0.01% hydrogen peroxide for 10 min. Slides were counter-stained with 1% methyl green solution for 2 min.

3. RESULTS

3.1 Tumor growth rate and metastases were increased by FGF overexpression

Four human breast tumor lines were tested in this study as shown in Table 1. MCF-7 is an estrogen-dependent, non-metastatic line, and produces little or no FGF mRNA. MCF-7 tumors usually grew slowly in nude mice and formed tumors of only 36-80 mm^3 two months after inoculation. However, the two MCF-7-derived transfectants, FGF1/MCF-7 and FGF4/MCF-7, as well as MDA-MB-435, grew quickly and had a relative large tumor size after two months (280-1440 mm^3) as shown in Table 1. After inoculation of $5x10^6$ cells, only 35% of MCF-7 tumors were detectable, and none of the seven tumors that did grow produced metastases to lung. The other three tumor xenografts had higher tumor take rates (65-85%) and frequently produced metastases (31-47% of tumors produced metastases).

TABLE 1. Tumor growth, lung metastasis and FGFs mRNA expression in four human breast carcinoma xenografts.

Cells	Endogenous FGFs mRNA	Tumor-take rate (%)	Tumor Size (mm^3)	Lung metastasis frequency
MCF-7	None	7/20 (35)	36-80	0/7
MBA-MB-435	FGF2	17/20 (85)	280-968	8/17 (47)
FGF1/MCF-7	FGF1	14/20 (70)	360-1440	6/14 (43)
FGF4/MCF-7	FGF4	13/20 (65)	240-1320	4/13 (31)

3.2 Vascular density did not correlate with FGF overproduction

As shown in Figure 1, FGF1/MCF-7 formed a purple-blue bloody tumor mass (Figure 1a) compared with other tumors, such as FGF4/MCF-7 (Figure 1d). Histologically, FGF1/MCF-7 tumors had very active angiogenesis, and enhanced vascularity was noted in both densely cellular tumor tissue and the surrounding stroma regions (Figure 1b and 1c). FGF4/MCF-7 tumors, however, were densely cellular with active tumor cell proliferation and less vascularity (Figure 1e and 1f). MCF7 tumor cells grew with a glandular structure surrounded by a fibrous capsule (Figure 2). MDA-MB-435, like the transfected tumor models, is an undifferentiated adenocarcinoma with almost no glandular structure (Figure 2). Vascular density was assessed immunohistochemically using antiCD-31 antibody. The number and density of vessels was similar based on CD31 staining in all four tumor models (Figure 3).

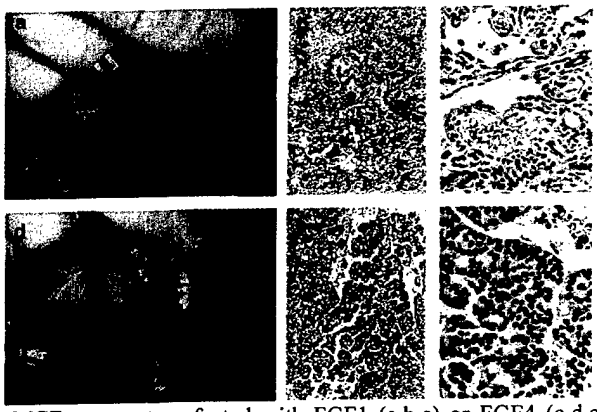

Figure 1. MCF-tumors transfected with FGF1 (a,b,c) or FGF4 (c,d,e). FGF1 transfected tumors had a particularly impressive vascular engorgement. All tumor models had a similar level of vascular density.

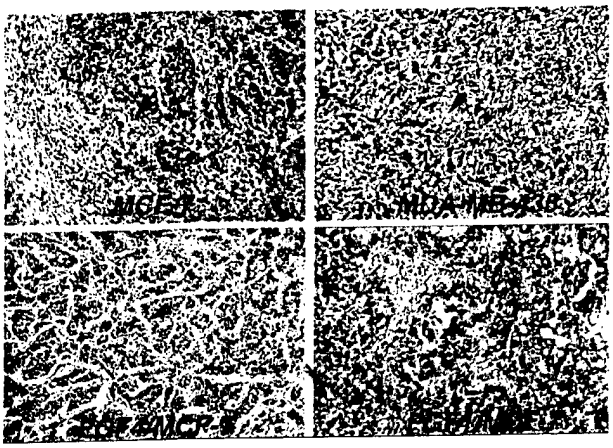

Figure 2. Tumor histology of MCF-7, MDA-MB-435 (FGF2 overexpressing tumor), FGF4/MCF-7 (FGF4 transfected tumor), and FGF1/MCF-7 (FGF1 transfected tumor). MCF-7 tumors had a more glandular histology than angiogenesis factor overexpressing tumor models.

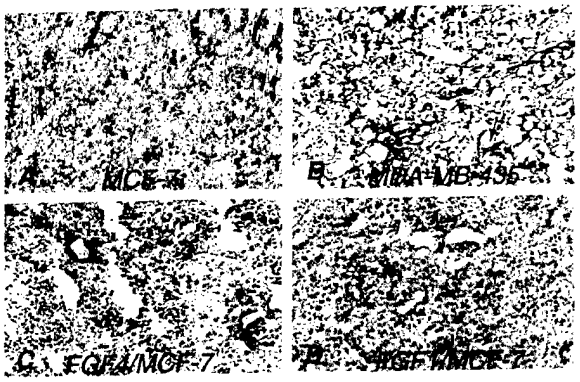

Figure 3. CD31 structural vessel staining of breast cancers grown in nude mice. (A) MCF-7, (B) MDA-MD-435, (C) FGF4/MCF-7, (D) FGF1/MCF-7. Number of positive staining cells per high power field is similar in all.

3.3 Blood flow increased by FGF overproduction

It is well known that tumor neovasculature is chaotic and frequently non-functional. Vascular function was then determined using ^{133}Xe washout in another set of tumors. As shown Figure 4, both FGF transfected tumors had increased ^{133}Xe clearance that was particularly obvious at large tumor sizes (100-500 mm^3) when compared with MCF-7 tumors (Figure 4). Tumor profusion in all three FGF overexpressing tumor models were often much higher than the levels seen in MCF-7.

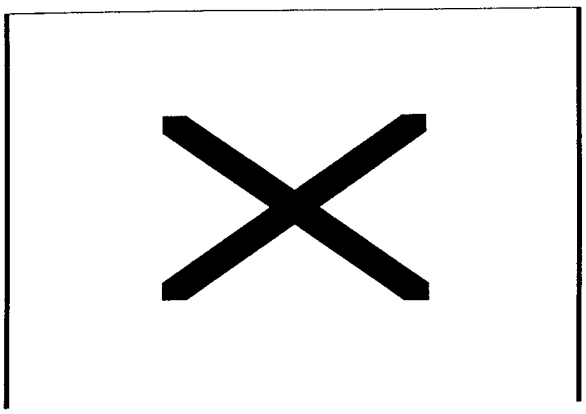

Figure 4. ^{133}Xe tumor blood flow measurements as a function of tumor size. The volume scale (x-axis) varies between tumor models due to size variation at the 2 month end-point. MCF-7 blood flow decreased with increasing tumor volume. FGF-overexpressing tumors maintained near normal flow, even for large tumors.

3.3.1 Mean pO_2 was increased by FGF overproduction

In a separate set of experiments, we also measured tumor median pO_2 levels using polarographic oxygen electrodes (Figure 5). Here again there appeared to be maintenance of vascular function by tumors overexpressing FGFs, evidenced by relatively higher median pO_2 values even for tumors of large size.

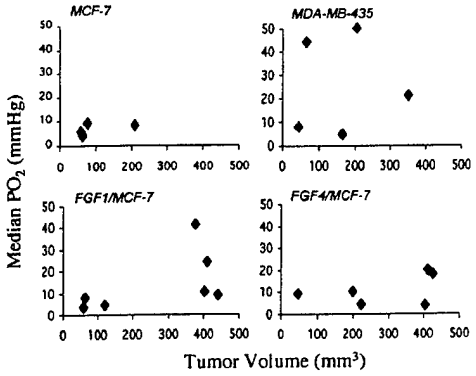

Figure 5. Median pO_2 of tumor versus tumor size. Median pO_2 was highly variable between tumors of similar size and histology. MCF-7 tumors, however, consistently had low median pO_2 values compared with FGF1/MCF-7 and FGF4/MCF-7 tumors.

4. DISCUSSION

Breast tumor progression and metastases require a number of physiological processes including access to adequate vasculature. Likewise, the tumor growth requires the delivery of nutrients and oxygen for activated cellular metabolism. Enhanced tumor growth and the higher rate of metastases therefore can be expected in tumors with robust blood perfusion. However, increased tumor blood flow does not necessarily result in the enhancement of oxygenation, and increased blood flow does not necessarily result in faster tumor growth. Finally, if tumors outgrow the functioning vasculature, tumor hypoxia could still develop. The present studies help delineate the major effects of FGFs on tumor microenvironment and vascular physiology.

Our study also demonstrated that overexpression of angiogenic growth factors results in a more malignant phenotype in breast tumors. This result supports the work of several other laboratory and clinical investigations (4, 5, 10, 11). The loss of normal glandular architecture is consistent with FGFs stimulating tumor proliferation. Similarly, overexpression of FGFs by tumor cells also likely stimulates tumor endothelial cell proliferation.

Our data suggest that overexpression of FGF1, FGF2 or FGF4 produces breast cancer tumors with less glandular architecture, faster growth rates, higher frequency of lung metastases, but no significant alteration of structural vascular density. The relatively stable vascular density occurs despite a preservation of tumor oxygenation and flow compared with MCF-7 tumors of large size. The physiology underlying this effect could result from (1) lower metabolic activity of FGF-overexpressing tumors causing lower consumption, or (2) better functional vasculature in FGF-overexpressing tumors leading to better nutrient delivery. Since faster growing tumors are unlikely to have lower metabolic requirements, we favor the second explanation.

5. CONCLUSION

The breast tumors overexpressing FGF1, FGF2, or FGF4 all had more rapid growth rates than the low FGF-expressing tumor model. These tumors produced a higher frequency of tumors and developed more lung metastases. For tumors of comparable size, the vascular densities of FGF-overexpressing tumors were similar to the parent model. Vascular function and perfusion were, however, preserved even for large tumor sizes among tumors expressing high levels of angiogenic factors. Therefore tumors that overexpress fibroblast growth factors are more aggressive tumors in part

through the production of a better functioning vascular network, and not a total structural vascular network.

REFERENCES

1. Folkman J. Angiogenesis inhibitors generated by tumors, Mol Med 1995; 1:120-122.
2. Folkman J. A new family of mediators of tumor angiogenesis, Cancer Invest 2001;19:754-755.
3. Kurebayashi J, McLeskey SW, Johnson MD, Lippman ME, Dickson RB, Kern FG. Quantitative demonstration of spontaneous metastasis by MCF-7 human breast cancer cells cotransfected with fibroblast growth factor 4 and LacZ, Cancer Res 1993;53:2178-2187.
4. McLeskey S W, Kurebayashi J, Honig SF, Zwiebel J, Lippman ME, Dickson RB, Kern FG Fibroblast growth factor 4 transfection of MCF-7 cells produces cell lines that are tumorigenic and metastatic in ovariectomized or tamoxifen-treated athymic nude mice, Cancer Res 1993;53:2168-2177.
5. Zhang L, Kharbanda S, Chen D, Bullocks J, Miller DL, Ding IY, Hanfelt J, McLeskey S W, Kern FG. MCF-7 breast carcinoma cells overexpressing FGF-1 form vascularized, metastatic tumors in ovariectomized or tamoxifen-treated nude mice, Oncogene 1997;15:2093-108..
6. Zhang L, Kharbanda S, McLeskey SW, Kern FG. Overexpression of fibroblast growth factor 1 in MCF-7 breast cancer cells facilitates tumor cell dissemination but does not support the development of macrometastases in the lungs or lymph nodes, Cancer Res 1999; 59:5023-5029.
7. Nguyen, M. Angiogenic factors as tumor markers, Invest New Drugs 1997;15:29-37.
8. Vaupel P, Schlenger KH, Hoeckel M, Okunieff P. Oxygenation of mammary tumors: from isotransplanted rodent tumors to primary malignancies in patients, Adv Exp Med Biol 1992;316:361-371.
9. Vaupel P and Hockel M. Blood supply, oxygenation status and metabolic micromilieu of breast cancers: characterization and therapeutic relevance, Int J Oncol 2000;17:869-879.
10. Compagni A, Wilgenbus P, Impagnatiello MA, Cotten M, Christofori G. Fibroblast growth factors are required for efficient tumor angiogenesis, Cancer Res 2000;60:7163-7169.
11. Hajitou A, Deroanne C, Noel A, Collette J, Nusgens B, Foidart J M, Calberg-Bacq C M. Progression in MCF-7 breast cancer cell tumorigenicity: compared effect of FGF-3 and FGF-4, Breast Cancer Res Treat 2000;60:15-28.

FGF1 AND VEGF MEDIATED ANGIOGENESIS IN KHT TUMOR-BEARING MICE

Ding I , Liu WM, Sun JZ, Paoni SF, Hernady E, Fenton BM, and Okunieff P
Department of Radiation Oncology, University of Rochester, Box 647, Rochester, NY, 14642

Abstract: Isotransplants of murine fibrosarcoma (KHT) cells were inoculated i.m. into the hind limbs of 6-8 week-old female C3H/HeJ mice. Intratumoral injection of FGF1 or VEGF proteins decreased hypoxic marker uptake in murine fibrosarcoma KHT. Reduction of tumor hypoxia did not correlate with mRNA expression of transcription factors in tumors. Likewise, there was no significant alteration in either apoptotic frequency or the mRNA levels of 10 apoptotic-related molecules in FGF1- or VEGF-treated tumors. mRNA expression for MCP-1, IL-1ß, IL-18 and IL-1Ra, however, were decreased in the tumors following FGF1 or VEGF treatment. Among the normal tissues tested (Brain, kidney, liver, spleen and lung), basal mRNA levels for cytokines as and chemokines varied. Intratumoral injection of FGF1 or VEGF (6 daily intra-tumor injections of 6μg/mouse) did not alter most cytokines or chemokines mRNA expression in spleen and lung. In summary, alteration of tumor oxygenation by local administration of angiogenic growth factors may be mediated by cytokine/chemokine production in the tumor.

Key words: VEGF, FGF, fibrosarcoma, cytokine and chemokine, apoptosis, transcription factors, gene expression

1. INTRODUCTION

Tumor angiogenesis requires at least four steps (1, 2) (i) local secretion of proteinase or cytokines/chemokines, (ii) degradation of the extracellular matrix of tumor stroma surrounding tissues, (iii) chemotaxis of endothelial cells and other cell types toward an angiogenic stimulus, and (iv) proliferation of endothelial cells and formation of tumor-specific blood vessels. A variety of tumor-related growth factors/cytokines have been identified as potential positive regulators of angiogenesis, including

fibroblast growth factors (FGFs) and vascular endothelial growth factor (VEGF) (3). Some of these factors are able to directly stimulate endothelial cell growth, while others lack direct stimulatory effects on endothelial cells, and are thought to require the paracrine release of growth factors from other cell types, such as tumor fibroblasts, infiltrating inflammatory cells, and tumor cells (1, 2, 4-6). In this study, we investigated the effects of exogenous FGF1 and VEGF on KHT tumor growth and hypoxia, and explored the underlying molecular mechanisms. Using FGF1- or VEGF-treated and control mice, mRNA expression for 7 transcriptional factors, 17 cytokines, 9 chemokines, and 10 apoptotic-related molecules were determined in tumors and five normal organs (brain, liver, lung, kidney and spleen) by RNase protection assay. Our goal was to further understand the role of these two angiogenic growth factors in the regulation of tumor oxygenation by alteration of gene expression for cytokine/chemokine, apoptosis and transcriptional factors.

2. METHODS

2.1 Tumor models and angiogenic growth factors treatment

Isotransplants of murine fibrosarcoma (KHT) cells were inoculated i.m. into the hind limbs of 6-8 week-old female C3H/HeJ mice (Jackson Laboratories, Bar Harbor, ME). Tumors were selected for treatment when they reached volumes of 100 and 300 mm^3 [as measured by calipers and the formula: volume = (Diameter^3/6)]. 6 μg of either FGF1 or VEGF (Pepro Tech Inc., Rocky Hill, NJ) was injected intratumorally once a day for 6 days. Control mice were given the same volume of saline as controls. Mice were sacrificed 24 hours after the final injection. Tumor, liver, spleen, lung, kidney and brain from tumor bearing mice were removed, and tissue RNA was isolated. Guidelines for the humane treatment of animals were followed as approved by the University Committee on Animal Resources.

2.2 EF5/Cy3 hypoxic marker

Localized areas of tumor hypoxia were assessed in frozen tissue sections by immunohistochemical identification of sites of 2-nitroimidazole metabolism. A pentafluorinated derivative (EF5) of etanidazole was injected i.v. one hour before tumor freezing. Protein conjugates of EF5 have been previously used to immunize mice from which monoclonal antibodies were

developed. These antibodies are extremely specific for the EF5 drug adducts that form when the drug is incorporated by hypoxic cell (7). Regions of high EF5 metabolism in tumors (hypoxic regions) were visualized immunochemically using a fluorochrome (Cy3) conjugated to the ELK3-51 antibody (8).

2.3 mRNA expression for transcriptional factors, apoptotic molecules, and cytokines/chemokine measured by RNase protection assay

Tumor and normal tissues from each treatment group were removed and immediately frozen. The RNA was then isolated by pulverizing the frozen tissue and dissolving it in TRIzol reagent (MRC, Cincinnati, OH). RNase protection was then performed using established multi-probe template sets (PharMingen, San Diego, CA). The MCK5 chemokines set includes Lymphotactin, Rantes, Eotaxin, MIP-1α, MIP-1β, MIP-2, IP-10, MCP-1, and TCA-3. The MCK3 inflammatory cytokine set includes tumor necrosis factors α and β, transforming growth factors β1, β2, β3, interferon β and γ, interleukine 6, and lymphotoxin. The MCK2 interleukine set includes IL-1α, IL-1β. IL-1Ra, IL-6, IL-8, IL-12, IL-18, and MIF. The transcriptional factors set includes c-jun, JunB, JunD, c-fos, FosB, Fra-1, and Fra-2. The apoptosis-related molecular set includes Caspase 8, FAS, FASL, FADD, FAP, FAF, Trail, TRADD, and TNFRp55. Two internal controls, L32 and GAPDH, were used. The mRNA expression levels for each sample were quantified by phosphorimaging (HP Company, Meriden, CT).

1.4 Statistical methods

mRNA expression from saline and FGF1 or VEGF treated mice was evaluated using the unpaired Students t-test or Mann-Whitney Rank Sum test. Differences were considered significant for $P < 0.05$.

3. RESULTS

3.1 Effects of FGF1 and VEGF intratumoral injection on tumor sections

Six daily intratumoral injections of either FGF1 or VEGF decreased the EF5 staining in tumor sections compared with saline-treated controls (Figure 1a-c). This phenomenon appears tumor size-dependent (Ding: Unpublished data). Although angiogenic growth factor-mediated improvement of tumor oxygenation could be the result of alteration in local tumor blood flow, other mechanisms may also be involved in this process, such as up- or down-regulation of angiogenic-related cytokines and/or chemokines. Angiogenic growth factors have been shown to lessen cell death from radiation by decreasing radiation-induced apoptosis. In our study, intratumoral injection of FGF1 and VEGF slightly increased tumor cell apoptosis, but not significantly (Figure 1d-f). We also examined mRNA expression of ten apoptosis-related molecules and seven transcriptional factors in these tumors. As shown in Figure 2, administration of FGF1 or VEGF in KHT tumors did not significantly alter mRNA expression of either the transcriptional factors (Fig 2a) or the apoptosis-related molecules (Fig 2b). Similarly, FGF1 and VEGF did not affect either the transcriptional factors or gene expression of the apoptosis-related molecules in five major normal organs (Fig 2c).

3.2 Effects of FGF1 and VEGF intratumoral injection on normal tissues

To explore the effects of intratumoral injection of VEGF or FGF1 on cytokine and chemokine mRNA expression in normal tissues, mRNA was determined for seventeen cytokine and nine chemokine samples of brain, liver, kidney, lung, and spleen tissue. As shown in Figure 1d, although different organs had varied baseline levels of each of the molecules, intratumoral injection of VEGF affected interleukine mRNA expression in kidney, liver, and brain. VEGF upregulated both liver and kidney IL-18 mRNA 1.6 fold, IL-1Ra mRNA 1.4 fold, and IL-1β mRNA 1.3- and 1.4-fold, respectively. Injection of FGF1 and VEGF did not alter expression of any of the TGFβ isoforms. The other cytokines, including TNFα, TNFβ, IFNβ, and IFNγ were also unaffected. Finally, injection of angiogenic growth factors also altered liver and tumor chemokine mRNA levels. As summarized in Table 1, both FGF1 and VEGF increased liver Rantes mRNA

expression (1.7 fold and 2.8 fold, respectively). VEGF also upregulated mRNA expression of two C-C family member chemokines in liver: MCP1 (3.7 fold) and TCA-3 (2.2 fold). Both VEGF and FGF1 also decreased tumor MCP-1 mRNA expression.

4. DISCUSSION

The effects of angiogenic growth factors on tumor angiogenesis and growth have been studied extensively (4). Active tumor cell proliferation is dependent on the tumor blood supply(2). It is believed that tumors larger than 1 mm^3 in volume require angiogenesis for further growth. In theory, local or systemic administration of angiogenic growth factors could improve blood vessel formation, and thus may alter tumor oxygenation. Our data support this notion. However, the underlying molecular mechanisms for angiogenic growth factor-mediated tumor pathophysiology are not clear (2). Most angiogenic growth factors not only stimulate endothelial cell proliferation, but also regulate tumor cell growth and differentiation. The process leading to tumor proliferation is either direct, acting on both endothelial and tumor cells, or indirect, regulating production of other growth factors, such as cytokines and chemokines. An example of the second mechanism comes from the work of Seghezzi et al (9) .They recently reported that both exogenous FGF2 administration and expression of endogenous FGF2 result in increased VEGF gene expression. They also concluded that endothelial cell-derived VEGF is a major autocrine mediator of FGF2-induced angiogenesis.

5. CONCLUSION

In this study, we explored the molecular mechanisms of angiogenic growth factor-mediated angiogenesis in KHT tumor-bearing mice treated with FGF1 and VEGF. Our findings indicate the following: (1) FGF1 and VEGF improved KHT tumor oxygenation without altering tumor transcriptional factors, tumor cell death-related molecule mRNA expression, or tumor cell apoptotic frequency. However, decreased tumor MCP1 and interleukin mRNA expression may indirectly affect local tumor angiogenesis. (2) Local tumor administration of FGF1 and VEGF altered cytokine or chemokine mRNA expression in some normal organs, with the greatest effects seen in kidney and liver. Increased C-C (MCP-1, Rantes and TCA-3) and C-X-C

(IP-10) mRNA expression generated by normal organs in animals with high intratumor cytokines may also participate in local tumor angiogenesis and immunoreactivity.

ACKNOWLEDGEMENTS

This work was supported in part by National Cancer Institue P01-CA11051-25A2 and National Cancer Institue R01CA52586.

REFERENCES

1. Couffinhal T, Silver M, Zheng LP, Kearney M, Witzenbichler B, and Isner JM. Mouse model of angiogenesis. Am J Pathol 1998;152:1667-79
2. Folkman J. Angiogenesis in cancer, vascular, rheumatoid and other disease. Nat Med 1995;1:27-31
3. Andre T, Chastre E, Kotelevets L, Vaillant JC, Louvet C, Balosso J, Le Gall E, Prevot S, Gespach C. Tumoral angiogenesis: physiopathology, prognostic value and therapeutic perspectives. Rev Med Interne 1998;19:904-13.
4. Battegay EJ. Angiogenesis: mechanistic insights, neovascular diseases, and therapeutic prospects. J Mol Med 1995;73:333-46
5. Folkman J. Fighting cancer by attacking its blood supply. Sci Am 1996;275:150-4
6. Folkman J. New perspectives in clinical oncology from angiogenesis research. Eur J Cancer 1996;32A:2534-9
7. Lord EM, Harwell L, and Koch CJ. Detection of hypoxic cells by monoclonal antibody recognizing 2- nitroimidazole adducts. Cancer Res 1993;53:5721-6
8. Fenton BM, Paoni SF, Lee J, Koch CJ, and Lord EM. Quantification of tumour vasculature and hypoxia by immunohistochemical staining and HbO2 saturation measurements. Br J Cancer 1999;79:464-71
9. Seghezzi G, Patel S, Ren CJ, Gualandris A, Pintucci G, Robbins ES, Shapiro RL, Galloway AC, Rifkin DB, and Mignatti P. Fibroblast growth factor-2 (FGF-2) induces vascular endothelial growth factor (VEGF) expression in the endothelial cells of forming capillaries: an autocrine mechanism contributing to angiogenesis. J Cell Biol 1998;141:1659-73

2000 Eleventh International Congress in the Chemical Modifiers of Cancer Treatment Series, Banff, Alberta, Canada.

ADMINISTRATION OF ENDOSTATIN PLASMID INHIBITS ANGIOGENESIS AND TUMOR GROWTH AND IN NUDE BUT NOT C3H MICE.

Paul Okunieff, Jianzhong Sun, Weimin Liu, Yuanying Jiang, Bruce Fenton, Ivan Ding
University of Rochester, Department of Radiation Oncology, Rochester, NY 14642.

Summary: Endostatin, a fragment of the C-terminal domain of collagen XVIII, is a recently discovered endogenous inhibitor of tumor angiogenesis and endothelial cell growth. In some hands, endostatin has little effect on tumors, in others it can arrest tumor growth, and in still others, cures are reported. The efficacy of endostatin, therefore, has been difficult to reliably reproduce. Further, very few measurements of tumor pathophysiology after endostatin treatment have been performed. For these reasons we sought to intramuscularly deliver an endostatin plasmid followed by measurement of a) tumor physiological parameters, b) tumor growth inhibition, and c) mRNA expression of some of the associated angiogenic and anti-angiogenic cytokines.

Methods: MCa-4 tumors were implanted in both thighs of C3H or nude mice. When tumors reached 7-8 mm in diameter, injections of either endostatin, saline, or vector were initiated (2 doses, 7 days apart) to the right thigh. Tumor diameters were measured, tumor vascularity and neovascularity were determined using CD31 and CD105 antibodies, perfusion was measured using $DiOC_7$ staining, and hypoxia was detected using EF5 uptake. All immunohistochemical images were analyzed by computer image analysis routines.

Figure 1 – Effect of endostatin on MCa-4 tumor weight and growth rate

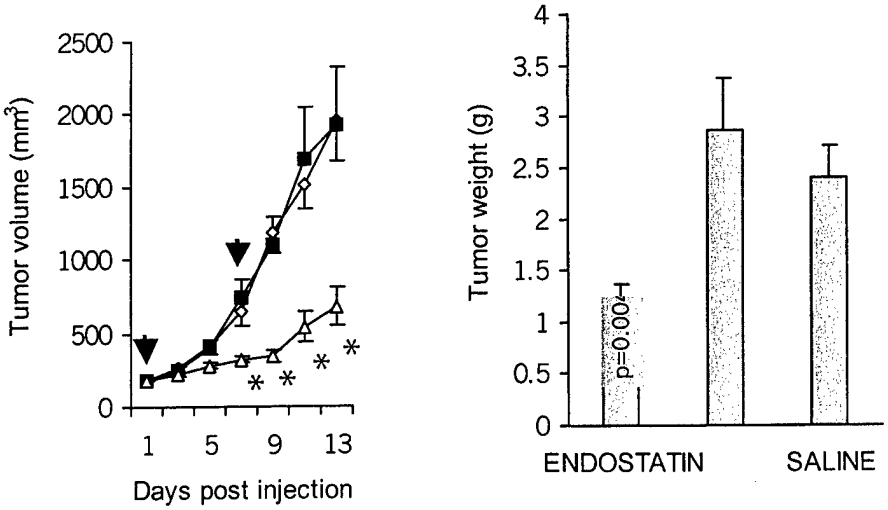

Results: Intratumoral injection of endostatin plasmid caused tumor growth reduction in nude mice, but not C3H/He mice. Although significant growth retardation was observed, there was no tumor shrinkage. The directly injected tumors (right thigh) had a greater response than the contralateral tumor (Fig. 1). Western analysis demonstrated endogenous endostatin in all tumors (Fig. 2). Endostatin treated animals, however, had very high levels in both the directly injected tumors and in the contralateral tumors. CD31 staining for total tumor vasculature was performed and distances to nearest vessels were computed automatically in multiple image montages (Fig. 3). Distances to nearest CD31 stained vessels (total vasculature) were not significantly different following endostatin treatment, for tumors grown in C3H mice, but were different in both the tumor interior (39.9 μm saline versus 51.8 μm endostatin) and periphery (36.7 μm saline versus 44.4 μm endostatin) for tumors in nude mice. Similarly for angiogenic staining (CD105), tumors in C3H mice were not effected by the endostatin injection, while significant differences were seen in nude mice (interior: 37.6

EFFECTS OF ANGIOGENIC GROWTH FACTOR ADMINISTRATION ON TUMOR VASCULAR DISTRIBUTION AND FUNCTION

Bruce Fenton, Paul Okunieff, and Ivan Ding, Department of Radiation Oncology
University of Rochester Medical Center, Rochester, New York 14642

Over the past ten years, the primary focus of our research has been the development of improved methods for measuring micro-regional heterogeneities in tumor vascular structure, oxygen delivery, and tumor hypoxia. These types of measurements are useful in terms of two fundamentally different approaches to cancer treatment: 1) the establishment of predictive assays of tumor radioresponse based on pathophysiological differences among tumors, and 2) the quantification of changes in tumor oxygenation or vascular structure following manipulations designed to either alter oxygen levels or blood vessel development (angiogenesis). The techniques available in our laboratories range from highly invasive measures of intravascular HbO_2 levels in frozen tumors to clinically applicable immunohistochemical staining of frozen or paraffin tumor sections. Using computer analysis of multiple field image montages, total anatomical blood vessels are quantified using anti-CD31 or anti-factor VIII staining, angiogenic vessels are determined by using anti-CD105, perfused vessels are measured by *i.v.* injection of fluorescent $DiOC_7$, and tumor hypoxia is determined using EF5 hypoxia marker uptake. Several ongoing research studies will be used to illustrate the range of measurements possible with these techniques. First, angiogenesis mediated by fibroblast growth factors (FGFs) and vascular endothelial growth factor (VEGF) is critically involved in physiological and pathological processes. These growth factors not only have beneficial effects on normal tissues undergoing radiation treatment, but can also contribute in varying degrees to tumor growth, invasion, and metastasis. Pathophysiological effects of growth factor administration were quantified using three murine mammary carcinomas: two fast-growing transplanted tumors (MCa-4 and MCa-35) contrasted with slow-growing 1^{st} generation transplants of spontaneous mammary tumors. Not only are basal levels of oxygenation and vascular density quite different among tumor models, but furthermore, response to specific growth factors varies markedly. To illustrate changes in tumor perfusion and oxygenation following oxygen manipulative agents, tumors were examined before and after hydralazine administration, an agent used to reduce tumor blood flow. Again, response was clearly tumor type dependent. To quantify the effects of anti-angiogenic agents, mice were treated with different schedules of COX-2 inhibitors, endostatin, and radiation. The combination of our pathophysiological measurements with corresponding molecular determinations allows a much more meaningful analysis of underlying mechanisms. Finally, while the majority of our work has thus far concentrated on animal models, similar approaches can be applied to clinical specimens and have recently been initiated using automated image analysis of anti-factor VIII stained prostate tumor sections.

versus 47.1 μm, peripheral: 41.9 versus 49.6 μm). In nude mice, endostatin gene therapy reduced functioning vasculature ($DiOC_7$), and increased hypoxia (Table 1). Also, mRNA expression was measured for several cytokines, including IL-1, IL-1Ra, IL-2, IL-6, IFNγ, TNF, and three TGFβ isoforms using RNase protection assay. No substantial changes were seen, although there were endostatin related reductions in the TGFβ and IL-6 in the nude mouse tumors. Although MCP-1 mRNA was reduced after endostatin treatment, this effect was also seen in vector treated tumors.

Conclusions: Endostatin effects are complex and are dependent on animal model. The success in nude but not C3H mice suggests that endostatin is less effective in the presence of normal T-cell function. MCa-4 tumors are weakly immunogenic, and immunogenic tumors may be less likely to respond to endostatin due to inflammation-associated enhancement of angiogenesis, as confirmed by preliminary data using immunogenic mammary MCa-35 tumors. Consistent with the proposed anti-vascular effects of endostatin, vascular density, perfusion, and oxygenation were all reduced by gene therapy with endostatin. Finally, although endogenous endostatin levels are already high in some tumors, further increases appear to be beneficial.

Figure 2

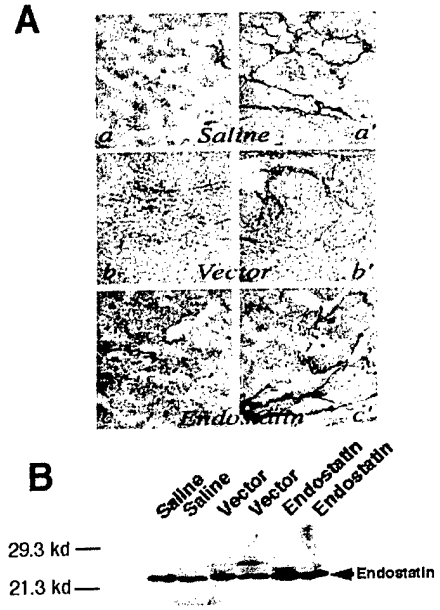

Figure 3 – Immunohistochemistry detection of tumor vasculature (top-bottom: control, vector, endostatin)

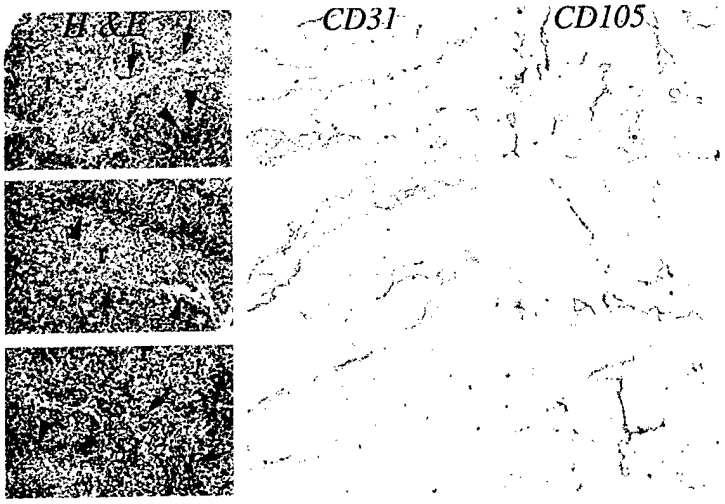

Table 1 – Effect of endostatin on tumor vasculature, growth, and apoptosis

	Median Distance to Tumor Vessels (μm)		Tumor Growth Parameters		
	CD31	CD105	% apoptosis	% mitosis	% necrosis
Saline	38.3 ± 1.6	39.8 ± 1.5	1.9 ± 0.32	3.6 ± 0.6	14.9 ± 2.9
Vector	41.5 ± 1.1	44.3 ± 1.6	2.0 ± 0.3	4.4 ± 0.4	11.3 ± 0.8
Endostatin	48.1 ± 3.8*	48.5 ± 1.5*	3.2 ± 0.5*	3.6 ± 0.2	8.6 ± 1.8

2001 American Association for Cancer Research Meeting, New Orleans, LA.

Endostatin-mediated Antitumor and Antiangiogenesis: Inhibition of Murine MCa-35 Mammary Tumor Growth and Metastasis are Associated with Decreased Tumor Structural and Perfused Vessels

J. Sun, W. Liu, C. Yang, W. Min, P. Keng, B. Fenton, P. Okunieff, and I. Ding. *University of Rochester School of Medicine Rochester, NY 14642.*

Endostatin, a fragment of the C-terminal domain of collagen XVIII has been recently demonstrated as an endogenous inhibitor of tumor angiogenesis by its selective inhibition of endothelial cell growth. Antiangiogenic therapy with endostatin in tumor-bearing mice requires multiple and prolonged administration of the protein. In addition, production of this functional polypeptide has proven difficult, perhaps due both to its physical properties and to variations in the purification procedures utilized by different laboratories. Although preliminary data have shown that local or systemic administration of endostatin by plasmid or viral-mediated delivery is an effective means of application in cancer therapy, direct transfection of endostatin gene into tumor cells is still commonly used in experimental systems. In the current study, we transfected murine, MCa-35, mammary tumors with endostatin cDNA and demonstrated that: 1) endostatin inhibited primary tumor formation and artificial lung metastasis, 2) secreted endostatin protein in conditional medium strongly inhibited FGF2 or VEGF-mediated HUVEC cell proliferation, 3) reduction of tumor growth correlated with a decrease in tumor structural (CD31-stained) and functional (DiOC7-stained) vessels, and 4) endostatin altered mRNA expression of angiogenic-related cytokines and chemokines, as well as angiogenic growth factors such as angiopoietin and VEGF. These results suggest that endostatin may have direct and indirect effects on tumor and endothelial cell growth.

2001 American Association for Cancer Research Meeting, New Orleans, LA.

Alteration of cytokine and chemokine mRNA expression in MCa-4 murine mammary carcinomas after intratumoral administration of endostatin plasmid.

I. Ding, J. Sun, L. Liang, W. Liu, W. Min, B. Fenton, and P. Okunieff, *University of Rochester School of Medicine, Rochester, New York 14642.*

Endostatin, a fragment of the C-terminal domain of collagen XVIII, is a recently demonstrated endogenous inhibitor of tumor angiogenesis and endothelial cell growth. We previously demonstrated that two intratumoral injections of endostatin plasmid reduced the number of vessels (structural, angiogenic and perfused) in murine mammary tumors. However, observed changes in oxygenation, apoptosis of tumor cells, and baseline expression of tumor endostatin cannot be explained by a single molecular mechanism. Therefore, we examined the effects of endostatin on mRNA expression of a series of cytokines, chemokines, and transcription factors by RNase protection assay in endostatin-treated MCa-4 tumors grown in nude and C3H mice. Endostatin inhibited MCa-4 tumor growth in nude mice, but not in C3H mice. In nude mice, a significant reduction of angiogenic vessels (CD105-stained) was seen in both peripheral (16%) and internal (21%) regions in endostatin-treated tumors. A similar reduction in structural vessels (CD31-stained) was also observed in these tumors in nude mice. Decreases in the number of blood vessels were associated with a significant down-regulation of Interleukin-6 (IL-6) mRNA expression after endostatin treatment. In addition, reductions in mRNA expression of TGF-b1, b2 and b3 (22-28% of controls) were seen in endostatin-treated tumors grown in nude mice. No obvious differences in chemokine mRNA expression were found between endostatin-treated and control tumors, except for the 25-28% reduction in mRNA expression of monocyte chemoattractant protein (MCP-1). A slight down-regulation of *fos* and *jun* transcription factor mRNA was coincident with the decrease of *myc* and *myc*-antagonist *mad* gene family mRNA. Endostatin therefore appears to slow tumor growth only when it is effective in down-regulating angiogenesis and vascular function. The antiangiogenic and subsequent anti-tumor growth effects of endostatin were associated with the down-regulation of some angiogenic-related inflammatory cytokines and chemokines, including IL-6, TGF-b and MCP-1.

Effect of Endostatin Administration on Tumor Growth Inhibition, Vascular Perfusion, and Hypoxia in Murine Mammary Carcinomas

Bruce M. Fenton[1], Scott Paoni[1], Brian Beauchamp[1], Li Liang[1], Brian G. Grimwood[2], and Ivan Ding[1]

[1]*Department of Radiation Oncology, University of Rochester Medical Center, Rochester, NY 14642 and* [2]*Wadsworth Center, Box 509, Albany, NY 12201.*
Email: bruce_fenton@urmc.rochester.edu

Endostatin, a fragment of collagen XVIII has been shown to potently inhibit both angiogenesis and the growth of experimental tumors, primarily through inhibition of endothelial cell migration and proliferation, with minimal direct effects on tumor cells. Recent studies have also demonstrated that endostatin can enhance the antitumor effects of ionizing radiation, when administered before and during radiotherapy (1). In order to optimize such combination therapies, an understanding of the accompanying changes in tumor pathophysiology, *i.e.*, oxygenation and blood flow, is clearly of prime importance. The primary aim of the current work was to determine the micro-regional effects of endostatin on total and perfused blood vessels, as well as hypoxic marker uptake, in two murine mammary carcinomas: MCa-35 and MCa-4. Total anatomical blood vessels were quantified using anti-CD31 stained frozen sections, perfused vessels were measured by *i.v.* injection of fluorescent $DiOC_7$, and tumor hypoxia was determined using EF5 hypoxia marker uptake. Tumors were grown in the hind legs of C3H/HeJ mice, and beginning when tumors had grown to between 100-200 mm^3, recombinant murine endostatin (rmNYendo) was administered *i.p.* at 20 mg/kg for 3 consecutive days. Tumors were frozen for sectioning and analysis at either day 4 or day 7, and 9.0 μm frozen sections were obtained for immunohistochemistry. Total and perfused vessel distributions, as well as EF5/Cy3 intensities, were determined using computer image analysis of multiple-field image montages. Although endostatin produced significant growth inhibition in MCa-4 tumors by day 4, growth of the more aggressive MCa-35 tumors was not substantially different from untreated controls. Total and perfused vessel densities were much higher in MCa-35 tumors than in MCa-4, but neither was significantly altered following endostatin. Compared to the untreated MCa-35 tumors, hypoxia was much higher in the untreated MCa-4 tumors but was significantly reduced at day 4. By day 7, a trend towards reduced hypoxia in the endostatin treated tumors was still present, although not significant. For the MCa-35 tumors, hypoxia was somewhat reduced at day 4, but no different by day 7. In summary, although the effects of endostatin on tumor growth inhibition varied markedly between the two tumor types, overall tumor hypoxia was similarly reduced in both cases. If confirmed in additional experiments, these results could provide an additional rationale for the reported improvement in response when combining endostatin with radiotherapy. Further more detailed studies are needed to interpret these somewhat puzzling findings, however, since the previously reported increase in endothelial cell apoptosis following endostatin (1) would more logically lead to a decrease in tumor oxygenation due to a compromise in vascular supply. Future experiments will investigate whether increased oxygen levels are only transient in nature, and whether response to fractionated radiotherapy can also be enhanced by extended endostatin administration.

1) N. N. Hanna, S. Seetharam, H. J. Mauceri, et al. Antitumor interaction of short-course endostatin and ionizing radiation. *Cancer Journal* **6**:287-293, 2000.

Supported by NIH Grant CA52586 and DOD Grant DAMD17-00-1-0420.

ABSTRACT SUBMISSION FORM
University of Rochester James P. Wilmot Cancer Center 6th Annual Scientific Symposium
October 16, 2001
Memorial Art Gallery – Rochester, New York
SUBMISSION DEADLINE: August 30, 2001

Use Times New Roman with a 12-point font
Limit text to one page
Abstracts must be electronically submitted
E-mail Marge Forth in the Continuing Professional Education Office at
maforth@cpe.rochester.edu

Presenting Author's Name : Bruce M. Fenton Degree(s): PhD

Affiliation: Department of Radiation Oncology
Address : Box 704

Telephone: 275-7911 Fax 273-1042
E-mail: bruce_fenton@urmc.rochester.edu
Indicate presentation format desired: _____ Poster _X___ Oral _____ Either

ABSTRACT
ALTERATIONS IN TUMOR GROWTH, PERFUSION, HYPOXIA, AND OXYGEN CONSUMPTION FOLLOWING ADMINISTRATION OF ENDOSTATIN

B Fenton*, S Paoni, B Beauchamp, L Liang, B Grimwood, B Tran, and I Ding
Box 704, University of Rochester Medical Center, Rochester, New York 14642

Endostatin, a fragment of collagen XVIII has been shown to potently inhibit both angiogenesis and tumor growth, primarily through inhibition of endothelial cell migration and proliferation. Recent studies have also demonstrated that endostatin can enhance the antitumor effects of ionizing radiation, when administered before and during radiotherapy. In order to optimize such combination therapies, an understanding of the accompanying changes in tumor oxygenation and blood flow is clearly of prime importance. The aim of the current work was to determine the micro-regional effects of endostatin on total and perfused blood vessel distributions and hypoxic marker uptake in two murine mammary carcinomas: MCa-35 and MCa-4. Total anatomical blood vessels were quantified using anti-CD31 stained frozen sections, perfused vessels were measured by *i.v.* injection of fluorescent $DiOC_7$, and tumor hypoxia was determined using EF5 hypoxia marker uptake. Tumors were grown in the hind legs of C3H/HeJ mice, and when tumors had grown to 100-300 mm^3, recombinant murine endostatin (rmNYendo) was administered *i.p.* at 20 mg/kg for 3 consecutive days. Tumors were frozen for sectioning and analysis at days four and seven, and 9.0 μm frozen sections were used for immunohistochemistry. Total and perfused vessel distributions, as well as EF5/Cy3 intensities, were determined using computer image analysis of multiple-field image montages. Although endostatin produced significant growth inhibition in MCa-4 tumors, growth of the more aggressive MCa-35 tumors was not substantially different from untreated controls. In MCa-4 tumors, vascular function was improved and tumor hypoxia was reduced, while oxygen consumption appeared unchanged. In MCa-35 tumors, however, no significant changes were seen in any of these parameters. If confirmed in additional experiments, these results could provide an additional rationale for the reported improvement in response when combining endostatin with radiotherapy.

Supported by NIH Grant CA52586 and DOD Grant DAMD17-00-1-0420.

Endostatin and angiostatin induce tumor and endothelial cell apoptosis through the down-regulation of VEGF/Akt signal transduction pathway

W.M. Liu, P. Keng, C.R. Yang, B. Fenton, P. Okunieff and I. Ding
Department of Radiation Oncology, University of Rochester, Rochester, NY 14642

Both endostatin and angiostatin have been identified and characterized as endogenous inhibitor for tumor angiogenesis and endothelial cell growth. Both of these antiangiogenic factors induce endothelial cell apoptosis in vitro and in vivo models. However, whether endostatin and angiostatin have antiapoptotic effect on tumor cells, as well the molecular mechanism of antiangiogenic action is currently unknown. In this study, we showed that transfection of endostatin and angiostatin fusion genes (endostatin/angiostatin) into murine breast cancer cell line, MCa35, caused a reduction of growth rate in vitro and tumor formation in vivo. The inhibition of MCa-35 tumor cell was associated with decreased S phase fraction and induction of apoptosis. Similarly, exogenous human or mouse recombinant endostatin (10μg/ml) treated MCa-35 cells also had significant increased apoptosis and altered cycle. 10 Gy radiation alone caused obvious apoptosis in both cultured MCa-35 and HUVEC cells, but combination of endostatin and/or angiostatin with radiation (endogenous transfected endostatin/angiostatin gene or exogenous protein application), leaded to more substantial induction of apoptosis in both tumor and endothelial cells. Endostatin/angiostatin transfected clones had a decrease of basal levels of phosphorylated Akt, in which the Akt reduction was more obvious if radiation added. We also found that in the downstream of Akt pathway, phosphorylated glycogen synthase kinase (GSK-3a and GSK-b) and transcription factor FKHK were significantly reduced in endostatin/angiostatin transfected clones. Finally we found there was decreased mRNA expression levels for VEGF, TGFb1, TGFb3 in two of three endostatin/angiostatin transfectants. These findings indicate that antiangiogenic agents endostatin or angiostatin, may down regulate endogenous growth factor gene expression, which is associated with reduction of survival factor Akt production, and resulted in tumor and endothelial cell apoptosis through Akt down stream signal GSK3 and FKHK down-regulation. It also suggests that endostatin or angiostatin may serve as radiation modulator to increase tumor cell apoptosis.

Discussion

Both endothelial cell and tumor cell were induced apoptosis after endostatin. Breast tumor cells are relatively refractory to apoptosis in response to modalities which induce DNA damage such as ionizing radiation and the topoisomerase II inhibitor, adriamycin. Various factors which may modulate the apoptotic response to DNA damage include the p53 status of the cell, levels and activity of the Bax and Bcl-2 families of proteins, activation of NF-kappa B, relative levels of insulin like growth factor and insulin-like growth factor binding proteins, activation of MAP kinases and PI3/Akt kinases, (the absence of) ceramide generation and the CD95 (APO1/Fas) signaling pathway. Prolonged growth arrest associated with replicative senescence may represent an alternative and reciprocal response to DNA-damage induced apoptosis that is p53 and/or

p21waf1/cip1 dependent while delayed apoptosis ma occur in p53 mutant breast tumor cells which fail to maintain the growth-arrested state. Clearly, the absence of an immediate apoptotic response to DNA damage does not eliminate other avenues leading to cell death and loss o self-renewal capacity in the breast tumor cell. Nevertheless, prolonged growth arrest (even if ultimately succeeded by apoptotic or necrotic cell death) could provide an opportunity for subpopulations of breast tumor cells to recover proliferative capacity and to develop resistance to subsequent clinical intervention.

Previous studies from this laboratory as well as others have demonstrated that breast tumor cells fail to undergo primary apoptosis in response to agents which induce DNA damage such as ionizing radiation and the topoisomerase II inhibitor adriamycin. Similarly, the primary response of breast tumor cells to vitamin D(3) [1,25-(OH)(2)-D(3)] and its analogs such as EB 1089 is growth inhibition, with apoptosis occurring in only a small fraction of the cell population. The possibility that the combination of vitamin D(3) compounds with radiation might promote cell death (i.e. through a differentiation stimulus plus DNA damage) was investigated by exposing both TP53 (formerly known as p53) wild-type and TP53 mutated breast tumor cells to 1,25-(OH)(2)-D(3) or EB 1089 for 48 h prior to irradiation. This combination resulted in enhanced antiproliferative effects in the TP53 wild-type MCF-7 cells based on both a clonogenic assay and the determination of numbers of viable cells. The combination of EB 1089 with radiation increased DNA fragmentation based on both the terminal transferase end-labeling (TUNEL) and bisbenzamide spectrofluorometric assays, suggesting the promotion of apoptosis. The observed increase in DNA fragmentation was not due to an enhancement of the extent of initial DNA damage induced by radiation. These findings suggest that vitamin D compounds may be useful in combination with radiation in the treatment of breast cancer.

Mouse endostatin protein and endostatin plasmid have differential effects on esophageal and mammary carcinomas at various growth stages. Ivan Ding , Min Guo, Dongping Hu, Weimin Liu, Yidan Ding, Lidong Wang, Brian Grimwood, Paul Okunieff and Bruce Fenton. *Department of Radiation Oncology, University of Rochester, Rochester, NY and Wadsworth Center, Albany, NY.*

The antiangiogenic agent, endostatin, has been shown to inhibit tumor growth in several experimental tumor models, whether administered by gene therapy or recombinant protein. However, endostatin-mediated, antitumoral effects on human esophageal carcinomas have not been studied. We investigated whether recombinant mouse endostatin (rmNYendo), given at three tumor growth stages, is effective against two human esophageal adenocarcinoma xenografts (Seg-1, which is highly angiogenic, and Bic-1, which is less angiogenic). The rmNYendo was administered *i.p.* at 20 mg/kg, twice per day, for four consecutive days to tumor-bearing mice at early (day of tumor cell inoculation), intermediate (tumors 3-4 mm in diameter), and late (tumors 10-12 mm in diameter) stages. Mean tumor weight in mice administered rmNYendo was slightly less than that in controls, with tumor growth inhibition of 6% and 10% (Bic-1 and Seg-1) at early, 5% and 4% at intermediate, and 34% and 21% at late stages, respectively. Total and functional vascular density, as well as endostatin-mediated endothelial and tumor cell growth inhibition were also determined. Altered tumor pathophysiology was associated with the inhibition of tumor growth. In a second experiment, endostatin plasmid (45μg DNA/mouse x 2) was intratumorally injected at similar stages in MCa-35 murine mammary tumors. Although tumor inhibition was present in endostatin plasmid-treated mice, this inhibition was treatment schedule dependent. In summary, endostatin administration, particularly endostatin recombinant protein, resulted in tumor inhibitory effects especially in the largest tumors. The effects were modest, and thus will require complementary cytotoxic or radiation therapies. Clinically, selection of tumor type (*e.g.*, highly versus poorly vascularized tumors) and appropriate administration times may both influence the overall efficacy of endostatin.

Celecoxib-mediated antitumor effects in murine mammary carcinomas: association of two signal transduction pathways involved in DNA damage and apoptosis. Weimin Liu, Bruce Fenton, Peter Keng, Paul Okunieff and Ivan Ding *Department of Radiation Oncology, University of Rochester, Rochester, NY 14642.*

Tumor growth and angiogenesis are interdependent. Cyclooxygenase (COX) mediates prostaglandin production, while nonsteroidal anti-inflammatory drugs (NSAIDs) inhibit the synthesis of prostaglandins and reduce tumor formation. Enhanced COX-2 expression has been related to the development of cancers. In previous studies, we have demonstrated differential effects of the selective COX-2 inhibitor, celecoxib, on mammary and lung carcinoma cell lines, but the molecular basis and celecoxib-mediated signal transduction pathways remain unclear. In the current study, celecoxib alone and in combination with radiation were investigated in vitro and in vivo using MCa-35 murine mammary tumors. Celecoxib dose-dependently inhibited MCa-35 clonogenic survival *in vitro* (at doses ranging from 10μM-100M). Similarly, 50 mg/kg celecoxib reduced tumor growth by 45% after 10 treatment doses. Celecoxib-mediated tumor inhibition was associated with activation of two signal-transduction pathways: DNA damage, which initiated G2/M arrest, and Akt inactivation, which triggered apoptosis. Celecoxib induced MCa-35 DNA damage, as detected by Comet assay (1 hr after treatment), and increased Ckh1, Chk2 and phospho-cdc2 protein levels, leading to G2/M arrest 8-24 hr after treatment. Similarly, administration of celecoxib significantly sensitized MCa-35 cells to radiation in vitro (increased SF2) and in vivo (increased tumor growth delay time). Tumor cells unrepaired after celecoxib demonstrated substantial apoptosis, in part due to inactivation of Akt phosphorylation. Elevated GSK and FKHR, as well as activated Caspase-9, were also observed beginning at 4 hr following celecoxib treatment. In celecoxib treated MCa-35 tumors, an association between tumor cell apoptosis and elevation of proapoptotic molecules was also noted. These results indicate that celecoxib-induced MCa-35 tumor cell DNA damage is the initiating event, then leading to repair processes via Chk1/Chk2 mediated G2/M arrest. However, unrepaired tumor cells progress through apoptosis by inactivation of Akt and induction of FKHR/GSK. Radiation can accentuate this process through its powerful G2/M blockade. In conclusion, celecoxib not only directly induces MCa-35 tumor cell apoptosis, but also facilitates radiosensitization through alteration of cell cycle check points. These results emphasize the importance of appropriate time scheduling of celecoxib and radiotherapy in the clinical setting.

Alterations in tumor growth, perfusion, hypoxia, and oxygen consumption following administration of endostatin

B Fenton, S Paoni, B Beauchamp, L Liang, B Grimwood, B Tran, and I Ding
University of Rochester Medical Center, Rochester, New York 14642

Endostatin, a fragment of collagen XVIII has been shown to potently inhibit both angiogenesis and tumor growth, primarily through inhibition of endothelial cell migration and proliferation. Recent studies have also demonstrated that endostatin can enhance the antitumor effects of ionizing radiation, when administered before and during radiotherapy. In order to optimize such combination therapies, an understanding of the accompanying changes in tumor oxygenation and blood flow is clearly of prime importance. The aim of the current work was to determine the micro-regional effects of endostatin on total and perfused blood vessel distributions and hypoxic marker uptake in two murine mammary carcinomas: MCa-35 and MCa-4. Total anatomical blood vessels were quantified using anti-CD31 stained frozen sections, perfused vessels were measured by *i.v.* injection of fluorescent $DiOC_7$, and tumor hypoxia was determined using EF5 hypoxia marker uptake. Tumors were grown in the hind legs of C3H/HeJ mice, and when tumors had grown to 100-300 mm^3, recombinant murine endostatin (rmNYendo) was administered *i.p.* at 20 mg/kg for 3 consecutive days. Tumors were frozen for sectioning and analysis at days four and seven, and 9.0 μm frozen sections were used for immunohistochemistry. Total and perfused vessel distributions, as well as EF5/Cy3 intensities, were determined using computer image analysis of multiple-field image montages. Although endostatin produced significant growth inhibition in MCa-4 tumors, growth of the more aggressive MCa-35 tumors was not substantially different from untreated controls. In MCa-4 tumors, vascular function was improved and tumor hypoxia was reduced, while oxygen consumption appeared unchanged. In MCa-35 tumors, however, no significant changes were seen in any of these parameters. If confirmed in additional experiments, these results could provide an additional rationale for the reported improvement in response when combining endostatin with radiotherapy.

Supported by NIH Grant CA52586 and DOD Grant DAMD17-00-1-0420.

Endostatin and angiostatin induce tumor and endothelial cell apoptosis through the down-regulation of VEGF/Akt signal transduction pathway

Wei Min Liu, Peter Keng, Chin-Rang Yang, Bruce Fenton, Brian Grimwood, Paul Okunieff and Ivan Ding

Both endostatin and angiostatin have been identified and characterized as endogenous inhibitors of tumor angiogenesis and endothelial cell growth. These antiangiogenic factors specifically induce endothelial cell apoptosis in *in vitro* and *in vivo* models. However, whether endostatin and angiostatin have anti-proliferative and/or apoptotic effects on tumor cells is unknown. Likewise, the molecular mechanisms of antiangiogenic action are currently unknown. In this study, we show that transfection of endostatin and angiostatin fusion genes (endostatin/angiostatin) into the murine breast cancer cell line, MCa35, caused a reduction in tumor cell growth rate *in vitro* and tumor formation *in vivo*. The inhibition of endostain/angiostatin transfected MCa-35 tumor growth was associated with a decreased S phase fraction and induction of apoptosis. Similarly, exogenous human or mouse recombinant endostatin (10-100μg/ml) treated MCa-35 cells also induced apoptosis and altered the cell cycle. 10 Gy radiation alone caused obvious apoptosis in both cultured MCa-35 and HUVEC cells, but combination of endostatin and/or angiostatin (either endogenous transfected endostatin/angiostatin gene or exogenous protein incubation) with radiation, resulted in a more substantial induction of apoptosis in both tumor and endothelial cells. Endostatin/angiostatin transfected clones had lower basal levels of phosphorylated Akt, and the Akt reduction was more obvious when radiation was added. We also found a reduction of phosphorylated glycogen synthase kinase (GSK-3a and GSK-3b) and transcription factor FKHR in endostatin/angiostatin transfected clones. Finally, decreased mRNA expression levels of VEGF, TGFβ1, and TGFβ3 were observed in two of three endostatin/angiostatin transfectants. These findings indicate that antiangiogenic agents endostatin or angiostatin, may downregulate endogenous growth factor gene expression, which is associated with reduction of survival factor Akt production and resulted in tumor and endothelial cell apoptosis through Akt downstream signal GSK3 and FKHR elevation. They also suggest that endostatin or angiostatin may serve as radiation sensitizers that increase tumor cell apoptosis.

"Endostatin: Structure, Function, and Application" Disparate effects of endostatin on tumor vascular perfusion and hypoxia in two murine mammary carcinomas.
Bruce M. Fenton, Scott F. Paoni, Brian G. Grimwood, and Ivan Ding

Endostatin has been shown to potently inhibit both tumor angiogenesis and the growth of experimental tumors, primarily through reduction of endothelial cell migration and proliferation with minimal direct effects on tumor cells. Recent studies have demonstrated that this agent can also enhance the antitumor effects of radiation when administered before or during radiotherapy. The current work was undertaken to investigate the effects of short-term recombinant endostatin administration on tumor microregional perfusion and hypoxic marker uptake in two murine mammary carcinomas, the poorly differentiated and highly vascularized MCa-35 tumor, and the well differentiated and less vascularized MCa-4. Specifically, the question was whether endostatin could produce pathophysiological changes in the tumor microenvironment, most notably alterations in oxygen delivery, that could lead to alterations in tumor radiosensitivity. Although antiangiogenic treatment might be expected to lead to a reduction in tumor blood flow, overall oxygenation was improved in one tumor model and unchanged in the other following short-term endostatin administration. Using recently devised image analysis techniques that allow correlation of multiply stained images of the same tumor frozen sections, changes in tumor hypoxia, apoptosis, and proliferation were quantified as a function of distance from the nearest anatomical or perfused blood vessel. In MCa-35 tumors, three daily doses of endostatin (20 mg/kg) had no effect on total or perfused vessel numbers, tumor hypoxia, or tumor growth. In MCa-4 tumors, total and perfused vessel counts were unchanged following endostatin, but tumor growth was inhibited by 30% and overall tumor hypoxia significantly decreased. Results suggest an initial increased vascular functionality in the endostatin treated tumors, without substantial alterations in tumor oxygen consumption rates. Following cessation of endostatin in the MCa-4 tumors, total and perfused vessel counts as well as vessel functionality decreased significantly with tumor growth, in conjunction with an increase in overall tumor necrosis. In summary, these results demonstrate striking intertumoral disparities in pathophysiological response following short-term endostatin administration. In those tumors in which hypoxia is reduced, acute treatment could prove extremely beneficial when combined with irradiation, providing that optimal treatment schedules can be defined. Improved predictive assays are clearly needed to characterize and select such tumors.

EFFECT OF ANTI-ANGIOGENIC AGENTS ON TUMOR VASCULATURE AND OXYGENATION IN MAMMARY CARCINOMAS

Bruce M. Fenton, PhD and Ivan Ding, MD

University of Rochester Medical Center

Bruce.Fenton@Rochester.edu

The effectiveness of therapy in human breast tumors is closely related to alterations in tumor vascular structure and oxygenation.These depend in part on the ability of the tumor to elicit new blood vessel formation (angiogenesis) to supply the rapidly expanding tumor mass. The primary objective of the current studies was to characterize changes in tumor vascular structure, perfusion, and oxygenation as a function of endogenous angiogenic growth factor expression. A second aim was to quantitate such pathophysiological changes following administration of various anti-angiogenic agents. Since such anti-angiogenic approaches will most likely be combined with conventional therapies, it is vital to understand acute and chronic alterations in the tumor micro-environment following specific dosing and scheduling. To investigate the interdependence among tumor growth factor expression and pathophysiology, MCF-7 xenografts were transfected with either fibroblast growth factor-1 (FGF1), FGF4, or three different VEGF isoforms. In addition, two murine mammary carcinomas were selected based on previously documented differences in: 1) VEGF expression, 2) p53 status, 3) metastatic potential, 4) vascularity, and 5) differentiation status. A combination of immunohistochemical stained images of the same frozen tumor sections were obtained to quantify changes in total and perfused vascular spacing and EF5 hypoxia marker intensities in relation to tumor growth in control and treated tumors. Overexpression of FGF or VEGF isoforms produced substantial alterations in tumor vascular configuration, tumor growth, and tumor oxygenation. Pathophysiological response to antiangiogenic therapy varied markedly among the different tumor types and results suggested a direct relationship to endogenous VEGF levels. An intriguing finding was that acute administration of some antiangiogenic agents produced an increase in tumor oxygenation and perfusion, rather than the expected increase in tumor hypoxia. This proposal is clinically relevant in terms of clarifying the relationships among tumor angiogenesis, vascular function, and metastatic potential and provides important clues as to the expected advantages and disadvantages of combining anti-angiogenic approaches with conventional therapies.

OVEREXPRESSION OF VEGF ENHANCES ESTROGEN-DEPENDENT AND -INDEPENDENT GROWTH OF MCF-7 BREAST TUMORS

Ping Guo,[1] Quan Fang,[1] Ivan Ding,[2] Bruce Fenton,[2] Bo Hu,[1] and Shi-Yuan Cheng[1]

[1]University of Pittsburgh Cancer Institute, Pittsburgh, PA 15213;
[2]Department of Radiation Oncology, University of Rochester, Rochester, NY 14642

chengs@msx.upmc.edu

Human breast cancers are dependent on estrogen or other estrogenic hormone for growth. Moreover, many estrogen-dependent breast tumors develop into more aggressive and malignant, estrogen-independent phenotype. Angiogenesis, a process of the formation of new blood vessels from preexisting vasculature, is important for the breast cancer growth. Vascular endothelial growth factor (VEGF) family, plays major roles in breast tumor angiogenesis. VEGF and its receptors are expressed at high levels in breast tumors. Modulation of VEGF functions regulated the angiogenicity and tumorigenicity of breast tumor cells in animals. VEGF regulates the functions of a similar set of estrogen (E_2)-modulated genes that contribute to breast cancer progression. In addition, E_2 directly regulates VEGF transcription expression by acting upon the estrogen response elements in the gene of VEGF. Early studies have demonstrated that factors induced by E_2 in E_2-dependent MCF-7 breast cancer cells could partially replace E_2 to promote tumor growth. Introduction of a human ras oncogene into these MCF-7 cells did not abrogate the E_2 dependency regarding for tumor growth in animals. Furthermore, E_2 dependent MCF-7 and T47D cells express VEGFR-1, VEGFR-2; and VEGF stimulates breast cancer cell mitogenesis. We therefore hypothesize that overexpression of VEGF in MCF-7 breast cancer cells might abolish E_2-dependency for breast tumor growth. To test our hypothesis, we constructed and characterized the MCF-7 breast cancer cell clones that overexpress two VEGF splicing isoforms, $VEGF_{121}$ and $VEGF_{165}$, as well as control LacZ gene. In vitro, the parental MCF-7 and MCF-7/LacZ cells express VEGF at low levels of 3.0 ng/ml/ 10^6 cells in 48 hrs. The derived MCF-7 clone cells express $VEGF_{121}$ or $VEGF_{165}$ at high levels of 300 ng to 500 ng/ml/10^6 cells. In cell culture, the MCF-7/VEGF expressing cells had increased proliferation rates than that of the parental MCF-7 cells and gained resistant to cell apoptosis induced by E_2-withdraw from the culture media. When these cells were implanted into mammary fat pads in mice that were inoculated with slow-release E_2 pellets, overexpression of $VEGF_{121}$ and $VEGF_{165}$ greatly enhanced E_2-dependent MCF-7 tumor growth. In 33 days, the parental MCF-7 or LacZ cells formed tumors in volumes of 250 mm^3, whereas the MCF/VEGF expressing tumor established tumor in volumes of 1250 to 1500 mm^3. Importantly, when the mice were no treated with E_2, no tumor were formed in mice that received the parental or MCF-7/LacZ cells. In contrast, in absence of E_2 treatment, the MCF-7/$VEGF_{121}$ or MCF7/$VEGF_{165}$ cells established tumors in mice with similar growth rate to that of the parental or MCF-7LacZ tumors in mice exposed to E_2 treatments. Analyses of the angiogenesis of the various types of MCF-7 tumors demonstrated that no differences were found in vessel densities among all types of the MCF-7 tumors. However, in the parental and MCF-7/LacZ tumors that only formed in E_2 treated mice, most vessels were on the periphery of the tumors. In MCF-7/$VEGF_{121}$ or MCF-7/$VEGF_{165}$ expressing tumors established both in E_2 or non-E_2 treated mice, the neovessels extended into the centers of the tumors. The vessels in these types of tumors were highly perfused, whereas vasculature in other types of tumors was less accessible. Our data demonstrate that in addition to stimulating breast tumor angiogenesis, VEGF might mediate, at least in part, estrogen responsiveness in human breast tumor growth or VEGF might activate subsets of genes that render E_2-independent breast tumor formation in mice.

ABSTRACT SUBMISSION FORM
University of Rochester
James P. Wilmot Cancer Center
7th Annual Scientific Symposium
October 4, 2002

Presenting Author's Name: Bruce M. Fenton
Department: Radiation Oncology
Box number 704
Telephone: 275-7911

E-mail: bruce.fenton@rochester.edu
Indicate presentation format desired: __X___ Poster___ Oral _____ Either

VEGF RECEPTOR-2 BLOCKING ANTIBODY INHIBITS MAMMARY TUMOR GROWTH, VASCULAR PERFUSION, AND OXYGENATION.

BM Fenton*, SF Paoni, WM Liu, and I Ding, Department of Radiation Oncology, University of Rochester Medical Center, Rochester, NY 14642

DC101, an antiangiogenic monoclonal antibody against vascular endothelial growth factor receptor-2 (VEGFR-2), has been shown to result in substantial tumor growth inhibition as well as enhanced radiosensitization. Since antiangiogenic treatments will most likely be combined with conventional therapies, it is important to understand acute and chronic alterations in the tumor microenvironment following specific dosing and scheduling. In the present study, MCa-4 mammary carcinomas were grown orthotopically in C3H/HeJ mice. Beginning at either day 8 (early stage) or day 17 (late stage) post-implantation, DC101 (Imclone, Inc.) was administered *i.p.* at 45 mg/kg every three days. Using computer analysis of multiple-field image montages, total blood vessels were identified on anti-CD31 stained frozen sections, perfused vessels were measured by *i.v.* injection of fluorescent $DiOC_7$, and tumor hypoxia was determined using EF5 hypoxia marker uptake. DC101 therapy, begun at either early or late timepoints, resulted in pronounced tumor growth inhibition. For the early initiation treatment, perfused vessel counts decreased significantly ($p = 0.026$), and overall tumor hypoxia increased significantly ($p = 0.006$). Total vessel densities were not significantly reduced, most likely because of the direct dependence of tumor growth on vascular development. Thus, although vascular growth was undoubtedly inhibited, tumor cell proliferation decreased accordingly, resulting in no net change in vascular density. Zonal analysis of hypoxia variations as a function of distance from perfused vessels suggests a decrease in oxygen delivery capacity in the early-stage tumors, with no corresponding change in tumor oxygen consumption rate. Treated tumors were also separated into responders and nonresponders according to tumor volume. Tumors that responded to DC101 were much more hypoxic than matched volume controls, while nonresponder hypoxia levels were essentially equivalent to controls. Interestingly, perfused vessel counts and tumor hypoxia were unchanged from controls following the late initiation treatments. Further studies are required to better characterize pathophysiological and molecular differences between these cohorts and to confirm the effects in additional tumor models.

Supported by NIH Grant CA52586 and DOD Grant DAMD17-00-1-0420.

Effects of vascular endothelial growth factor receptor-2 antibody on vascular function and tumor hypoxia in two disparate murine mammary carcinomas, BM Fenton, SF Paoni, and I Ding.

DC101 (ImClone Systems), an antiangiogenic monoclonal antibody against vascular endothelial growth factor receptor-2 (VEGFR-2), has been shown to result in substantial tumor growth inhibition and enhanced radiosensitization in numerous tumor models. Since antiangiogenic treatments are likely to be ultimately combined with conventional therapies, it is vital to understand accompanying acute and chronic alterations in tumor pathophysiology. In the current study, two murine mammary carcinomas were grown orthotopically in C3H/HeJ mice: poorly differentiated, highly vascularized, MCa-35 tumors, and well-differentiated, less vascularized MCa-4 tumors. DC101 treatment (45 mg/kg every 3 days) was initiated at tumor volumes of either 50 mm^3 (early) or 500 mm^3 (late). Using computer analysis of multiple-field image montages from frozen tumor sections: 1) total blood vessels were identified using anti-CD31, 2) perfused vessels were found using *i.v.* injection of fluorescent $DiOC_7$, and 3) tumor hypoxia was quantified by uptake of the EF5 hypoxia marker. DC101 produced significant tumor growth inhibition for both tumor types, although somewhat more pronounced for the MCa-4. For the MCa-4 tumors, DC101 produced no alterations in total vessels densities, but significantly fewer perfused vessels ($p = 0.03$) and increased overall tumor hypoxia ($p = 0.03$). Zonal analysis of hypoxia variations as a function of distance from perfused vessels also suggested a decrease in oxygen delivery capacity in the early treated tumors, with no corresponding change in tumor oxygen consumption rate. For the late initiation treatments, DC101 again produced significant tumor growth inhibition, with no alterations in total vessel counts. Here, however, perfused vessel counts were not decreased and tumor hypoxia was not increased, suggesting a relative enhancement of radiosensitivity and drug delivery in comparison to early treatment tumors. For the MCa-35 tumors, pathophysiological responses were quite different. Following DC101, overall hypoxia was unchanged, but total and perfused vessel counts were strikingly decreased ($p = 0.001$ and $p = 0.02$, respectively). Although oxygen delivery capacity significantly declined with increasing tumor volume, perivascular hypoxia levels in treated MCa-35 tumors were not significantly different from controls for large or small tumors. In conclusion, treatment-induced, temporal variations in tumor oxygenation clearly have important implications in terms of the timing of subsequent therapies, and predictive assays of tumor response are critically needed. Further studies are in progress to better characterize the underlying rationale for the differential response in these tumors, including spatial measurements of endogenous pro- and anti-angiogenic cytokine levels as well as differences in vessel angiogenic status.

6243

Overexpression of VEGF by MCF-7 breast cancer cells enhances estrogen-dependent and estrogen-independent tumor growth

Ping Guo, Quan Fang, Houquan Tao, Christopher Anthony Schafer, Bruce M. Fenton, Ivan Ding, Bo Hu, Shiyuan Cheng, University of Pittsburgh, Pittsburgh, PA; University of Pittsburgh Cancer Institute, Pittsburgh, PA; University of Rochester Medical Center, Rochester, NY.

Human breast cancers are dependent on estrogen forgrowth.† Clinically, estrogen-dependentbreast tumors often evolve into more aggressive, malignant,estrogen-independent phenotypes.†Estrogen (E2) can stimulate severalgenes that are involved in breast cancer progression, one of which is vascularendothelial growth factor (VEGF) .†Studies have shown that growth factors induced by 17 b-estradiol (E2)in E2-dependent MCF-7 breast cancer cells can partially replace E2and promote tumor growth.† Therefore, wehypothesize that overexpression of VEGF by MCF-7 breast cancer cells mightabolish the E2-dependency of MCF-7 breast tumor growth in vivo.† To test our hypothesis, we generated MCF-7breast cancer cell clones that overexpress either LacZ or one of the two VEGFisoforms, VEGF121 or VEGF165.† The transfected MCF-7 clones stably expressed the isoforms, VEGF121or VEGF165, at levels of 300 ng/ml/106 cells after 48 hrsin culture, whereas the level of VEGF produced by parental MCF-7 or MCF-7/LacZcells was only 3.0 ng/ml/106 cells.†The parental MCF-7 or MCF-7/LacZ or the VEGF isoform overexpressingcells were all individually injected into the mammary fat pads in separateovariectomized female nude mice.† Withimplanted E2-release pellets, MCF-7 tumors derived from VEGF121or VEGF165 overexpressing cells had a 4-fold increase in volumesthan that of the tumors derived from the parental MCF-7 cells or MCF-7/LacZcells 45-day post implantation.† Incontrast, in the absence of E2, no tumorigenesis was observed in themice that received either the parental MCF-7 cells or MCF-7/LacZ cells.†† However, the tumors derived from eitherVEGF121 or VEGF165 overexpressing cells without E2treatment showed growth rates similar to, or greater than that of the tumorsestablished by the parental or MCF-7/LacZ cells in the mice that were exposedto estrogen. † Regardless, with orwithout estrogen exposure, a 3-fold increase of vessel density was found inboth types of tumors derived from either VEGF121 or VEGF165overexpressing cells.† Expression ofVEGF receptor-1 (Flt-1) was detected in tumor cells by IHC and RT-PCR analysesin the MCF-7 tumor tissues and in the cultured MCF-7 cells, respectively.† Overexpression of either VEGF121or VEGF165 led to a 2-fold increase in the proliferation of MCF-7cells in cell culture.† Theproliferation of MCF-7 VEGF overexpressing cells was inhibited by aneutralizing antibody against VEGF.†Thus, we showed that overexpression of VEGF in MCF-7 breast cancer cellscould indeed abolish E2-dependency on breast tumor growth throughboth paracrine and autocrine pathways.†These results also suggest that in addition to the well-defined functionof VEGF on tumor angiogenesis, VEGF might also render E2-independent growth ofbreast cancers.

EFFECT OF ANTIANGIOGENIC STRATEGIES ON THE PATHOPHYSIOLOGY AND PROGRESSION OF SPONTANEOUS AND TRANSPLANTED MAMMARY TUMORS.

Bruce M Fenton, Scott F Paoni, and Ivan Ding, University of Rochester Medical Center, Rochester, NY 14642

On the basis of successful preclinical data, numerous antiangiogenic agents are now in clinical trials, either alone or in combination with conventional therapies. Several key questions arise in regards to such combination therapies. The first is whether antiangiogenic agents produce detrimental effects on tumor vascular function and oxygen delivery, since conventional therapies are usually directly dependent on the supply of either chemotherapeutic drugs or oxygen. The second is whether experimental results based on fast-growing, transplanted tumors differ substantially from those in more slowly growing spontaneous murine tumors, which may be more representative of response in human primary tumors. To investigate changes in tumor pathophysiology, three antiangiogenic agents were compared: a) endostatin, a naturally occurring inhibitor of endothelial proliferation and migration, b) DC101, an antibody to vascular endothelial growth factor receptor-2, and c) celecoxib, a COX-2 inhibitor that can also inhibit angiogenesis. Using computer analysis of multiple-field image montages from frozen tumor sections: 1) total blood vessels were identified using antibodies to CD31 or panendothelial cell antigen, 2) perfused vessels were visualized using i.v. injection of fluorescent $DiOC_7$, and 3) tumor hypoxia was quantified by uptake of the EF5 hypoxia marker. Spontaneous mammary tumors developed in C3H/HeJ strain retired breeder mice over a period of 6 months to 1.5 yr, and were compared to two transplanted murine mammary tumors, MCa-4 and MCa-35, which differ substantially in both vascular configuration and overall hypoxia. Although spontaneous tumor growth rates varied substantially, even within a given treatment group, distinct differences were noted between treatment groups. Based on the slopes of the growth curves, 55% of the DC101 treated tumors responded to therapy, versus 12% of the endostatin tumors and 0% of the celecoxib tumors. Vessel spacing was significantly increased following both endostatin and DC101 treatment, while perfused vessel spacing was significantly increased for only the DC101. Overall tumor hypoxia and perivascular hypoxia were significantly higher following both endostatin and DC101, while celecoxib produced no changes in vascular configuration or hypoxia. DC101 also resulted in a substantial growth delay in the transplanted tumors, although less pronounced in the MCa-35 tumors. Vessel spacing was significantly increased in the MCa-35, but not the MCa-4, perfused vessel spacing was increased in both, and overall hypoxia was increased in only the MCa-4. Response to these antiangiogenic agents varied substantially both within and between the three tumor models. While DC101 reduced growth rate in roughly half of the spontaneous tumors, the remaining half of the tumors grew as rapidly as controls. Although vascular structure and function varied markedly among the three models, overall response to DC101 was, however, quite similar in most respects. Despite variations in absolute values, DC101 tended to both decrease vascular perfusion and increase hypoxia. While not conclusive proof, these studies support the idea that fast-growing, transplanted tumors reflect the effects of antiangiogenic agents on the pathophysiology of slower-growing, spontaneous tumors. A key focus of future studies will be to investigate the underlying rationale for the widely varying antiangiogenic response among tumors that outwardly appear so similar.